NASA HANDBOOK

NASA-HANDBOOK 8719.14

National Aeronautics and Space Administration
Washington, DC 20546

Approved: 2008-07-30
Expiration Date: 2013-07-30

HANDBOOK FOR LIMITING ORBITAL DEBRIS

Measurement System Identification: Metric

APPROVED FOR PUBLIC RELEASE – DISTRIBUTION IS UNLIMITED

This page intentionally left blank.

DOCUMENT HISTORY LOG

Status	Document Revision	Approval Date	Description
Baseline		2008-07-30	Initial Release

This page intentionally left blank.

FOREWORD

This NASA-Handbook (NASA-HDBK) is published by the National Aeronautics and Space Administration (NASA) to provide the scientific background to NASA's Orbital Debris Program as defined in NASA Procedural Requirements (NPR) 8715.6, Procedural Requirements for Limiting Orbital Debris, and NASA Standard (NASA-STD) 8719.14, Process for Limiting Orbital Debris.

This NASA-HDBK serves as a companion to NPR 8715.6 and NASA-STD 8719.14 and provides each NASA program and project with supporting material to assist in implementing the NPR and the NASA-STD. The uniform engineering, processes, procedures, practices, and methods that have been endorsed in NPR 8715.6 and NASA-STD 8719.14 are further explained in this NASA-HDBK during the selection, application, and design criteria of an item.

This NASA-HDBK is consistent with the objectives of the U.S. National Space Policy (August 2006), the U.S. Government Orbital Debris Mitigation Standard Practices (February 2001), the Inter-Agency Space Debris Coordination Committee (IADC) Space Debris Mitigation Guidelines (October 2002), the Space and Missile Center Orbital Debris Handbook, Technical Report on Space Debris (July 2002), and the space debris mitigation guidelines of the Scientific and Technical Subcommittee of the United Nations Committee on the Peaceful Uses of Outer Space, (A/AC.105/720, 1999 and A/AC.105/890, Feb 2007).

This NASA-HDBK is approved for use by NASA Headquarters and NASA Centers, including Component Facilities.

Requests for information, corrections, or additions to this NASA-HDBK shall be submitted via "Feedback" in the NASA Technical Standards System at **http://standards.nasa.gov**. This NASA-HDBK was developed by the NASA Headquarters Office of Safety and Mission Assurance with the Orbital Debris Program Office at Johnson Space Center.

Bryan O'Connor — July 30, 2008

Bryan O'Connor
Chief, Safety and Mission Assurance

Approval Date

This page intentionally left blank.

TABLE OF CONTENTS

LIST OF FIGURES

LIST OF TABLES

Handbook for Limiting Orbital Debris

1 SCOPE

1.1 Purpose

This NASA-HDBK serves as a companion to NASA Procedural Requirements (NPR) 8715.6, NASA Procedural Requirements for Limiting Orbital Debris and NASA-STD 8719.14, Process for Limiting Orbital Debris and contains the background and reference materials to aid in understanding the foundation and science for predicting and limiting orbital debris.

1.2 Applicability

a. This NASA-HDBK may be used by any program which launches material into space, but is most useful in assisting those programs using NPR 8715.6 and NASA-STD 8719.14.

b. This NASA-HDBK may be cited in contract, program, and other Agency documents as a reference for guidance.

2 APPLICABLE AND REFERENCE DOCUMENTS

The applicable documents for this NASA-HDBK include:

14 CFR Chapter III	Commercial Space Transportation, Federal Aviation Administration, Department Of Transportation.
NPR 8715.6	NASA Procedural Requirements for Limiting Orbital Debris.
NASA-STD 8719.14	Process for Limiting Orbital Debris.

Additional reference documents are listed in the last sub-section of each section topic area.

3 ACRONYMS AND DEFINITIONS

3.1 Acronyms

A/M	Area-to-mass
AHaB	Atmospheric Heating and Breakup
Al_2O_3	Aluminum oxide
ALCOR	ARPA-Lincoln C-band Observables Radar
AMOS	USAF Maui Optical Station
ASCC	Alternate Space Control Center
BLEs	Ballistic limit equations
CCDs	Charged-couple devices
CDR	Critical Design Review
CDT	CCD Debris Telescope
CGRO	Compton Gamma Ray Observatory
CIPAA	Cure-in-Place Ablator Applicator
CIS	Commonwealth of Independent States
CME	Chemistry of Meteoroids Experiment
CNES	Centre National d'Etudes Spatiales
COPUOS	Committee on the Peaceful Uses of Outer Space
CTIO	Cerro Tololo Inter-American Observatory
CTs	Correlated targets
DAS	Debris Assessment Software
DECR	Debris Environment Characterization Radar
DELTA	Debris Environment Long-Term Analysis
DoD	Department of Defense
DoT	Department of Transportation
DRAMA	Debris Risk Assessment and Mitigation Analysis
EISCAT	European Incoherent Scatter Scientific Association
EM	Expectation-Maximization

EOS	Earth Observation System
ESA	European Space Agency
EVA	Extravehicular activity
FCC	Federal Communications Commission
FGAN/TIRA	German Research Establishment for Applied Science Tracking and Imaging Radar
FOV	Field-of-view
GEO	Geosynchronous orbit
GEODSS	Ground-based Electro-Optical Deep Space Surveillance
GRAVES	Grande R'eseau Adapt'e a la Veille Spatiale
GTO	Geosynchronous transfer orbit
GUI	Graphical User Interface
HANDS	High Accuracy Network Determination System
HAX	Haystack Auxiliary
HST	Hubble Space Telescope
HST-SA	Hubble Space Telescope Solar Array
HTG	Hyperschall-Technologie Gottingen
HVIs	Hypervelocity impacts
IADC	Inter-Agency Space Debris Coordination Committee
ISAS	Institute of Space and Astronautical Science
ISCL	Inhibited shaped-charge launcher
ISS	International Space Station
JAXA	Japan Aerospace Exploration Agency
JSC	Johnson Space Center
KSGC	Kamisaibara Space Guard Center
LAD-C	Large Area Debris Collector
LDEF	Long Duration Exposure Facility
LEGEND	LEO-to-GEO Environment Debris model
LEO	Low Earth orbit

LGG	Light-gas guns
LMT	Liquid Mirror Telescope
LOC	Loss of crew
LOM	Loss of mission
LOV	Loss of vehicle
LRIR	Long Range Imaging Radar
MASTER	Meteoroid and Space Debris Terrestrial Environment Reference
MC	Monte Carlo
MCAT	Meter-class autonomous telescope
MCP	Microchannel plate
MEO	Medium Earth orbit
MIT/LL	Massachusetts Institute of Technology’s Lincoln Laboratory
MLI	Multi-layer insulation
MMOD	Micro-Meteoroid Orbital Debris
MODEST	Michigan Orbital DEbris Survey Telescope
MPAC	Micro-PArticle Captured
MPIfR/Effelsberg	Max Planck Institute for Radio Astronomy
MSISe-90	Mass Spectrometer Incoherent Scattering - extended 1990
MSX	Midcourse Space Experiment
NaK	Sodium-potassium
NASA-HDBK	NASA Handbook
NASA-STD	NASA Standard
NASDA	National Space Development Agency (Currently named “JAXA”)
NASS	NASA AMOS Spectral Study
NCAR	National Center for Atmospheric Research
NORAD	North American Air Defense Command
NPD	NASA Policy Directive
NPOESS	National Polar-orbiting Operational Environment Satellite System

NSS	NASA Safety Standard
NSSC	National Space Surveillance Control Center
ODAR	Orbital debris assessment reports
ODC	Orbital Debris Collector
ODERACS	Orbital DEbris RAdar Calibration Spheres
ORDEM	Orbital Debris Engineering Model
ORSAT	Object Reentry Survival Analysis Tool
PDR	Preliminary Design Review
PINDROP	Particle Impact Noise Detection and Ranging On autonomous Platform
PL	Phillips Laboratory
PMD	Postmission disposal
PNP	Probability of no penetration
POST	Program to Optimize Simulated Trajectories
RA	Reentry Assessment
RA	Right ascension
RAAN	Right ascension of the ascending node
RCS	Radar cross section
REBR	Reentry Breakup Recorder
RFP	Request for Proposal
ROSAT	German ROentgen SATellit
ROSCOSMOS	Russian Federal Space Agency
RWA	Reaction Wheel Assembly
SAO	Smithsonian Astrophysical Observatory
SBM	Standard Breakup Model
SBSS	Space-based space surveillance system
SBV	Space-Based Visible
SCARAB	Space Craft Atmospheric Reentry and Aerothermal Break-up
SCC	Space Control Center

SDM	Semi Deterministic Model
SDPA	Space Debris Prediction and Analysis
SEM	Size estimation model
SFU	Space Flyer Unit
SMA	Safety and mission assurance
SPADATS	Space Detection and Tracking System
SPASUR	Space Surveillance
SRM	Solid rocket motor
SSC	Space Surveillance Center
SSEM	Statistical Size Estimation Model
SSF	Space Station Freedom
SSN	U.S. Space Surveillance Network
SSS	Space Surveillance System
STP	Space Test Program
STSC	Scientific and Technical Subcommittee
SwRI	Southwest Research Institute
TIP	Tracking and Impact Prediction
TLE	Two-Line Element Set
TPS	Thermal protection systems
UCTs	Uncorrelated targets
UN	United Nations
USAF	U.S. Air Force
USN	U.S. Navy
USNA	U.S. Naval Academy
USSC	U.S. Satellite Catalog

3.2 Definitions

Apogee: The point in the orbit that is the farthest from the center of the Earth. The apogee altitude is the distance of the apogee point above the surface of the Earth.

Apsis (pl. apsides): The point in the orbit where a satellite is at the lowest altitude (perigee) or at the highest altitude (apogee). The line connecting apogee and perigee is the *line of apsides*.

Argument of perigee: The angle between the line extending from the center of the Earth to the ascending node of an orbit and the line extending from the center of the Earth to the perigee point in the orbit measured from the ascending node in the direction of motion of the satellite.

Ascending node: The point in the orbit where a satellite crosses the Earth's equatorial plane in passing from the southern hemisphere to the northern hemisphere.

Ballistic Coefficient: Mass, multiplied by the inverses of the drag coefficient and the area.

Cratering flux: The number of impacts per square meter per year of objects which will leave a crater at least as large as a specified diameter.

Debris flux: The number of impacts per square meter per year expected on a randomly oriented planar surface of an orbiting space structure.

Debris flux to limiting size: The number of impacts per square meter per year of debris objects of a specified diameter or larger.

ΔV: The change in the velocity vector caused by thrust measured in units of meters per second.

Disposal: An end-of-mission process for moving a spacecraft (if necessary) to an orbit considered acceptable for orbital debris limitation.

Eccentricity: The apogee altitude minus perigee altitude of an orbit divided by twice the semi major axis. Eccentricity is zero for circular orbits and less than one for all elliptical orbits.

f10: An index of solar activity; often a 13-month running average of the energy flux from the Sun measured at a wavelength of 10.7 cm, expressed in units of 10^4 janskys.

Geosynchronous Earth Orbit (GEO): An orbit with a period equal to the sidereal day. A circular GEO with 0° inclination is a geostationary orbit; i.e., the nadir point is fixed on the Earth's surface. The normal altitude of a circular GEO is 35,786 km and the inclination is normally +/- 15 degrees latitude.

Geosynchronous Transfer Orbit (GTO): A highly eccentric orbit with perigee normally within or near the LEO region altitude and apogee near or above GEO altitude.

High Earth Orbit (HEO): An orbit with a mean altitude greater than 2000 km or, equivalently, an orbit with a period greater than 127 minutes.

Inclination: The angle an orbital plane makes with the Earth’s equatorial plane.

Jansky: A unit of electromagnetic power density equal to 10^{-26} watts/m^2/Hz.

Launch vehicle: Any space transportation mode, including expendable launch vehicles (ELVs), reusable launch vehicles (RLVs), and the Space Shuttle.

Line of apsides: The line connecting the apogee and perigee points in an orbit. This line passes through the center of the Earth.

Line of nodes: The line formed by the intersection of the orbit plane with the Earth's equatorial plane. This line passes through the center of the Earth. The ascending node is the point where a satellite crosses the equator from the southern hemisphere to the northern hemisphere.

Low Earth Orbit (LEO): An orbit with a mean altitude less than or equal to 2000 km, or equivalently, an orbit with a period less than or equal to 127 minutes.

Meteoroids: Naturally occurring particulates associated with solar system formation or evolution processes. Meteoroid material is often associated with asteroid breakup or material released from comets.

Mission operations: All activities executed by the spacecraft; includes design mission, primary mission, secondary mission, extended mission, and disposal.

Orbital debris: Artificial objects, including derelict spacecraft and spent launch vehicle orbital stages, left in orbit which no longer serve a useful purpose. In this document, only debris of diameter 1 mm and larger is considered. If liquids are to be released, they should explicitly be shown to be compliant with all mitigation requirements.

Orbital lifetime: The length of time an object remains in orbit. Objects in LEO or passing through LEO lose energy as they pass through the Earth’s upper atmosphere, eventually getting low enough in altitude that the atmosphere removes them from orbit.

Orbital Stage: A part of the launch vehicle left in a parking, transfer, or final orbit during or after payload insertion; includes liquid propellant systems, solid rocket motors, and any propulsive unit jettisoned from a spacecraft.

Passivation: The process of removing stored energy from a space structure at EOM which could result in an explosion or deflagration of the space structure to preclude generation of new orbital debris after End of Mission. This includes removing energy in the form of electrical, pressure, mechanical, or chemical.

Penetration debris flux: The number of impacts per square meter per year that will penetrate a surface of specified orientation with specified materials and structural characteristics.

Perigee: The point in the orbit that is nearest to the center of the Earth. The perigee altitude is the distance of the perigee point above the surface of the Earth.

Postmission Disposal: The orbit/location where a spacecraft/launch vehicle is left after passivation at EOM.

Right ascension of ascending node: The angle between the line extending from the center of the Earth to the ascending node of an orbit and the line extending from the center of the Earth to the vernal equinox, measured from the vernal equinox eastward in the Earth’s equatorial plane.

Semi-major axis: Half the sum of the distances of apogee and perigee from the center of the Earth. Half the length of the major axis of the elliptical orbit.

Semi-synchronous Orbit (SSO)*:* An orbit with approximately a 12-hour period. A circular SSO is at an altitude of approximately 20,200 km.

Solar flux unit (sfu): Equal to 10^4 janskys measured at a wavelength of 10.7 cm.

Space debris*:* General class of debris, including both meteoroids and orbital debris.

Space Structures: Spacecraft and launch vehicle orbital stages. This includes all components contained within the object such as instruments and fuel.

Spacecraft: This includes all components contained within a space borne payload such as instruments and fuel.

Stabilized: When the spacecraft maintains its orientation along one or more axes.

Vernal equinox*:* The direction of the Sun in space when it passes from the southern hemisphere to the northern hemisphere (on March 20 or 21) and appears to cross the Earth's equator. The vernal equinox is the reference point for measuring angular distance along the Earth's equatorial plane (right ascension) and one of two angles usually used to locate objects in orbit (the other being declination).

4 Technical Material

4.1 Introduction

Earth orbiting spacecraft have become an integral part of our everyday lives. We depend on them for communications, weather information, scientific research, and national security. A real and growing concern for the safety and reliability of these satellites is the threat from collision with other orbiting objects including space debris. Even small particles can damage, degrade, or destroy spacecraft due to the very high velocities involved in a collision, on the average about 11 km/sec.

For example, during the flight of STS-7 in 1983, a paint fleck only 0.2 mm in size impacted the window and created a pit 0.4 mm deep, which exceeded the allowable damage criteria for reuse of the window outer pane during subsequent launches. This was the first documented example of damage to the Space Shuttle from an orbital debris impact. The orbital debris environment in this size regime has grown to the point where currently, the Space Shuttle program replaces, on average, one to two windows per shuttle flight due to hypervelocity impacts (HVIs) from space debris including micrometeoroids (Figure 4.1-1).

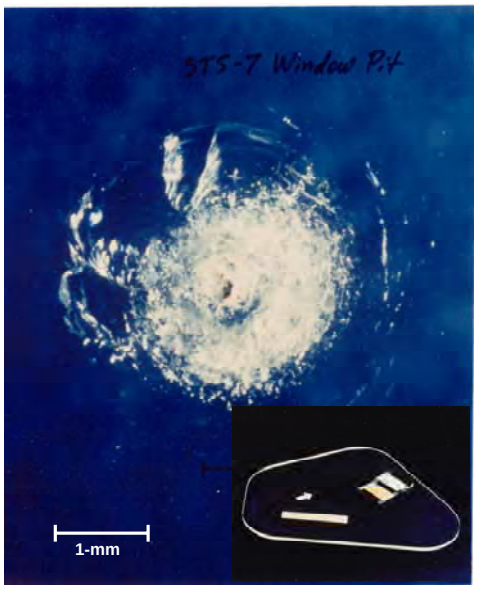

Figure 4.1-1. STS-7 window strike.

Damage caused by a paint fleck only 0.2 mm in size.

The STS-115 flight in 2006 returned with damage to the starboard payload bay radiator number 4 from a hypervelocity debris impact. The debris penetrated both walls of the honeycomb structure, and the shock wave from the penetration created a crack in the rear surface of the radiator 6.8 mm long (Figure 4.1-2). Scanning electron microscopy and energy dispersive X-ray detection analysis of residual material around the hole and in the interior of the radiator shows that the impactor was a small fragment of circuit board material.

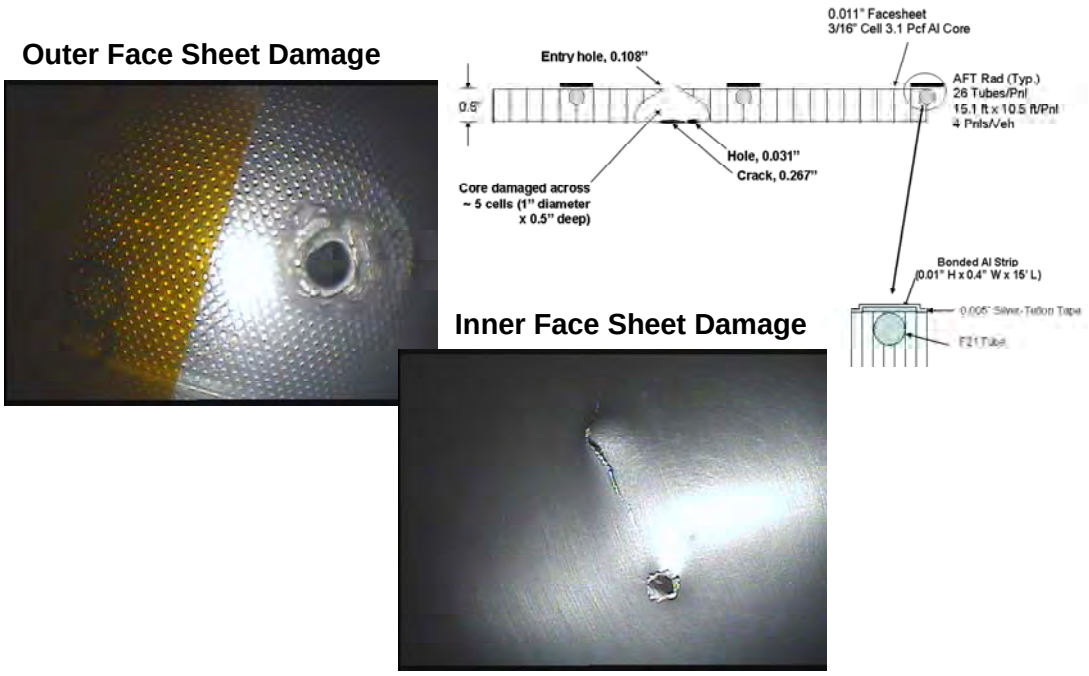

Figure 4.1-2. Radiator damage on STS-115.

This damage was caused by a small piece of circuit board material.

There are also examples of unplanned collisions in orbit involving larger objects tracked by the U.S. Space Surveillance Network (SSN). By 2006, three collisions between tracked objects are known to have occurred [anon. 2005]. Fortunately, none of these collisions has been catastrophic, producing only one to four additional pieces of tracked debris per collision.

An intentional collision in January 2007 demonstrated the potential for collisions to significantly pollute the near Earth orbital environment. On the 11th of that month the People's Republic of China launched an anti-satellite ballistic missile that struck a Chinese meteorological satellite, Fengyun-1C. The resulting debris cloud represents the single worst contamination of low Earth orbit (LEO) during the past 50 years. More than 2200 fragments have been cataloged by the SSN to date, with more expected in the future. Extending from 200 km to more than 4000 km in altitude, the debris frequently transit the orbits of hundreds of operational spacecraft, including the human space flight regime, posing new risks to current and future space systems. Moreover, the majority of the debris were thrown into long-duration orbits, with lifetimes measured in decades and even centuries [anon. 2007].

Orbital debris is an issue that cannot be solved unilaterally by any one organization or country. NASA has taken the lead in both researching the orbital debris issue and raising the awareness of the issue within other U.S. government agencies, with commercial spacecraft launchers and operators, and with other space-faring nations.

President Ronald Reagan's update of the U.S. National Space Policy, signed 5 January 1988, was the first White House declaration to address specifically the topic of orbital debris and to recognize the need for its mitigation to preserve near-Earth space for future generations. Each

succeeding president has updated and expanded upon this directive in subsequent national space policies. The most recent, signed by President George W. Bush on 31 August 2006 states:

> Orbital debris poses a risk to continued reliable use of space-based services and operations and to the safety of persons and property in space and on Earth. The United States shall seek to minimize the creation of orbital debris by government and non-government operations in space in order to preserve the space environment for future generations. Toward that end:
>
> - Departments and agencies shall continue to follow the United States Government Orbital Debris Mitigation Standard Practices, consistent with mission requirements and cost effectiveness, in the procurement and operation of spacecraft, launch services, and the operation of tests and experiments in space;
> - The Secretaries of Commerce and Transportation, in coordination with the Chairman of the Federal Communications Commission, shall continue to address orbital debris issues through their respective licensing procedures; and
> - The United States shall take a leadership role in international fora to encourage foreign nations and international organizations to adopt policies and practices aimed at debris minimization and shall cooperate in the exchange of information on debris research and identification of improved debris mitigation practices.

Internationally, NASA began bilateral discussions with the space agencies of Russia, Japan, China, and the European Space Agency (ESA) in an effort to increase the awareness of orbital debris issues within these agencies. From these initial meetings, the Inter-Agency Space Debris Coordination Committee (IADC) was formed in 1993 to study and reach consensus on technical issues related to space debris. The IADC is an association of the space agencies from 10 countries plus ESA and is recognized internationally as the leading technical authority on space debris.

NASA has also led the U.S. delegation in discussions of the issue at the United Nations' (UN) Committee on the Peaceful Uses of Outer Space (COPUOS) Scientific and Technical Subcommittee (STSC) meeting held annually in Vienna, Austria.

NASA's first set of comprehensive mitigation requirements was the *NASA Safety Standard (NSS) 1740.14, Guidelines and Assessment Procedures for Limiting Orbital Debris*, approved in August 1995. In 1997, NASA and the Department of Defense (DoD) drafted a set of *U.S. Government Orbital Debris Mitigation Standard Practices* (see Appendices) under the auspices of the Interagency Working Group on Orbital Debris, which was headed by the White House Office of Science and Technology Policy whose membership, along with NASA and DoD, included the Department of State, the Department of Transportation (DoT), the Department of Commerce, the Federal Communications Commission (FCC), the Department of Justice, and other White House Offices. The Standard Practices were formally adopted in February 2001 when all the applicable U.S. Government Agencies approved the Standard Practices in writing.

Current NASA direction for orbital debris assessments comes from *NASA Policy Directive (NPD) 8700.1, NASA Policy for Safety and Mission Success*. This document addresses the inclusion of safety and mission assurance (SMA) as an integral part of every NASA program and project. One of the responsibilities of all NASA programs and projects placing objects into space is to limit the generation of debris on orbit.

NASA requirements are more explicitly addressed in two documents: NASA Procedural Requirement (NPR): 8715.6, *NASA Procedural Requirements for Limiting Orbital Debris*, and NASA Standard (NASA-STD) *8719.14, Process for Limiting Orbital Debris*. NPR 8715.6 specifies how to implement an orbital debris program as a part of the NASA SMA activities. Those requirements and responsibilities for limiting orbital debris, which are solely the responsibility of NASA personnel, are defined in the NPR. NASA-STD 8719.14 provides details on orbital debris assessment reports (ODAR), reporting, and engineering processes needed for limiting orbital debris. The Orbital Debris Program Office has also developed a software package, Debris Assessment Software (DAS) Version 2.0, to facilitate the creation of the ODARs.

This handbook, as a companion to NASA-STD 8719.14, contains the background and reference materials to aid in understanding the foundation and science for predicting and limiting orbital debris.

4.1.1 References

Anon., "Accidental Collisions of Cataloged Satellites Identified," The Orbital Debris Quarterly News, NASA JSC, p. 1, April 2005. Available online at http://www.orbitaldebris.jsc.nasa.gov/newsletter/pdfs/ODQNv9i2.pdf.

Anon., "Chinese Anti-satellite Test Creates Most Severe Orbital Debris Cloud in History," The Orbital Debris Quarterly News, NASA JSC, p. 2, April 2007. Available online at http://www.orbitaldebris.jsc.nasa.gov/newsletter/pdfs/ODQNv11i2.pdf

4.2 The Current Orbital Debris Environment

4.2.1 Introduction

The orbital debris environment is a growing concern for operational spacecraft, in both the LEO and geosynchronous orbit (GEO) regimes. This risk will unequivocally grow as more and more nations gain the technology to launch satellites into Earth orbit. In the last decade, there has been an increased focus from the international community as a whole in attempting to categorize and model this ever-changing environment.

The LEO and GEO environment has over 10,000 objects with a size of 10 cm or larger. These objects include operational (functional) spacecraft, non-operational (inactive or retired) spacecraft and rocket bodies, as well as debris from a variety of sources. Debris can be released intentionally from a spacecraft or rocket body, but many times are generated as intact spacecraft and rocket bodies deteriorate or explode. The next section will go into more detail about the types of intact objects and debris in the LEO and GEO environments.

4.2.2 Sources of Debris and Distributions

4.2.2.1 Mission-Related

Mission-related debris are objects intentionally discarded during satellite delivery or satellite operations, including lens caps, separation and packing devices, spin-up mechanisms, empty propellant tanks, payload shrouds, or a few objects thrown away or dropped during EVA

activities. Most missions have very few pieces of this type of debris, and many times the objects have lower ballistic coefficients (mass, multiplied by the inverses of the drag coefficient and the area). LEO objects of this type will reenter the Earth's atmosphere more rapidly.

4.2.2.2 Fragmentation

Since the first recognized fragmentation in June 1961, over 200 objects (payloads, rocket bodies, and mission-related debris) have experienced on-orbit breakups. On-orbit fragmentations can result from accidental or intentional explosions, accidental or intentional collisions, or aerodynamic forces as an object nears atmospheric reentry. Accidental collisions are relatively uncommon to date, but are expected to increase as more objects are placed into orbit. Aerodynamic breakups, while relatively common, produce very few long-lived debris and are a non-factor in the long-term orbital debris problem. However, the intentional breakup of the Fengyun-1C spacecraft in January 2007 via hypervelocity collision with a ballistic object created the most severe artificial debris cloud in Earth orbit since the beginning of space exploration. More than 2200 debris on the order of 10 cm or greater in size have been identified and tracked by the SSN. The majority of these debris appear to reside in long-lived orbits.

Before the Fengyun-1C event, accidental explosions have dominated the long-lived debris generating events. Because of the energy associated with an explosion, these events can have hundreds of trackable objects, and probably tens-of-thousands of smaller pieces. It is these events that the international space agencies are focusing on reducing or eliminating. The accidental explosion event causing the most objects still in orbit today was the explosion of the Soviet Cosmos 1275 (International ID, 1981-053A) payload. A (probable) battery explosion 50 days into the lifetime of the satellite led to 259 objects that are still trackable over 25 years later [McKnight 1987]. A close second place is the United States Nimbus 4 rocket body (1970-025C), which first fragmented in 1970, but has experienced up to six sub-events as late as 1995. These events released over 370 trackable objects, with over 240 pieces of debris still in Earth orbit for over 35 years [Johnson 1991]. More discussion of the breakup causes will be contained in Section 4.7.2.3.

4.2.2.3 Anomalous/Deterioration

As spacecraft spend many years in the space environment, many deteriorate to the point of pieces or parts separating from the original spacecraft and causing what is referred to as "anomalous debris." An anomalous event is the unplanned separation, usually at low velocity, of one or more detectable objects from a satellite that remains relatively intact [Johnson *et al.* 2004].

The disintegration of spacecraft exterior paint is thought to create many sub-millimeter pieces of debris. The cause of this paint flaking is believed to be atomic oxygen erosion of the organic binder in the paint. Stage and spacecraft separation processes that occur in orbit also frequently release small debris.

4.2.2.4 Slag/NaK/Other

Many small orbital debris particles are created by solid rocket motor (SRM) firings, which produce aluminum oxide (Al_2O_3) particles called slag. These particles are formed during SRM tail-off, or termination of burn, by the rapid expansion, dissemination, and solidification of the molten Al_2O_3 slag accumulated during the burn. Since the transfer orbits are elliptical orbits,

most of the particles reenter quickly because of the effects of atmospheric drag and other forces at the orbit perigee. However, the propensity of SRMs to generate particles of 100 μm and larger has caused concern regarding their contribution to the debris environment. Particle sizes as large as 1 cm have been witnessed in ground tests, and comparable sizes have been estimated via ground-based and in-situ observations of sub-orbital tail-off events [Horstman and Mulrooney 2007]. Due to the large number of particles ejected by each motor, these Al_2O_3 particles can represent a significant surface erosion and contamination threat to spacecraft. Studies are ongoing to better understand the Al_2O_3 environment because, due to their smaller sizes, they are difficult to track from ground-based sensors.

Another class of debris is the Sodium-potassium (NaK) droplets that are released from RORSAT spacecraft launched between 1971 and 1988 by the former Soviet Union. The nuclear reactors on board routinely released many drops of coolant into the orbital environment. The spherical NaK droplets released over a period of decades number in the thousands. Because the RORSAT objects are in circular orbits over 800 km, the lifetime of the NaK droplets will be measured in thousands of years. Attempts to quantify the NaK population have been ongoing, with observations originally coming from only the DoD radar telescopes, but now also from the Haystack Radar telescopes at Lincoln Laboratories. There may be over 50,000 NaK droplets that are 5 mm or larger in orbit today [Foster *et al.* 2003].

4.2.3 Debris Count (> 10 cm) Graphs and Figures

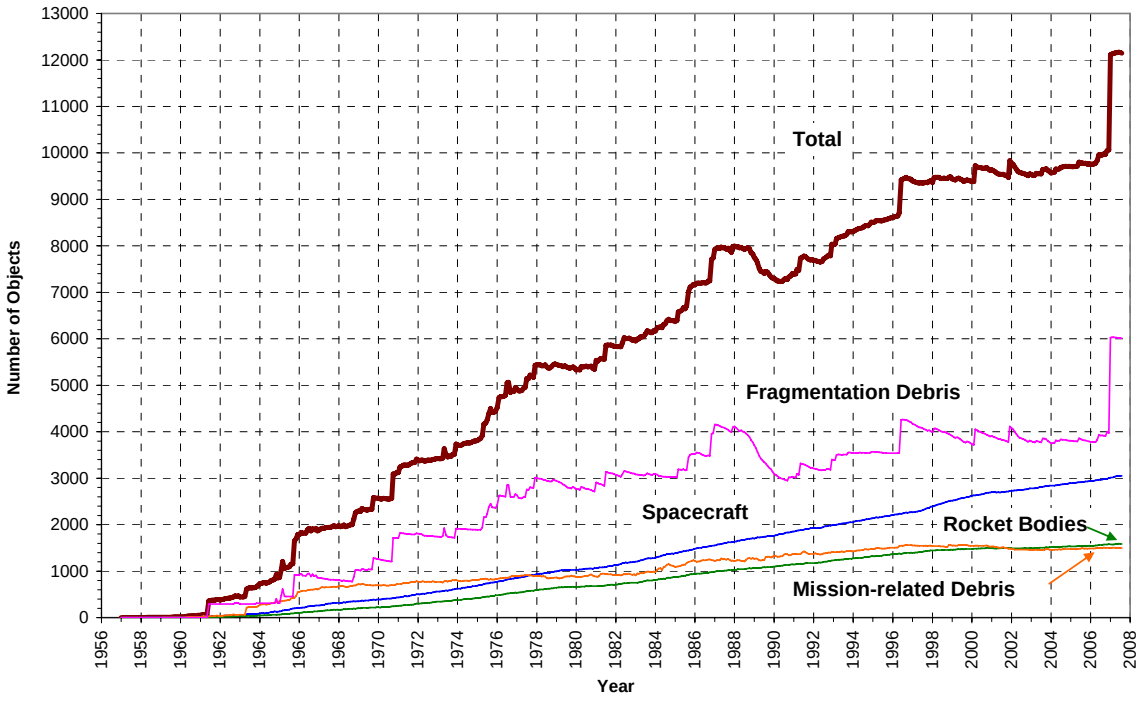

Figure 4.2-1. Monthly number of cataloged objects in Earth orbit by object type.

This chart displays a summary of all objects in Earth orbit officially cataloged by the SSN. "Fragmentation debris" includes satellite breakup debris and anomalous event debris, while "mission-related debris" includes all objects dispensed, separated, or released as part of the planned mission (epoch date of 2 August 2007).

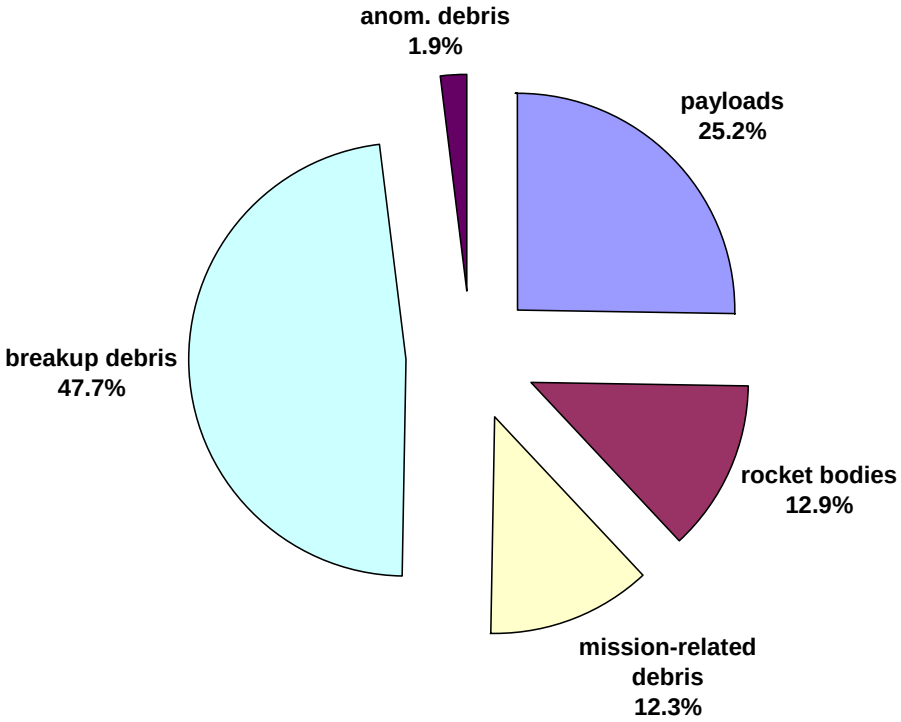

Figure 4.2-2. On-Orbit objects by type.

Relative segments of the cataloged in-orbit Earth satellite population (epoch date of 2 August 2007).

Table 4.2-1. Source vs. Type Accounting: Types of Objects Both In-Orbit, and Decayed, by Country of Origin (Epoch Date of 2 August 2007).

on-orbit									
	US	CIS	France	PRC	India	Japan	ESRO/ESA	Other	totals
payloads	1063	1324	44	61	33	103	36	387	3051
rocket bodies	542	837	97	37	8	35	6	27	1589
debris dispensed	0	0	0	0	0	0	0	0	0
mission related debris	781	507	92	62	1	36	12	5	1496
fragmentation debris	1666	1524	126	2315	97	2	18	35	5783
anomalous debris	142	82	3	0	0	0	0	0	227
totals	4194	4274	362	2475	139	176	72	454	12146

decayed or beyond Earth orbit									
	US	CIS	France	PRC	India	Japan	ESRO/ESA	Other	totals
payloads	800	1860	8	50	9	22	18	49	2816
rocket bodies	631	2367	55	68	8	53	5	7	3194
debris dispensed	0	1250	0	0	0	0	0	0	1250
mission related debris	783	4300	123	113	8	81	8	54	5470
fragmentation debris	2835	3272	474	179	249	22	4	4	7039
anomalous debris	74	5	2	0	0	2	0	0	83
totals	5123	13054	662	410	274	180	35	114	**19852**

Grand Total ->	**31998**

4.2.4 Breakups

4.2.4.1 Causes

The cause of over one-in-six, debris-generating, fragmentation events is still unknown. Causes that are known include deliberate explosion (or collision), propulsion events, battery explosion events, unintentional collisions, and aerodynamic events. Their definitions follow.

Deliberate: Deliberate actions, often associated with activities related to national security, were formerly the most frequently occurring class, but only four such events have happened since 1997, the latest being the aforementioned Fengyun 1C deliberate collision. Historically, deliberate fragmentations are performed such that many of the resulting debris are short-lived, which was not the case with the Fengyun event.

Propulsion: Propulsion-related events are the most frequent type of satellite fragmentation. Over half of all breakups with known causes are a result of a propulsion explosion (88 propulsion events as of February 2007). Causes of propulsion events include catastrophic malfunctions during orbital injection or maneuvers, subsequent explosions based on residual propellants, and failures of active attitude control systems. Breakups of rocket bodies due to propulsion failures are usually more prolific and produce longer-lived debris than the intentional destruction of payloads, often due to higher altitudes of the malfunctioning rocket bodies rather than the mechanics of the explosive event.

Battery: Explosions of pressurized batteries present a non-trivial contribution to the debris environment. While only eight events have been confirmed as related to battery explosions, debris remaining from these eight events are the second largest contributor to the debris still on-orbit. There has not been a known battery explosion event since 1987, as battery designs and safety mechanisms have improved.

Collisions: There have only been three accidental collisions of objects in space [Johnson 1996, anon. 2005]. All three involved a large intact body colliding with a much smaller piece of debris, and all three produced less than ten pieces of cataloged debris.

Aerodynamic events: These events occur when an object is undergoing its final atmospheric demise, but puts off a small number of debris that are briefly trackable, before they demise as well.

4.2.5 Debris Causes and Counts

The following figures display debris events and debris counts separated by breakup type. Aerodynamic events are excluded, because their contribution to the debris environment is negligible.

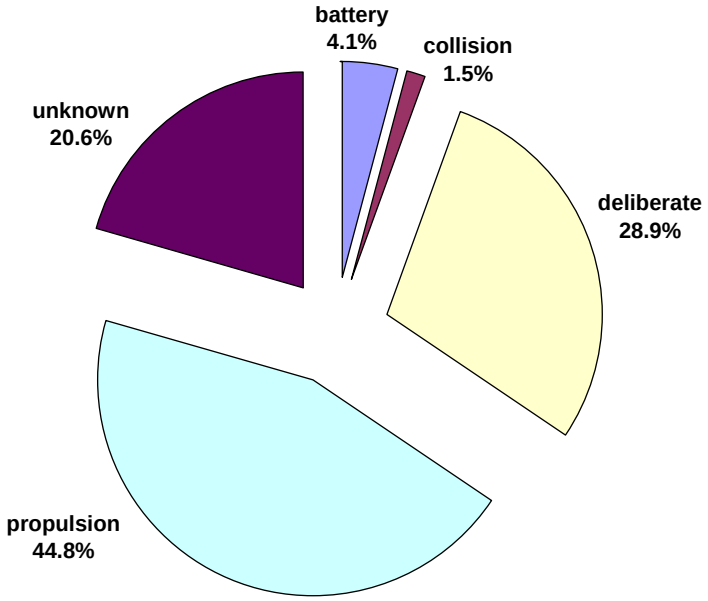

Figure 4.2-3. Causes of satellite breakups.

Percentage by number of events (epoch date of 2 August 2007).

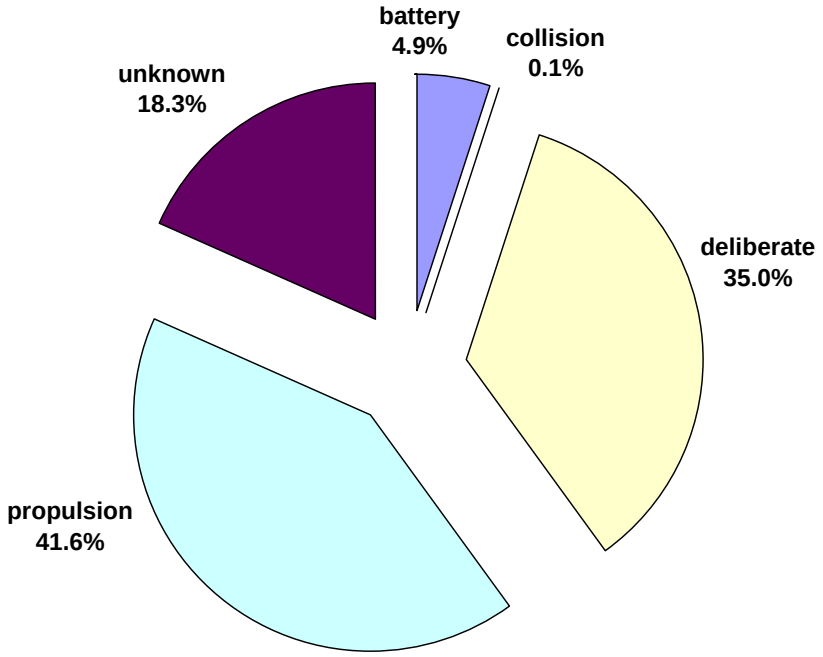

Figure 4.2-4. Proportion of all cataloged satellite breakup debris.

Percentage by number of pieces cataloged (epoch date of 2 August 2007).

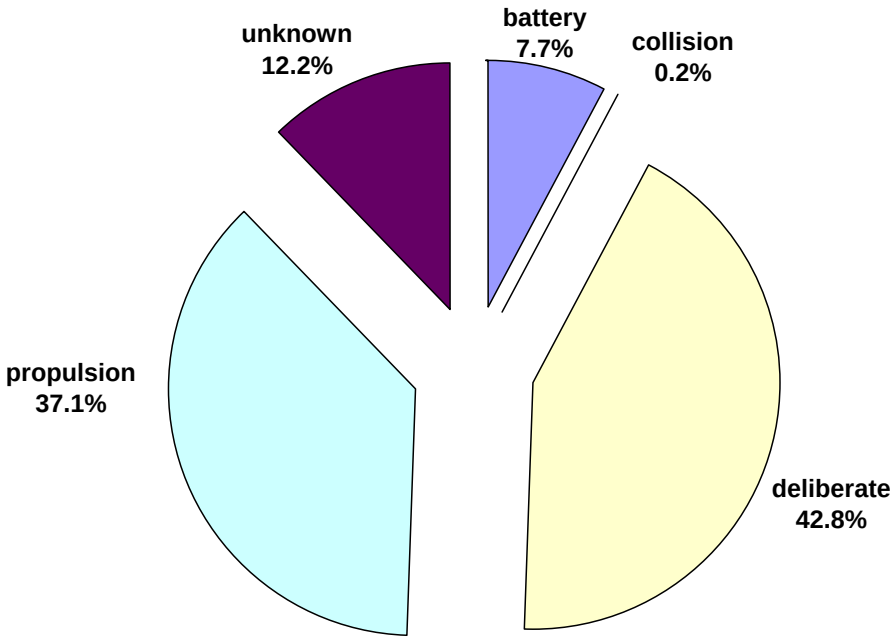

Figure 4.2-5. Proportion of cataloged satellite breakup debris remaining in orbit

Percentage by number of pieces remaining in orbit (epoch date of 2 August 2007).

4.2.6 Effects of Debris Collisions

In the next half-century, collisions most likely will become a much larger contributor in the debris generation in LEO. One study has shown that even if there were no new launches, the collision of existing spacecraft, rocket bodies, and debris would lead to a growing debris count, as more and more pieces of debris are generated and collide with other objects [Liou and Johnson 2006]. The three accidental collisions mentioned above have been non-catastrophic, meaning a small piece collided with a large piece and did not produce a significant amount of resultant debris. The Fengyun 1C event has shown that if there was indeed a catastrophic collision between two large objects at high velocity in which both are significantly damaged, the resultant debris count could be on the order of the largest fragmentations seen to date. The area of debris collisions is garnering more focus from the international community in recent years, particularly with a noticeable rise in fragmentation events seen in the last 12 months.

4.2.7 Uncertainty

Because of the inherent limits of ground-based sensors, debris events can only be known and discussed if there are pieces larger than approximately 10 cm. There may be other events that produce only a handful of very small debris that have gone undetected. Similarly, objects in the GEO regime must be on the order of 1 m in size or larger, so events in GEO are difficult to detect and a source of speculation among different space agencies. In addition, objects in certain

inclinations are difficult to track routinely, and therefore some events are not known until well after the event, when many of the debris may have reentered the atmosphere or been undetected too long to be associated with another parent object. As sensors improve, as well as the knowledge and shared information associated with international cooperation, detection of events may increase with time, but this may not be an indication that there are more events, just that we are detecting more of them.

4.2.8 References

Anon., "Accidental Collisions of Cataloged Satellites Identified," The Orbital Debris Quarterly News, NASA JSC, p. 1, April 2005. Available online at http://www.orbitaldebris.jsc.nasa.gov/newsletter/pdfs/ODQNv9i2.pdf.

Foster, J.L., et al., "NaK Droplet Source Modeling," *Space Debris and Space Traffic Management Symposium 2003,* American Astronautical Society. IAA 03-5.2.02, Bremen Germany, 29 September - 3 October 2003.

Horstman, M.F. and M. Mulrooney, "An Analysis of the Orbital Distribution of Solid Rocket Motor Slag," *58th International Astronautical Congress,* IAC-07 – 6.2.03 (CD-ROM), Hyderabad, India, September 2007.

Johnson, N.L., "Analysis of the Nimbus 4 Rocket Body Breakup and Subsequent Debris Anomalies," Kaman Sciences Corporation, February 1992.

Johnson, N. "First Natural Collision of Cataloged Earth Satellites," The Orbital Debris Quarterly News, NASA JSC, p. 1, September 1996. Available online at http://www.orbitaldebris.jsc.nasa.gov/newsletter/pdfs/ODQNV1i2.pdf.

Johnson, N.L., et al., History of On-Orbit Satellite Fragmentations, ed. 13, JSC-62530, NASA JSC, Houston, Texas, 2004.

Liou, J-C. and N.L. Johnson, "Risks in Space from Orbiting Debris," Science, Volume 311, pp. 340-341, 20 January 2006.

McKnight, D.S., Determining the Cause of a Satellite Breakup: A Case Study of the Kosmos 1275 Breakup, *38th Congress of the International Astronautical Federation*, IAA-87-573, Brighton, England, October 1987.

4.3 Future Environment

4.3.1 Introduction

Management of the future debris environment is critical to space operations for all nations of the world. Consequently, in the 1990s, international policies and procedures began to take form, such that all space-faring nations were making a concerted effort to maximize the ability to use space, while minimizing operations and procedures that might be destructive to the environment in the long term. As more countries gain the technology and economic means to launch spacecraft, more focus is being exerted on standardizing the procedures in each individual country, while adhering to the international agreements.

Space activity is placing debris in orbit faster than the natural effects of drag can remove it. As a result, since 1980, the tracked population of orbital debris is increasing by about 160 objects per year, even though launch rates have remained relatively constant for the last couple of decades. This increase in objects per year only includes those having sizes of 10 cm or larger; the increase in the number of smaller pieces is most likely much larger. Since 1980, the population of intact spacecraft, rocket bodies, and mission-related debris is increasing by about 120 objects per year, demonstrating that despite launch rates that are relatively stable, the increase in number of objects is still dominated by intact objects.

4.3.2 Debris Count

4.3.2.1 Trends

The major source of both large and small debris in LEO has been fragmentation of satellites and rocket bodies. This process has produced more large, trackable debris than has space operations, and very many more small untrackable debris. The launching of a payload into space from a booster or rocket upper stage generates orbital debris composed of spent rocket stages, clamps, shrouds, covers, and so forth, but does not produce many untrackable debris (sizes smaller than 10 cm) in LEO.

As launch activity has stabilized, and a greater focus has been placed on engineering spacecraft and rocket body hardware to avoid fragmentation events, the fragmentation debris count has been relatively stable since about 1987. While there certainly have been catastrophic, large debris count-generating events since this time, the slight decrease in the number of events, combined with two solar maxima during this time period, caused the number of debris to remain around 5000 pieces of fragmentation and mission-related debris 10 cm or larger (see Figure 4.2-1). This was until the Fengyun 1C event boosted that count by over 2000 pieces.

As mentioned, the debris count can be noticeably affected by the solar cycle, which lasts approximately 11 years. During periods of high solar activity, an object will see more drag from the atmosphere. Because in most cases, debris has lower ballistic coefficients (higher area-to-mass, A/M) than intact objects, debris tends to reenter the atmosphere more quickly. Figure 4.3-1 shows the last three solar cycles (with monthly average flux values), as shown previously in Figure 4.2-1 when debris counts were lower.

While it is certain that the cycle will continue indefinitely, the magnitude of the solar cycle and its effect on orbital debris is difficult to predict. If the peak of the next solar cycle is abnormally high, this would lead to shorter lifetimes for most LEO objects. The next solar maximum should occur near 2012, and there are differing opinions as to whether this cycle could be abnormally high or abnormally low. A team of scientists led by Mausumi Dikpati, from the National Center for Atmospheric Research (NCAR), maintains that the next solar cycle will have peaks 30% - 50% higher than the previous cycle [Dikpati *et al*. 2006]. However, solar cycle expert Dr. Ken Schatten has asserted that cycle #24 will be abnormally low [Schatten 2003]. The impact that this solar cycle has on the environment will have a propagative effect on debris over the next century. Figure 4.3-2 shows a comparison for the two opinions for the next solar maxima.

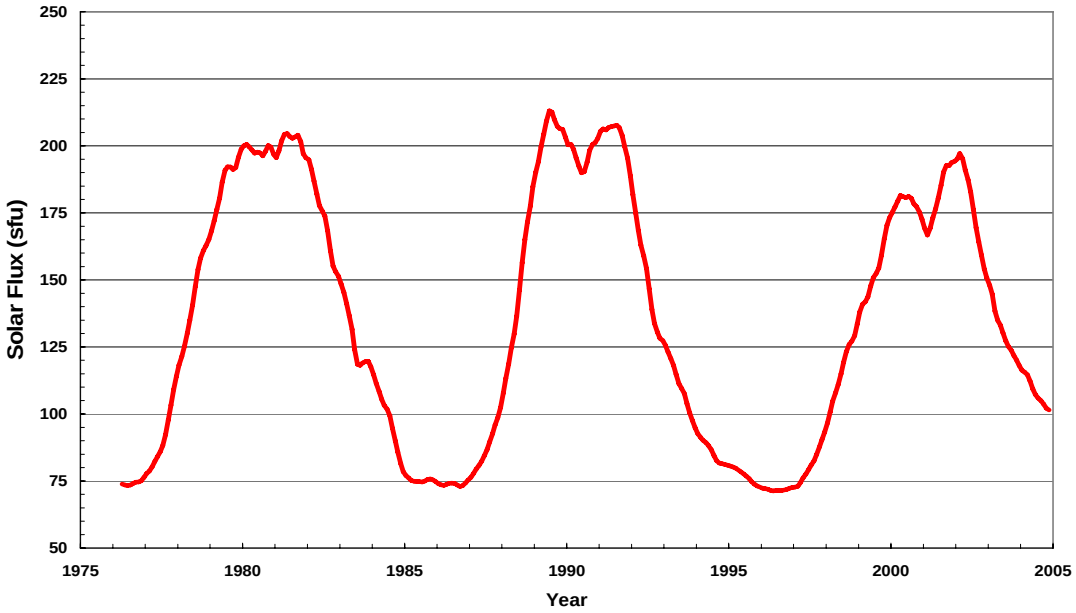

Figure 4.3-1. Average historical solar flux.

A smoothed average of solar flux for the last three cycles.

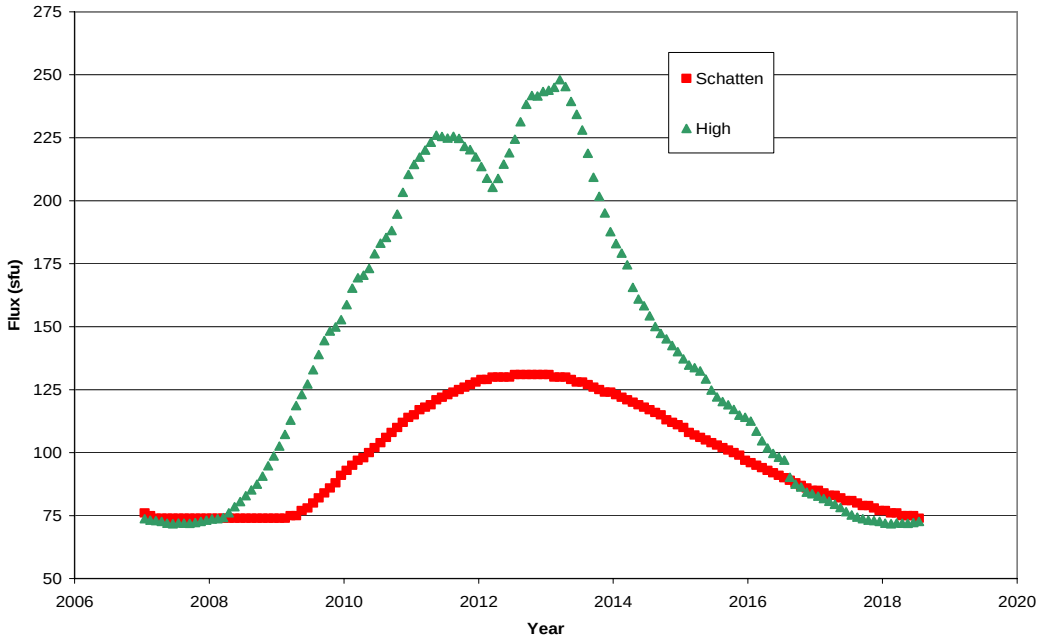

Figure 4.3-2. Solar model comparison.

A comparison of average monthly solar flux values, as predicted by two different organizations. "Schatten" data obtained from the Flight Dynamics Facility Data Center (https://wakata.nascom.nasa.gov//prod_center/pc_frame_page.htm) (epoch date of October 2006), while the "high" prediction is the previous solar cycle (23) augmented by 40% as suggested by the NCAR paper.

4.3.2.2 Future Outlook

There are very large uncertainties involved with predicting future debris environments. Making these predictions requires estimates of future debris sources and sinks. This includes estimates of future world launch activity (when, how much mass on orbit, what orbit), estimates of future on-orbit explosions and collisions (when, where, what, how many), estimates of future solar cycle activity, and estimates of mitigation strategies and their effect on the debris environment. Another aspect of future predictions that is not modeled by NASA or DoD is the impact of future technology and its effect on reducing the hazard of debris to operational assets.

As the international community focuses more on the elimination of circumstances that lead to fragmentation (*i.e.*, improved battery design, passivation of pressurized and energized systems, reduction in deliberate events, etc.), it is reasonable to assume that the current rate of fragmentation events may remain relatively constant at only a few per year. However, as more traffic is introduced to the LEO environment (*i.e.*, the 160 objects per year), it is also reasonable to assume that collisions of objects could become a much larger player in debris generation. While there have only been three, relatively small, accidental collision events to date (see Section 4.2.3.1), it is understood that a catastrophic event could lead to as many or more pieces as large propulsion-related events.

4.3.3 Launch Activity

4.3.3.1 Trends

For the first 25 years of human involvement in space, only the U.S. and the former Soviet Union launched significant numbers of spacecraft. Currently, the seven countries or groups listed in Table 4.3-1 (plus the “others”) are the primary contributors of spacecraft and rocket bodies into the LEO and GEO environments. After hitting a peak in the 1980s, the number of successful launches per year has stabilized since 2000. Figure 4.3-3 shows the number of launches per year. Some launches might have multiple payloads, but for each launch around three or four intact objects, on average, are cataloged.

There is little to suggest politically or economically that the launch rate might increase significantly in the near future. In many NASA models, it has been assumed that the launch rate will remain as it has been for the past 8 years. This assumption has been valid for the past 10 years, but will always be revisited as the launch climate changes.

4.3.3.2 Future Outlook

In the past 2.5 years, objects launched into LEO by countries other than the seven listed in Table 4.3-1 have increased by 25%, while the U.S. and Russia combined have only increased by 7% (Johnson et al. 2004). While evaluating 30 months of data does not necessarily make a trend, it is important to understand that other nations are expanding their presence in LEO. Figure 4.3-4 shows a comparison of launches by the U.S., Russia (including the former Soviet Union), and all other countries combined.

Table 4.3-1. Source vs. Orbit Accounting: Objects by Orbit Type, Both Currently In-Orbit and Decayed, by Country of Origin (Epoch Date of 3 October 2006).

on-orbit									
	US	CIS	France	PRC	India	Japan	ESRO/ESA	Other	totals
LEO	3043	3567	244	347	119	127	38	117	7602
GEO	202	226	10	27	19	43	14	222	763
BTH	3	0	98	0	0	0	4	16	121
OTH	819	426	3	2	1	13	14	37	1315
totals	**4067**	**4219**	**355**	**376**	**139**	**183**	**70**	**392**	**9801**

decayed or beyond Earth orbit									
	US	CIS	France	PRC	India	Japan	ESRO/ESA	Other	totals
LEO	4783	12814	655	386	269	134	26	90	19157
GEO	1	0	0	0	0	0	0	0	1
BTH	1	0	2	0	0	0	1	1	5
OTH	284	153	1	0	0	8	8	3	457
totals	5069	12967	658	386	269	142	35	94	**19620**

Grand Total -->	**29421**

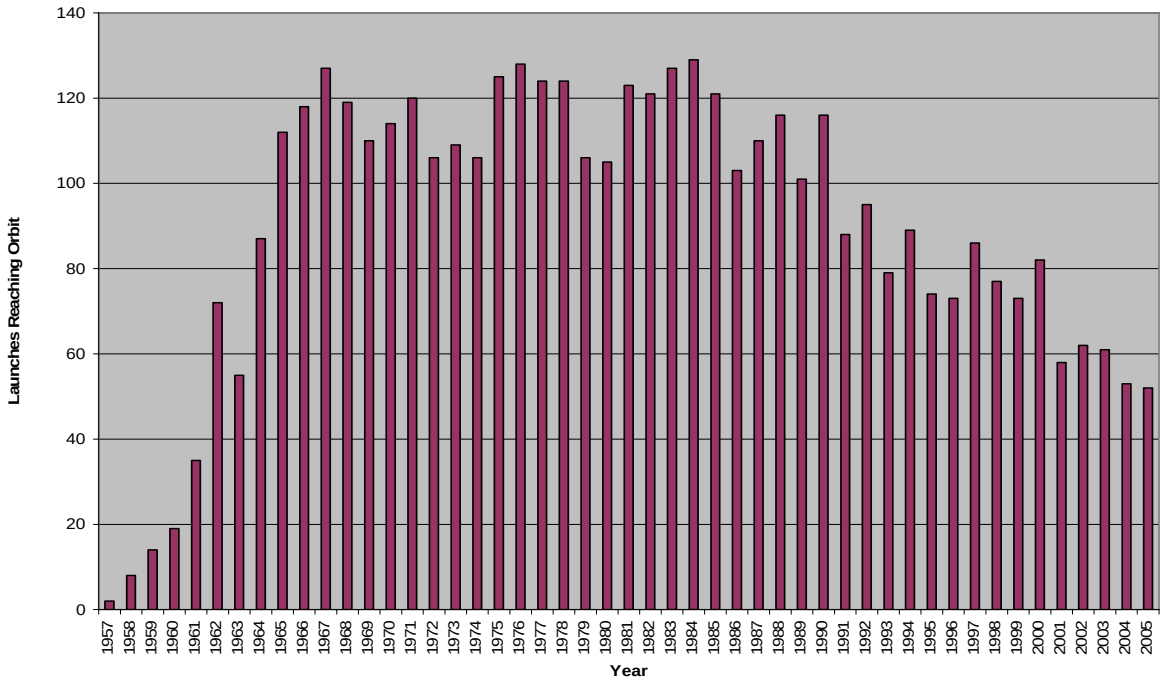

Figure 4.3-3. Launches per year: number of unique launches each year since 1957.

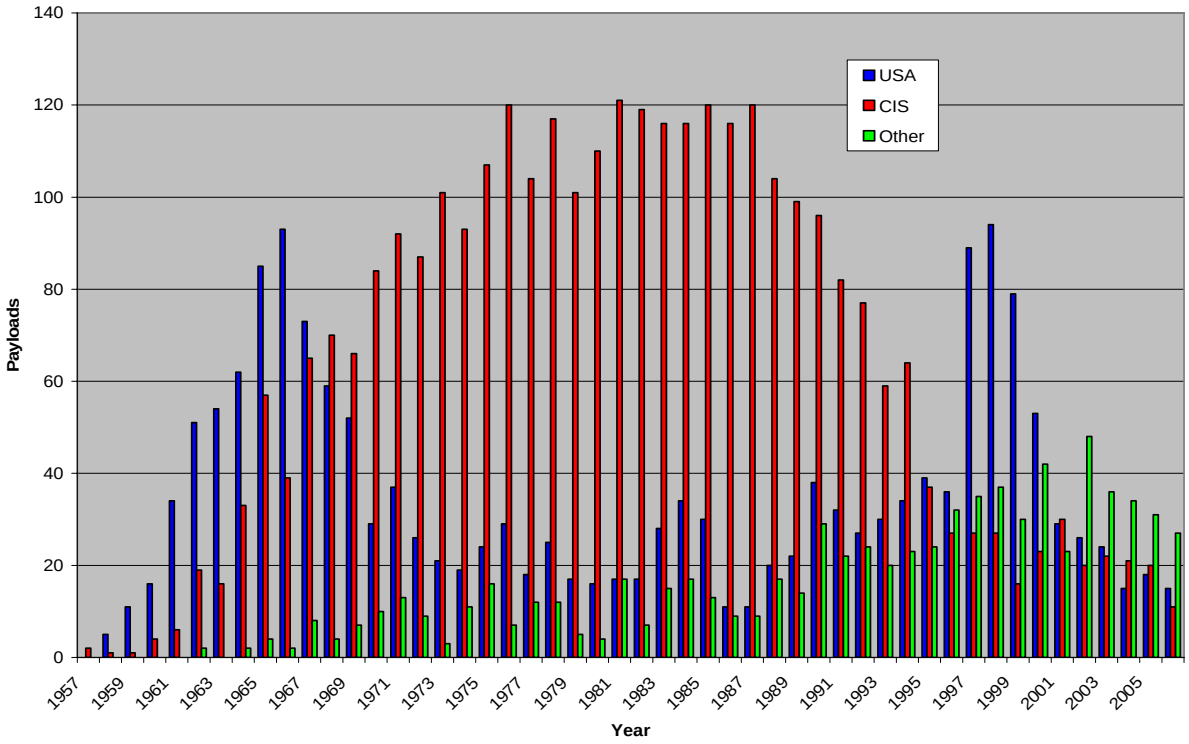

Figure 4.3-4. Payloads by country of origin and year.

Launched payloads only - all countries besides the U.S. and Russia are included in the other.

4.3.4 Implications

4.3.4.1 Future Missions and Constellations

The advent of LEO satellite constellations could present a new and significant issue for the orbital debris environment around LEO. Constellations may use a variety of planes and inclinations with expected spacecraft lifetimes of less than 10 years. Therefore, in the near future, more spacecraft will have to be launched to replace derelict craft. Many of the bands for future systems would probably be the most heavily used regions of LEO, such as the sun-synchronous inclinations. Including the large numbers and cross-section characteristic of constellations increases the probability of collisions, particularly because the high inclination leads to high spatial density over the poles.

Adding to the complexity is the uncertainty of how economically profitable constellations will be in the future, as the three most extensive constellations – GLOBALSTAR, ORBCOMM, and IRIDIUM all filed for bankruptcy protection at some point during the implementation phase of their respective programs. Should constellations show more profitability, it is unclear how many of these systems will be deployed. This is particularly true since many current and proposed constellations are at some of the higher LEO regimes, thus requiring a massive upper stage, which may or may not be reentered in a timely fashion. In addition, should there be an explosion

event; the debris will certainly contaminate the LEO environment for many years, as most objects over 600 km in altitude do not reenter for decades.

4.3.4.2 Human Space Flight

The International Space Station (ISS) began operations in 1998. Since November 2, 2000 there has been a constant human presence in space. While this presence is invaluable for research, the expanding debris environment presents a significant risk to the humans on board. Because the ISS is at a relatively low altitude (~350 km), debris in this regime' tends to deteriorate below the ISS altitude very quickly. This has mostly been evident during extravehicular activities when there have been several pieces of debris intentionally released or inadvertently dropped from the ISS. In each case, within hours, the debris was confirmed to have been safely below ISS altitude, and of no threat to the station. That is not to say this risk is negligible. As evident by the damage to the STS-115 Orbiter discussed in Section 4.1, there will always be a risk of debris colliding with an inhabited spacecraft, and consequently a risk to human life.

Moreover, it is a certainty that there will be impacts with objects too small to cause a penetration or significant structural damage. Most impacting particles will be in the size range of grains of sand. These very small impacts will cause surface degradation on sensitive surfaces, such as instruments and solar panels. This type of damage has been, and will be repaired during the routine maintenance operations. In fact, in the case of the Hubble Space Telescope (HST), the solar array surfaces can be returned and analyzed to better understand the environment to which the shuttle or station is exposed.

One of the more important design constraints for the new Crew Exploration Vehicle will be the design of the exterior to withstand a reasonable debris impact. As we attempt to define the environment over the next 20 years, it will be important to make sure enough shielding is provided, but without unreasonable or detrimental impact to weight and cost. Because the mission profiles may vary widely from that of the Space Shuttle, a comprehensive understanding of the debris environment throughout LEO is a necessity.

4.3.5 References

Anon., "Monthly Number of Cataloged Objects in Earth Orbit by Object Type" (Chart), The Orbital Debris Quarterly News, NASA JSC, p. 10, April 2006. Available online at http://www.orbitaldebris.jsc.nasa.gov/newsletter/pdfs/ODQNv10i2.pdf.

Dikpati, M., et al., "Predicting the Strength of Solar Cycle 24 Using a Flux-transport Dynamo-based Tool", Geophys. Res. Lett., 33, L05102, doi:10.1029/2005GL025221, 2006.

Johnson, N.L., et al., History of On-Orbit Satellite Fragmentations, ed. 13, JSC-62530, NASA JSC, Houston, Texas, 2004.

Schatten, K.H., "Solar Activity and Solar Cycle," 2003. Available online at: http://www.ai-solutions.com/Resources/Papers/cospar-schatten-D1.1-D2.1-E3.1-0001-05_final.pdf.

4.4 Measurements of the Orbital Debris Environment

4.4.1 Introduction

The NASA Orbital Debris Program Office places great emphasis on obtaining and understanding direct measurements of the orbital debris environment. The Orbital Debris Program Office's environmental models are all based on these measurements. The Orbital Debris Engineering Model (ORDEM) is the result of combining all of the most current measurements and projecting the short-term future (~30 years) based on historical environment changes and trends. NASA's long-term evolutionary model uses measurements and historical data to reach the current environment and then projects that environment into the distant future (~100 years typically) using different operational assumptions or scenarios.

Because OD measurements must cover a very wide range of sizes and altitudes, one technique realistically cannot be used for all measurements. In general, radar measurements have been used for lower altitudes and optical measurements for higher altitude orbits. For very small debris, *in situ* measurements such as returned spacecraft surfaces are utilized.

The DoD maintains a catalog and ephemeris of orbital objects and debris for sizes as small as 5- to 10-cm diameter in LEO and about 1 m diameter in GEO using its worldwide network of radar and optical sensors that comprise the SSN. NASA concentrates on statistically measuring size and orbit distribution of the debris environment for sizes smaller than these limits.

For statistical measurements of the LEO debris environment for sizes less than 10 cm, NASA uses the Haystack, the Haystack Auxiliary (HAX), and the Goldstone radars. Of these, the Goldstone radar is the most sensitive and can detect objects as small as 2- to 3- mm diameter at ISS altitudes. However, Goldstone, as part of the Deep Space Network, is highly subscribed, and collects only a few hours of data each year on an "as available" basis. NASA, through an agreement with United States Strategic Command, receives 1000 hours per year of data collected with Haystack and HAX, with a minimum of 600 hours from Haystack. Haystack is capable of detecting debris as small as 5 mm at ISS altitudes, while HAX is capable of detecting debris as small as 1 - 2 cm.

The radar cross section (RCS) of a target determines how much transmitted radar energy will be reflected back to the radar receiver. RCS is a very complicated function of the radar wavelength and the material composition, shape, and orientation of the debris object, and as a result, interpreting radar data can be very challenging. To develop a model, NASA measured a representative set of fragmentation debris from a ground HVI test in a controlled radar range. The pieces were measured over all orientations and a wide range of radar wavelengths to create a size estimation model (SEM) to statistically relate RCS to physical size.

To measure the debris population at GEO altitudes, NASA currently uses the Michigan Orbital DEbris Survey Telescope (MODEST) located at the Cerro Tololo Inter-American Observatory (CTIO) in Chile through a grant to the University of Michigan. Because optical brightness must also be related to physical size, comparisons of RCS to optical brightness indicates that, on average, orbital debris only reflects 10-20% of the incident visible light. Developing a statistical model using more direct measurement techniques is an on-going research topic.

Another on-going area of research is determining material composition of debris from remote spectral reflectance measurements. NASA has developed a large database of measured spectra of common spacecraft materials. It is currently developing and testing the tools to compare remote spectral measurements with this database to estimate the material combinations and percentages present in debris pieces.

For statistically measuring the debris environment for debris sizes smaller than can be measured from ground sensors, NASA relies on examination of materials that have been exposed to the orbital space environment and other *in situ* measurements. Some notable examples of this type of measurement are the Long Duration Exposure Facility (LDEF), solar arrays from the HST, the Orbital Debris Collector (ODC), and of course, the Space Shuttles. Size of the impacting debris can be related to the crater or hole size produced. Often residual material from the impactor can be analyzed to determine the material composition of the debris particle.

4.4.2 The U.S. Space Surveillance Network

4.4.2.1 History and Overview

Although the origin of the SSN predates the launch of the world's first artificial satellite on 4 October 1957, the dramatic appearance of Sputnik 1 profoundly altered the course of satellite tracking in the U.S. In keeping with the civilian nature of the goal to orbit a scientific spacecraft during the International Geophysical Year, the Smithsonian Astrophysical Observatory (SAO) was assigned the responsibility of designing and deploying a worldwide, satellite-tracking network. The first of the famous Baker-Nunn cameras was completed on 2 October 1957, just two days before the Space Age was inaugurated. An equally important milestone was achieved on 5 October 1957 when the Millstone Hill radar, a product of the Massachusetts Institute of Technology's Lincoln Laboratory (MIT/LL), became operational.

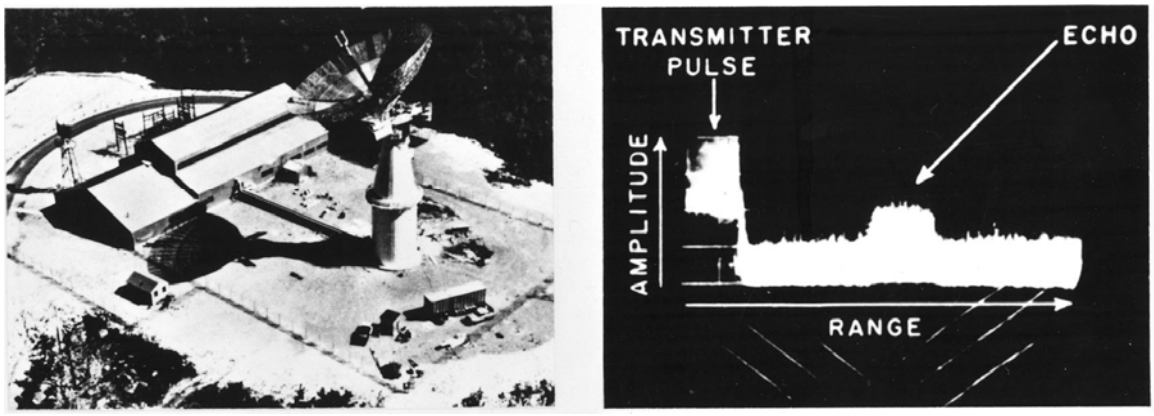

Figure 4.4-1. Millstone Hill radar in 1957 (left) and an A-scope trace of Sputnik (right).

During October 1957, the U.S. Air Force (USAF) also organized Project Harvest Moon, the direct predecessor of the service's SPACETRACK network. Harvest Moon became operational at the Cambridge Research Center, Massachusetts, on 30 November 1957 with three radars and an assortment of optical sites supplying observations on the fledgling Earth artificial satellite population, which had grown to three objects.

As the SAO, the USAF, and the U.S. Navy (USN) developed independent space surveillance systems, the need to coordinate and to integrate U.S. satellite tracking activities led to the creation of the National Space Surveillance Control Center (NSSC), which became operational on 1 January 1960 at Hanscom Field, Massachusetts, with the support of an IBM 709 computer. In the fall of that year the North American Air Defense Command (NORAD; the word "Air" was changed to "Aerospace" in May 1981) was assigned operational control of the NSSC and the Space Detection and Tracking System (SPADATS) that supported it. Meanwhile, the primary components of SPADATS – USAF's SPACETRACK (496L) System and the USN's Space Surveillance (SPASUR) System – remained under the command of their respective services. On 14 March 1961 the NSSC was renamed the SPADATS Center, and by the summer of 1961 the SPADATS Center and the SPACETRACK Center were both operational at Ent Air Force Base in Colorado Springs, Colorado.

That same year, the mammoth construction project commenced to carve out nearly 700,000 tons of granite from Cheyenne Mountain to provide a secure command and control center for NORAD's space surveillance, attack warning, and national defense functions. At that time, the only full-time radar systems contributing to SPADATS were USN's SPASUR and USAF's AN/FPS-17 detection radar at Laredo, Texas. However, five other radars at Millstone Hill; Moorestown, New Jersey; Shemya Island, Alaska; Trinidad Island; and Diyarbakir, Turkey, were serving as contributing space surveillance sensors.

By 23 March 1964, SPADATS had officially cataloged 769 satellites of which 418 from four countries were still in orbit. Actually, the satellite population was higher due to incomplete cataloging of debris from the fragmentations of the Transit 4A rocket body on 29 June 1961 and the Atlas Centaur 2 rocket body on 27 November 1963. In fact, in September 1961, NORAD informed NASA of the problem associated with the detection and tracking of space 'junk'.

For four decades, the Cheyenne Mountain Complex was the principal fusion center for all space surveillance tracking and identification information. The name of the center in which these functions are accomplished has changed over the years with titles including the Space Control Center (SCC), the NSSC, the Space Surveillance Center (SSC), and most recently, back to SCC. In August, 2007, the center was moved to Vandenberg Air Force Base and the name changed yet again to the Joint Space Operations Center (JSpOC). The 1st Space Control Squadron of the USAF Space Command is responsible for the operation of the SSN, including tasking individual sensors and data collection and analysis. Five crews work around the clock, 365 days a year, in the JSpOC.

Space surveillance involves detecting, tracking, cataloging, and identifying man-made objects orbiting the Earth; *e.g.*, active and inactive spacecraft, spent rocket bodies, mission-related debris, and fragments. The smallest objects currently tracked (~ 5 cm in diameter) are droplets of NaK which served as the primary coolant for Soviet nuclear reactors and which were released during disposal operations from 1980 to 1988.

- Space surveillance accomplishes the following:
- Detects new man-made objects in space;
- Produces a running catalog of man-made space objects;
- Determines which country is responsible for an orbiting or reentering space object;
- Charts the present position of space objects and plots their anticipated trajectories; and

- Predicts when and where a space object will reenter the Earth's atmosphere.

The average number of satellite observations being forwarded to the SCC has risen from 10,000 per day in the mid-1960s to more than 100,000 in 2006. A radar observation normally consists of a number of returns from the object. A series of observations taken during a single pass over the sensor is called a track.

In order to meet its mission of maintaining a satellite catalog, the SSN need not observe every satellite at each sensor opportunity. Such a volume of data is both unnecessary and inefficient. For example, a single track of 10 observations each day can be sufficient to maintain the orbital parameters of higher altitude objects. Space objects more susceptible to the influences of atmospheric drag (typically at altitudes below 500 km) and solar radiation pressure, and those with maneuver capabilities can be the subject of multiple tracks per day by the SSN.

Specific orbital accuracy tolerances are assigned to each satellite based upon a number of considerations. Solar activity also affects the accuracy of orbital element sets not only due to atmospheric disturbances, but also due to direct effects on the performance of SSN radars.

Inherent radar errors (both random and bias errors) may combine to further reduce the accuracy of satellite element sets. One method of calibrating radar sensors is to employ specifically designed satellites for fine-tuning RCS measurements, as well as metric data. The U.S. has orbited a variety of calibration satellites for this purpose, most during the 1960s, and more than a dozen remain in orbit. The wide range of sizes (typically 0.3 to 1.1 m diameter), shapes (spheres, polygons, cylinders), and altitudes (600 to 2800 km) permits calibration across a broad set of conditions. In addition, in the case of RCS measurements, the irregular shape and instability of most Earth satellites results in large standard deviations.

A wide variety of radar, optical, and electro-optical sensors have been a part of the SSN since 1961. The original optical telescopes have given way to more sensitive and accurate electro-optical systems (first with vidicon technology, but now with charge-coupled devices), while many mechanical dish radars have been replaced with phased-array radars capable of tracking multiple objects simultaneously. Moreover, the radar frequencies have moved to progressively higher bands from VHF and UHF to L-band, C-band, and X-band in order to observe smaller objects. The 2006 configuration of the SSN is described in the following section.

4.4.2.2 SSN Sensors

The SSN uses a "predictive" technique to monitor space objects; *i.e.*, it spot checks them rather than tracking them continually. This technique is used because of the limits of the SS; *e.g.*, the number of sensors, geographic distribution, capability, and availability. Below is a brief description of each type of sensor.

a. Phased-array radar**s** can maintain tracks on multiple satellites simultaneously and scan large areas of space in a fraction of a second. These radars have no moving mechanical parts to limit the speed of the radar scan – the radar energy is steered electronically.

b. Conventional radars use moveable tracking antennas or fixed detection and tracking antennas. A detection antenna transmits radar energy into space in the shape of a large fan. When a satellite intersects the fan, energy is reflected back to the detection antenna, where the location of

the satellite is computed. A tracking antenna steers a narrow beam of energy toward a satellite and uses the returned energy to compute the location of the satellite and to follow the satellite's motion to collect more data.

c. Electro-optical sensors consist of telescopes linked to video cameras and computers. The video cameras feed their space pictures into a nearby computer that drives a display scope. The image is transposed into electrical impulses and stored on magnetic media. Thus, the image can be recorded and analyzed in real-time or later.

d. The Midcourse Space Experiment (MSX) satellite is an Earth-orbiting satellite with a payload containing a variety of sensors, from ultra-violet to very-long-wave infrared. Originally a platform for Ballistic Missile Defense Organization projects, the MSX was moved to the SSN in 1998. Since that time, the visible-light *Space-Based Visible (SBV)* sensor on MSX has contributed significantly to the tracking of geosynchronous objects and is serving as a pathfinder for a future space-based space surveillance system (SBSS).

In general, electro-optical sensors are used to track objects at high altitudes (above 5000 km), and radar sensors are used for lower altitude objects. However, a few radars have deep space capabilities; *e.g.*, Millstone, Altair, and Globus II.

The SSN sensors are categorized as dedicated (those with the primary mission of performing space surveillance) or contributing and collateral sensors (those with a primary mission other than space surveillance) (see Table 4.4-1). Combined, these types of sensors make over 100,000 observations each day. This enormous amount of data comes from SSN sites such as Maui, Hawaii; Eglin, Florida; Thule, Greenland; and Diego Garcia, Indian Ocean. The data are transmitted directly to the SCC at Cheyenne Mountain Air Force Station in Colorado Springs via satellite, ground wire, microwave, and/or phone. An Alternate Space Control Center (ASCC) is operational at Dahlgren, Virginia. Every available means of communication is used to ensure a backup is readily available if necessary.

The SSN can track space objects as small as 5 cm in diameter in LEOs. At geosynchronous altitudes, the sensitivity of the SSN is approximately 1 m. By 2007, the SSN had cataloged more than 30,000 space objects in orbit about the Earth. The SSN currently tracks and monitors nearly 10,000 cataloged satellites, of which about 800 represent operational spacecraft. More than 19,000 cataloged objects have already reentered Earth's turbulent atmosphere and are no longer in orbit. The cataloged objects now orbiting the Earth range from debris with masses of less than 1 kg to the ISS with a mass of 186,000 kg (as of June 2006). An historical overview of the SSN Catalog was shown in Figure 4.2-1.

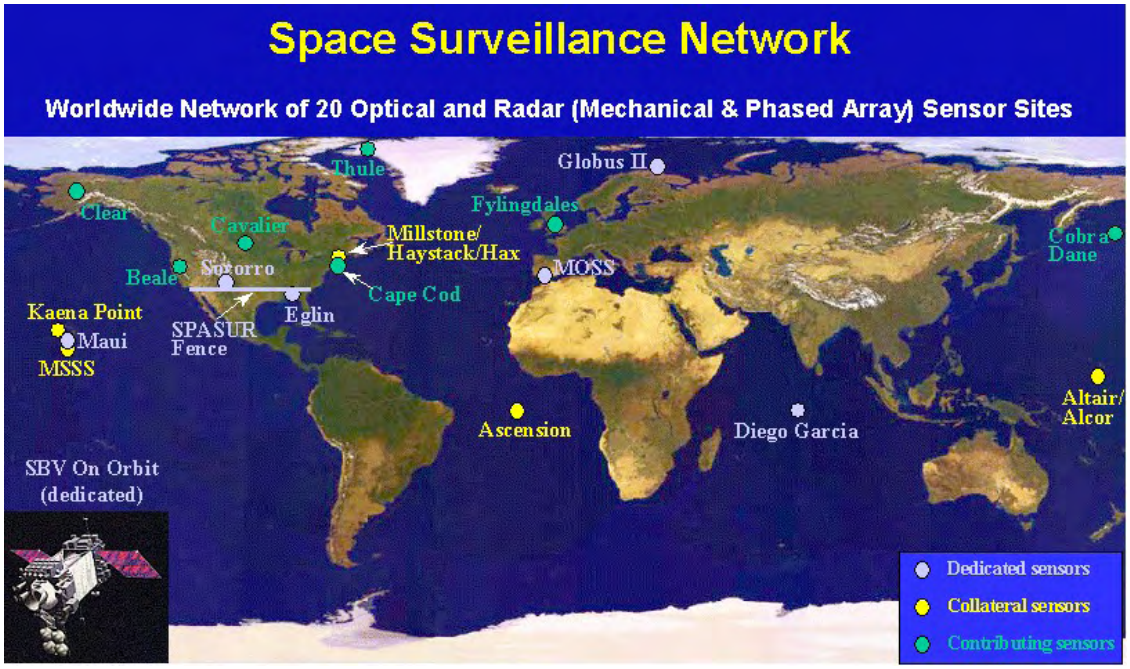

Figure 4.4-2. Configuration of the SSN in 2006.

Table 4.4-1. SSN Sensors – 2006

Sensor	Sensor Desig.	Rng Type	Collector Type	Data Type	Mission Support	# Sensors	Owner
Ascension	ASC	NE	Radar (Mechanical Tracker)	Metric / Intel	Collateral	1	AFSPC
Beale - PAVE PAWS	BLE	NE	Solid State Phased Array Radar (SSPAR)	Metric / Intel	Collateral	2	AFSPC
Cape Cod - PAVE PAWS	COD	NE	SSPAR	Metric / Intel	Collateral	2	AFSPC
Cavalier - PARCS	CAV	NE	Radar PA	Metric / Intel	Collateral	1	AFSPC
Clear - BMEWS	CLR	NE	3 Detection Radars / 1 Tracking Radar	Metric / Intel	Collateral	2	AFSPC
Diego Garcia - GEODSS	DGC	DS	E-O	Metric / Intel	Dedicated	3	AFSPC
Eglin	EGL	NE/DS	Radar PA	Metric / Intel	Dedicated	1	AFSPC
Feltwell - DSTS	FLT	DS	Passive RF	Metric	Dedicated	2	AFSPC
Fylingdales - BMEWS	FYL	NE	SSPAR	Metric / Intel	Collateral	3	AFSPC/UK
Haystack Aux - LSSC	HAX	NE/DS	Radar (Mechanical Tracker)	Intel	Contributing	1	MIT/LL
Haystack LRIR - LSSC	HAY	NE/DS	Radar (Mechanical Tracker)	Intel	Contributing	1	MIT/LL
Kaena Point	KAE	NE	Radar (Mechanical Tracker)	Metric / Intel	Collateral	1	AFSPC

Sensor	Sensor Desig.	Rng Type	Collector Type	Data Type	Mission Support	# Sensors	Owner
Kwajalein - ALCOR	ALC	NE	Radar (Mechanical Tracker)	Intel	Contributing	1	Army/SMDC
Kwajalein - ALTAIR	ALT	NE/DS	Radar (Mechanical Tracker)	Metric / Intel	Contributing	1	Army/SMDC
Kwajalein - TRADEX	TRX	NE/DS	Radar (Mechanical Tracker)	Metric / Intel	Contributing	1	Army/SMDC
Kwajalein - MMW	MMW	NE	Radar (Mechanical Tracker)	Intel	Contributing	1	Army/SMDC
Maui - GEODSS	MAU	DS	E-O	Metric / Intel	Dedicated	3	AFSPC
Misawa - DSTS	MSW	DS	Passive RF	Metric	Dedicated	2	AFSPC
Millstone - LSSC	MIL	NE/DS	Radar (Mechanical Tracker)	Metric / Intel	Contributing	1	MIT/LL
MSSS – 3.7m	AEOS	DS	E-O	Intel	Contributing (Oct 00)	1	AFMC/AFRL
MSSS - 1.6m	AMS	DS	E-O	Metric / Intel	Contributing (Oct 00)	1	AFMC/AFRL
MSSS - 1.2m	MOT	DS	E-O	Metric	Contributing (Oct 00)	1	AFMC/AFRL
MSSS - .8m	BDT	DS	E-O	Metric	Contributing (Oct 00)	1	AFMC/AFRL
MSX/SBV	MSX	NE/DS	E-O	Metric	Dedicated (Oct 00)	1	AFSPC
AF Detection Fence (formerly SPASUR)	NAV	NE/DS	Radar (Detection Fence/Interferometer)	Metric	Dedicated	6 (Rcv) 3 (Trx)	AFSPC
Globus II	GB2	NE/DS	Radar (Mechanical Tracker)	Metric	Dedicated	1	AFSPC
Socorro - GEODSS	SOC	DS	E-O	Metric / Intel	Dedicated	3	AFSPC
Spain - MOSS	MOSS	DS	E-O	Metric / Intel	Dedicated	1	AFSPC
Shemya	SHY	NE	Radar PA	Metric	Contributing	1	AF/AIA
Thule - BMEWS	THU	NE	SSPAR	Metric / Intel	Collateral	2	AFSPC

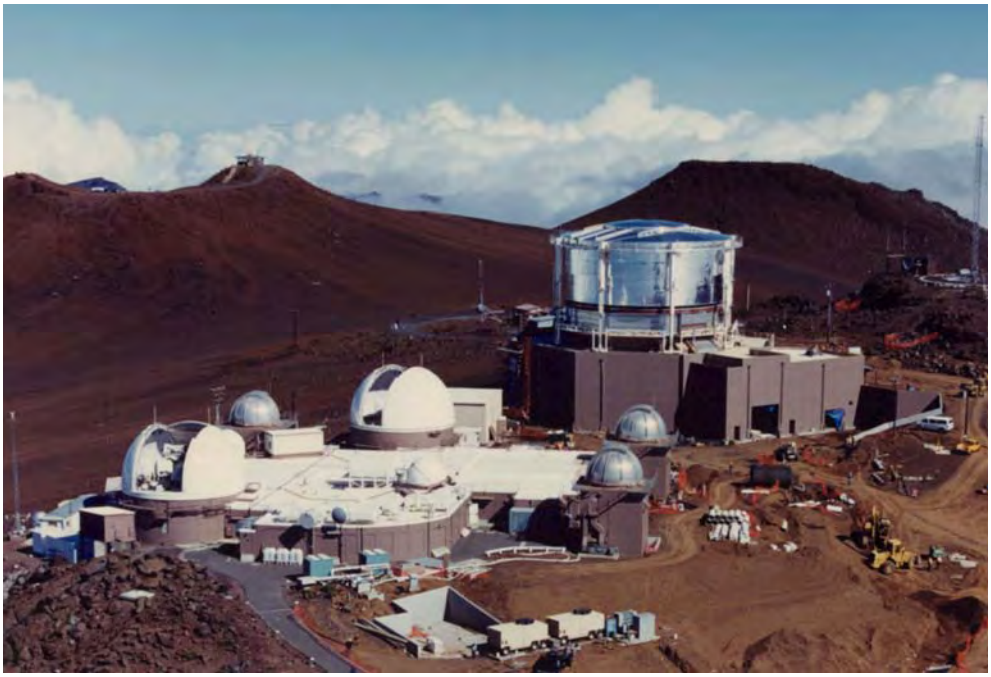

Figure 4.4-3. Maui Space Surveillance Complex.

Includes the Maui Ground-based Electro-Optical Deep Space Surveillance (GEODSS) site (the three smaller silver domes).

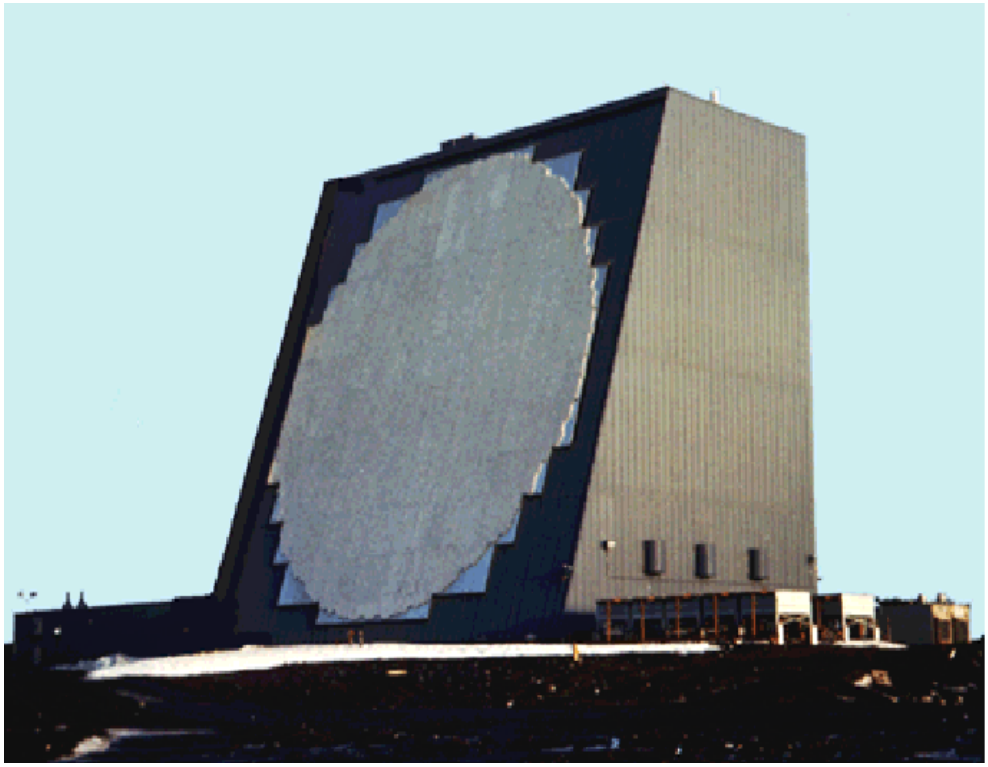

Figure 4.4-4. The Cobra Dane L-band phased-array radar at Shemya, Alaska.

Figure 4.4-5. PAVE PAWS 2-sided phased-array radar.

Figure 4.4-6. The FPS-85 phased array radar at Eglin AFB, Florida.

The transmitter array is on the left, and the receiver array is on the right.

Figure 4.4-7. The Haystack (left) and the HAX (right) mechanical dish radars in Massachusetts.

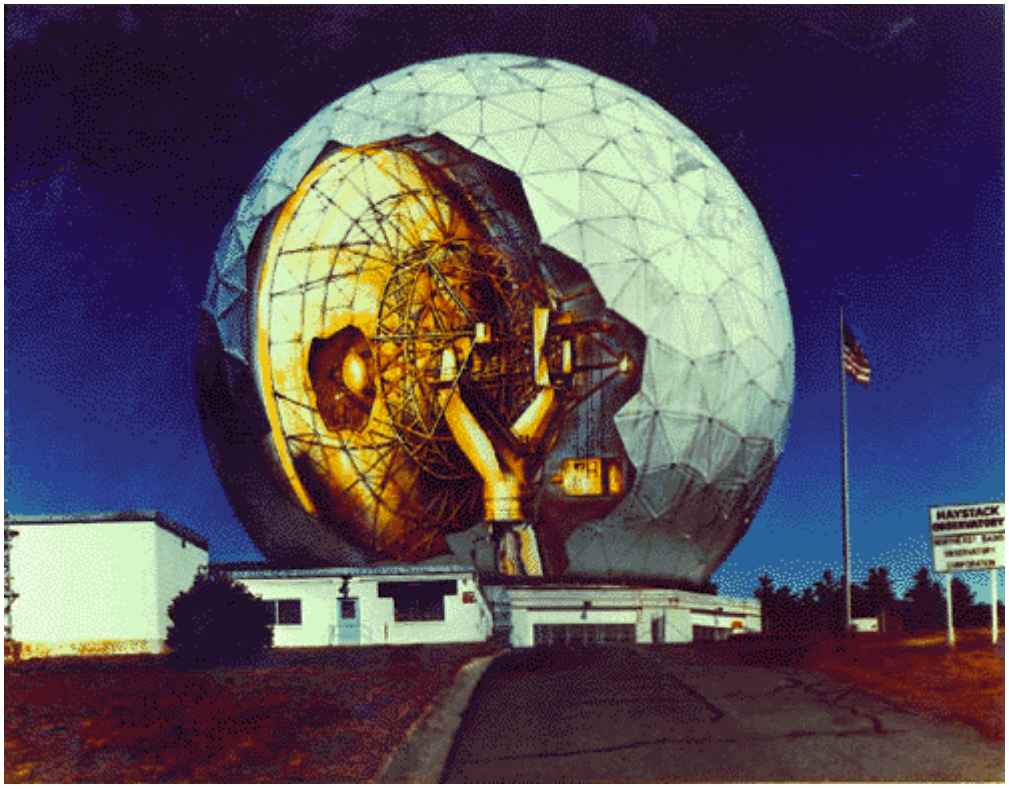

Figure 4.4-8. Interior view of the Haystack radar.

Figure 4.4-9. ALTAIR

(top of the photo) and other radars on the Kwajalein Atoll in the Pacific Ocean.

Figure 4.4-10. Globus II radar in Vardo, Norway.

Figure 4.4-11. Jordan Lake transmitter of the USAF Space Surveillance Fence near Wetumpka, Alabama.

Figure 4.4-12. Red River receiver of the USAF Space Surveillance Fence near Lewisville, Arkansas.

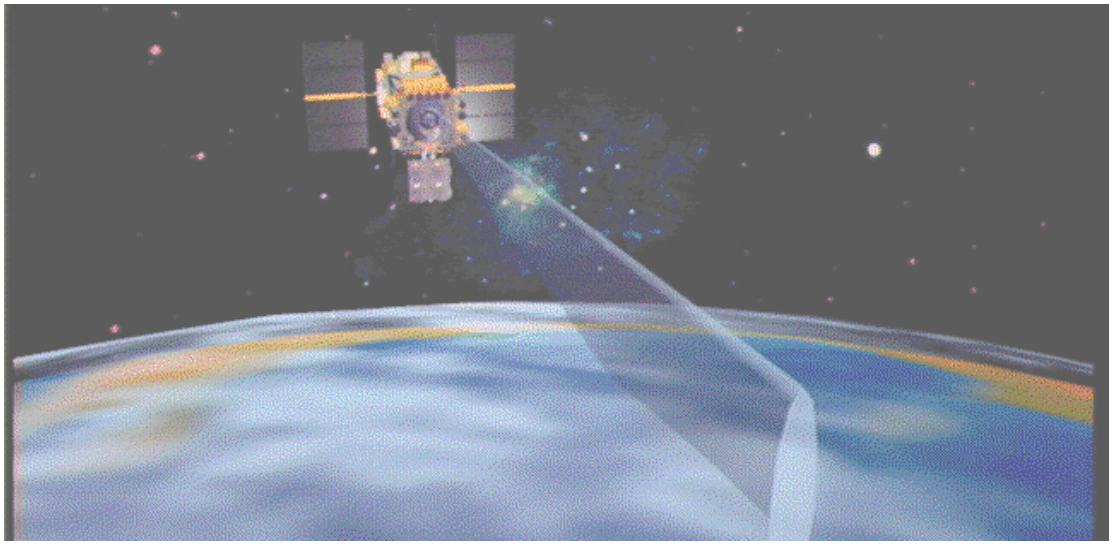

Figure 4.4-13. MSX spacecraft with the SBV sensor used for tracking geosynchronous satellites.

4.4.2.3 SSN Products and Cataloging Procedures

The SCC has at its disposal two basic types of astrodynamic theories that can be applied when creating or updating a satellite's orbit: general perturbations, employing analytic techniques and a simplified force model; and special perturbations, based on numerical integration methods and a much more comprehensive force model. Both capabilities are available to perform differential correction when updating orbital element data.

Historically, the faster, though less accurate, general perturbation technique has been used for maintaining the orbits of the vast majority of satellites. However, increased computer capabilities in recent years have led to a growing use of special perturbation orbit determinations; *e.g.*, when calculating satellite conjunctions for the purpose of collision avoidance. Another use of special perturbations occurs when large objects are within two weeks of their projected natural reentry into the atmosphere. Data made available to the general public via the DoD Space-Track website (www.space-track.org) are in the form of general perturbation mean element sets rather than the more precise osculating orbital parameters. An explanation of the format of mean elements sets is provided in Table 4.4-2.

A principal publication of the SCC is the U.S. Satellite Catalog (USSC), which is an historical record of all man-made objects placed into or created in Earth orbit since 1957. Each object is given a sequential number normally based upon the date of its entry into the catalog. Below is the entry for the first element of ISS:

Interanational Designator	Satellite Number	Common Name	Owner	Launch Date	Launch Site	Decay Date	Period (minutes)	Inclination (degrees)	Apogee (km)	Perigee (km)	Admin Character	Radar Cross-Section (m2)	Observing Radar
1998-067A	25544	ISS (ZARYA)	ISS	20-Nov-98	TTMTR		91.34	51.64	349	331		529.38	FYL

If the object is still in Earth orbit, the orbital parameters will represent those of the object at the time the catalog was published. If the object has decayed, the orbital parameters will reflect the last orbit recorded prior to reentry. For objects which are beyond Earth orbit or for which no data are available, a descriptive text will appear in the columns reserved for the orbital

parameters, *e.g.*, "Mars Orbit" or "No Elements Available." A version of the USSC, called the Satellite Situation Report, is available via the DoD Space-Track website.

The SSC also produces a summary of all cataloged objects which are still in orbit about the Earth or elsewhere in the solar system or which have reentered the Earth's atmosphere or "landed" on bodies such as the Moon, Mars, or Venus. This summary is called a Box Score and is indexed by the nation or organization that is responsible for the object. The Box Score can be found on the Space-Track website. A very simplified version of the Box Score is included in each issue of NASA's *Orbital Debris Quarterly News* (www.orbitaldebris.jsc.nasa.gov).

Table 4.4-2. Explanation of Two-Line Element Set (TLE) Format.

Example TLE for ISS (ZARYA)

```
1 25544U 98067A   04236.56031392  .00020137  00000-0  16538-3 0  5135
2 25544  51.6335 341.7760 0007976 126.2523 325.9359 15.70406856328903
```

```
1234567890123456789012345678901234567890123456789012345678901234567890
(reference column numbering)
```

Line 1		
Columns	**Example**	**Description**
1	1	Line Number
3-7	25544	Object Identification Number Search by object ID
8	U	Elset Classification
10-17	98067A	International Designator Search by International Designator
19-32	04236.56031392	Element Set Epoch
34-43	.00020137	1st Derivative of the Mean Motion with respect to Time
45-52	00000-0	2nd Derivative of the Mean Motion with respect to Time (decimal point assumed)
54-61	16538-3	B* Drag Term
63	0	Element Set Type
65-68	513	Element Number
69	5	Checksum
Line 2		
Columns	**Example**	**Description**
1	2	Line Number
3-7	25544	Object Identification Number
9-16	51.6335	Orbit Inclination (degrees)
18-25	344.7760	Right Ascension of Ascending Node (degrees)
27-33	0007976	Eccentricity (decimal point assumed)
35-42	126.2523	Argument of Perigee (degrees)
44-51	325.9359	Mean Anomaly (degrees)
53-63	15.70406856	Mean Motion (revolutions/day)
64-68	32890	Revolution Number at Epoch
69	3	Checksum

International Designator: `98067A`

This is another format for identifying an object.

- The first two characters designate the launch year of the object.
- The next three characters indicate the launch number, starting from the beginning of the year.
  This particular launch was the 67th launch of 1998.
- The remainder of the field (one to three characters) indicates the piece of the launch. Piece 'A' is usually the payload.

Element Set Epoch: `04236.56031392`

- The first two digits ('04') indicate the year. Add 1900 for years >= 57, and 2000 for all others.
- The remainder of the field ('236.56031392') is the decimal day of the year.

Checksum

The checksum is the sum of all of the character in the data line, modulo 10. In this formula, the following non-numeric characters are assigned the indicated values:

- Blanks, periods, letters, '+' signs -> 0
- '-' signs -> 1

Individual SSN sensors are normally tasked each day to track a tailored set of satellites, taking advantage of each sensor's location and capabilities. If the sensor can correlate the observations with a cataloged satellite, the observations are tagged accordingly and are sent to Cheyenne Mountain. If the observations cannot be associated with a known object, the observations are sent as uncorrelated targets (UCTs). Sometimes these UCTs can be correlated automatically with cataloged objects in Cheyenne Mountain, since the SCC database might have more accurate or more recent orbital data than the sensor. If no correlation is possible, the observations are retained as UCTs and can be compared with other UCTs at a later date by SCC analysts. See Figure 4.4-14 below.

If a new object is discovered by the SSN (*e.g.*, insulation material that has separated from a spacecraft), the observations of that object are collected and correlated, a two-line element set is developed, and a provisional satellite number between 80,000 and 90,000 is assigned. Unlike official satellite numbers, these 8X,XXX satellite numbers are assigned on a temporary basis until the object is cataloged, decays, or becomes lost. TLEs for the new object are sent to SSN sensors for follow-up observations.

Before an object can be officially cataloged and assigned a permanent satellite number, the object must be well-tracked, normally by multiple SSN sensors, and its launch of origin must be determined. The former requirement is usually determined quickly, but the latter requirement dictates a human assessment, which can occur rapidly, *e.g.*, in the case of an object thrown overboard from ISS, or can take weeks, months, or years, if determining the parent of the object is difficult. Once the object has been cataloged, the 8X,XXX provisional number can be reused for another newly discovered object. During the past several years, the size of the provisional satellite catalog has grown and now can typically include 3,000 objects or more.

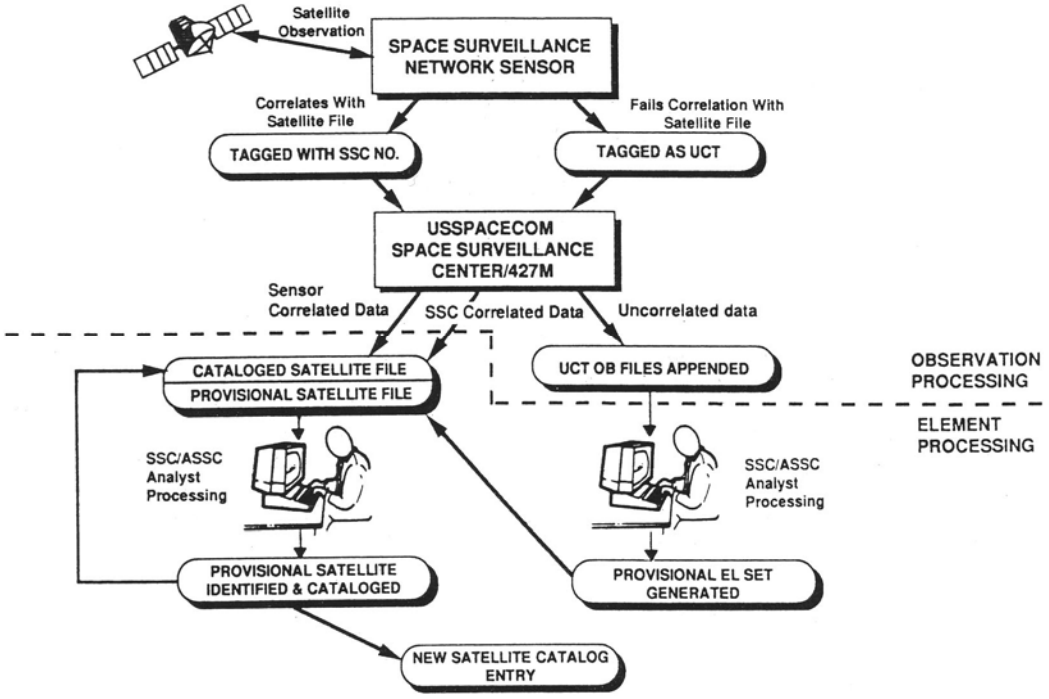

Figure 4.4-14. Catalog Process.

This figure illustrates the tracking and catalog maintenance process in 1992. Although the organization names and computer systems have changed, the overall process remains the same.

Another important function of the SSN is to monitor the orbital decay of satellites and to predict when and where they will reenter the atmosphere. This process is called Tracking and Impact Prediction (TIP), sometimes referred to as Reentry Assessment (RA). The TIP process typically begins two weeks before the expected reentry date. The SCC normally increases sensor tasking on the object because the orbit can change significantly between sensor tracking opportunities.

Official TIP messages, including the time and location of reentry at a reference altitude of 10 km, are issued at the following times prior to reentry: 96 hours, 72 hours, 48 hours, 24 hours, 12 hours, 6 hours, and 2 hours. However, due to several inherent uncertainties, including atmospheric density and stability of the object, the accuracies of these predictions are less than desired and can lead to significant errors in the predicted location of the nominal impact location. A final, post-event assessment is issued a few hours after reentry.

4.4.2.4 The SSN and Debris Detection

The major sources of orbital debris, other than derelict spacecraft and rocket bodies, are mission-related debris and fragmentation debris. During the past 25 years, approximately 15% of all cataloged objects in Earth orbit have fallen into the category of mission-related debris (see Figure 4.2-1 and Table 4.2-1). Since the turn of the century, the absolute number of mission-related debris in Earth orbit has declined due to increasing adoption of mitigation measures and design modifications. Mission-related debris includes the release of payload attachment devices,

sensor covers, explosive bolt fragments, and straps and wires. Such objects are often seen immediately after launch or release and are cataloged quickly. Historically, some small debris have evaded, and will continue to evade, detection until more capable SSN sensors have become operational, or until perturbations in the debris orbits make them easier to detect. These effects can result in cataloging delays of months, years, or more.

The release of debris from space stations has been a common occurrence for more than 30 years. The generation of debris onboard a space station is a natural consequence, but its accumulation can present a direct or indirect hazard to the crew as well as result in reduced productivity. Although it is normally preferable to dispose of debris via a logistics vehicle, the size of the debris could prevent its transfer to another vehicle or the nature of the debris could pose a health hazard to the space station crew. Hence, the jettison of debris into space, in special cases, can be the most viable option.

During 3 months of human operations with the Soviet Salyut 4 space station in 1975 more than a dozen debris from the orbital complex were detected and cataloged by the SSN. Salyut 6, the first long-duration Soviet space station, housed crews for 4 years and in the process produced more than 100 new debris, whereas its successor, Salyut 7, was responsible for twice as many debris in a similar time interval. The Mir space station, which supported crews over a span of 14 years, created more than 300 cataloged debris, but its rate of release was significantly lower than its predecessor's rate. By contrast, the amount of cataloged debris released from ISS has been considerably less: only three dozen in more than 7 years of operations.

Debris can be generated either deliberately or accidentally. Salyuts 6 and 7 and Mir possessed a special airlock that could be used for conducting experiments, launching small satellites, or ejecting debris into space. Even with Progress resupply vehicles almost constantly docked with Salyuts 6 and 7; refuse removal via the small airlock was not uncommon. However, dumping debris through the airlock appeared to be practiced less in the latter years of operations with the Mir space station.

During spacewalks, debris, both small and large, are often thrown off the station for convenience, although sometimes tools unintentionally slip away. Such was the case in December 1998 when a slidewire carrier and a worksite interface were lost by the STS-88 crew while conducting an extravehicular activity (EVA) for ISS. These objects were large enough to be tracked by the SSN and were cataloged (U.S. satellite numbers 25564 and 25565). Three other objects were also released by STS-88 spacewalkers, one inadvertently (an insulation blanket), and two by design (antenna spools), although only the former was officially cataloged.

The sizes of debris released from space stations vary dramatically from small, untrackable debris (normally less than 5 cm in diameter with today's SSN) to the 10 m diameter KRT-10 antenna, which had to be kicked off the rear of Salyut 6 by a crewmember when it failed to eject automatically. Several untrackable pieces of debris are known to have come off ISS, such as a small object in June 2003.

As of October 2006, 39 debris arising from ISS operations had been officially cataloged since the launch of the first station element in November 1998 (see Table 4.4-3). Typically, debris experience rapid orbital decay and reenter the atmosphere within about one month. However, some objects have taken more than 100 days to fall back to Earth.

Table 4.4-3. Cataloged Debris from the ISS (Nov 1998 – Oct 2006).

Int. Desig.	Sat. No.	Common Name	Parent Launch Date	Release Date	Decay Date	Orbital Lifetime (days)	RCS (m2)	RCS Source
1998-067C	25570	ISS DEB	20-Nov-98	7-Dec-98	14-Dec-98	7	0.1446	EGL
1998-067D	25846	ISS DEB	20-Nov-98	29-May-99	18-Aug-99	81	0.0837	EGL
1998-067E	26572	ISS DEB	20-Nov-98	18-Oct-00	1-Nov-00	14	0.0352	EGL
1998-067F	26943	ISS DEB	20-Nov-98	8-Oct-01	10-Oct-01	2	0.4448	EGL
1998-067G	26944	ISS DEB	20-Nov-98	8-Oct-01	18-Oct-01	10	0.0555	EGL
1998-067H	26945	ISS DEB	20-Nov-98	8-Oct-01	19-Oct-01	11	0.0398	EGL
1998-067J	26946	ISS DEB	20-Nov-98	8-Oct-01	17-Oct-01	9	0.1222	EGL
1998-067K	26950	ISS DEB	20-Nov-98	8-Oct-01	12-Oct-01	4		
1998-067L	26951	ISS DEB	20-Nov-98	15-Oct-01	26-Oct-01	11	0.0125	EGL
1998-067M	26952	ISS DEB	20-Nov-98	15-Oct-01	26-Oct-01	11	0.0046	EGL
1998-067N	27166	ISS DEB	20-Nov-98	14-Jan-02	16-Jan-02	2	0.2732	SHY
1998-067P	27167	ISS DEB	20-Nov-98	14-Jan-02	26-Feb-02	43	0.1023	SHY
1998-067Q	27328	ISS DEB	20-Nov-98	25-Jan-02	6-Feb-02	12	0.0091	SHY
1998-067R	27505	ISS DEB	20-Nov-98	23-Aug-02	4-Sep-02	12	0.0106	CAV
1998-067S	27506	ISS DEB	20-Nov-98	23-Aug-02	3-Sep-02	11	0.0019	CAV
1998-067T	27507	ISS DEB	20-Nov-98	23-Aug-02	4-Sep-02	12	0.0111	CAV
1998-067U	27521	ISS DEB	20-Nov-98	23-Aug-02	11-Sep-02	19	0.076	EGL
1998-067V	27522	ISS DEB	20-Nov-98	23-Aug-02	11-Sep-02	19	0.0319	EGL
1998-067W	27523	ISS DEB	20-Nov-98	23-Aug-02	12-Sep-02	20	0.0452	EGL
1998-067X	27524	ISS DEB	20-Nov-98	23-Aug-02	12-Sep-02	20	0.016	EGL
1998-067Y	27539	ISS DEB	20-Nov-98	23-Aug-02	26-Oct-02	64	0.0024	CAV
1998-067Z	28408	ISS DEB	20-Nov-98	3-Sep-04	12-Oct-04	39	0.058	SHY
1998-067AA	28409	ISS DEB	20-Nov-98	3-Sep-04	12-Oct-04	39	0.1303	SHY
1998-067AB	28410	ISS DEB	20-Nov-98	3-Sep-04	14-Oct-04	41	0.1501	CAV
1998-067AC	28411	ISS DEB	20-Nov-98	3-Sep-04	3-Oct-04	30	0.1382	EGL
1998-067AD	28412	ISS DEB (PIG)	20-Nov-98	3-Sep-04	25-Jan-05	144	0.6365	COD
1998-067AE	28386	ISS DEB	20-Nov-98	3-Sep-04	5-Oct-04	32	0.0919	SHY
1998-067AF	28635	ISS DEB	20-Nov-98	28-Mar-05	10-Apr-05	13	0.8027	COD
1998-067AG	28792	ISS DEB	20-Nov-98	18-Aug-05	24-Aug-05	6	0.3523	SHY
1998-067AH	29191	ISS DEB (FOOT RESTRAINT)	20-Nov-98	1-Jun-06		137	0.0766	EGL
1998-067AJ	29257	ISS DEB (TPS REPAIR TOOL)	20-Nov-98	12-Jul-06	29-Sep-06	79	0.0540	FYL
1998-069D	25564	STS 88 DEB (WIRE CARRIER)	4-Dec-98	7-Dec-98	8-Apr-99	122	0.0972	EGL
1998-069E	25565	STS 88 DEB (SOCKET)	4-Dec-98	7-Dec-98	24-Mar-99	107	0.0184	EGL
2000-053B	26492	STS 106 DEB	8-Sep-00	11-Sep-00	20-Sep-00	9	0.045	EGL
2000-053C	26493	STS 106 DEB	8-Sep-00	11-Sep-00	25-Sep-00	14	0.01	FYL
2000-078B	28896	FPP	1-Dec-00	7-Nov-05	25-Feb-06	110	0.3444	SHY
2001-010B	26723	STS 102 DEB (PAD)	8-Mar-01	12-Mar-01	7-Jun-01	87	0.1046	EGL
2005-035C	28933	SUITSAT	8-Sep-05	3-Feb-06	7-Sep-06	216	0.5269	CAV
2005-035D	28934	SUITSAT DEB	8-Sep-05	6-Feb-06	20-Mar-06	42	0.0057	SHY
					Total Object days	**1661**		
					Total Object years	**4.55**		
Total: 39 Debris								
* Does not include TNS-0 spacecraft released from ISS on 28 March 2005 (lifetime = 155 days)								
* Does not include Kolibri spacecraft released from Progress M1-7 after separation from ISS								
Red indicates object is still in orbit as of report date								

Most EVAs do not involve the jettison of large objects from ISS, but they often result in small objects being cast off. During an EVA performed by the ISS Expedition 10 crew on 26 January 2005, a total of 20 objects were released: 16 electrical caps and 4 covers. These items ranged in mass from 25 to 50 grams each and in size from 6 to 7 cm. None were tracked and cataloged by the SSN, and all probably reentered rapidly.

By far the greatest source of debris in Earth orbit has been the often violent break-up of spacecraft and rocket bodies. In January 2007, the Chinese intercepted the Fengyun 1C spacecraft with an ASAT weapon which created the single worst debris event in history. Prior to that event, explosions from faulty propulsion systems were by far the most prevalent source of break-up debris. In fact, the vast majority of these propellant- or pressurant-induced break-ups occur after a spacecraft or launch vehicle orbital stage has successfully completed its mission.

In terms of official debris, the explosion of a Pegasus HAPS orbital stage in June 1996 is the worst explosion on record creating more than 700 cataloged debris pieces. (Some more prolific break-ups have occurred in very low altitude orbits, but the majority of the debris reenter the atmosphere before they could be cataloged.) A severe fragmentation poses considerable challenges to the SSN, including spatial resolution and sheer numbers of UCTs. Immediately after the fragmentation many debris will be close to other debris or the parent object. Hence, discriminating between discrete objects might take days, as the debris gradually separate. Secondly, the SCC will be flooded with UCTs, some of which will be tagged incorrectly with the parent object. Often, considerable work is required by SCC analysts to sort through the large number of UCTs to determine which UCTs are associated with a single piece of debris. Then, a preliminary TLE can be constructed and an 8X,XXX number can be assigned for follow-up tracking.

Once TLEs are developed for individual debris, the SCC and the ASCC can determine when and where the fragmentation occurred, using internally developed software. Next, using conjunction assessment methods, analysts can determine if any other tracked object was in the vicinity of the fragmented object at the time of the event. Three accidental collisions in space (one each in 1991, 1996, and 2005) have been identified using this technique. Perturbations in the orbit of the other satellite near the time of the breakup can verify that a collision indeed occurred.

Finally, the TLEs can be used by the NASA Orbital Debris Program Office to define the nature of the fragmentation and the resultant debris; *e.g.*, by determining the ejection velocities and ballistic coefficients of each of the debris. In turn, this information might shed light on the cause of the breakup and can be used to refine NASA fragmentation models.

4.4.2.5 Future Outlook

The SSN continues to evolve in both sensors and data processing capabilities. The addition of the Globus II X-band radar in 2001 and the return of the Cobra Dane radar to the SSN in 2003 at full power and continuous operations significantly improved the capabilities of the SSN in the high and low altitude regimes, respectively. Likewise, the recent upgrading of the GEODSS system with charged-couple devices (CCDs) has greatly increased high altitude detection and tracking.

The FPS-85 radar at Eglin AFB in Florida, operating since 1969, is scheduled to undergo a service life-extension program by 2010 to permit it to continue operations until 2025. Improvements to other existing phased-array radars are also possible. The X-band Haystack dish radar will be upgraded and a new W-band capability will be added to it.

On the other hand, the Antigua C-band radar was removed from the SSN in 2001 and budgetary pressure could force additional closures in the coming years. The USAF Fence, transferred from the USN in 2004 after 43 years of operations, will possibly be closed during 2007. A new, S-band fence, originally slated for initial operations by 2008-2009, is no longer funded, and a new design, if adopted, is unlikely to be fielded until after 2010.

In August, 2007 the SCC moved from Cheyenne Mountain to Vandenberg AFB, California, where it was integrated with the new Joint Space Operations Center. After this transfer has been completed, the ASCC at Dahlgren, Virginia, is scheduled to be deactivated.

The future of the SSN rests in part on the plan to deploy a SBSS system in Earth orbit. Considered since the 1970s under a wide variety of project names, an SBSS system using visible light sensors has the potential for dramatically improving the SSN in both observation opportunities and sensitivity. The current plan is to field a LEO pathfinder mission, called Block 10, in late 2008 or 2009 and to follow it with a preliminary SBSS constellation of four Block 20 spacecraft sometime after 2010. This “all-weather” system will be able to monitor all Earth orbital altitude regimes.

Figure 4.4-15. 2006 concept of an SBSS spacecraft.

The overall objectives for improving the SSN include greater detection sensitivity and more rapid event discovery. The general sensitivity of the SSN in LEO is 10 cm, with some capability down to 5 cm for objects at low altitudes and high inclinations. Since current shielding technology is limited in practical terms to objects of 1 cm diameter or less, the ability to detect and to track objects as small as 1 cm would help close the gap between the risk mitigation strategies of collision avoidance and shielding. However, the number of objects of 1-10 cm is approximately an order of magnitude greater than the population of objects greater than 10 cm, which are currently in the USSC. Consequently, any increase in detection sensitivity must be accompanied with significant improvements in data processing.

The prompt detection of satellite fragmentations will also contribute to the evaluation of collision risks to operational spacecraft, especially activities associated with human space flight, and, if

necessary, to the implementation of countermeasures. In practice, such breakups should be identified by the SSN within one hour of their occurrence.

4.4.3 Radar Measurements

4.4.3.1 History

In the early 1980s, NASA proposed building a large, permanently-crewed space station, which was approved by President Reagan in his 1984 State of the Union address and later designated as Space Station Freedom (SSF). In July of 1984, NASA published the "Orbital Debris Environment for Space Station" [Kessler 1984]. Played against SSF requirements for probability-of-no-penetration, this model indicated that the SSF should be shielded to protect against debris about 1 cm in diameter. At that time, no measurements were available for debris between about 100 microns and 10 cm, so the environment model used information from ground fragmentation tests and interpolated between the two measured values. This resulted in an estimated 300% uncertainty in the modeled 1 cm population.

Protecting the SSF against the high end of the debris uncertainty estimate would have added significant additional weight and volume of shielding. A measurement of the 1 cm orbital debris population at SSF altitudes was needed prior to the SSF Critical Design Review (CDR) scheduled for 1991. Several different options were considered including ground- and space-based optical systems and ground- and space-based radars. The University of Texas proposed a system of two 8 m f/4.3 Cassegrain telescopes located 100 m apart that was estimated to cost ~$100 million [Portree and Loftus 1993]. The Jet Propulsion Laboratory (JPL) proposed Quicksat, utilizing twin 25 cm f/1.0 telescopes on an orbiting platform, also estimated in the $100 million range [Kessler 1988].

NASA settled on the concept of a ground based radar. It was recognized that part of what limited the SSN radars to objects larger than 10 cm was that the SSN radars operated at long wavelengths of 70 cm. A 1 cm object was very far into the Rayleigh scattering regime at these wavelengths. The original concept for the NASA radar was for a simple, non-steerable radar located near the equator that pointed vertically and counted orbital debris passing through its field-of-view. A monopulse feed could be used to estimate the location of the debris in the beam and the path through the beam. It was quickly realized that the best way to calibrate the radar was to track on-orbit calibration spheres, so the radar did need some tracking capability although the radar would "stare" at a fixed pointing direction during debris data collection. The concept was designated the Debris Environment Characterization Radar (DECR) and was approved by the NASA Administrator in July 1987.

Two notable precursor experiments were performed. JPL performed an experiment using the Arecibo radar located in Puerto Rico, which demonstrated that high-power, short-wavelength radars can detect orbital debris with sizes less than a centimeter [Thompson *et al.* 1992]. Ninety objects larger than 5 mm were detected in the main-beam of the radar between 500- and 1000-km altitude in 18.8 hours of data collection during June and July 1989. The NASA Johnson Space Center (JSC) performed an experiment using the ALCOR (ARPA-Lincoln C-band Observables Radar) radar in Kwajalein, which provided experience with open-loop monopulse data [Stansbery 1990].

Figure 4.4-16. Arecibo and ALCOR antennas.

Arecibo 305 m diameter antenna (left). The experiment was conducted at S-band in a bistatic mode with a second 30 m dish located about 11 km away. ALCOR C-band antenna dome (right). This radar had a similar field-of-view compared to the proposed DECR.

In an unrelated effort, the MIT/LL collected debris data from its Haystack Long Range Imaging Radar (LRIR) for the USAF in a similar time frame [Kupiec 1988]. This experiment detected 11 objects in just one hour, most between 850-1000 km.

JPL released a Request for Proposal (RFP) for DECR in January 1989. Shortly after the release of the RFP, MIT/LL and the USAF proposed that NASA use the money earmarked for DECR to build the HAX. Haystack was primarily used by the USAF for range-Doppler imaging of orbiting satellites. However, the Haystack antenna shared time with the radio astronomy community and the imaging capability was only intermittently available. MIT/LL proposed HAX, which would have less sensitivity than Haystack, but higher imaging resolution and would be available full time. In return, the USAF would provide debris data from Haystack and HAX. The USAF-MIT/LL proposal was attractive to NASA for several reasons, but primarily from a schedule point of view. The schedule to procure and operate DECR to collect enough statistical debris data to meet the SSF CDR was very tight and had virtually no room for schedule slips. NASA agreed to the Haystack/HAX proposal in September 1989 and cancelled the DECR procurement.

Haystack began successfully collecting statistical orbital debris data in October 1990 [Stansbery 1991] and has been NASA's primary source of statistical data on the 1 cm size debris population since that time. HAX became operational in 1993 and collected debris data for the first time in March 1994 [Settecerri 1997].

NASA has supplemented the Haystack/HAX data with data from other radars as well. Dr. Richard Goldstein of JPL, who was involved in the Arecibo test, remained interested in the orbital debris issue and began running experiments with the more sensitive Goldstone radar. This radar played a key role in identifying the NaK debris from the RORSATs. As mentioned previously, Goldstone has limitations and is available for debris measurement for only a few hours each year.

In 1996, ESA conducted debris measurements utilizing the German Research Establishment for Applied Science Tracking and Imaging Radar (FGAN/TIRA) system and the Max Planck Institute for Radio Astronomy (MPIfR/Effelsberg) radio telescope in a bistatic staring mode.

The IADC Working Group 1, assigned to measurements, decided to expand the ESA concept into a coordinated international campaign of duration of ~24 near contiguous hours. Similar campaigns are now conducted by the IADC on a biannual schedule. In addition to Haystack and HAX, the U.S. has utilized the Cobra Dane radar in Alaska and the TRADEX radar in Kwajalein for some of these campaigns. In addition to FGAN/TIRA, ESA has used the European Incoherent Scatter Scientific Association (EISCAT) radar in Norway [IADC 2006].

4.4.3.2 Size Estimation Model

A separate study was done by XonTech, Inc. [Everett 1991(1), Everett 1991(2), Dalquist 1991, and Bohannon 1994] to develop a SEM to relate RCS to physical size. "Representative" debris objects were selected from two HVIs of simulated satellites conducted at the Arnold Engineering Development Center by the DoD (Figure 4.4-17). Some artificial, debris-like objects were also included in the sample to better represent the postulated orbital debris environment. This included a printed circuit board and a piece of SRM Al_2O_3 slag.

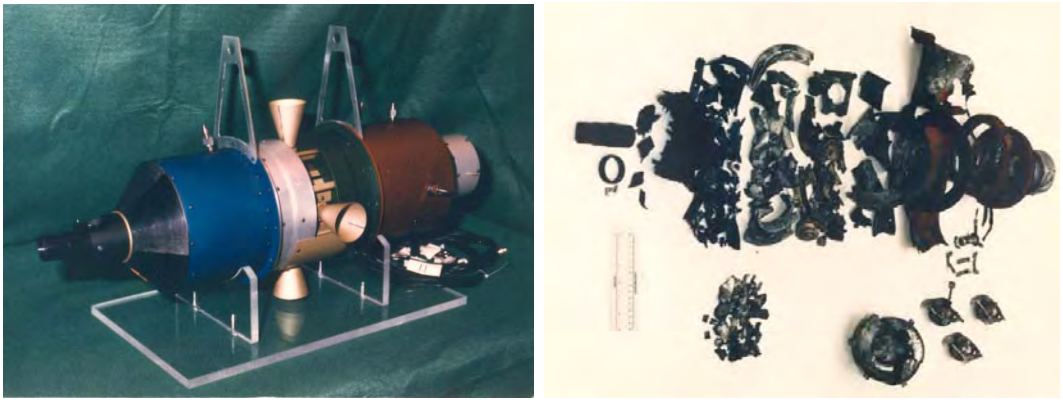

Figure 4.4-17. Simulated Target

The simulated target (left) was impacted by a 1 cm aluminum sphere traveling at 7 km/sec, the pieces for the SEM (right) were taken primarily from this test.

The RCS values of these 39 debris objects were measured at a controlled RCS radar range operated by the System Planning Corporation (Figure 4.4-18). The RCSs of these objects were measured over 4 radar frequency bands (2.5647-3.9111 GHz, 4.116-7.986 GHz, 8.1544-12.7684 GHz, and 12.924-17.538 GHz) with 8 steps in the band of the lowest frequency and 16 steps in the band for the other three, and with hundreds of source-object orientations. These frequencies, S-, C-, X-, and Ku-band, respectively, were chosen since they represent radar frequencies often used for orbital debris observations.

Consistent with the Maxwell's equations of electromagnetics, radar data from different wavelengths can be compared by normalizing the size by the wavelength of the measuring frequency and the RCS by the wavelength squared. This results in a size parameter $x = size/wavelength$ and a RCS parameter $z = RCS/wavelength^2$. No divergences from the scaling law invariances were observed from the analysis of the radar data by XonTech, but this may be a consequence of the limited size range chosen for the 39 pieces.

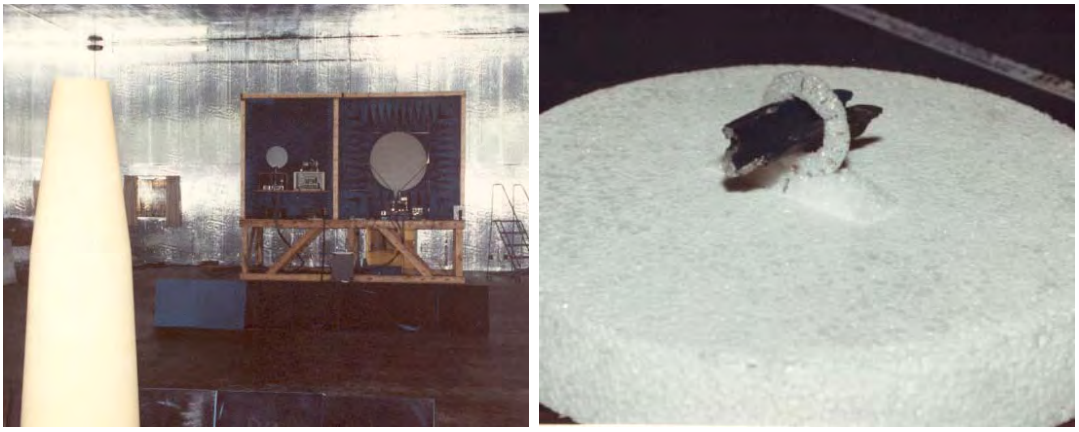

Figure 4.4-18. The indoor RCS range at SPC.

A computer controlled, rotating foam column is in the left foreground. Representative cradle used to rotate the debris along its second axis (right).

Figure 4.4-19 shows the relationship between the measured RCS parameter and the object's physical size parameter. Each of the 2072 points on this plot is a weighted average for a single object over hundreds of different orientations at a single frequency. The data was weighted to account for nonuniform sampling of the object orientations as the data was collected.

The physical size parameter, or characteristic length of an object, is defined as the average of the largest dimensions for an object measured along three orthogonal axes. The first axis was chosen to coincide with the largest dimension, the second axis to coincide with the largest dimension in a plane orthogonal to the first axis, and the third axis to be orthogonal to the first two axes. The characteristic length is referred to here as simply the size or diameter of the object.

From this plot a scaling curve (smooth solid line) was developed that represents the mean of the measured RCS for each size/wavelength. For debris sizes much smaller or larger than the radar wavelength, the scaling curve approaches the Rayleigh or optics region curves, as expected. Between the Rayleigh and optics region curves is the Mie resonance region that results in an enhanced RCS measurement on average for a given size. In the resonance region, the scaling curve deviates from the optical curve (not shown) such that, for a given RCS, the object is smaller in characteristic length than through an interpretation based on an optical approximation. The scaling curve may be expressed as:

$$x = \sqrt{\frac{4z}{\pi}} \text{ , for } z>5, \text{ Optical Regime}$$

$$x = \sqrt[6]{\frac{4z}{9\pi^5}} \text{ , for } z<0.03, \text{ Rayleigh Regime}$$

$$x = g(z) \text{ , in between, Mie Resonance Regime}$$

where $z = RCS/\lambda^2$, $x = diameter/\lambda$, and λ is wavelength. In the above equations, the quantity z is assumed to not be expressed in dB. The smooth function g(z) is expressed by 23 points in Table 4.4-4

Table 4.4-4. The NASA SEM Curve x=g(z) in the Mie Resonance Region.

$x = diameter/\lambda$	$z = RCS/\lambda^2$
0.10997	0.001220
0.11685	0.001735
0.12444	0.002468
0.13302	0.003511
0.14256	0.004993
0.15256	0.007102
0.16220	0.01010
0.17138	0.01437
0.18039	0.02044
0.18982	0.02907
0.20014	0.04135
0.21237	0.05881
0.22902	0.08365
0.25574	0.1190
0.30537	0.1692
0.42028	0.2407
0.56287	0.3424
0.71108	0.4870
0.86714	0.6927
1.0529	0.9852
1.2790	1.401
1.5661	1.993
1.8975	2.835

Note that most of the debris detected by Haystack is in the Rayleigh region, which allows size estimates that are relatively insensitive to errors in the RCS measurements.

For comparison, the oscillating RCS-to-size curve for a spherical conductor is also shown in Figure 4.4-19 . The NASA SEM is not applicable to estimate sizes of spherical conductors (such as NaK droplets) in the Mie Resonance region. The oscillations result from constructive and destructive interference of electromagnetically induced waves on the surface of the conducting sphere

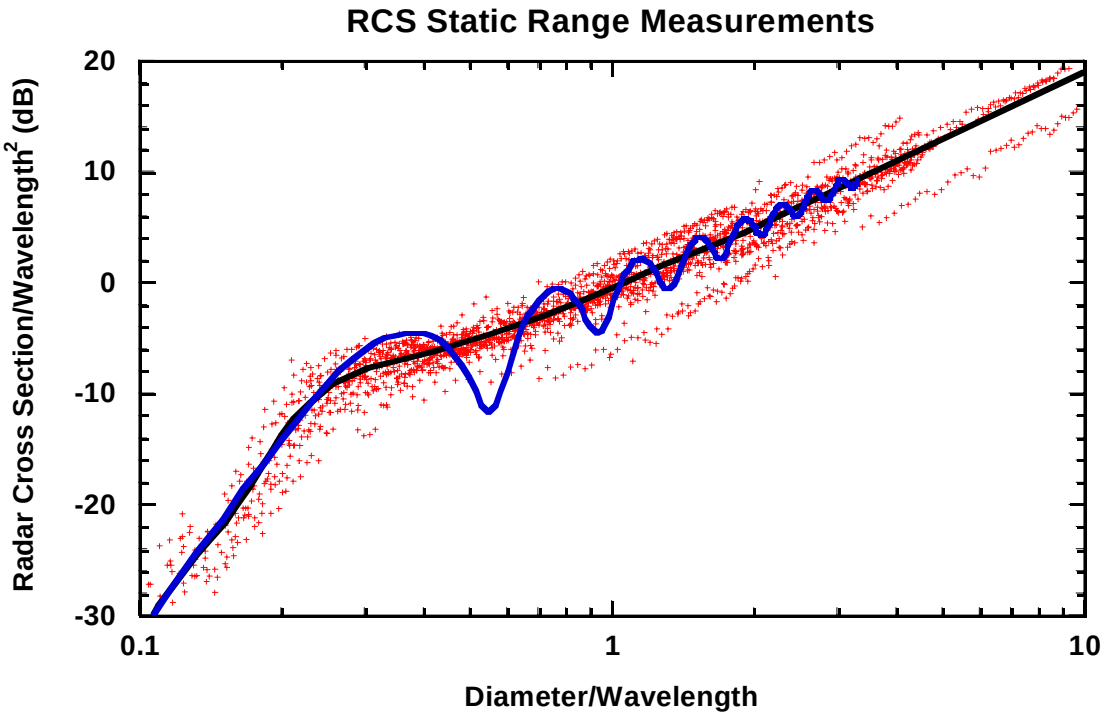

Figure 4.4-19. Results of RCS-to-Physical size measurements.

39 "representative" debris objects over the frequency range 2.0 - 18 GHz (15 - 1.67 cm wavelength). Each point represents an average RCS for a single object measured at a single frequency over many orientations. The oscillating line is the RCS for a spherical conductor while the smooth line is the polynomial fit to the data.

The size-to-RCS curve for a spherical conductor is expressed theoretically as:

$$z = \frac{1}{\pi}\left|\sum_{n=1}^{\infty}(-1)^n\left(n+\frac{1}{2}\right)(b_n - a_n)\right|^2$$

where the coefficients a_n and b_n are:

$$a_n = \frac{j_n(2\pi x)}{h_n^{(2)}(2\pi x)} \qquad b_n = \frac{2\pi x \cdot j_{n-1}(2\pi x) - n \cdot j_n(2\pi x)}{2\pi x \cdot h_{n-1}^{(2)}(2\pi x) - n \cdot h_n^{(2)}(2\pi x)}$$

where $h_n^{(2)}(x) = j_n(x) - i \cdot y_n(x)$, in which $j_n(x)$ and $y_n(x)$ are the spherical Bessel functions of the first and second kinds, respectively [Knott *et al.* 1993].

Further work has shown that the size implied by a single-valued smooth RCS-to-size curve, as seen in Figure 4.4-19, needs to be adjusted slightly. Thus, for any given size there is a distribution of RCS values that are not necessarily symmetric about a mean or median RCS value. Sometimes an object will appear to be larger than the mean value and sometimes it will appear to be smaller. The radars measure a number of similar RCS values. Of these, some will be smaller objects that appear bigger, some will be objects that appear to be the correct size, and some will be larger objects that appear to look smaller. Because the SEM is a simple model for

one-to-one, RCS-to-size mapping, it does not provide an uncertainty estimate for the derived size distribution, nor does it take into account the specific distribution of RCS values for a given size.

To improve the original NASA SEM, a Statistical Size Estimation Model (SSEM) has been developed [Xu and Stokely 2005]. The SSEM is based on the expectation maximization theorem clarified and further developed by Vardi and Lee [Vardi and Lee 1993]. The SSEM utilizes conditional probability distributions of RCS given a specific size, which were an outcome of the analysis done by XonTech on the RCS radar range measurements.

4.4.3.3 Current Status

4.4.3.3.1 NASA/U.S. Measurements

To obtain debris data down to 2 mm in diameter, NASA has been utilizing radar observations of the LEO debris environment for more than a decade from the NASA JPL Goldstone Deep Space Network radars, the MIT/LL Haystack LRIR, and the MIT/LL HAX. The Goldstone radar is located in southern California's Mojave Desert at a latitude of 35.2° and the Haystack and HAX radars are co-located in Massachusetts near Boston at a latitude of 42.6°. Unlike Goldstone, whose primary mission is to monitor deep space probes, Haystack and HAX are both extensively utilized for debris observations, typically collecting several hundred hours each year.

Both Haystack and HAX are monostatic radars that measure the range, radial velocity, the principal polarization RCS, the orthogonal polarization RCS, and the position within the radar beam using a monopulse system. The HAX radar has less sensitivity than Haystack, but has a larger beamwidth. Both radars are capable of full-sky pointing. The Goldstone radar can measure the range, radial velocity, and principal polarization RCS of debris. Currently, the Goldstone radar can only point toward the zenith for debris observations. Haystack's availability, along with its very high sensitivity, makes it the primary source of data for characterizing the small debris environment.

For debris observations, the radars statistically sample the debris populations by operating in a staring, or "beam park," mode. In this mode, the antenna is pointed at a specified elevation and azimuth and remains there while debris objects randomly pass through the field of view (FOV) of the radar beam. This operational mode provides a fixed detection area important to the measurement of the debris flux, or number of objects detected per unit area per unit time, which is the defining quantity for debris risk analysis.

Each radar is ideally suited to measure debris within a specific altitude region. The Goldstone radar generally observes objects at altitudes from 300 km to 3200 km with near-zenith pointing. Commonly, both Haystack and HAX collect data by pointing the radars east at 75° elevation. Sometimes, Haystack points south at 10° elevation or 20° elevation. With 75° east-pointing, both radars observe debris from 350 km to 1800 km. Figure 4.4-20, Figure 4.4-21, and Figure 4.4-22 show diameter versus altitude for each radar. The overlapping size regions among the radars allow a continuous measurement of debris with diameters from less than 1 cm to several meters. Moreover, the overlapping size regions allow comparisons in order to understand systematic and statistical variations in the data. Figure 4.4-23 shows cumulative debris flux versus diameter from altitude 600 km to 800 km for all three radars.

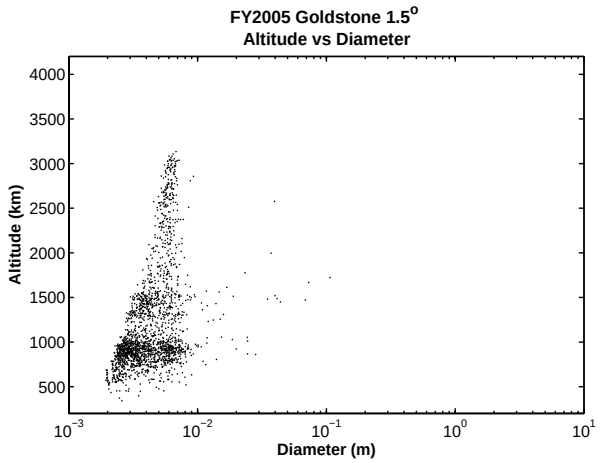

Figure 4.4-20. Altitude vs. size estimated for FY2005 Goldstone detections.

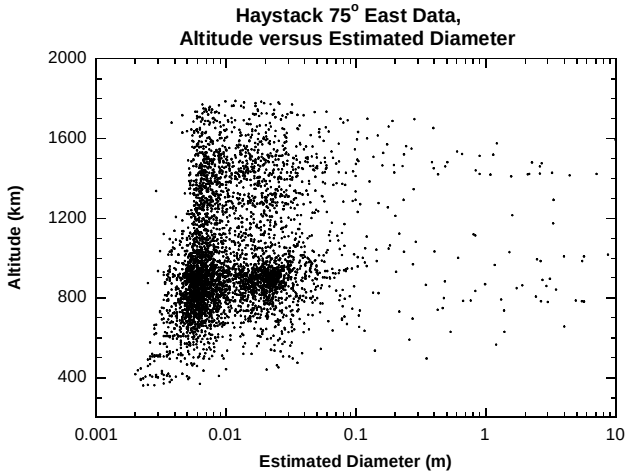

Figure 4.4-21. Altitude vs. size estimated for FY2003 Haystack detections.

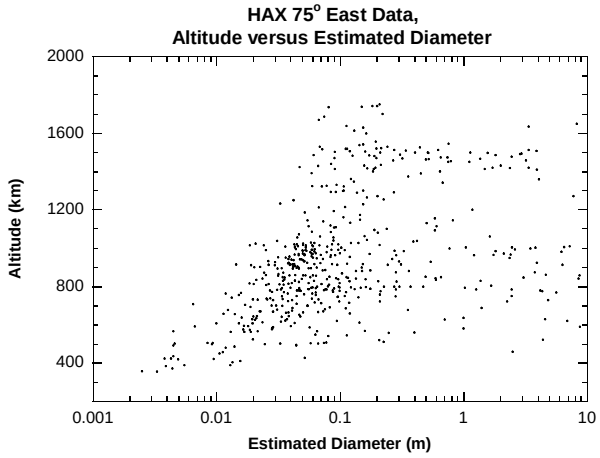

Figure 4.4-22. Altitude vs. size estimated for FY2003 HAX detections.

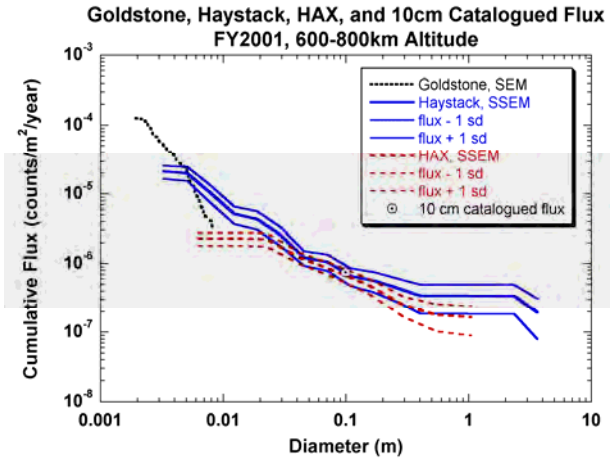

Figure 4.4-23. Cumulative Flux.

The cumulative debris flux versus diameter measured by the Goldstone radar, Haystack radar, and HAX radar. The flux of 10 cm catalogued objects is also shown for comparison.

A precise measurement of the object's orbit is sacrificed by operating the radars in a stare mode and not tracking detected debris objects. By examining the signals from the monopulse angle channels on Haystack and HAX, the path through the beam can be roughly determined and the orbital inclination may be deduced with moderate accuracy, especially for debris with large signal-to-noise ratios. The orbital inclination may also be estimated by assuming a circular orbit and using the measured radial velocity via the Doppler-shifted return signal. As seen in Figure 4.4-24 of altitude versus inclination, this method allows “families” of debris objects to be defined and studied separately [Stansbery 1997].

While it is impossible to say whether an individual detection is in a particular family because of the uncertainty in its eccentricity, the data in Figure 4.4-24 shows detections clumping into distinct families defined by limits of inclination and altitude. Extracting the data by choosing a narrow range of orbital parameters should minimize the number of “interlopers” and insures that the large majority of the extracted detections are of objects in the target family. The Goldstone radar cannot estimate an orbital inclination since it does not possess a monopulse system and because there are limitations to orbital inclination estimates from zenith pointing.

In 1995, the large population of debris between 850-km to 1000-km altitude in an inclination band centered near 65° inclination was identified as small spherical droplets of eutectic NaK coolant [Kessler 1997; Sridharan 1999]. The NaK coolant leaked from fast neutron reactors that had separated from the RORSATs at the end of their useful lifetime. Other debris families that have been examined include Cosmos 1275, Cosmos 1484, Pegasus/HAPS [Settecerri 1997 - 1] and Ops 4682, commonly referred to as SNAPSHOT [Stansbery 2006].

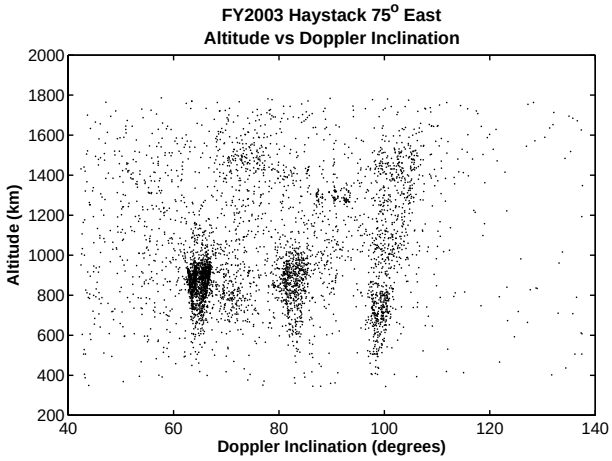

Figure 4.4-24. Altitude versus Doppler inclination for FY2003 Haystack detections.

The NASA Orbital Debris Program has conducted two independent reviews of the Haystack radar debris observations using experts on radar and statistics. The first panel of experts made recommendations regarding processing and analysis [Barton *et al.* 1992]. The second panel examined NASA's statistical treatment of the data and its use in characterizing the debris environment [Barton *et al.* 1998]. Each group commended NASA for its efforts and found NASA procedures and conclusions to be sound. In addition, NASA conducted space flight experiments in 1994 and 1995, Orbital DEbris RAdar Calibration Spheres (ODERACS) [Cress *et al.* 1996], to investigate Haystack's calibration and validate the processing at NASA JSC. In summary, the ODERACS experiments showed that the Haystack radar is calibrated within nominal limits.

The radar observations have shown that the debris environment is dynamic and can change rapidly. Therefore, continued monitoring, or at least frequent, periodic sampling of the debris environment to sizes below 1 cm should be continued.

4.4.3.3.2 Other Agencies

The Russian Space Surveillance System (SSS) employs a variety of ground-based radars and electro-optical sensors in and outside of the Russian Federation and maintains a satellite database similar to the USSC [Anisimov 2004]. Russia is the only country other than the U.S. that operates a significant SSS, although France has a limited network and ESA has proposed a network similar to the French system. However, several countries and ESA have performed experiments designed to periodically sample the debris environment.

ESA has funded the FGAN/TIRA system to conduct a number of experiments [Mehrholz 2004]. The FGAN/TIRA is an L-band (25 cm wavelength), monopulse, dish radar with a 0.5-deg beamwidth that is capable of detecting 2 cm debris at a 1000 km slant range. It was first used for debris measurements in 1996 and has been used in every IADC LEO debris campaign. For debris, it operates in a staring mode very similar to the Haystack radar. In 1996, FGAN/TIRA combined with the MPIfR/Effelsberg radio telescope to operate in a bi-static mode similar to the NASA's Goldstone radar. In this mode, the Effelsberg receiver is capable of detecting 0.9 cm

debris at 1000 km. The combined operation was repeated in the 2006 IADC campaign (Figure 4.4-25) [Leushacke 2006].

Figure 4.4-25. FGAN/TIRA radar (left) and Effelsberg radio telescope (right).

When operated together in a bi-static configuration, this system can detect orbital debris as small as 0.9 cm.

Beginning in 2000, ESA also began sponsoring the EISCAT ionospheric research radars (Figure 4.4-26), located near Tromso, Norway and on Svalbard, to measure space debris in parallel with the standard EISCAT ionospheric measurements. The Tromso radar operates at 930 MHz (32 cm wavelength) and can detect objects as small as 2 cm at a 1000km slant range. The Svalbard radar operates at 500 MHz (60 cm wavelength) and can detect 2.7 cm at the same slant range [Markkanen 2005]. Since debris data collection is a “piggy back” mission, the radar parameters and pointing are not optimized for debris. In addition, their location at high latitudes (69° and 79°N) limits the inclinations that the radars can see. Unfortunately, due to funding constraints, these measurements were suspended in 2006.

Figure 4.4-26. EISCAT radar installations in Tromso (left) and Svalbard (right)

Russia, in cooperation with the Ukraine, China, and Italy has conducted bi-static measurements using a very long baseline system comprised of the 70 m diameter Evpatoria radar (Ukraine) as the transmitter and large dishes as receivers at Bear Lakes – 64 m diameter, Russia (Figure 4.4-

27); Simeiz – 22 m, Ukraine; Noto – 32 m, Italy; and Urumqi – 25 m, China [Molotov 2005]. The instantaneous altitude coverage using widely-separated transmit and receive antennas is limited, but debris have been observed at GEO altitudes. Russia has also experimented with an ionospheric research radar in Irtusk in a similar experiment set up as EISCAT [Agapov 2006].

Figure 4.4-27. Evpatoria radar (left) located in Ukraine and the Bear Lakes facility (right) in Russia.

The French have built and tested the Grande R'eseau Adapt'e a la Veille Spatiale (GRAVES) radar. The GRAVES radar is a bi-static, continuous wave, phased-array radar operating at VHF [Michal 2005]. The transmit array is located near Dijon and the receive array is located 380 km away near Apt, France (Figure 4.4-28). The transmitter has four antenna panels, each of which covers ~45° in azimuth (180° total azimuth coverage) by scanning an 8° azimuth by 20° elevation beam across the sky in roughly 20 seconds. The receive array uses digital beam forming and tracks the satellite using the Doppler (frequency shift of the received signal) and angles-only information from the receive array. The GRAVES radar is the basis for the proposed European SSS [Donath 2005] for low altitude satellite tracking. ESA design studies have proposed a UHF system to be located in Spain, which has a slightly lower latitude than the current French system and could therefore track satellites with lower inclinations. Neither the GRAVES, nor the proposed ESA system, will detect debris smaller than 10 cm.

Figure 4.4-28. GRAVES radar.

One of four transmit panels (left) and some of the Yagi antennas comprising the receive array (right).

Japan has also conducted debris experiments with its Middle and Upper atmosphere radar. This HF radar is also a mono-static phased array radar operating at 6.4 m wavelength utilizing 475 Yagi antenna elements in a 103 m circle. This radar's primary purpose is investigating atmospheric and plasma dynamics in the troposphere to the ionosphere. The long wavelength severely limits the size of debris that is visible to it. At best, this radar can detect 20 cm debris at 500 km slant range. Japan has also recently built the Kamisaibara Space Guard Center (KSGC) radar (Figure 4.4-29). This is an S-band, phased array radar mounted on a rotating platform [Hirose 2005]. The face of the radar is set at 54° elevation, but can electronically steer from 15° to 75° elevation and +/- 45° in azimuth. The radar can only detect 1 m objects at 600 km slant range, but can track 10 objects simultaneously.

Figure 4.4-29. Japanese radars used in experiments to track space debris.

Middle and Upper atmospheric radar (left); and (right) the KSGC radar.

4.4.3.4 Potential Future Enhancement

The Haystack radar will soon be undergoing major modifications. The MIT/LL is planning to add an additional frequency band to the radar. Haystack currently operates in the 9.5 GHz- to 10.5 GHz-frequency band. As part of the upgrade, a millimeter-wave radar that operates in the 92 GHz- to 100 GHz-frequency band will be added to the system. The new radar will use an innovative transmitter design and signal processing to achieve image resolution that is about ten times better than what is currently available. The existing 37 m antenna will be replaced by a new dish, accurate to 0.1 mm over its entire surface, which is a factor of three better than at present. The upgrade program is currently in the design stage and will take at least two years to implement. In the near future, the 45 m diameter Haystack radome will be temporarily lifted and set aside to permit the removal of the existing antenna and the installation of the new antenna. The new radar transmitter and processing system will be integrated and tested with the final testing of the new radar scheduled to be completed in 2010. The smaller wavelength will dramatically increase the antenna gain from the 37 m antenna, but will conversely reduce the antenna beamwidth. Depending on the transmitter and receiver capabilities, the new system should be able to detect objects smaller than the current Haystack limit of about 5 mm at low altitudes. In addition, the X-band system will still be available.

Upgrades are also underway at the Goldstone radar. The Goldstone radar is currently being upgraded to allow pointing away from the zenith during debris observations. With this capability, estimates can be made of orbit inclinations for debris detections.

4.4.4 Optical Measurements

4.4.4.1 Role in Debris Detection

Optical sensors, which typically have been employed for detection and tracking of high altitude "deep space" satellites, are becoming viable and cost-effective, low-altitude orbital debris hunters. In the 1990s, the three-site global network of 1.0 m class GEODSS telescopes demonstrated the ability to probe for debris not only at GEO, but at LEO and medium Earth orbit (MEO), as well. Optical observations also provide a complementary and independent set of statistics that can be correlated with the radar observations and can yield a more complete picture of the debris population. This is especially important because some objects have large optical cross-sections but very small RCSs, and vice versa. One advantage to using optical measurements is that the telescope can more easily detect debris objects in higher altitudes due to the $1/r^4$ fall off in received radar signal with altitude.

Most optical measurements are taken in survey mode where objects are detected as they go through the FOV of the telescope. By using this method, large sections of the sky can be examined in one night. In addition, objects are in the FOV for a short time and thus, only a small part of the object's orbit is detected. Therefore, a circular orbit assumption is usually made when calculating the orbital parameters of objects detected in survey mode.

By comparing observations to the SSN Catalog, it can be determined which objects might be classified as debris. A detected object that is found to match an object in the optical measurements section of the catalog will be called a correlated target (CT), while an object that can not be found in the catalogue will be termed a UCT.

4.4.4.2 History

4.4.4.2.1 Phillips Lab at the USAF Maui Optical and Supercomputing Site and MIT/LL Electronic Telescope Site at Socorro, New Mexico

Beginning in 1988, the DOD sponsored an optical measurements program using facilities located at the Phillips Laboratory USAF Maui Optical Station (PL/AMOS) and the MIT/LL Electronic Telescope Site in Socorro, New Mexico. In this program, the focus was to estimate the debris population and the development of observational techniques to allow orbital determination of uncorrelated debris. These observations provided the first direct measurements of the orbital elements of small UCT debris and exposed significant differences between the orbital distribution of the total space population and the catalog at that time. Hundreds of hours of data were collected and analyzed to derive a population estimate. Results indicated that there were approximately 20,000 objects larger than 5 cm in 1991, a result that was consistent with the Haystack results in the same size regime in 1995.

Among numerous parallel efforts, an attempt was made to differentiate and characterize optical and radar signatures by launching calibration objects to be observed by each sensor system. The ODERACS were a series of diffuse and specular spheres, of varying size and mass, launched on

STS-60 (1993) and STS-63 (1995) and then tracked and detected by various radar and optical assets. Optical observations [Cress *et al.* 1996] of the ODERACS 4-inch and 6-inch spheres were carried out with variety of optical sensors. The sensors were very useful for verifying the optical observational techniques and data analysis of orbital debris. Prior knowledge of the albedo and geometry of the object allowed the determination of size based only on the astronomical photometric instrumentation and techniques. An analysis of the CCD image of the ODERACS 4-inch diffuse sphere by the CCD Debris Telescope (CDT) Hawaii yielded a 3.93±0.24 inch measurement [Cress *et al.* 1996].

4.4.4.2.2 CDT Hawaii

In 1992 there was some evidence that debris might be accumulating in GEO. Consequently, the CDT, a transportable 32 cm Schmidt telescope (for instrumental details see Section 4.4.3.2.5), began a search for debris near GEO altitudes from Maui, Hawaii (20.7° N, 156.3° W, 3058 m). The results showed that a generalized albedo of 0.2 was good for GEO as well as that 70% of the GEO detections were UCTs [Henize and Stanley 1992]. The CDT was built during the 1988 to 1989 time frame under the guidance of Dr. Karl Henize. The original specification was for a 12.5-in. (32 cm) diameter, f/1.3 Schmidt utilizing a Vidicon television system yielding a 1.8 by 1.2 deg FOV and a limiting magnitude of 13.5. In 1990, well before the Maui deployment, system linearity and limiting magnitude was vastly improved by upgrading to a CCD detector. A Thompson 7882-384x576 pixel CCD with 27-micron pixels (11 arcseconds) was installed that yielded a 17.1-magnitude sensitivity for a 30-second exposure. Later upgrades to CDT included numerous CCDs, culminating in a 512x512, 24μm-pixel back-illuminated detector with enhanced blue sensitivity, 1.6 deg FOV, a 13-arcsecond plate scale, and a 17.1 limiting magnitude for a 20-second exposure.

During the interval from December 1992 through August 1994, five observing runs were conducted on Haleakala in Maui, Hawaii by personnel from NASA JSC. Prior to the CDT GEO observation campaign, historical events had indicated the likelihood of a significant debris population in GEO. On 21 February 1992, a Titan 3C Transtage was observed to break up by a Maui GEODSS Sensor. At least 20 pieces of debris were seen. No orbital data were generated for these fragments, thus all were subsequently lost. Earlier, on 23 June 1978, another historical breakup, that of EKRAN 2, took place and was completely undetected. Its existence only became known when the Commonwealth of Independent States (CIS) revealed the event in 1992.

A total of 13,516 CCD images (6758 GEO fields) were recorded by CDT Hawaii; an object of some type was detected in 26.7% of these fields [Talent *et al.* 1997]. During the data reduction, instrumental brightness units were measured and recorded for each object. By using standard stars these were converted to astronomical magnitudes. Equivalent sizes were calculated for the object population, following flux correction for atmospheric extinction, range correction to 36,000 km, utilizing a value of albedo of 0.2 obtained from employing the observed magnitudes of cataloged objects which were observed and for which accurate size information was known.

Primary conclusions of the observing program carried out by CDT Hawaii were:

- A measurable debris population exists in and near the GEO environment.
- Approximately 27% of all objects in GEO observable down to a magnitude limit of 17.1 are objects not being tracked and maintained as catalogued objects.

- The uncorrelated population described above is sufficiently bright that it could be tracked by existing facilities.

4.4.4.2.3 GEODSS Program

Similar searches to those conducted by the CDT were being conducted by the Air Force Space Command at the Maui GEODSS site. Today, there are three operational GEODSS sites that report to the 21st Space Wing, headquartered at Peterson Air Force Base, Colorado. The sites are located at Socorro, New Mexico; Maui, Hawaii; and Diego Garcia, British Indian Ocean Territories. The GEODSS system is the successor to the Baker-Nunn camera, which was developed in the mid-1950s to provide surveillance data. The GEODSS concept was developed and researched by MIT/LL at an experimental test site located at Socorro that is still used by MIT. To perform its mission, GEODSS brings together three proven technologies: the telescope, the low-light-level television, and the computer. Each site has three telescopes, two main and one auxiliary, with the exception of Diego Garcia, which has three main telescopes. The main telescopes have a 40-inch aperture and a 2 deg FOV. The system only operates at night when the telescopes are able to detect objects 10,000 times dimmer than the human eye can detect. Since it is an optical system, cloud cover and local weather conditions influence its effectiveness

Figure 4.4-30. GEODSS site

The optical telescopes move across the sky at the same rate as the stars appear to move. Thus, the distant stars appear to maintain their same positions in the FOV. As the telescopes slowly move, the GEODSS cameras take very rapid electronic snapshots of the FOV. Four computers then take these snapshots and overlay them on each other. Then, star images, which remain fixed, are electronically erased. Man-made space objects, however, do not remain fixed and their movements show up as tiny streaks that can be viewed on a console screen. The computers measure these streaks and use the data to figure the positions of objects, such as satellites in orbits, from 3,000 to 22,000 miles. This information is used to update the list of orbiting objects.

4.4.4.2.4 Liquid Mirror Telescope

NASA began LEO optical measurements in 1996 with the construction of the 3 m Liquid Mirror Telescope (LMT) at Cloudcroft, New Mexico (33.0° N, 105.9° W, 2772 m) between October 1997 and December 2001 [Jarvis *et al.* 2001, 2003]. Liquid mirror technology was an extremely cost-effective way of providing a large aperture primary mirror and a relatively large FOV of

0.26 deg. [Potter and Mulrooney 1997]. The LMT's major limitation of zenith staring did not hinder it from statistically sampling the LEO orbital debris environment but only orbits with inclinations greater than 33 degrees could be sampled. This telescope was built to characterize the optical orbital debris environment, especially in the important, but hard to track, 1- to 10-cm-size range in LEO.

The primary mirror of the LMT was a parabolic dish of mercury. As the dish was spun, the mercury spread over the dish to form a reflective surface. The 3 m dish was spun at a rate of 10 rpm to form an f/1.5 primary mirror whose beam was then corrected to yield a field free of coma and astigmatism with a final focal ratio of f/1.77. The LMT was able to detect orbital debris objects as dim as 16th magnitude and stars down to 17th magnitude. Between October 1997 and December 2001, the LMT collected 1105 hours of data and detected 830 CTs and 1833 UCTs [Africano *et al.* 1999, Barker *et al.* 2005a].

The first LMT report [Africano *et al.* 1999] analyzed data gathered from October 1997 through January 1999 using a microchannel plate (MCP) with a FOV of about 0.42 deg, which is designated period 1 (P1). The second report [Jarvis *et al.* 2004] presented the results of LMT observations of the LEO orbital debris environment using a more sensitive 25 mm MCP and a decreased FOV of 0.275 deg, for March 1999 through September 2000, or period 2 (P2). The third report, in preparation, will cover data collected from October 2000 through the closure of the LMT in December 2001, or period 3 (P3). A soon-to-be-released summary report will contain the summary dataset with uniform data reduction and analysis parameters and inter-comparison of the three periods of observation. The entire dataset, discussed below, emphasizes the LEO environment ($\leq$ 2100 km). Any direct comparison between period 1 data and data from periods 2 and 3 must be evaluated recalling that period 1 data used a less sensitive MCP and a larger FOV than the two other periods.

Although objects often passed through the FOV of the LMT in just a few tenths of a second, an amazing quantity of information was gleaned. By measuring the object's entry and exit positions and its time to cross the FOV, its altitude and orbital inclination could be calculated. After the data processing program identified moving targets in the data, human screeners reviewed the results and classified the computer generated detections as meteors, CTs, or UCTs. Manual reviews of the data showed that the automated software missed less than 5% of the debris objects.

The data reduction software packages produced astrometric positions for all detections. These positions were fitted under the assumption of a circular orbit to produce inferred values for the inclination and range. With this information and its apparent magnitude, the absolute magnitude was calculated and used to estimate an object's size by assuming an albedo. The object's FOV crossing angle was then calculated from the entry and exit positions of the object. A reasonably well-defined plane of the orbit, defined by the inclination and right ascension (RA) of the ascending node (RAAN), was derived from the object's FOV crossing angle. By assuming a circular orbit, the altitude of the object was estimated based upon its velocity through the FOV. Errors seen in the estimated orbital altitude were due largely to departures from the circular orbit approximation used in the calculations. The height of the Earth's shadow for the time of each event was calculated and detected objects that were in Earth shadow were classified as meteors (debris reflects light whereas meteors produce their own illumination), and removed from the data set.

In 2004, NASA carried out a comparison of extracted estimates of the altitudes and inclinations for observed targets with known values for SSN-cataloged objects [Barker *et al.* 2005a]. The LMT dataset was restricted to targets with altitudes less than 2100 km and nearly circular orbits. The comparison showed that the assumption of circular orbits introduces small biases that are removable. After separately removing the biases for each period, the remaining bias offsets were: (1) the inclination bias is -0.1 deg with an uncertainty of ±2.1 deg, and (2) the altitude estimate is 0.0 with an uncertainty of ±53 km. Figure 4.4-32 shows the flux of objects 10 cm in diameter as a function of altitude compared to LMT period 2, LMT period 3, HAX radar 2001, and the flux predicted by the ORDEM2000 model for 2001 [Barker *et al.* 2005a]. Below 600 km altitude, it is believed that the LMT data still suffers from meteor contamination and is not reliable. From 700 km to 1050 km, LMT 10 cm flux matches both HAX and ORDEM data extremely well, though the LMT flux is a little higher at 850 km. At 1350-1450 km, the LMT flux matches ORDEM data. In addition, LMT period-3 flux mimics the trend, if not the value, of ORDEM extremely well. However, the LMT period 2 is not as good a match, generally being a little higher in flux.

Previous differences between LMT and HAX fluxes suggested that each instrument might detect slightly different populations where some objects are optically bright but radar dim, although other explanations were not ruled out. Bias corrections for phase angle, solar distance, assumed circular orbits, and a correction for small object bias significantly improved the flux values and put ORDEM and LMT in much closer agreement. The difference in flux at 850 km occurs near the center of the RORSAT altitude band, leaving the possibility that the RORSAT debris had been imperfectly removed from the datasets. For the optical datasets, all uncorrelated debris between 63.5 deg and 66.5 deg inclination at altitudes between 700 and 1000 km were removed for the purpose of the flux calculation. A spike in flux was seen predominantly at 82 deg inclination, making it possible that LMT had seen Cosmos 1275 debris.

Figure 4.4-31. Image of the 3-meter LMT.

Located in Cloudcroft, New Mexico. Photograph credit to Chip Simmons.

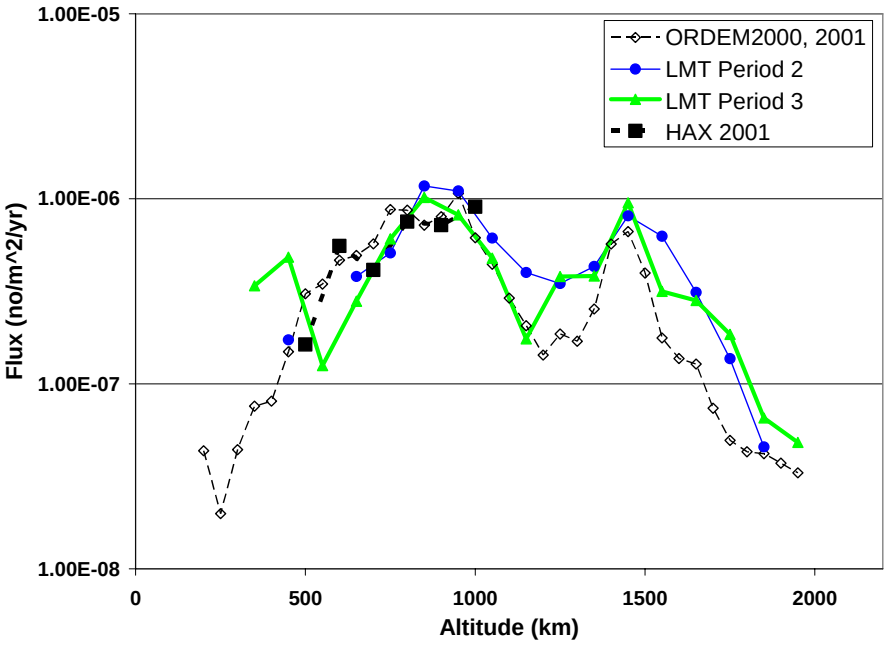

Figure 4.4-32. 10 cm flux comparison of LMT period 2, LMT period 3, HAX 2001, and the ORDEM2000 model for calendar year 2001.

4.4.4.2.5 CDT Cloudcroft

Beginning in 1998, NASA used the CDT, a transportable 32 cm Schmidt telescope co-located with the LMT near Cloudcroft, New Mexico (33.0° N, 105.9° W, 2772 m), to help characterize the debris environment in GEO. The CDT, shown in Figure 4.4-33, was equipped with a SITe 512x512 CCD camera capable of detecting down to 18th magnitude. The pixels were 24 microns square (12.5 arcseconds), resulting in a 1.7 by 1.7 deg FOV. In addition, the telescope pointing and CCD operation were computer controlled to automatically collect data for an entire night. Using the CDT, researchers conducted systematic searches of the GEO environment as part of an international measurement campaign under the auspices of the IADC. The objectives for this survey were to determine the extent and character of debris in GEO, specifically by obtaining distributions for the brightness, inclination, RAAN, and mean motion for the debris. Between 1998 and 2002 the CDT collected data on 240 nights, or a total of 1420 hours, and detected 15,725 cataloged and 3096 un-correlated objects. The sensitivity roll-off began at 15th magnitude, but objects were detected as faint as 18th magnitude, which corresponded to an object size of 0.36 meters when a 0.2 albedo with a specular reflection was assumed [Jarvis *et al*. 2002, Barker *et al*. 2005b]. When an assumption of diffuse Lambertian scattering was made for an 18th magnitude object, a size of 0.22 meters was derived.

In general, all 4 years of CDT UCT data show similar distributions in inclination, eccentricity, RAAN, mean motion and magnitude, thereby indicating a general stability in the UCT environment between 1998 and 2002 for objects brighter than 18th magnitude (Barker *et al.* 2005b). A plot shown in Figure 4.4-34 depicts the RAAN versus inclination distribution over the 4 years of CDT data collection. Overall, the conclusions of the CDT survey of GEO showed:

- The inclination distribution of non-functional CTs is similar to those seen for UCTs.
- Analysis of the repeatability of non-functional CTs within each observing year provides evidence that each unique UCT is seen ~5.5 times a year, which reduces the total number of unique UCTs to about 100 per year.
- UCTs and CTs show the same amount of drift in the angular momentum plot between calendar years, confirming the same behavior related to gravitational perturbations of their orbital planes.
- The ratio of detected UCTs to CTs is similar over the 4 years.
- The absolute magnitudes of the UCTs are 1-2 magnitudes fainter than the non-functional CTs for all 4 years.
- If a Lambertian phase function is used instead of a specular phase function to convert the observed magnitudes into characteristic sizes, the resulting size is a factor of 1.63 smaller. The detection limit of 60 cm (specular assumption) for the CDT becomes 35 cm when a diffuse Lambertian scatter is used.
- Probability charts shown that the CDT has good coverage for most RAAN values with inclinations less than 15 deg.

Although, the CDT was shutdown in the fall of 2001, the data can still be used for modeling efforts in the GEO regime. Subsequently, NASA has transferred the CDT to the Aerospace Engineering and Physics Departments of the Embry-Riddle University in Prescott, Arizona, where it is being used as a teaching tool for space physics.

Figure 4.4-33. CDT located in Cloudcroft, New Mexico.

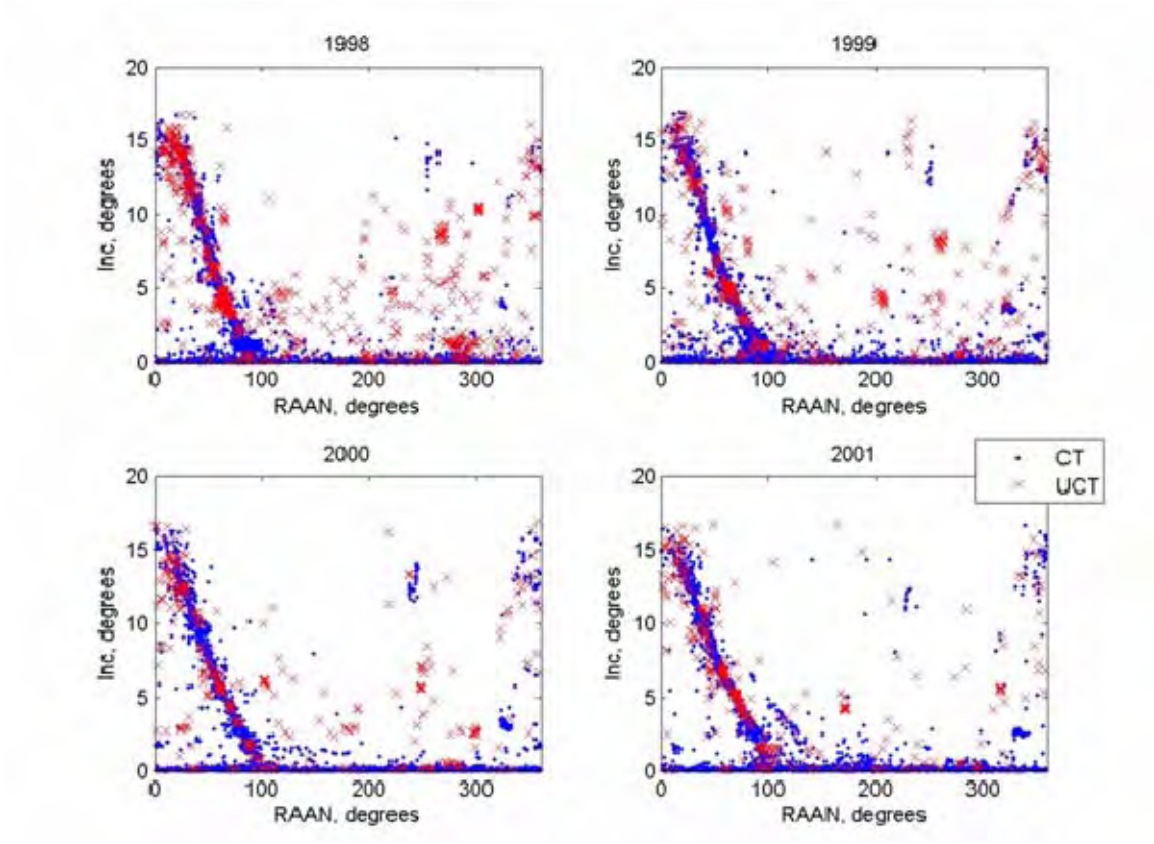

Figure 4.4-34. RAAN versus inclination distribution for the 4 years of CDT data collection.

The CTs are the blue dots and the UCTs are the red x's.

4.4.4.3 Current Status

Currently, optical measurement research continues with MODEST, the NASA AMOS Spectral Study (NASS), the meter-class autonomous telescope (MCAT), the Optical Measurement Center, and projects for the U.S. as well as other agency studies on the orbital debris environment.

4.4.4.3.1 NASA Related

4.4.4.3.1.1 MODEST

Since 2002, the University of Michigan's Curtis Schmidt telescope has operated through a NASA grant and is located at the CTIO in Chile (30.2° S, 70.8° W, 2216 m altitude) [Seitzer *et al.* 2001, 2005]. Part of the observatory is shown in

Figure 4.4-35 and MODEST, specifically, is shown in

Figure 4.4-36. The MODEST system is 0.6/0.9 meter f/3.5 and has a 1.3 deg by 1.3 deg FOV. All images are obtained through a broad R filter with a standard 5-second exposure that yields a S/N of 10 for a 18th magnitude object. The total time between exposures is approximately 38 seconds [Seitzer *et al.* 2005 and Abercromby *et al.* 2005a, 2006a].

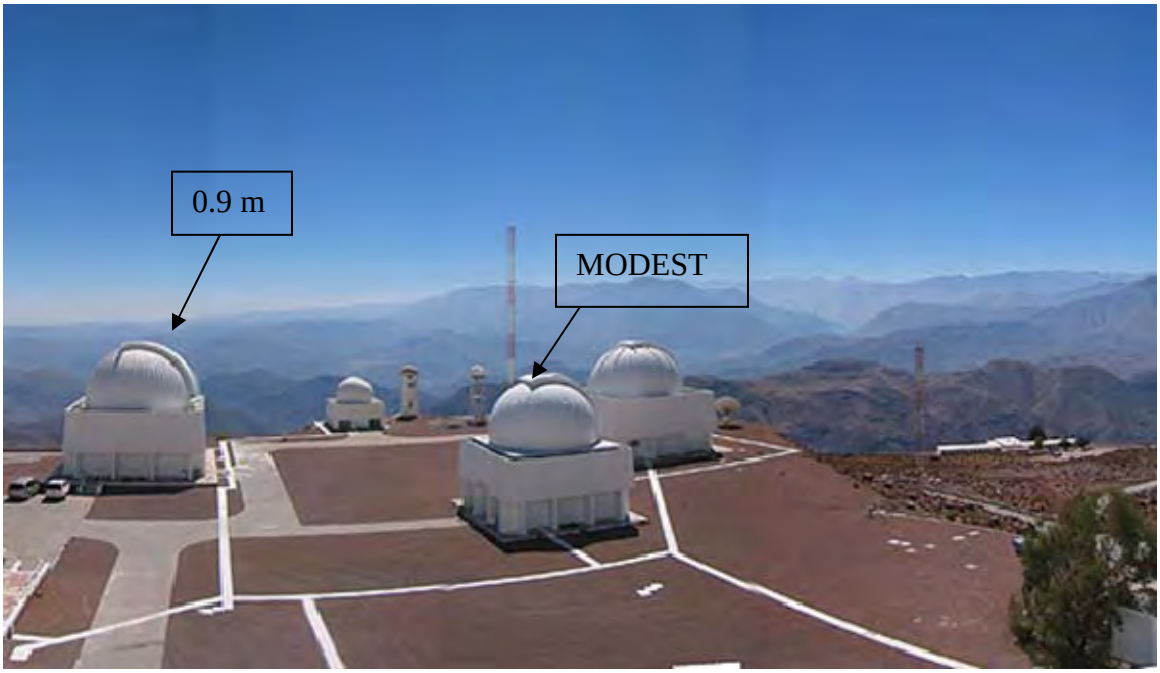

Figure 4.4-35. View looking north from CTIO of MODEST and the 0.9-meter telescopes.

To date, 131 days of data have been collected and 3724 objects detected. With a 5-minute sample of the orbital arc, a circular orbit can be determined. As in the CDT and LMT observational programs, studies are being carried out to assess the biases introduced by the assumption of circular orbits for UCTs. The sensitivity limit of the MODEST system is near 18th

magnitude, which corresponds to a 0.36 m object when a 0.2 albedo and a specular reflection are assumed. The telescope operates nominally in survey mode, near the Earth's shadow, in an effort to optimize brightness. By observing at a specific RA and declination for an entire night, MODEST generates nearly 7 gigabytes of data.

By the end of 2006, the MODEST system had enough survey coverage to build a complete statistical map of the GEO environment [Matney *et al.* 2006]. By applying the Johnson Law [Johnson *et al.* 2004] of breakups to the uncorrelated section of the environment, it can be shown that the population continues to grow following the power law similar to what was found in LEO. The results are shown in Figure 4.4-37. This information is useful when using optical data in a model of the GEO environment and needing the size to be near 10 cm (or a magnitude of 20.8 in R).

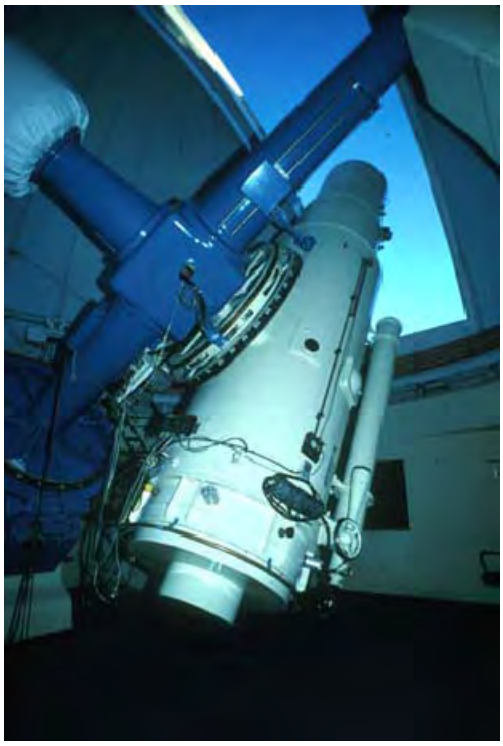

Figure 4.4-36. MODEST telescope.

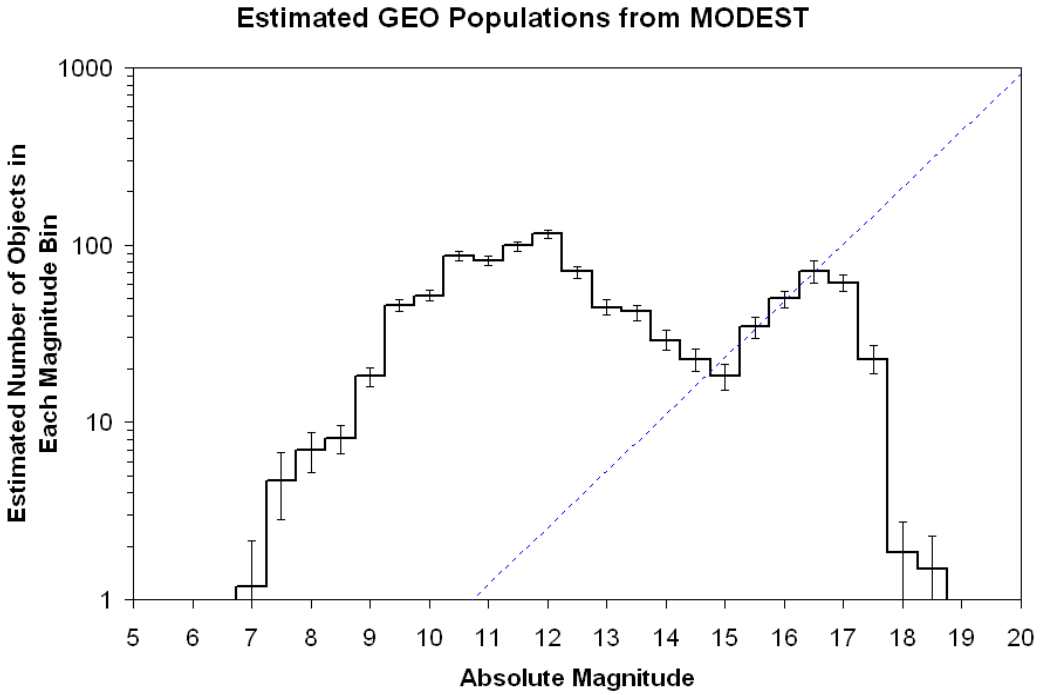

Figure 4.4-37. Debiased MODEST debris population.

The dotted line is the power law of fragmentations similar to what is seen in LEO.

4.4.4.3.1.2 AMOS-NASS (1.6m, 3.0m, 3.6m)

In order to characterize the space environment, the physical characteristics of orbiting objects need to be determined. These properties are used in current space environment models and the building of shields for spacecraft, as well as in providing base work for future environment studies. Some of these characteristics, including material type, currently are assumed. Each material shows a different reflectance spectrum based on its composition [Jorgensen *et al.* 2004a, 2004b]. Using low-resolution spectrophotometry and comparing absorption features to those taken in a laboratory, it is possible to determine material type of human-made orbiting objects in both LEO and GEO. Using the 1.6-meter and 3.67-meter telescopes at the AMOS [Africano *et al.* 2004] site (shown in Figure 4.4-38) and NASA's 3.0-meter Infrared Telescope Facility located at Mauna Kea, Hawaii, remote spectral observations have been taken on many rocket bodies and spacecraft through the wavelength ranges of 0.3 to 2.5 microns [Jorgensen *et al.* 2004a, 2004b, Abercromby *et al.* 2005b, 2006b]. Examples of the data are shown in Figure 4.4-39. The image on the left is from a rocket body identified as being covered with white paint, but showing the organics in the longer wavelengths. The image on the right is from another rocket body and identified as being covered with paint, shown by the bad gap feature at 3900 angstroms.

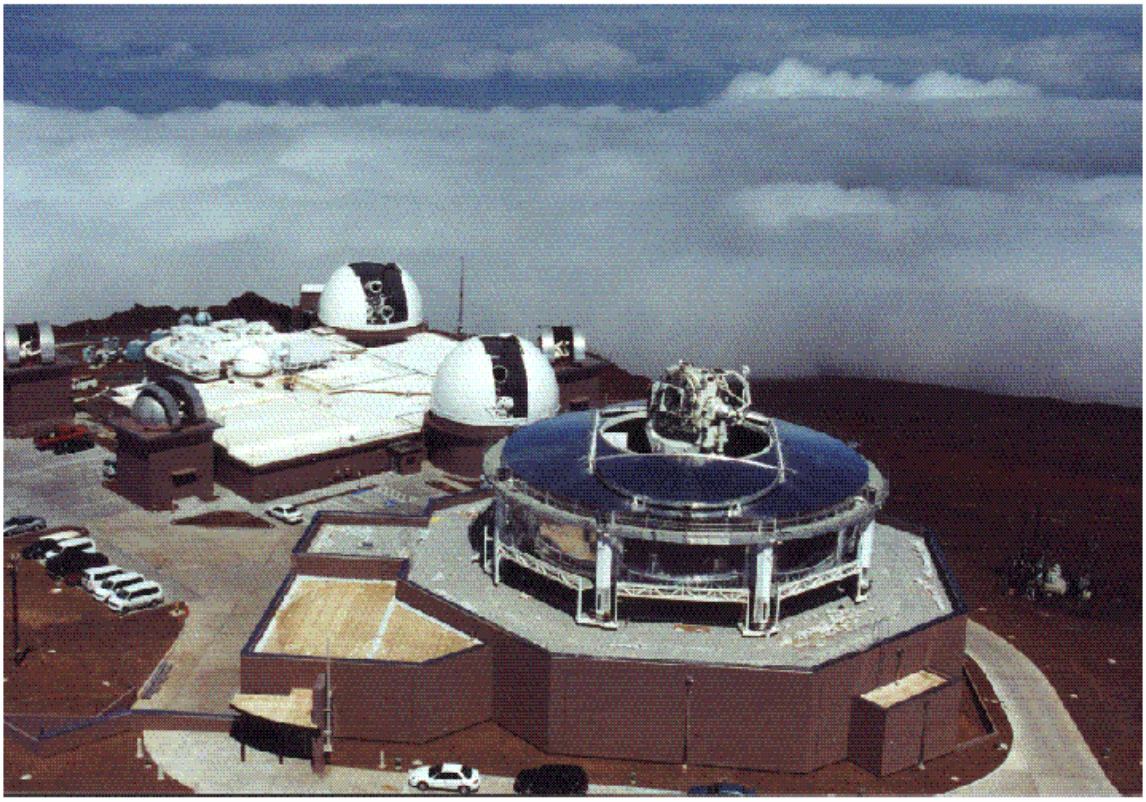

Figure 4.4-38. Picture from AMOS at Haleakala, Maui, Hawaii.

The 3.6 m telescope is in the foreground with the dome down, while the 1.6 m with Spica is the dome in the center of the photo.

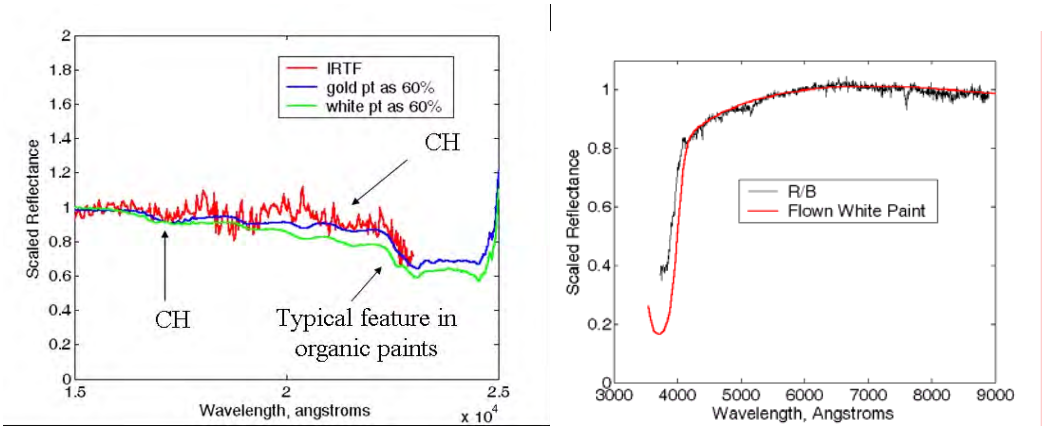

Figure 4.4-39. Two examples of spectra.

The image on the left is from a rocket body identified as being covered with paint, but showing the organics in the longer wavelengths. The image on the right is from another rocket body and identified as being covered with white paint, shown by the band gap feature at 3900 angstroms.

4.4.4.3.2 Other Agencies

The IADC has carried out several campaigns to help define the GEO orbital debris environment. NASA and ESA have been the prime contributors to finding and defining the fainter debris environments. ESA [Schildknecht *et al.* 2004, 2005, 2006] and MODEST [Seitzer *et al.* 2005, Abercromby *et al.* 2005, 2006, Matney *et al.* 2006] have described their operations and primary results, which indicate an evolving debris population including a possible cluster of objects, presumably from breakups in GEO.

The current IADC campaign is to study the high A/M objects that were first detected by Schildknecht [Schildknecht 2005]. Members of the IADC with participating optical sensors for this high A/M campaign are the:

- ESA
    - Tenerife-Teide (28.3° N, 16.5° W, 2374 m) (1 meter aperture, 40’ x 40’ FOV, 19^m limiting magnitude)
    - Zimerwald (AUIB) (46.9° N, 7.5° E, 951 m) (1 meter aperture, 30’ x 30’ FOV, 19^m limiting magnitude)
- Russian Federal Space Agency (ROSCOSMOS)
    - Mondy (ISTP RAS) (51.6° N, 100.9° E, 2008 m) (1.6 meter aperture, 19^m limiting magnitude)
    - Nauchnyi (CrAO RAS, ZTSh) (44.7° N, 34.0° E, 580 m) (2.6 meter aperture, 8.4’ x 8.4’ FOV, 20^m limiting magnitude)
    - Nauchnyi (CrAO RAS, AT-64) (44.7° N, 34.0° E, 580 m) (0.64 meter aperture, 53’ x 34’ FOV, 18^m limiting magnitude)
    - Zelenchukskaya (SA) RAS) (43.6° N, 41.4° E, 2059 m) (0.60 meter aperature, 18.2’ x 18.2’ FOV, 19^m limiting magnitude)
- Japan Aerospace Exploration Agency (JAXA)
    - Nyukasa (35.9° N, 138.2° E, 1870m)
- Centre National d'Etudes Spatiales
    - Cote d’Azur (CNRS) (43.7° N, 6.9° E, 1270 m, 0.25m aperture, 1.86°x 1.86° FOV, 16.5^m limiting magnitude))
- British National Space Centre
    - Cyprus (PIMS) (34.9° N, 32.9° E, 1810 m)
    - Hersmonceux (PIMS) (50.9° N, 0.2° E, 31 m)
- Agenzia Spaziale Italiana
    - Collepardo (CAT) (41.8° N, 13.4° E, 555 m)
- China National Space Administration

4.4.4.4 Potential Future Achievements

4.4.4.4.1 MODEST Hand-Off

Hand-off operations between MODEST and the 0.9 m telescope at CTIO have been tested [Seitzer *et al.* 2006] to determine better defined orbits for debris instead of assuming circular orbits. During some future IADC observing runs, MODEST will operate in a regular survey mode and all objects fainter than 15^{th} magnitude will be followed with the 0.9 m at CTIO

(4.4-35) to determine orbits and colors of these fainter objects. Optimum operations of this mode would include other telescopes world-wide.

4.4.4.4.2 HANDS/Raven

AMOS developed the autonomous Raven class telescopes (~0.4 m diameter aperture) to offload the tracking workload of the GEODSS for brighter satellites [Nishimoto 1999]. The autonomous data reduction scheme used for Raven yielded very accurate "angles only" metric observations. It was realized that sub-arcsecond observations were possible with some modifications to the Raven system. The High Accuracy Network Determination System (HANDS) Program is an outgrowth of Raven that seeks to combine sub-arcsecond angle information with accurate range data to greatly improve orbit estimation of near-geostationary satellites [Sabol and Culp 1998, Nishimoto 2002]. The HANDS telescopes will use a proprietary K-Star telescope design that utilizes economical spherical mirrors. An advantage of this design is that it can be configured with a very large FOV (up to 5 deg) and is scalable to apertures approaching 2 m.

4.4.4.4.3 MCAT

NASA (through the Orbital Debris Program Office) and the AMOS site are cooperating to place a wide field-of-view, 1 m aperture telescope on two islands (Roi and Legan) in Kwajalein Atoll (167.0° E, 9.1° N) for space debris research. The MCAT system will be deployed as a part of the HANDS by Oceanit, Inc. and will use a Ritchey Chrétien design with a 0.9 deg FOV. The telescope will operate in primarily two different modes. During the twilight hours it will sample low inclination orbits in a "track before detect" mode. In the middle of the night it will perform a more standard GEO survey similar to MODEST [Stansbery *et al.* 2003]. These two modes will address major limitations of the previous LEO and GEO surveys by extending the LEO survey down to 0 deg inclination from 33 deg and the GEO survey to fainter limits (20^{th} vs. 18^{th} magnitude). A temporary 0.4 m telescope was deployed in February 2007 on Roi (Figure 4.4-40) as part of HANDS to test remote operations from the Kwajelein Atoll. Tentatively the full MCAT is scheduled for deployment in 2010 on Legan, shown in

Figure 4.4-41.

A key to the success of MCAT will be the autonomous operational mode. The Raven telescopes have highlighted the productivity and cost savings offered by remote, uninhabited (except for maintenance) operations. In the case of Raven, which collects metric observations on known, cataloged satellites, the telescope is remotely tasked on which satellites to observe by an automated scheduler. The Raven system has an integrated weather station that monitors rain, humidity, wind speed, and other conditions. Whenever the weather conditions are within acceptable bounds, the Raven dome is opened and the telescope collects data.

In the case of MCAT, the telescope will be conducting blind searches. For GEO searches, the search strategy will be similar to that developed for the CDT and MODEST, which takes into consideration such things as solar phase angle and location of the Earth's shadow, as well as complete coverage of the inclination versus RAAN parameter space for GEO objects.

Automation is particularly important for the low inclination searches. The track-before-detect mode searches find very limited segments of the RA arcs of an orbit. It is anticipated that most CCD exposures taken during low inclination searches will contain no detections. Having no

human involved in either the operation of the telescope or in the data reduction and detection makes this type of search economically feasible.

Figure 4.4-40. The Roi site is within the cluster of buildings in the lower center.

Figure 4.4-41. Island of Legan in Kwajalein Atoll.

4.4.4.4.4 Laboratory Measurements

Laboratory measurements have been undertaken at both AMOS and NASA to obtain light curves of various satellite shapes and debris fragments. AMOS will concentrate on satellites [Deiotte *et al.* 2006] while NASA will concentrate on ESOC debris [Rodriguez *et al.* 2006]. These laboratory programs will generate light curves, which should assist in the interpretation of observational light curves obtained with AMOS facilities [Hall *et al.* 2003]

4.4.5 *In Situ* Measurements

4.4.5.1 History

Both meteoroids and man-made orbital debris exist in the near-Earth environment. While the former is a natural component of the Solar System, the latter is a byproduct of half a century of human space activities. Meteoroids originated primarily from collisions among asteroids, or the

disintegration of comets near the Sun. The existence of meteoroids and orbital debris in the near-Earth space presents challenges for space scientists and mission operators. Since the beginning of the space age, it has been recognized that impacts by meteoroids pose a threat to satellite operations in the near-Earth environment and in interplanetary space [anon. 1969]. As the orbital debris population increases, it becomes a new impact threat to operational satellites as well.

To protect critical space assets (including satellites, the ISS, the Space Shuttle, and future exploration vehicles), a reliable meteoroid and orbital debris environment definition is needed. A better understanding of the environment is also a key to cost-effective shielding designs for appropriate protection. The primary concern for impact risk assessments is focused on particles about 0.1 mm and larger. Ground-based optical telescopes and radars are limited to objects several millimeters and larger. An *in situ* sensor with a large detection area, and long mission duration, is the only means to characterize the particles between a meter and a few millimeters in size.

Early *in situ* measurements of the near-Earth meteoroid environment were carried out by acoustic sensors and penetration cells. Examples include Explorer 1, Pioneer 1, Pioneer 16, and Pegasus 1, 2, and 3. Surfaces returned from space, such as windows from Gemini missions, were also analyzed to deduce the meteoroid populations [Zook 1970]. A major milestone for *in situ* measurements was reached when the LDEF was launched in 1984. After a long delay, the facility was retrieved in 1990. Due to its large surface areas, and the unique fixed orientations of different surfaces, its data has been utilized extensively to improve the knowledge of both meteoroid and orbital debris populations.

After the return of the LDEF, major *in situ* measurements included the European Retrievable Carrier (EURECA) between 1992 and 1993 and Japan's Space Flyer Unit between 1995 and 1996. Surfaces returned from space, such as Space Shuttle window panels and radiators [Hyde and Bernhard 2006] and the HST Solar Arrays [Moussi *et al.* 2005] have also been used to deduce meteoroid and orbital debris populations in the low-Earth environment. Additional sensors also included the SPAce DUSt (SPADUS) instrument [Tuzzolino *et al.* 2005], DEBris In orbit Evaluator (DEBIE) [Schwanethal *et al.* 2005] and the Micro-PArticle Captured (MPAC) [Neish *et al.* 2005]. The Geostationary ORbit Impact Detector (GORID) was placed in GEO between 1997 and 2000 [Drolshagen *et al.* 2001]. Due to the small detection areas of the last four systems, detections were limited to particles about 20 μm and smaller.

Aerogel has been used in recent years to capture meteoroids and orbital debris for additional sample-return laboratory analysis. The ODC was deployed on the *Mir* Station between 1996 and 1997 [Hörz 1999], and the MPAC system was placed on the ISS in 2001 [Kitazawa *et al.* 2004]. The unique property of aerogel for intact capture of hypervelocity particles was further demonstrated by the successful mission of Stardust. For near-Earth *in situ* measurements, the utilization of aerogel has the potential to further our understanding of the origin and composition of the meteoroid and orbital debris populations.

4.4.5.2 Current Status

Although ground-based sensors have been used on a regular basis to monitor meteoroid and orbital debris populations of a few millimeters in size and larger, there has been a lack of large

area *in situ* sensors to characterize and update the smaller particle environment. This is illustrated by Figure 4.4-42. *In situ* data for particles between 0.1 and 1 mm collected by LDEF, EURECA, and Space Flyer Unit (SFU) are more than 10 years old. For meteoroid populations where a significant change in time is not expected, this is not an issue. For orbital debris populations that are fast-growing and dynamic in nature, however, the lack of new data is a major problem.

Currently the only data for particles between 0.1 and 1 mm that are being collected on a regular basis come from the damage inspection of the Orbiter surfaces (windows, radiator panels, etc.) after each Space Shuttle mission. The results, however, are not as useful as those collected by sensors specifically designed for *in situ* measurements. Additional factors, such as the lack of impact timing information, and the difficulty to distinguish meteoroids from orbital debris, also add deficiency to the Space Shuttle surface data. From the safety and satellite operations perspective, there is an immediate need for a large and dedicated meteoroid and orbital debris sensor to monitor and update the populations between 0.1 and 1 mm.

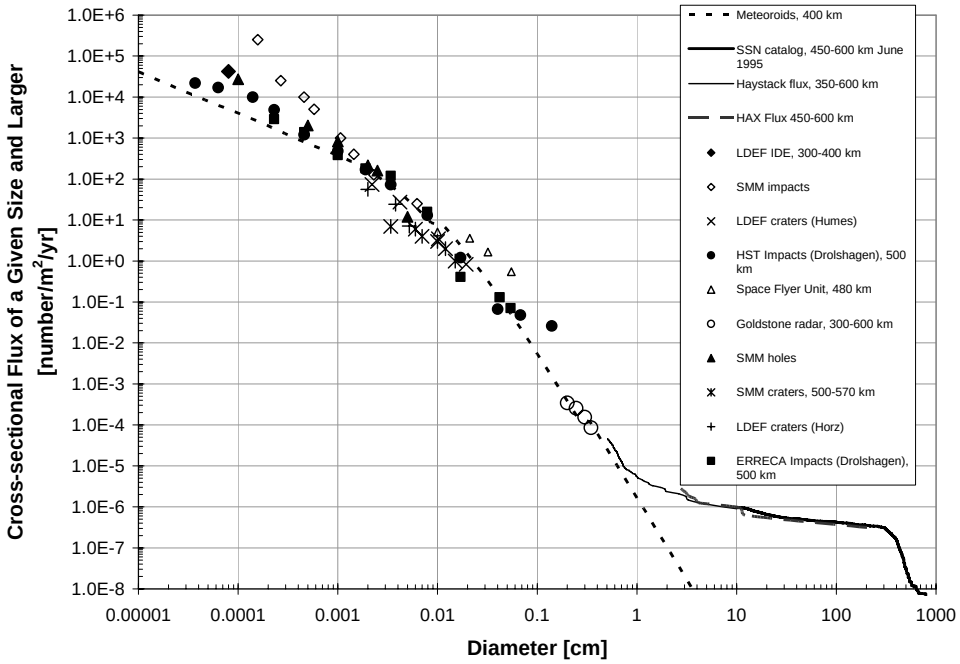

Figure 4.4-42. Sample of approximate-measured debris flux in LEO, by object size adopted from the United Nations Technical Report on Space Debris [anon. 1999].

Particles 1 mm and smaller are detected by space-based in situ sensors or surfaces returned from space, including LDEF, Solar Maximum Mission (SMM), SFU, EURECA, and HST solar panel post flight analyses 1 and 2.

4.4.5.3 Potential Future Achievement

4.4.5.3.1 Large Area Debris Collector

The Large Area Debris Collector (LAD-C) project attempted to utilize the ISS as a scientific platform to characterize the near-Earth meteoroid and orbital debris environment in the size regime where little data existed. The two primary objectives were safety and science. For the safety objective, LAD-C would provide a good meteoroid and orbital debris environment definition, including impact flux and impact velocity distribution for reliable risk assessments for critical space assets. For the science objective, *in situ* measurements and sample return of orbital debris and meteoroids from the ISS would provide a cost-effective way to capture and collect small meteoroids as samples from asteroids and comets. The extracted information, including mineralogical and isotopic compositions, could be used to understand the physical processes that formed the asteroids and comets and to improve knowledge of conditions when the Solar System was formed.

The LAD-C project was developed by a consortium of members from international space agencies and universities. Their roles and responsibilities were: U.S. Naval Academy (USNA) (lead, mission sponsor, management, electronics), U.S. Naval Research Lab (acoustics, engineering), NASA Orbital Debris Program Office (project development support, science planning and operations), JAXA/Institute of Space and Astronautical Science (ISAS) and Chiba University (aerogel manufacture, calibration), ESA Space Debris Office (system software, hardware manufacture, thermal analysis, calibration), University of Kent (HVI calibration), and the University of California – Berkeley (aerogel and mission support). The U.S. DoD Space Test Program (STP) Office was in charge of system launch manifesting, deployment, and retrieval.

The LAD-C system included two major components: aerogel tiles and acoustic sensors. The tiles were used for intact capture of HVI particles, while the sensors were designed to record impact characteristics of the collected samples. The basic structure of LAD-C consisted of 1 m by 1 m by 2.2 cm trays, with each tray further divided into two half-panels. Each aluminum (6061-T6) panel contained many small aerogel tiles and twelve acoustic sensors attached to an aluminum frame. Although the total number of trays was limited by the STS/ISS transportation, installation, and attachment constraints, the goal was to have a total aerogel exposure area reach 10 m^2.

The LAD-C acoustic sensor system was called the Particle Impact Noise Detection and Ranging On autonomous Platform (PINDROP) [Corsaro *et al.* 2004, 2006]. Development of the system was supported by the NASA Planetary Instrument Definition and Development Program between 2004 and 2006. The sensor design was optimized by fabricating and testing sensors of various configurations and materials. Because it has high acoustic sensitivity, low mass, and good transient response, the final sensor material selected for LAD-C was poly-vinylidene fluoride copolymer.

The LAD-C aerogel was a special, silica hydrophobic aerogel originally developed for Cherenkov counters at Japan's national KEK high energy lab [Adachi *et al.* 1995, Tabata *et al.* 2005]. Similar KEK-produced aerogel was flown on the ISS as part of the MPAC package [Kitazawa *et al.* 2004]. Selection of the aerogel density for LAD-C was based on a balance between two competing factors – strong acoustic signals, with a higher density, and longer

aerogel tracks, with a lower density. After a series of HVI tests were conducted at the University of Kent, 0.06 g/cm3 was selected as the density for LAD-C aerogel [Liou *et al.* 2007]. Additional impact tests were planned to better characterize the relationship between the impact characteristics and features embedded in the aerogel.

The combination of acoustic sensors and aerogel tiles would make it possible to estimate the impact locations and velocities of some of the collected samples. Acoustic sensors would record impact time, location, signal strength, and acoustic waveform data of the largest collected samples. From the inspection of aerogel impact features, impact angle and impact speed could be estimated. The combined information could be used to reconstruct the orbits of some of the collected samples, and lead to the possible identification of their sources (asteroidal, cometary, or orbital debris). Compositional analysis of the collected samples could easily separate debris from meteoroids, and provide additional breakdown of the orbital debris populations (*e.g.*, Al, paint, steel, Al_2O_3).

In addition to PINDROP and aerogel, several small area subsystems, proposed by ESA, JAXA/ISAS, and the University of California – Berkeley, were considered to be integrated into one of the trays. These passive subsystems included thin, multi-layer, film sensors, and calorimetric aerogel. Their different sensing capabilities could be used to cross-calibrate the acoustic and aerogel data. A simple transmitter might also be added to LAD-C for additional monitoring purposes.

Deployment of the LAD-C was driven by two factors: to maximize the sample collection and to minimize potential particle contamination on aerogel. Meteoroid and orbital debris impact rates and impact speeds were very sensitive to the orientation of the collection surface. Possible contaminations on ISS included STS/Progress/Soyuz thruster plume particles, water and waste dumps from ISS, and outgassing from other ISS components, making the location and orientation of the sensor very important. After a careful analysis of the factors involved, the decision was made to place LAD-C on the starboard side (near the S3 Truss) of the Space Station with the aerogel facing the starboard direction.

The LAD-C Preliminary Design Review (PDR) was held in May 2006. An ideal deployment opportunity in August 2008 was identified by the STP, with system retrieval planned in late 2009. However, the DoD sponsorship of LAD-C was transferred from National Research Laboratory to USNA in August 2006. As a result of this change, LAD-C was required to be recertified by the DoD Space Experiment Review Board. Unfortunately, after the review was completed, STP was unable to continue its support to manifest the project due to a budget constraint. Currently, the NASA Orbital Debris Program Office is exploring other possibilities to develop new *in situ* experiments to better characterize the small debris populations in the near future.

4.4.5.3.2 Other Agencies

The Japanese MPAC system was placed on the ISS in 2001. The three subsystems were brought back separately in 2002, 2004, and 2005, respectively. Each subsystem consists of aerogel tiles, polyimide foam, and aluminum plates. The system was mounted near the Russian module with the aerogel surfaces facing in both ram and anti-ram directions. Each surface had a total area of 329 cm^2. Preliminary analysis on the returned subsystems indicates that the aerogel surface was

heavily contaminated, possibly by thruster plume particles [Neish *et al.* 2005, Kitazawa *et al.* 2006]. A similar MPAC system is planned to be deployed with the Japanese Experiment Module on the ISS.

4.4.6 References

Abercromby, K. J. et al., "Orbital Parameters for Objects Observed by the Michigan Orbital DEbris Survey Telescope (MODEST)," *56th International Astronautical Congress*, IAC-5-B6.1.05 (CD-ROM), Fukuoka, Japan, 17-21 October 2005a.

Abercromby, K.J. et al., "Apply Space Weathering Models to Common Spacecraft Materials to Predict Spectral Signatures," *Proceedings of the 2005 AMOS Technical Conference* (CD-ROM), Wailea, Maui, Hawaii, pp. 154-161, 2005b.

Abercromby, K.J. et al., "Survey and Chase: A New Method of Observations for the Michigan Orbital DEbris Survey Telescope (MODEST)," *57th International Astronautical Congress*, IAC-06-B6.1.2 (CD-ROM), Valencia, Spain, 2006a.

Abercromby, K.J. et al., "Comparisons of Ground Truth and Remote Spectral Measurements of the FORMOSAT and ANDE Spacecraft," *Presented at The AMOS Technical Conference*, Wailea, Hawaii, 11-14 September 2006b.

Africano, J.L. et al., "Liquid Mirror Telescope Observations of the Orbital Debris Environment: October 1997 – January 2001," JSC – 28826, Houston, Texas, 1999.

Africano, J.L. et al., "The Optical Orbital Debris Measurement Program at NASA and AMOS," Adv. Space Research, 34, pp. 892-900, 2004.

Agapov, V., A. Medvedev, and I. Molotov, "Results of LEO, HEO, and GEO object's radar observations in 2005," *Presentation at the 24th IADC Meeting*, Tsukuba Space Center, Japan, 10-13 April 2006.

Anisimov, V.D., G.S. Batyr, A.V. Menshikov, and V.D. Shilin, "Russia's Space Surveillance System: Yesterday, Today, and Tomorrow," Vozdushno-Kosmicheskaya Oborona, Moscow, 15 February 2004.

Anon., "The NORAD Space Detection and Tracking System," *NORAD Fact Sheet*, Headquarters North American Air Defense Command, Peterson Air Force Base, September 1977.

Anon., "Space Detection and Tracking, A Chronology, 1957-1983," History Office, USAF Space Command, March 1990.

Barker, E. S. et al., "The LEO Environment as Determined by the LMT between 1998 and 2002," *Proceedings of the 2005 AMOS Technical Conference*, pp. 206-215, Wailea, Maui, Hawaii, 2005a.

Barker, E. et al., "The GEO Environment as Determined by the CDT between 1998 and 2002," *Proceedings of the 4th European Conference on Space Debris*, ESA SP-587, pp. 135-140, Darmstadt, Germany, August 2005b.

Barker, W.N., “The Accuracy of General Perturbations and Semianalytic Satellite Ephemeris Theories,” *AAS/AIAA Astrodynamics Specialist Conference*, Paper AAS 95-432, Halifax, Nova Scotia, Canada, August 1995.

Barton, D. K., et al., “Orbital Debris Radar Technology Peer Review,” Final Report, NASA/Johnson Space Center, Houston, Texas, March 1992.

Barton, D. K., et al., “Final Report of the Haystack Orbital Debris Data Review Panel,” NASA TM 4809, Houston, Texas, February 1998.

Bohannon, G., T. Caampued, and N. Young, “First Order RCS Statistics of Hypervelocity Impact Fragments,” XonTech Report 940128-BE-2305, April 1994.

Coffey, S.L., H.L. Neal, and M.M. Berry, “Uncorrelated Observations Processing at Naval Space Command,” *Proceedings of the Third U.S./Russian Space Surveillance Workshop*, pp. 211-234, Washington, DC, October 1998.

Coombs, C., Spacetrack, Watchdog of the Skies, William Morrow & Company, New York, 1969.

Cress, G.H. et al., “Radar and Optical Measurements Final Report: Orbital Debris Radar Calibration Spheres,” JSC – 27241, June 1996.

Dalquist, C. and G. Bohannon, “Physical Descriptions of Debris Objects Used in Static RCS Measurements,” XonTech Report 910555-1978, August 1991.

Deiotte, R. et al., “Maui Space Surveillance System (MSSS) Satellite Categorization Laboratory,” *Proceedings of the 2006 AMOS Technical Conference* (CD-ROM), Wailea, Maui, Hawaii, Sept. 10-14 September 2006.

DeVere, G.T. and N.L. Johnson, "The NORAD Space Network," Spaceflight, pp. 306-309, July-August 1985.

Donath, T., et.al., “Proposal for a European Space Surveillance System,” *Proceedings of the 4th European Conference on Space Debris*, ESA SP-587, pp. 31-38., August 2005.

Everett, R., T. Caampued, and J. Chu, “Summary of Data Processing of September 1990 SPC Debris Data,” XonTech Report 910147-1937, March 1991.

Everett, R., C. Dalquist, and T. Caampued, “Summary of Data Processing of January 1991 SPC Debris Data,” XonTech Report 9100393-1965, July 1991.

Furniss, Tim, “NORAD – The Inside Story,” Satellite & Space Technology, pp. 12-13, December 1985.

Hall, D. et al., “AEOS I-Band Photometry of Moving Targets,” *Proceedings of the 2003 AMOS Technical Conference* (CD-ROM), Wailea, Maui, Hawaii, 2003.

Henize K. and Stanley, “Optical Observations of Space Debris: Technical Issues and Future Directions,” AE Potter (ed.), NASA Conference Publication 10077, pp. 241-244, 1992.

Hirose, C., et al., "Observation of Space Debris by the Kamisaibara Radar System," *Proceedings of the 4th European Conference on Space Debris*, ESA SP-587, pp. 73-78, Darmstadt, Germany, August 2005.

IADC Working Group 1, "IADC 24-Hour Space Debris Campaign 200,4, Inter-Agency Space Debris Coordination Committee Final Report on Action Item 21.1, October 2006.

Jackson, P., "Space Surveillance Satellite Catalog Maintenance," *AIAA/NASA/DoD Orbital Debris Conference: Technical Issues & Future Directions*, AIAA 90-1339, Baltimore, Maryland, April 1990.

Jarvis K.S., et al., "2001: Observations of the Geosynchronous Earth Orbital Debris Environment Using NASA's CCD Debris Telescope," *Proceedings of the 3rd European Conference on Space Debris*, ESA SP-473, Darmstadt, Germany, October 2001.

Jarvis, K.S. et al., "CCD Debris Telescope Observations of the Geosynchronous Orbital Debris Environment: Observing Year: 1999," Technical Report, NASA JSC, Houston, Texas, 2002.

Jarvis, K.S. et al., "Observational Results of NASA's Liquid Mirror Telescope," IAA-01-IAA.6.4.01, 2003.

Jorgensen, K. et al., "Observations of J002E3: Possible Discovery of an Apollo Rocket Body," *Presented at the Division of Planetary Sciences*," Monterey, California, October 2004a.

Jorgensen, K. et al., "Reflectance Spectra of Human-made Objects," *Presented at the AMOS Technical Conference*, Maui, Hawaii, 13-17 September 2004b.

Johnson, N.L. and D.J. Nauer, "Orbital Debris Detection: Techniques and Issues," Journal of Spacecraft and Rockets, 28 (4), pp. 465-469, 1991.

Johnson, N.L., "U.S. Space Surveillance," Adv. Space Research, 13 (8), pp. 5-20, 1993.

Johnson, N.L., "The Reentry of Large Orbital Debris," *48th International Astronautical Congress*, Turin, Italy, October 1997.

Johnson, N.L., "The Cause and Consequences of a Satellite Fragmentation: A Case Study," Adv. Space Research, 23 (1), pp. 165-173, 1999.

Johnson, N.L. et al., History of On-Orbit Satellite Fragmentations, ed. 13, JSC-62530, NASA JSC, Houston, Texas, 2004.

Johnson, N.L., "The New Jettison Policy for the International Space Station," *36th COSPAR Scientific Assembly*, Beijing, China, July 2006.

Kessler, D. J., Orbital Debris Environment for Space Station, JSC-20001, 1984.

Kessler, D. J., and E.G. Stansbery, "NASA's Planned and Proposed Techniques for Monitoring 1 cm to 1 mm Space Debris," *Smart Catalog Working Group Session II – Proceedings*, Cooke, Maj. D. G. (Chairman) HQ AFSPACECOM, 25-26 May 1988.

Kessler, D. J., et al., "A Search for a Previously Unknown Source of Orbital Debris: The Possibility of a Coolant Leak in Radar Ocean Reconnaissance Satellites," 48th International Astronautical Congress, IAA-97-IAA.6.3.03, Turin, Italy, October 1997.

Kupiec, I., "Small Object Detection by the LRIR (Haystack)," *Smart Catalog Working Group Session II – Proceedings,* Cooke, Maj. D. G. (Chairman) HQ AFSPACECOM, 25-26 May 1988.

Leushacke, L., G. Ruiz, "Improved TIRA/Effelsberg Bi-Static Beam-Park Campaign 2006," *Presentation at the 24th IADC Meeting,* Tsukuba Space Center, Japan, 10-13 April 2006.

Liou, J.-C., F. Giovane, R. Corsaro, and E. Stansbery, "LAD-C: A Large Area Cosmic Dust and Orbtial Debris Collector on the International Space Station," *Proceedings of "Dust in the Planetary System,"* ESA SP-643, pp. 227-230, 2007.

Markkanen, J., M. Lehtinen, M. Landgraf, "Real-time Space Debris Monitoring with EISCAT," Adv. Space Research, 35 (7), pp. 1197-1209, 2005.

Matney, M. et al., "Extracting GEO Orbit Populations from Optical Surveys," *Proceedings of the 2002 AMOS Technical Conference,* Maui, Hawaii, 2002.

Matney, M. et al., "Calculating Statistical Orbit Distribution Using GEO Optical Observation with the Michigan Orbital DEbris Survey Telescope (MODEST)," *57th International Astronautical Congress,* IAC-06-B6.2.2 (CD-ROM), Valencia, Spain, 2006.

Mehrholz, D., L. Leushacke, and D. Banka, "Beam-park Experiments at FGAN," Adv. Space Research, 34 (5), pp. 863-871, 2004.

Michal, Th., J. Eglizeaud, and J. Bouchard, "GRAVES: The New French System for Space Surveillance," *Proceedings of the 4th European Conference on Space Debris,* ESA SP-587, pp. 61-66, Darmstadt, Germany, August 2005.

Molotov, I., et al., "International Radar Space Debris Research," *Proceedings of the 4th European Conference on Space Debris*, ESA SP-587, pp. 83-88, Darmstadt, Germany, August 2005.

Nishimoto, D. L., "Raven: The Evolution of Small Telescopes," *Proceedings of the 1999 AMOS Technical Conference*, pp. 389-394, Wailea, Maui, Hawaii, 1999.

Nishimoto, D. L., "High Accuracy Networked Orbit Determination System." *Proceedings of the 2002 AMOS Technical Conference*, pp. 48-67, Wailea, Maui, Hawaii, 2002.

Payne, T.P., "Satellite Observation Correlation Processing," *Proceedings of the Third U.S./Russian Space Surveillance Workshop,* pp. 201-210, Washington, DC, October 1998.

Portree, D.S.F., and J.P. Loftus Jr., "Orbital Debris and Near-Earth Environmental Management: A Chronology," NASA-RP-1320, 1993.

Potter, A. and M. Mulrooney, "Liquid Mirror Telescope for Debris Measurement," *Presentation at the 13th IADC meeting*, Houston, Texas, 1997.

Rodriguez. H.M. et al., "Using Light Curves to Characterize Size and Shape of Pseudo-Debris," *Proceedings of the 2006 AMOS Technical Conference* (CD ROM), Wailea, Maui, Hawaii, 10-14 September 2006.

Ruck, G.T. ed., Radar Cross Section Handbook Volumes 1 and 2, New York, Plenum Press, 1970.

Sabol, C. and R. Culp, "Improved Angular Observations in Geostationary Orbit Determination," AIAA 98-4281, 1998.

Sato, K., et al., "MU Radar Observations of Space Debris," *Proceedings of the 4th International Space Conference of Pacific-basin Societies*, pp. 273-282, Kyoto, Japan, November 1991.

Schildknecht, T. et al., "Geostationary Orbit Objects Survey, Final Report," European Space Agency Contract Report 10623/93/D/IM, Bern, Switzerland, 2004.

Schildknecht, T. et al., "Optical Observations of Space Debris in High-Altitude Orbits," *Proceedings of the 4th European Conference on Space Debris*, ESA SP-587, pp. 113 - 118, Darmstadt, Germany, 2005a.

Schildknecht, T. et al., "Properties of the High Area-to-mass Ratio Space Debris Population in GEO," *Proceedings of AMOS 2004 Technical Conference Proceedings*, Wailea, Maui, Hawaii, 2005b.

Seitzer, P. et al., "A Survey for Space Debris in Geosynchronous Orbit," *Proceedings of AMOS 2001 Technical Conference*, Wailea, Maui, Hawaii, 2001.

Seitzer, P. et al., "An Optical Survey for GEO Debris in High Inclination Orbits," *Proceedings of the 2005 AMOS Technical Conference* (CD-ROM), pp. 224-229, Wailea, Maui, Hawaii, 2005.

Settecerri, T. J., et al., "Haystack-Pegasus Debris Measurements," Proceedings of the 1997 Space Control Conference, Project Report STK-249, Vol. II., pp. 93-108, MIT/Lincoln Laboratory, Lexington, Massachusetts, 25-27 March 1997.

Settecerri, T.J., and E.G. Stansbery, Measurements of the Orbital Debris Environment: Comparison of the Haystack and HAX Radars, JSC-27971, August 1997.

Sridharan, R., et al., "Radar and Optical Characterization of an Anomalous Orbital Debris Population," Journal of Spacecraft and Rockets, Vol. 36, No. 5, pp.719-725, 1999.

Stansbery, E.G. and H. Schaeper, "Orbital Debris Radar Design Verification Tests Using ALCOR," *Presentation at the 1990 Space Surveillance Workshop*, MIT/Lincoln Laboratory, Lexington, Massachusetts, 3 April 1990.

Stansbery, E.G., et al., Size and Orbit Analysis of Orbital Debris Data Collected Using the Haystack Radar, JSC-25245, August 1991.

Stansbery, G., et al., "Debris Families Observed by the Haystack Orbital Debris Radar," Acta Astronautica, Vol. 41, No. 1, pp 53-56, 1997.

Stansbery, E. et al., "Meter-Class Autonomous Telescope for Space Debris Research," *Proceedings of the 2003 AMOS Technical Conference* (CD-ROM), Wailea, Maui, Hawaii, 2003.

Stansbery, E. G., and C.L. Stokely, "Identification of a Debris Cloud from the Nuclear Powered SNAPSHOT Satellite with Haystack Radar Measurement," *Presented at the 36th COSPAR*, PEDAS1-002-06, Beijing, China, 2006.

Stokes, G.H. and R. Sridharan, "Contributing Sensor Operations of the Space-Based Visible (SBV)," *Proceedings of the Third U.S./Russian Space Surveillance Workshop*, pp. 27-37, Washington, DC, October 1998.

Stringer, M.E. and R. Teets, "Tools and Databases Used to Maintain the Space Catalog at 1CACS," *Proceedings of the Fourth U.S./Russian Space Surveillance Workshop*, pp. 149-164, Washington, DC, October 2000.

Talent, D. et al, "A Search for Orbital Debris in GEO," *Proceedings of the 2nd European Conference on Space Debris*, ESA SP-393, pp. 99-104, Darmstadt, Germany, May 1997.

Thompson, T.W., et al., "Radar Detection of Centimeter-Sized Orbital Debris: Preliminary Arecibo Observations at 12.5-cm Wavelength," Geophys. Res. Lett., Vol. 19, No. 3, pp. 257-259, 7 February 1992.

Vallado, D. and S. Alfano, "A Future Look at Space Surveillance and Operations," *Proceedings of the Third U.S./Russian Space Surveillance Workshop*, pp. 235-262, Washington, DC, October 1998.

Vardi, Y., and D. Lee, "From Image Deblurring to Optical Investments: Maximum Likelihood Solutions for Positive Linear Inverse Problems," J.R. Statist. Soc., B 55, pp. 569-612, 1993.

Xu, Y.-L., and C.L. Stokely, "A Statistical Size Estimation Model for Haystack and HAX Radar Detections," *56th International Astronautical Congress*, Fukuoka, Japan, 2005.

4.5 Modeling the Orbital Debris Environment

4.5.1 Introduction

Models are used to take the information obtained by measurements and turn them into useful estimates of the population of debris and how they are divided into different orbits and debris types. The idea is to put together as accurate a picture of the past, present, and future environments as possible.

Sometimes, information is needed on the long-term behavior of orbital debris evolution. Future projections are linked to human activities – launch rates and explosion rates. Heavy-duty modeling tools have been developed to answer these types of questions. The modeling tools require information on historical launch and explosion behavior, as well as other models that propagate the orbits, describe the orbital behavior of breakup clouds, and compute rates of accidental collisions and their effects on the environment. Typically, these tools are used to look at how the environment is expected to change over time scales of decades and even centuries. In addition, there needs to be the capability to investigate the effectiveness of changes in behavior (e.g., the effectiveness of mitigation techniques). Due to the complexity of these models, they are not set up for the needs of general users, and are mostly for internal use by the Orbital Debris Program Office. However, the results of these models are often shared and compared with our colleagues in the orbital debris community.

The NASA modeling program of the orbital debris environment began in the late 1970s with simplified, stand-alone breakup models and orbital propagators that included the lowest order terms in gravity and drag. By the mid 1980s these models were combined with intact populations in LEO and pre-computed average explosion and collision rate codes in the model AVERAGE. However, fidelity was compromised in this early program by the requirement to execute within a reasonable amount of time. By the late 1980s, NASA made the commitment of resources to upgrade the AVERAGE code into a higher-fidelity modeling tool. The result was the EVOLVE series of programs.

The EVOLVE series introduced Monte Carlo (MC) processing to estimate future fragmentations for the first time. Five distinct versions of the EVOLVE code were completed over the next decade. All were 1-dimensional models in LEO in the sense that collision events were assigned within spherical altitude shells from 200 to 2000 km altitude. Model development proceeded from a phenomenological representation of debris spatial density with a debris cloud as an altitude, fragment size, and time-dependent mathematical function to a model of individual fragments and intacts, and their propagation. The later versions also included software for testing future post-mission-disposal scenarios and their effect on the future collision rate.

Advances in the supporting models within EVOLVE were driven by added observational data. For the fragmentation model this meant a longer period of object-decay profiling during high and low solar activity and additional ground breakup test data. The main result was a fragment A/M distribution for each size range. A new orbital element propagator was developed by comparing predicted decay files and long-term orbital evolution to actual tracking data of a number of intact objects in orbit. This led to the addition of higher order gravity terms, an oblate Earth, a rotating atmosphere, advanced lunar and solar gravity effects, and solar radiation pressure effects with Earth-shadowing. Other advances included fragment initial ΔV distribution and traffic file upgrades.

The final version of the EVOLVE model included the new propagator and a tagging of collision pairings by type: intact-on-intact, intact-on-fragment, fragment-on-fragment. Still, computation time and array sizes remained a concern and EVOLVE remained a 1-dimensional model in the collision calculation. This restricted the fidelity of the collisional breakup pairings since only pair type could be identified, not individual objects.

In the early 2000s the LEO-to-GEO Environment Debris (LEGEND) model took over as the standard NASA model for long-term orbital debris environment studies. LEGEND includes the traffic, breakup, and LEO propagator models of the final EVOLVE model, but also a geosynchronous orbital element propagator that extends the range of this model. The 3-dimensional character of LEGEND is realized in the propagators noted above, and in the consideration of collision pairs individually. This is done through an efficient and innovative algorithm to evaluate collision probabilities in the 3-dimensional space. This type of calculation requires a much higher level of knowledge than has been needed in the past of launch and maneuver traffic, and also fragmentation orbital position of historical events. This is an ongoing priority for the historical launch and fragmentation event files that are inputs to LEGEND.

In contrast to the evolutionary models, engineering models are tools for estimating the orbital debris populations such that they can be used to predict fluxes on spacecraft and measurement instruments. As such, they need to be much more “user-friendly” than the heavy-duty

LEGEND-type models. The models need to provide the user accurate results in a timely fashion. Two main constituencies compose the user community for engineering models: spacecraft designers and operators, and debris observers. A third user group includes spacecraft designers and analysts using the DAS package. Engineering models form the heart of the DAS orbital debris environment subroutines.

The requirements of each user group differ somewhat, although they share many common requirements, of course. For example, the designer of an oriented spacecraft requires more detailed estimates of the flux than the designer of a randomly oriented or randomly tumbling spacecraft. In the case of the first vehicle, a designer may prefer the flux to be described in terms of azimuth in the local horizontal plane so as to design shielding in the most cost-effective manner. Such detail is not required in the case of a randomly tumbling spacecraft. Both designers, however, would be concerned with the distribution of debris flux as a function of size, altitude, and relative velocity. Because of the long lead times in new satellite designs, the long-term temporal behavior of the debris environment over a satellite life cycle is of interest. In the case of an observer planning a debris observation campaign, results will be dependent upon the inclination distribution of resident space objects visible to the ground-based sensor site and the latitude of the observer. Further complications arise depending upon whether the sensor is fixed in its orientation or is steerable in azimuth and elevation.

Thus, any engineering model must include an accurate assessment of the orbital debris environment as a function of altitude, latitude, and debris size. This means the engineering model needs to be based on debris populations with a variety of orbital and size distributions consistent with the populations around the Earth. The model must be able to provide a complete description of the environment in terms of debris flux onto spacecraft surfaces or debris detection rate observed by a ground-based sensor.

Beginning in the mid 1980s, debris environment curve fits (to the SSN catalog for objects > 10 cm, and to in-situ data of returned surfaces for objects < 10 cm) were derived by NASA for special programs (i.e., Strategic Defense Initiative Program, Space Station Program Office, and various LEO spacecraft programs). A significant requirement of these models was that they be easily executed by a programmable calculator or be capable of manipulation “by hand” in a reasonable amount of time. The last of this type was the NASA90 model.

The ORDEM series began in the mid 1990s with ORDEM96. This series is distinguished by the requirement of a personal computer for effective manipulation. ORDEM96 also implemented curve fits of a pre-modeled environment, but it pioneered the use of debris population ensembles characterized by altitude, eccentricity, inclination, and size.

The second model in the series, ORDEM2000, is the NASA standard today. It adopts debris population ensembles similar to those of ORDEM96, but it replaces the curve fitting technique with a finite element model to represent the debris environment. With an advanced Graphical User Interface (GUI), ORDEM2000 give users NASA's state-of-the-art LEO debris environment represented by informative graphics and concise data files. A third model, ORDEM2008, is currently under development.

4.5.2 Applicability of an Engineering Model

Engineering models are applicable to questions regarding what debris environment a particular spacecraft/sensor might encounter/measure. Some problems, however, are beyond the scope of an engineering model. For example, one cannot evaluate the short-term collision risk from the fragments of a recent breakup event, because the risk is a function of the detailed orbital state vectors of the breakup parent body and the asset spacecraft at the time of breakup. For random breakups, this information is not known *a priori*, so the risks can only be calculated *ex post facto*. However, the long-term effects of breakups integrated over time can be included in a statistical manner within an engineering model.

An engineering model also cannot be used to test the long-term impact of various mitigation measures on the debris environment. However, models that are used to investigate this long-term behavior, such as EVOLVE and LEGEND, are used to help compute future projections of the environment for the engineering models.

4.5.2.1 An Historical Overview of Engineering Models

Engineering models were first assembled for agency internal use. Kessler developed the first debris engineering model for the ISS Program Office [Kessler 1984]. Further models were assembled for the Strategic Defense Initiative Organization and various LEO spacecraft programs [Kessler *et al.* 1989] and, again, the ISS Program Office [Kessler *et al.* 1991]. Each of these models portrayed the environment in terms of curve fits to describe the distributions of large objects (the SSN catalog of objects larger than approximately 10 cm) and small objects (as recorded by the inspection of exposed spacecraft surfaces returned from space). Debris populations in the intermediate size regimes (1 mm to 10 cm in size) were based on model calculations by programs such as EVOLVE. However, there was little data at the time with which to calibrate these models, so the results for some regions and regimes had significant errors. These models were designed to be easily executed by a programmable calculator or be capable of manipulation “by hand” in a reasonable amount of time. The important effects of inclination distribution and velocity/direction dependencies were handled in a very general way.

The need to better define the debris environment eventually outgrew this latter requirement. This was primarily driven by the addition of Haystack radar data in the early 1990s, which, for the first time, gave an accurate assessment of the 1- to 10-cm debris population in LEO. In addition, it became clear from the Haystack data that, in some cases, debris in the centimeter size regime showed qualitatively different orbit distributions from the catalogued populations. ORDEM96 was developed to capture not only the improved centimeter populations, but also the improved knowledge in the distribution of debris in inclination, altitude, and eccentricity [Kessler *et al.* 1996]. In addition, improved computer technology allowed for numerical integration of the debris flux equations to obtain better direction/velocity spacecraft flux distributions. This precluded the use of simple formulae for describing spacecraft flux, but the debris populations in ORDEM96 were still described by a set of analytic equations for each debris population. These debris populations were divided into discrete “families,” each assigned a single value of inclination and eccentricity based on the limited information that was available and to aid in calculations. The analytic equations described the distribution of each inclination “family” in terms of perigee and size distribution, and the future predicted behavior of the population. The resulting model gave a much higher fidelity directional flux distribution that

greatly aided in modifying ISS shield designs and Space Shuttle operational orientations to minimize debris risks.

By the late 1990s it became clear from accumulated Haystack radar observations and Space Shuttle returned surfaces that it was time to update the NASA engineering model. In addition, improvements in computer power and storage made many of the limitations of ORDEM96 no longer necessary. In addition, new techniques were developed to extract higher fidelity orbit data from the available data. The resulting engineering model, released in 2000, is called ORDEM2000 [Liou *et al.* 2002].

4.5.2.2 ORDEM2000

Instead of using a few discrete populations, ORDEM2000 uses a finite element approach with a spatial grid around the Earth, binned in altitude, latitude, and velocity (longitude is considered to be randomized, so there is no explicit dependence). The model describes the orbital debris environment between 10 μm and 1 m in size for altitudes up to 2000 km, projecting out to the year 2030. Size distribution is handled by defining the environment at six key reference sizes (10 μm, 100 μm, 1 mm, 1 cm, 10 cm, 1 m), with other values obtained using interpolation. The flux on an orbital spacecraft is computed by integrating over the complete orbit through the spatial and velocity distribution. ORDEM2000 is currently the standard NASA model and is used by the Space Shuttle Program and the ISS Program. It will be used for future mission designs until it is replaced by the next generation of the engineering ORDEM model.

One of the goals of ORDEM2000 was to make it as data-dependent as possible. This required a number of new tools to statistically extract detailed orbit distributions from the data sets. Ten data sources form the basic database of ORDEM2000 (see details in Table 4.5-1 below):

- SSN catalog
- Haystack and HAX radar data [Settecerri *et al.* 1999]
- Goldstone radar data [Matney *et al.* 1999]
- Impact measurements from the LDEF [Levine 1991, 1992, 1993]
- HST Solar Array (HST-SA) impact data [Drolshagen *et al.* 1997, McDonnell *et al.* 1998a,b]
- EURECA impact data [Drolshagen *et al.* 1996, McDonnell *et al.* 1998a,b]
- Space Shuttle window and radiator impact data [Hyde *et al.* 2000a,b]
- SFU data [Yano 1999, Kuriki *et al.* 1997]
- Mir impact data [Hörz *et al.* 1999, Humes 1998)

The ORDEM2000 model was computed on five of the six pre-calculated, debris population-reference sizes: 10 μm and greater, 100 μm and greater, 1 cm and greater, 10 cm and greater, and 1 m and greater (hereafter referred to as 10-μm, 100 μm, 1 cm, 10 cm, and 1 m populations). Major sources were used to build the debris populations, while the other sources were used to verify and validate the model predictions.

The following major data sources were used to obtain the five populations:

- SSN catalog 1 m and 10 cm reference populations
- Haystack radar data 1 cm reference population
- LDEF measurements 10 μm and 100 μm reference populations

As no direct measurements at 1 mm were available, the 1 mm debris population in the model is based on an interpolation between the 100 μm and 1 cm populations. Goldstone radar data for the 3 mm objects and Space Shuttle returned surface data for the 100-μm to 1-mm-size regime were used to adjust the interpolation.

The model was constructed for a reference date as the reference baseline of the environment, chosen as 1 January 1999. For projections in time, the relative growth rates (not the absolute population estimates) were computed using the EVOLVE 4.0 model [Krisko *et al.* 2000]. For the 1 cm and larger populations, this data was projected forward in time directly. For the micron size debris, the populations were propagated from the LDEF mission time frame (1984-1990) forward in time using the intact population (from the catalog for historical behavior and the future populations using EVOLVE 4.0) as constant sources of debris, with the micron particles evolved in time including the effects of atmospheric drag and solar radiation pressure.

The 10 mm and 100 mm orbit distributions were computed using the LDEF spacecraft data. LDEF was a spacecraft oriented so that the crater distributions on the oriented surfaces preserved information (albeit in a cryptic manner) on the size, velocity, and directional distribution of the meteoroid and orbital debris environment. For ORDEM2000, 13 Space Debris Impact Experiment surfaces (12 sides plus the space-facing side for meteoroids) [Humes 1991, 1993], the Chemistry of Meteoroids Experiment (CME) gold and aluminum plates [Hörz *et al.* 1991, 1992], and 12 aluminum frame intercostal elements that were examined after the mission by the M/D Special Investigation Group were used. Of these, the space-facing Humes experiment and the gold CME surface were able to distinguish meteoroids and debris and thus provide a control to statistically separate the two populations.

Table 4.5-1. The Ten Data Sources

	Size range	Altitude Range (km)	Inc. Range (degree)	Time of Collection
SSN	10 cm to 10 m	200 to 2000	All	up to Dec. 99
Haystack	0.3 cm to 10 m 0.5 cm to 10 m 0.5 cm to 10 m 0.5 cm to 10 m 1.0 cm to 10 m	350 to 1100 350 to 650 350 to 650 700 to 1100 1200 to 2100	40 to 140 28 to 152 32 to 148 32 to 148 40 to 140	91 to 99 91 to 99 91 to 94 94 to 98 93,94,96,97
HAX	1.0 cm to 10 m 0.8 cm to 10 m	450 to 1050 450 to 1050	40 to 140 40 to 140	94 to 97 98 to 99
LDEF[a]	0.01 to 1 mm	330 to 480	All	Apr. 84 to Jan. 90
HST-SA	0.01 to 1 mm	586 to 614	All	Apr. 90 to Dec. 93
EURECA	0.005 to 0.5 mm	502 to 508	All	Aug. 92 to Jun. 93
Space Shuttle[b]	0.1 to 1 mm	300 to 400	All	95 to 98
SFU	10 μm to 1 mm	480	All	Mar. 95 to Jan. 96

Mir	10 to 100 μm	170 to 300	All	Mar. 96 to Oct. 97
Goldstone	2 mm to 2 cm	280 to 2000	32 to 148	Oct. 94 to Oct. 98

[a] LDEF: Space Debris Impact Experiment [D. Humes 1991, 1993], Chemistry of Meteoroid Experiment [F. Hörz 1991, 1992], Interplanetary Dust Experiment - Singer, [Levine 1991, 1992, 1993], LDEF frame - M/D Special Investigation Group [Levine 1991, 1992, 1993].

[b] Space Shuttle: STS-50, 56, 71, 72, 73, 75, 76, 77, 79, 80, 81, 84, 85, 86, 87, 88, 89, 91, 94, 95, 96.

The contributing populations were computed using a version of the Expectation-Maximization (EM) algorithm [Vardi and Lee 1993] originally adapted by NASA for use in computing debris size from RCSs. This proved to be an effective method for extracting statistical populations from measurement data and was applied to both the LDEF and Haystack data, although the detailed implementation differed in each case. The EM algorithm yielded distributions of small debris in terms of velocity (eccentricity) and inclination. These had to be extrapolated from the LDEF altitudes to other altitudes using the EVOLVE model mentioned above.

The Haystack data was used to compute the 1 cm population, and specifically to identify how the population was distributed in perigee, eccentricity, and inclination. Because the state vectors of objects detected with Haystack are not of sufficient accuracy to calculate accurate orbits, the most accurate metric data – range and Doppler range-rate – were used as the input into the EM algorithm. The data from a variety of Haystack pointing angles and range limits totaling over 5000 hours of observations over a period of years were used (Table 4.5-2). The EM analysis yielded 1 cm orbit distributions in eccentricity, perigee, and inclination bins.

Table 4.5-2. Haystack Data Sets Used

Pointing	Time (hours)*	Ranges Used (km)	Range-Rates (km/s)	Years
10 deg South	1279.6	1160 – 2340	+/-11	1991-1999
20 deg South	1534.1	630 – 2570	+/-10	1991-1999
90 deg South	802.0	300 – 2000	+/-6	1991-1998
75 deg East	1270.4	310 – 1620	+/-6	1994-1999
82 deg East	93.8	1200 – 2000	+/-6	1996-1997
20 deg East	149.9	760 – 1740	+/-10.5	1993-1994

**Total hours observed at that pointing direction. Different ranges were observed for different lengths of time over different years.*

The SSN data was relatively easy to use in the formulation for ORDEM2000 because of the detailed orbit information. Size data was extracted from the RCS database also obtained from

the SSN. Because the catalog population at 10 cm was incomplete, ORDEM2000 required some adjustment to bias-correct the population at the 10 cm reference size.

The Space Shuttle returned surfaces data consisted of all measured impacts from the windows and radiators broken out by impact type (debris, meteoroid, or unknown) for STS flights 71, 76, 79, 81, 84, 86, 89, and 91 [Hyde *et al.* 2000a] and STS flights 50, 56, 72, 73, 75, 77, 80, 85, 87, 88, 94, 95, and 96 [Hyde *et al.* 2000b]. Detailed flight timeline information for each mission was used to compute the contribution from all the various flux directions on the relevant surfaces.

When the Space Shuttle results were compared to the preliminary ORDEM2000 fluxes, it became clear that the small particle populations needed to be adjusted to reflect the Space Shuttle's *in situ* from the 1990s which was different from what the LDEF measured in the 1980s. Combining the Space Shuttle's impact data experience along with the Goldstone radar measurements, the overall numbers of elliptical and circular orbits were adjusted, without changing the distributions of either in inclination. Therefore, in the final version, ORDEM2000 used the LDEF for the small particle orbit distributions, and the Space Shuttle and Goldstone data for the actual population numbers.

Data results from ORDEM2000 are shown in Figures 4.5-1 through 4.5-16 that follow.

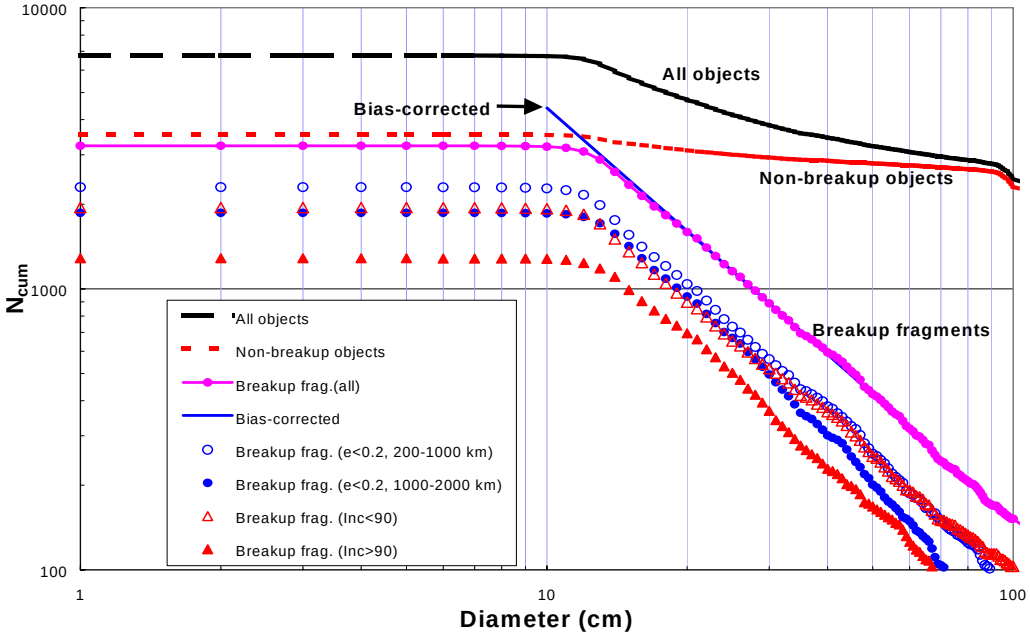

Figure 4.5-1. Cumulative size distribution of LEO-crossing SSN objects in 1999.

ORDEM2000 uses the bias correction to estimate the 10 cm population

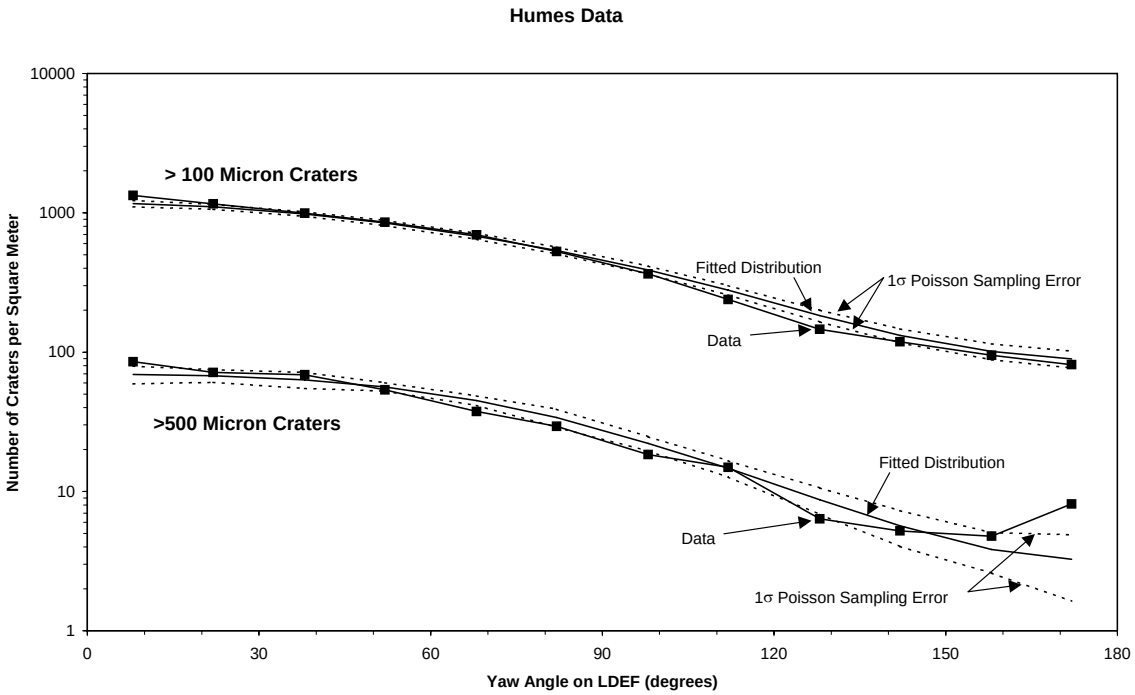

Figure 4.5-2. Crater feature distributions at two different limiting sizes.

Various Humes surfaces along the LDEF sides as a function of yaw angle. Both the fit and the data represent a mix of meteoroids and debris.

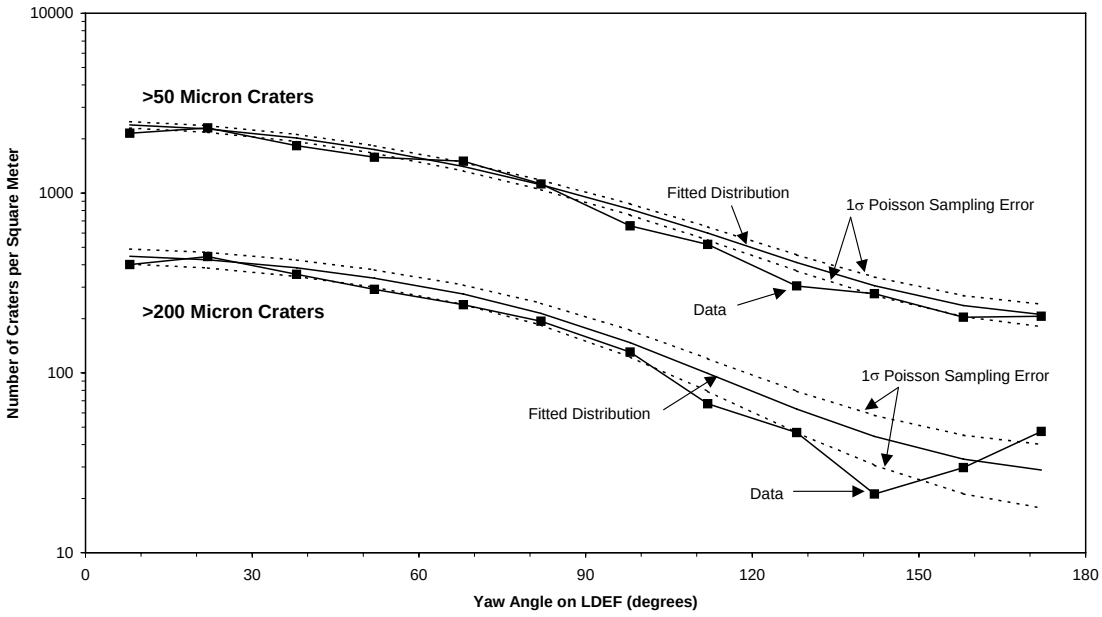

Figure 4.5-3. Crater feature distributions at two different limiting sizes.

Various intercostal surfaces along the LDEF sides as a function of yaw angle. Both the fit and the data represent a mix of meteoroids and debris.

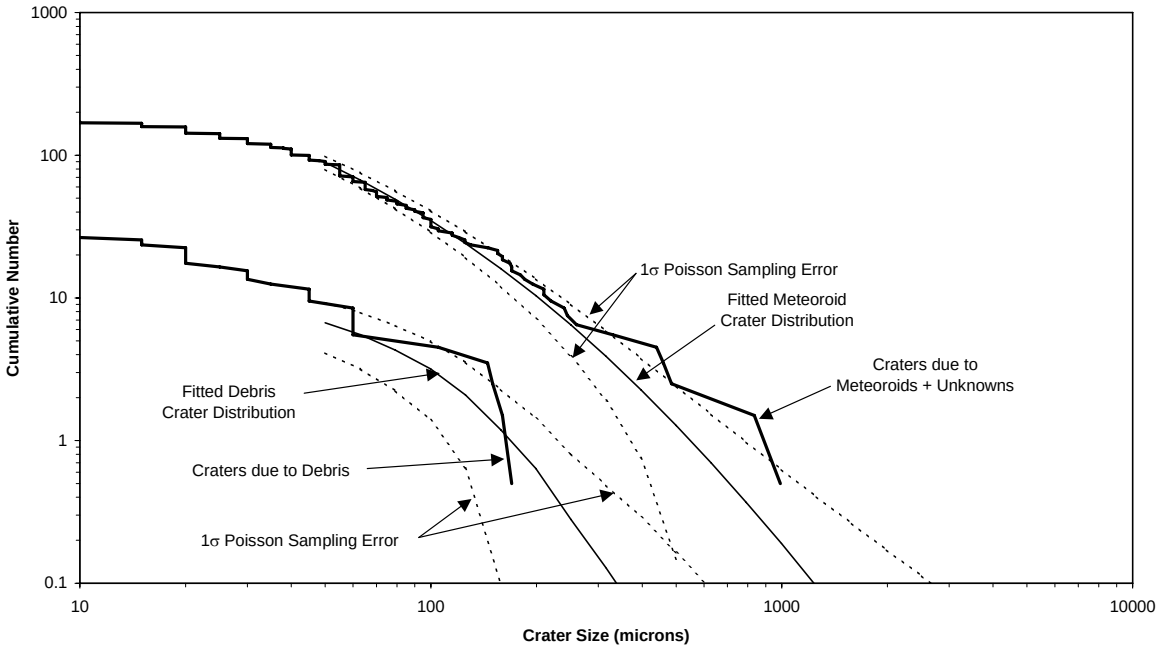

Figure 4.5-4. Crater feature distributions on CME gold surface on the rear side of LDEF.

Broken out by craters made by debris only and meteoroids only (meteoroids + unknowns). This is the only LDEF surface other than the space-facing surface that can unambiguously determine between meteoroids and debris (based on reasonable assumptions). The fitted curves are also shown for debris only and meteoroids only.

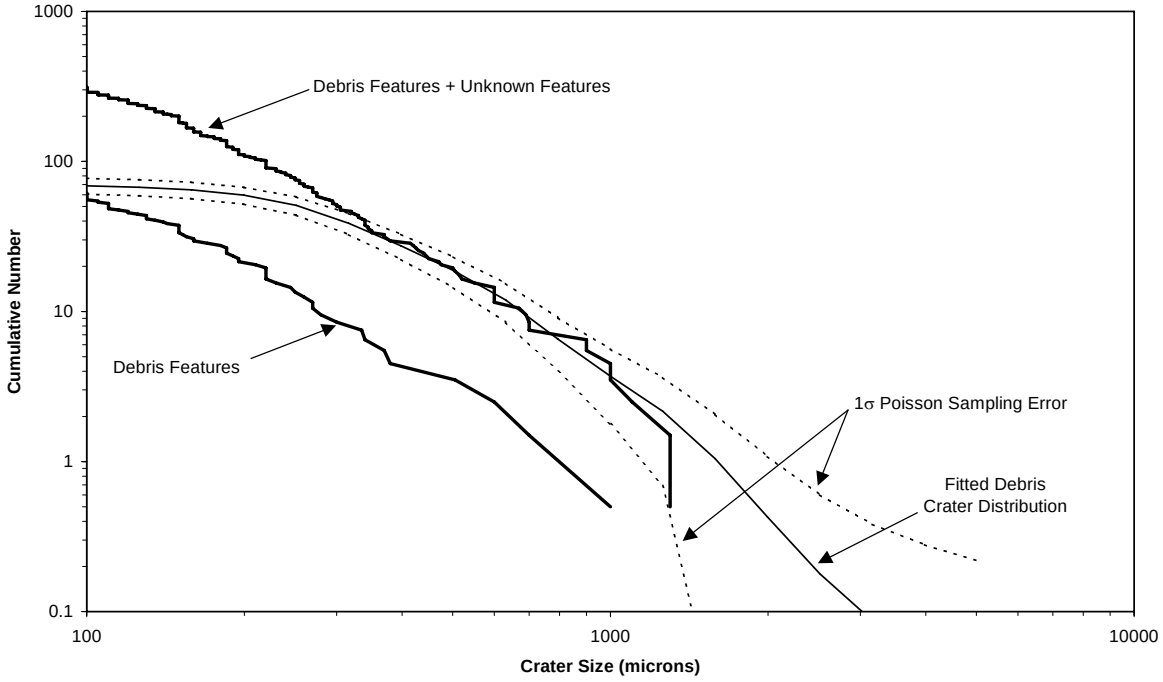

Figure 4.5-5. On the LDEF CME aluminum surface.

Craters identified as "unknowns" could be due to either meteoroids or debris. The true debris crater distribution should lie somewhere between "debris only" and "debris + unknowns." As can be seen in this figure, the fitted debris distribution stays between these two extremes. The fit also implies that the largest "unknown" craters are caused by debris, but the smallest ones are dominated by meteoroids.

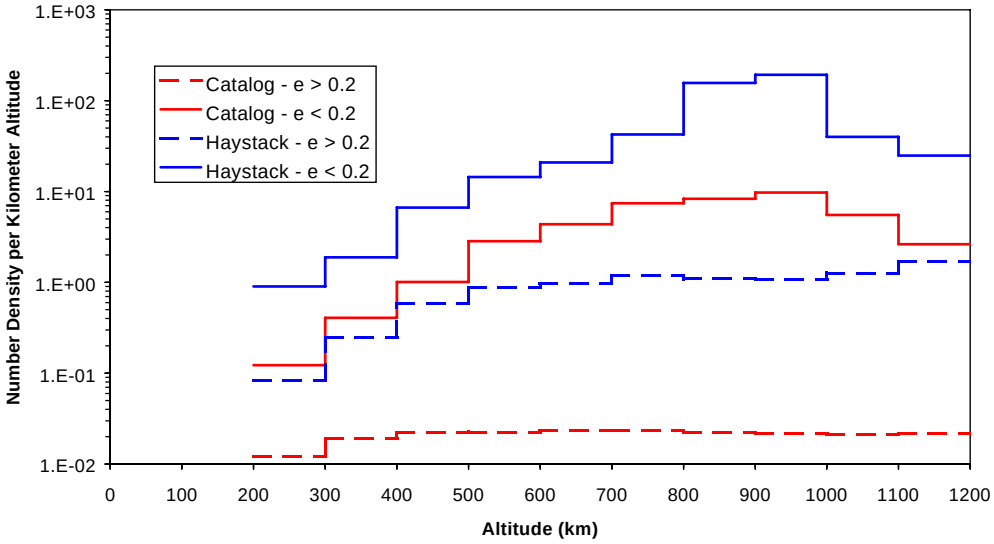

Figure 4.5-6. The 1 cm orbit families estimated from Haystack data using the EM method.

Distributions have been broken out by eccentricity and the spatial density with altitude is shown in comparison to the equivalent populations in the catalog.

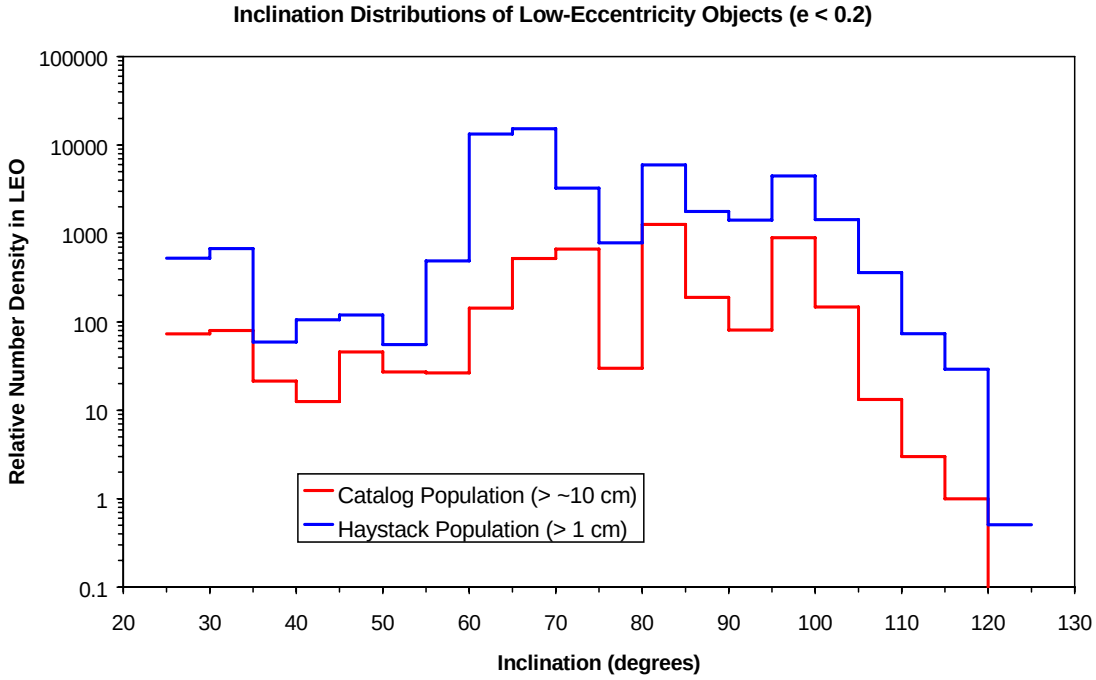

Figure 4.5-7. The 1 cm orbit families estimated from the Haystack data have been broken out by inclination for the low-eccentricity population.

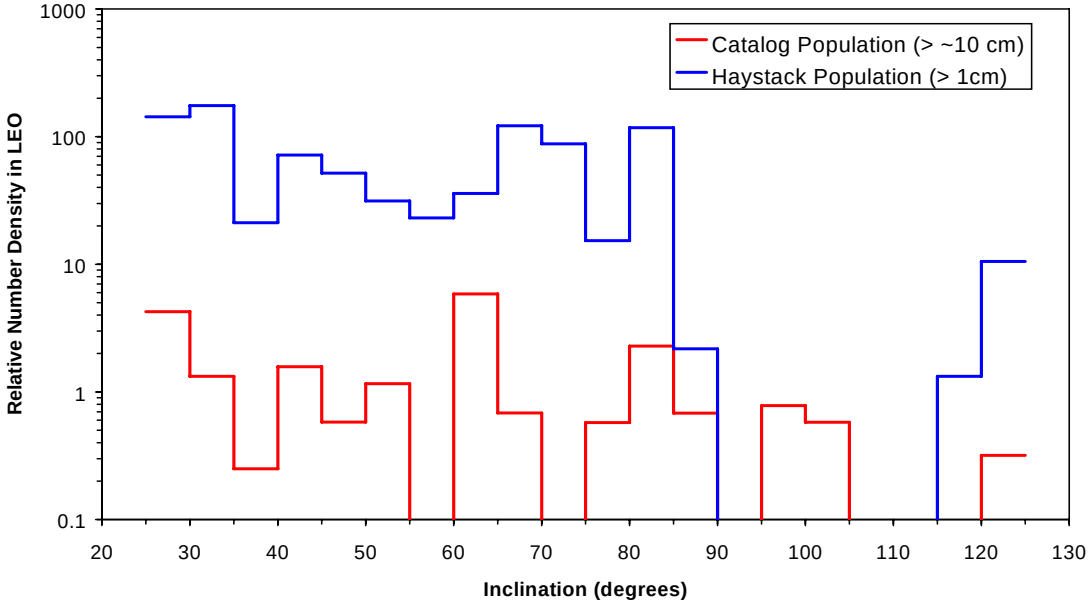

Figure 4.5-8. The 1 cm orbit families estimated from the Haystack data have been broken out by inclination for the high-eccentricity population.

The Haystack population shows a relatively high relative population of elliptical orbits, especially at low inclinations.

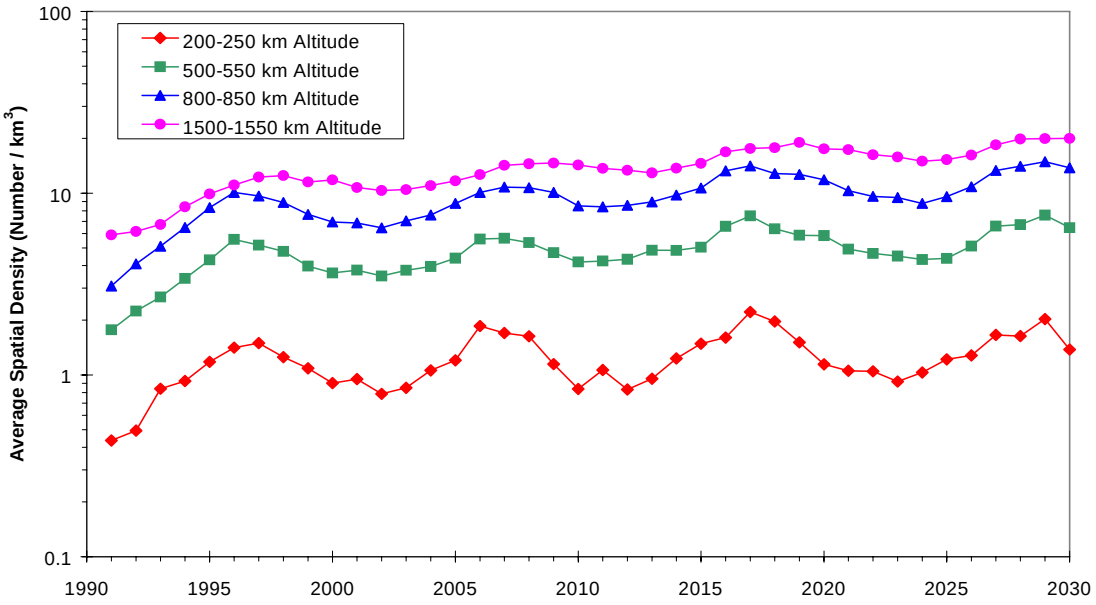

Figure 4.5-9. ORDEM2000 spatial density variation between 1991 and 2030 for debris >10 μm in size.

The densities are benchmarked from in situ data in the 1980s and 1990s, and the future projections are estimated using a small-particle production model based on future traffic estimates.

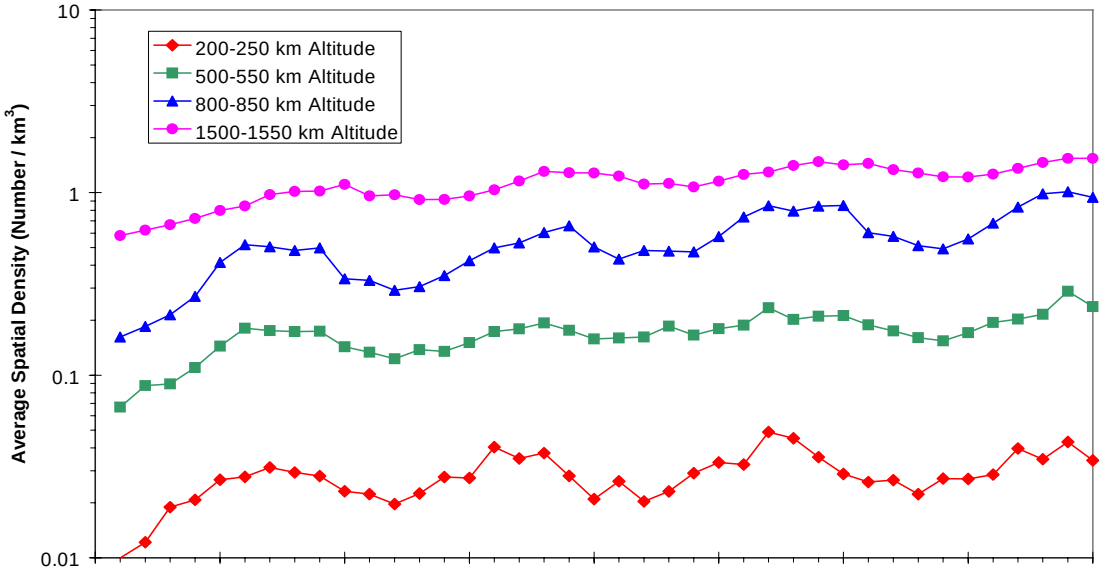

Figure 4.5-10. The ORDEM2000 spatial density variation between 1991 and 2030 for debris >100 μm in size.

The densities are benchmarked from in situ data in the 1980s and 1990s, and the future projections are estimated using a small-particle production model based on future traffic estimates.

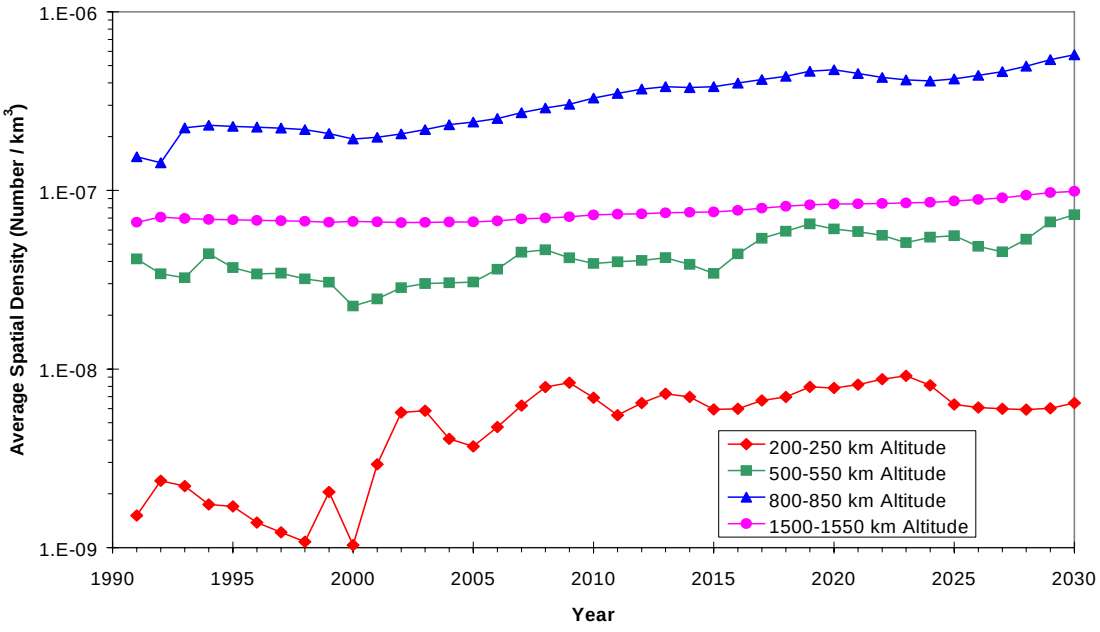

Figure 4.5-11. The ORDEM 2000 spatial density variation between 1991 and 2030 for debris >1 cm in size.

The densities are benchmarked from Haystack data in the 1990s and the future projections are estimated from EVOLVE.

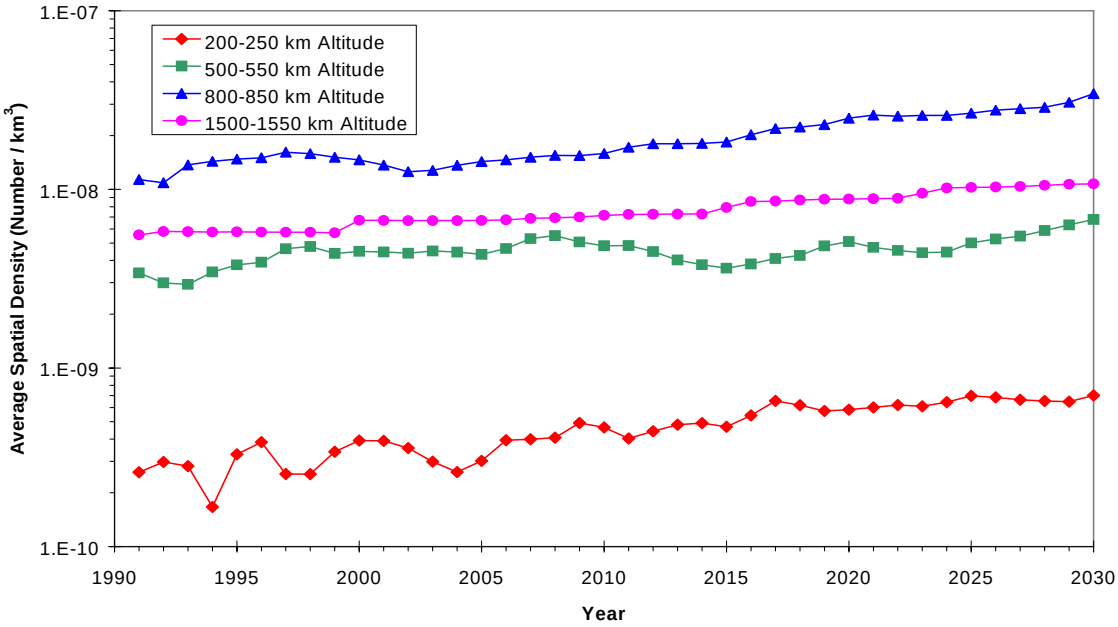

Figure 4.5-12. Spatial density variation between 1991 and 2030 for debris >10 cm in size.

The densities are benchmarked from the SSN data and the future projections are estimated from EVOLVE.

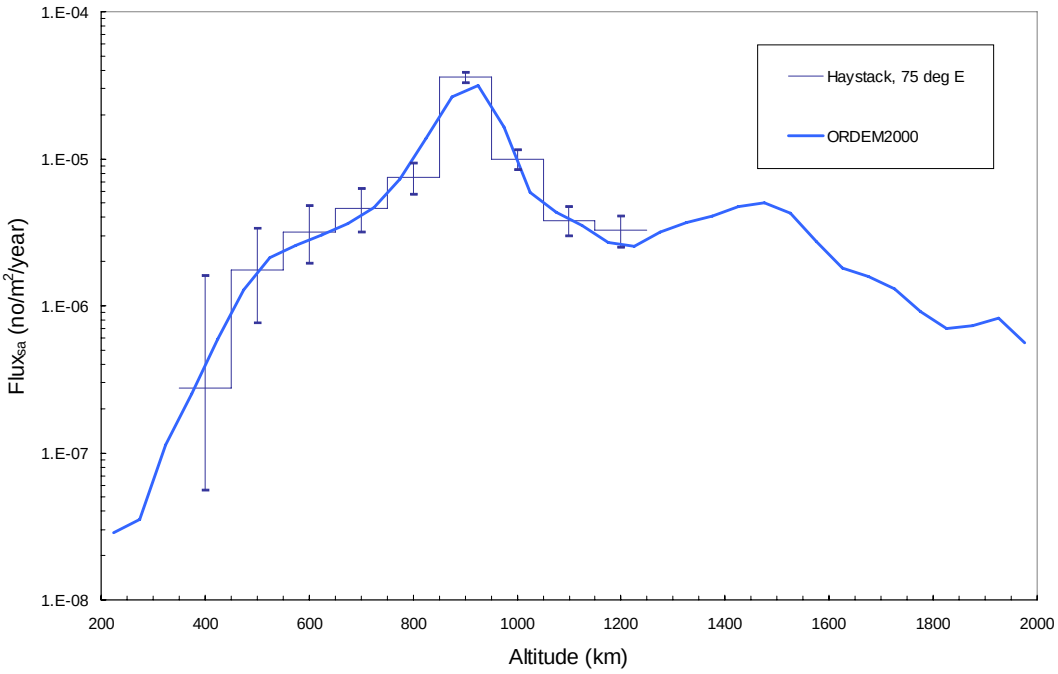

Figure 4.5-13. ORDEM2000 vs. Haystack data (1998, objects ≥1 cm).

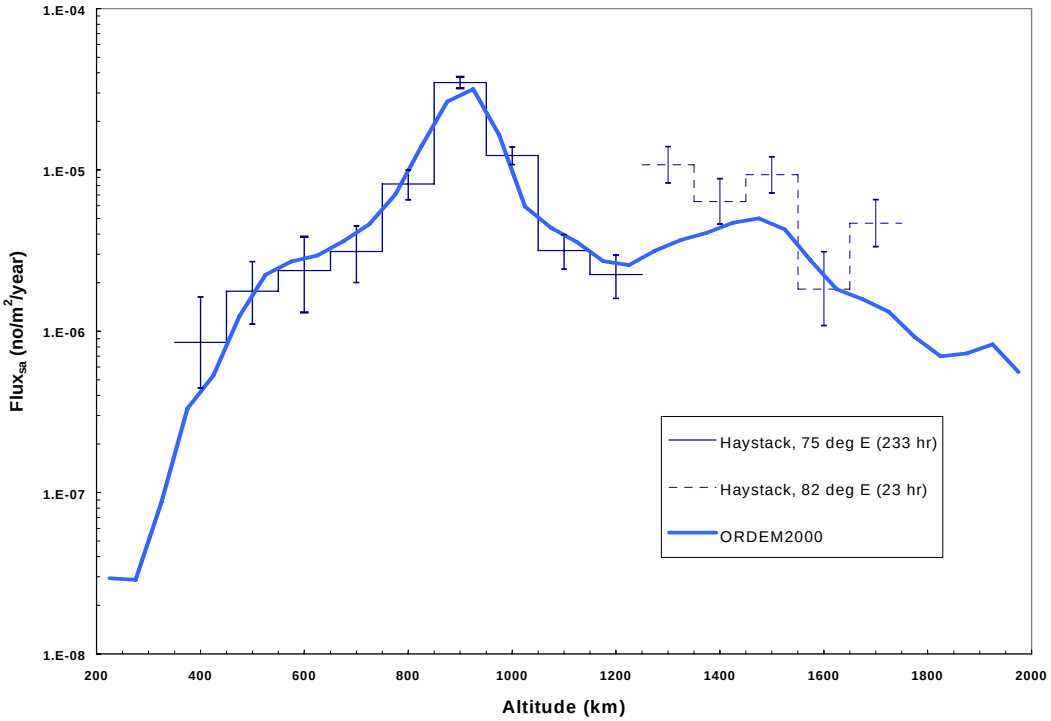

Figure 4.5-14. ORDEM2000 vs. Haystack data (1997, objects ≥1 cm).

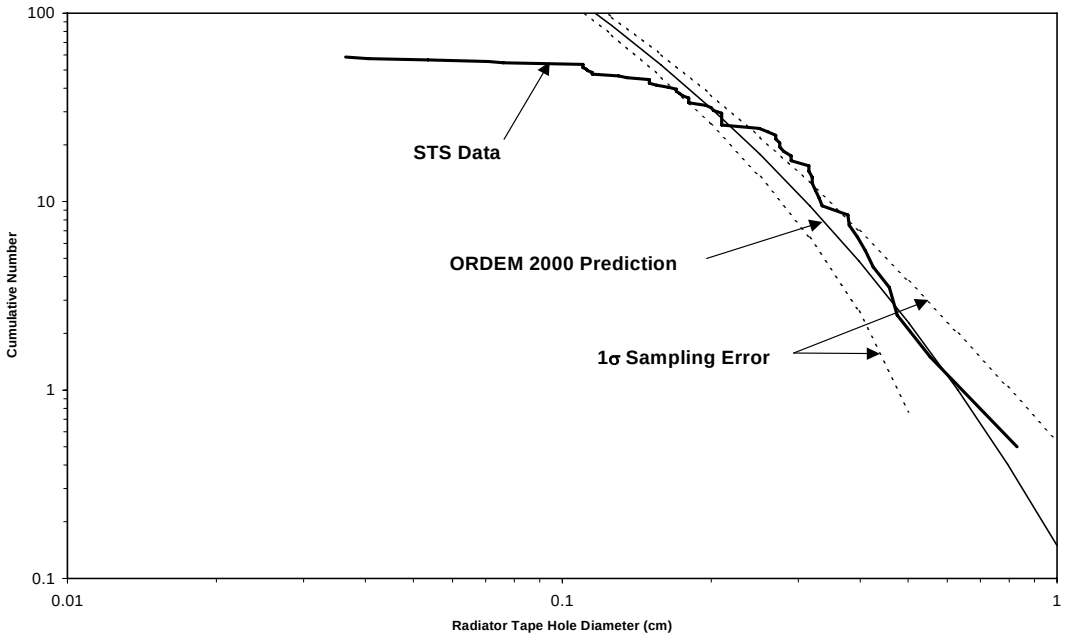

Figure 4.5-15. ORDEM2000 predictions of the Space Shuttle radiator tape-hole-diameter distributions.

These data consist of those impacts known to be debris from their chemistry. The fit originally derived from LDEF data was adjusted to fit this data set.

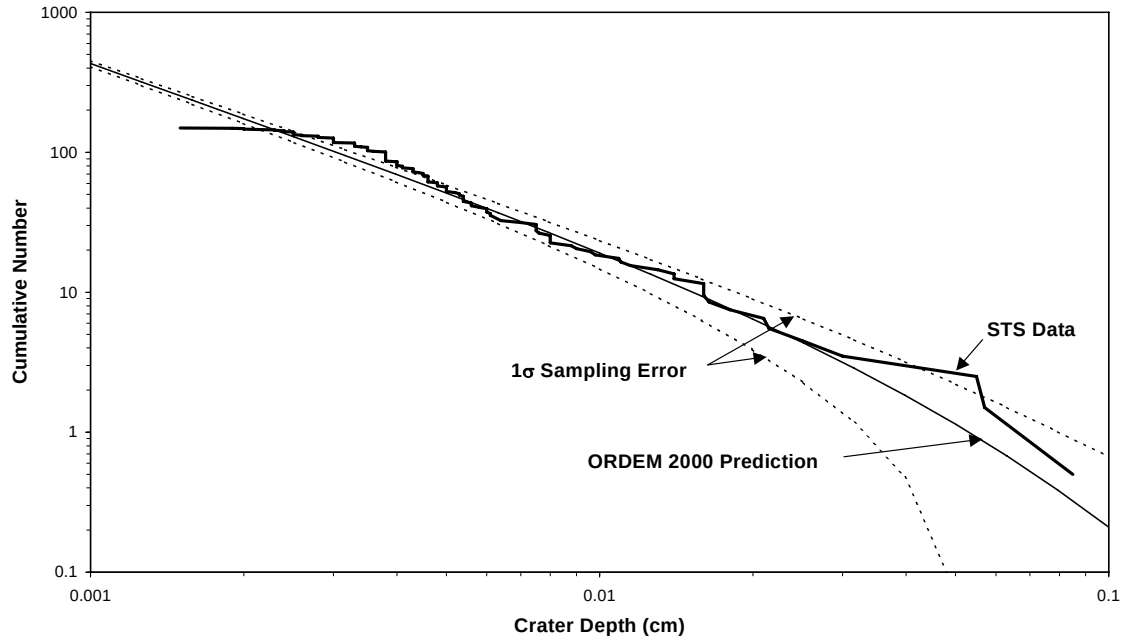

Figure 4.5-16. ORDEM2000 population predictions of the Space Shuttle window crater-depth distributions.

These data consist of those impacts known to be debris from their chemistry. The fit originally derived from LDEF data was adjusted to fit this data set.

4.5.2.3 ORDEM2008

NASA is in the process of developing the next generation of ORDEM models. There are several reasons for this. The most important is that the future predictions of the changing orbital debris environment are always uncertain, so engineering models need to be updated at regular intervals to conform to new measurements. In addition, new types of measurements become available over time, adding new insight into the environment. Also, new analysis techniques become available to better analyze new and existing data.

For ORDEM2008, there is an interest in quantifying some factors that are known to be important for risk analyses, but have been difficult to obtain so far. One of these is an estimate of the uncertainty in the hazard calculations. This requires an estimate of the uncertainty in the modeled populations and the accompanying measurements and estimates of the uncertainties in the calculations themselves.

Another desired feature is information on the makeup of debris – their shape and material composition. At this stage, the plan is to include uncertainty estimates in the flux results and include a simple model of debris material types. Research is ongoing to determine if it is feasible to include debris shapes as well.

The new model will cover an altitude range of 200 to 39,000 km. This will include the GEO regime. Table 4.5-3 summarizes the types of information planned to be in the ORDEM2008. Note that the size limits are altitude-dependent, reflecting a lack of knowledge of small debris populations in higher altitude regimes.

Table 4.5-3. Summary of ORDEM2008 coverage

Altitude range	200 to 39,000 km	
Time range	1995 to 2035	
Size range	200 - 600 km alt	≥10 μm
	600 - 2000 km alt	≥1 mm
	2000 - 33,000 km alt	≥1 cm
	33,000 - 39,000 km alt	≥10 cm
Reference epoch	1/1/2006	

As with previous engineering models, ORDEM2008 will be able to compute fluxes on spacecraft. However, previous models were limited to calculations in the LEO environment, where the debris fluxes were mostly confined to the local horizontal plane. ORDEM2008 will not have this restriction. The model is expected to be completed for beta testing soon.

4.5.2.4 Other agencies' equivalent models

To date there are two engineering models series in the public domain that have been designed for the same purpose as that of the ORDEM model series – to provide satellite operators with an accurate and quick estimate of the present and future vulnerability of their vehicles to debris. The first model was developed by ESA, called the Meteoroid and Space Debris Terrestrial Environment Reference (MASTER) model. The other, developed by ROSCOSMOS, is called the Space Debris Prediction and Analysis (SDPA) model. The versions concurrent with ORDEM2000 are MASTER 2001 and SDPA 2000.

The MASTER model describes the man-made and natural particulate environment of the Earth and its incident flux on user-defined target orbits down to an impactor diameter of 1 μm. All relevant meteoroids and debris source terms are also considered.

Apart from spent payloads and upper stages (TLE background), MASTER 2001 considers fragmentation from on-orbit collisions and explosions, dust and slag from SRM firings, NaK coolant droplets from RORSAT satellites, surface degradation particles (paint flakes), ejecta, and West Ford needles (as part of the TLE population).

For each simulated source, a corresponding debris generation model in terms of mass/diameter distribution, additional velocities, and directional spreading has been developed. A comprehensive perturbation model was used to propagate all objects to the reference epoch of 1 May 2001.

The MASTER model offers a full 3-dimensional description of the terrestrial debris distribution reaching from LEO ($r > 6564$ km) up to the GEO region ($r < 45164$ km). Flux results relative to an orbiting target or to an inertial volume can be resolved into source terms, impactor characteristics, and orbit, as well as impact velocity and direction. Simultaneously, a 3-dimensional flux analysis with respect to any two of these parameters is possible.

The SDPA model is a semi-analytical, stochastic model for the medium- and long-term forecast of the man-made debris environment (with sizes larger than 1 mm), for construction of spatial density and velocity distributions in LEO and GEO, as well as for risk evaluation. The latest

version, SDPA 2000, consists of ten individual modules related to the aforementioned tasks. The total characteristics of space debris of the different sizes are considered (without partition of these characteristics into specific sources). The current space debris environment is characterized by the spatial density dependence on the altitude and latitude of a point, as well as on size of objects, and by the statistical distribution of the magnitude and direction of a space object's velocity in an inertial geocentric coordinate system. These characteristics are constructed on the basis of the complex application of the accessible measuring information and series of *a priori* data. Basic files of the space debris' initial state are prepared by the SDPA 2000 model and then used as inputs to an engineering version of the model, SDPA-E. This information is generally provided to spacecraft operators for their risk analysis.

As noted in Table 4.5-4 , the model regions of applicability vary. For example, ORDEM2000 is a LEO model only, while both MASTER 2001 and SDPA 2000 extend to the GEO region. All three models also extend to different, small-size regimes: MASTER 2001 to 1µm, ORDEM2000 to 10 µm, and SDPA 2000 to 1 mm.

Table 4.5-4. A Comparative Survey of Model Characteristics

	ORDEM2000	MASTER 2001	SDPA 2000
Minimum size	10 µm	1µm	1 mm
Upper altitude border	2000 km	37000 km	36200 km
Elliptical debris orbits implemented	Yes (if Ha < 3000 km)	Yes	Yes (if Ha < 3000 km)
Elliptical target orbits possible	Yes (if Ha < 2000 km)	Yes	Yes (if Ha ≤ 2000 km)
Source terms	Primarily an empirical fit to data, avoiding source term assumptions as much as possible	TLE breakup frag's paint flakes NA/K SRM slag SRM dust ejecta West-Ford Needles	Sum of all source terms
Modeling approach	Fit to measurement data, populations template define environment around the Earth	Semi deterministic including some measurement data	Semi-analytical, stochastic

A major comparison study of the models was completed by the IADC in 2003. The analysis entailed parametric studies that applied the models to a number of target orbits specified by grids in terms of:

- impactor size
- perigee altitude
- inclination
- eccentricity

The models were applied where they were valid, as displayed in the following tables.

Table 4.5-5. Impactor Size Grid

Model	>1 μm	>10 μm	>100 μm	>1mm	>1 cm	>10 cm
ORDEM2000	no	yes	yes	yes	yes	yes
MASTER 2001	yes	yes	yes	yes	yes	yes
SDPA 2000	no	no	no	yes	yes	yes

Sixteen grid points covered perigee altitudes between 300 km and 2000 km with a step size of 100 km.

Table 4.5-6. Perigee Altitude Grid

Model	perigee grid applicable	exceptions
ORDEM2000	yes	eccentricity must be such that Ha $\leq$ 2000 km
MASTER 2001	yes	none
SDPA 2000	yes	eccentricity must be such that Ha $\leq$ 3000 km

Fifteen inclination grid points covered inclinations between 0° and 140° with a step size of 10°.

Table 4.5-7. Inclination Grid

Model	inclination grid applicable	exceptions
ORDEM2000	yes	none
MASTER 2001	yes	none
SDPA 2000	yes	none

Four eccentricity grid points included e=0.0, e=0.1, e=0.5, and e=0.73, with argument of perigee set to 180°.

Table 4.5-8. Eccentricity Grid

Model	e=0.0	e=0.1	e=0.5	e=0.73	exceptions	μ= 180°
ORDEM2000	yes	yes	no	no	See Table 4.5-6	yes
MASTER2001	yes	yes	yes	yes	none	yes
SDPA 2000	yes	yes	no	no	See Table 4.5-6	yes

The study also included four orbit case studies of particular interest:

- ISS (hp = 400 km, i = 51.5°; e =0)
- STS (hp = 380 km, i = 28.5°; e =0)
- sunsynch (hp = 780 km, i = 98.5°; e =0)
- GEO (hp = 42165, i =0°; e =0)

The metrics of comparison for all these studies are listed in Table 4.5-9.

Table 4.5-9. Study Metrics

FLUX vs.	min	max	classwidth	scale
impactor diameter	10 micron	10 meters	N/A	log
impact velocity	0 km/s	18 km/s	0.5 km/s	lin
impact azimuth angle	-180°	180°	5°	lin
impact elevation angle	45°	45°	2°	lin

The flux vs. elevation angle results applied to MASTER2001 and SDPA2000 only. For ORDEM2000 the elevation dependency is specified in the Telescope Assessment/Telescope Arbitrary Pointing mode only, which was not applied in this comparison.

Results from each model displayed the regions of agreement and disagreement among them. These have been the only comparative tests of the models to date. The section that follows relates these comparisons.

4.5.2.5 Similarities and Differences Among Model Results

The main differences between the three model results lie in the flux vs. particle diameter distributions, with ORDEM2000 predicting fluxes higher than MASTER 2001 and SDPA 2000 for particles smaller than 1 cm with differences of up to one order-of-magnitude. For particle sizes > 1 cm, ORDEM2000 produces fluxes similar or somewhat smaller than the other models. For particle sizes > 10 cm, the models are in general agreement. These observations are demonstrated for the case of the e=0.0 orbits below (Figure 4.5-17, Figure 4.5-18, Figure 4.5-19), over the range of inclinations and perigee altitudes in the study.

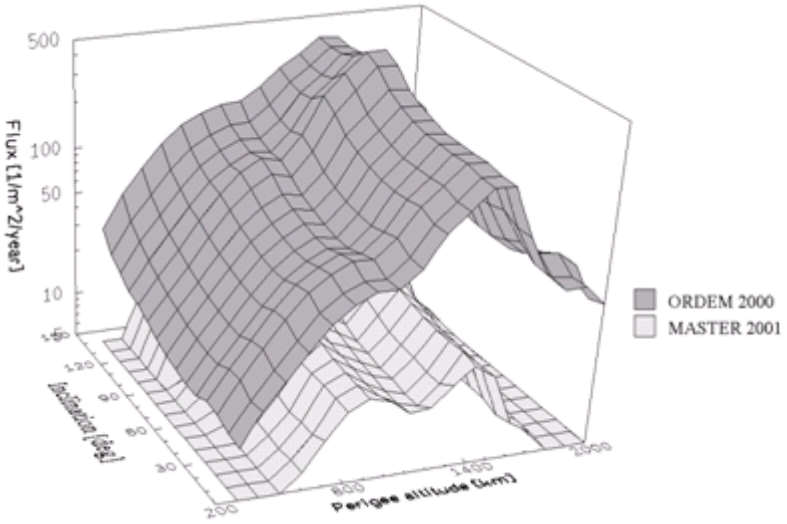

Figure 4.5-17. Flux of particles larger than 100 µm for eccentricity = 0.

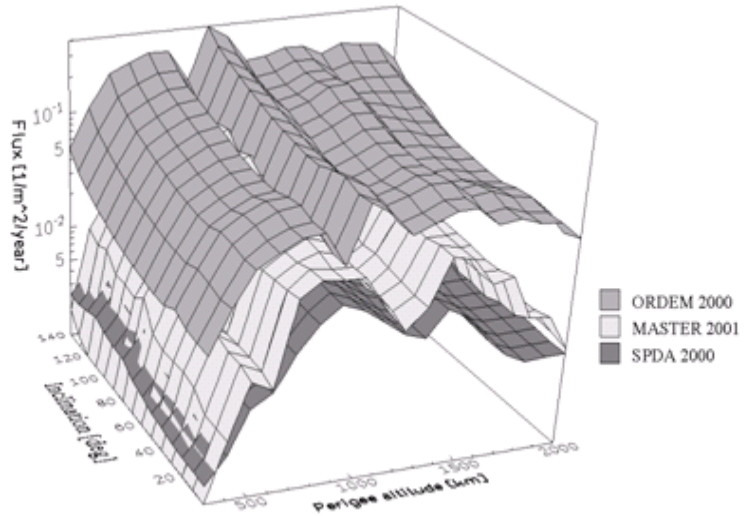

Figure 4.5-18. Flux of particles larger than 1 mm for eccentricity = 0.

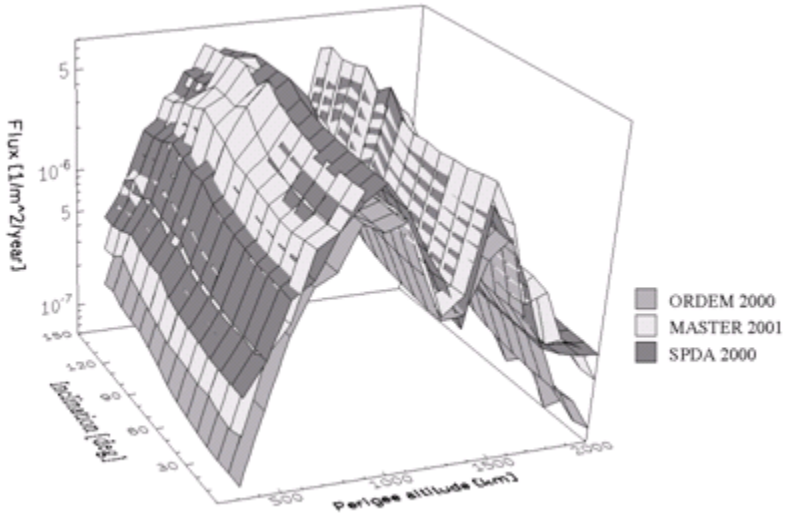

Figure 4.5-19. Flux of particles larger than 10 cm for eccentricity = 0.

This behavior is also noted in the individual cases studied. This example of the ISS orbit is illustrative of the other cases.

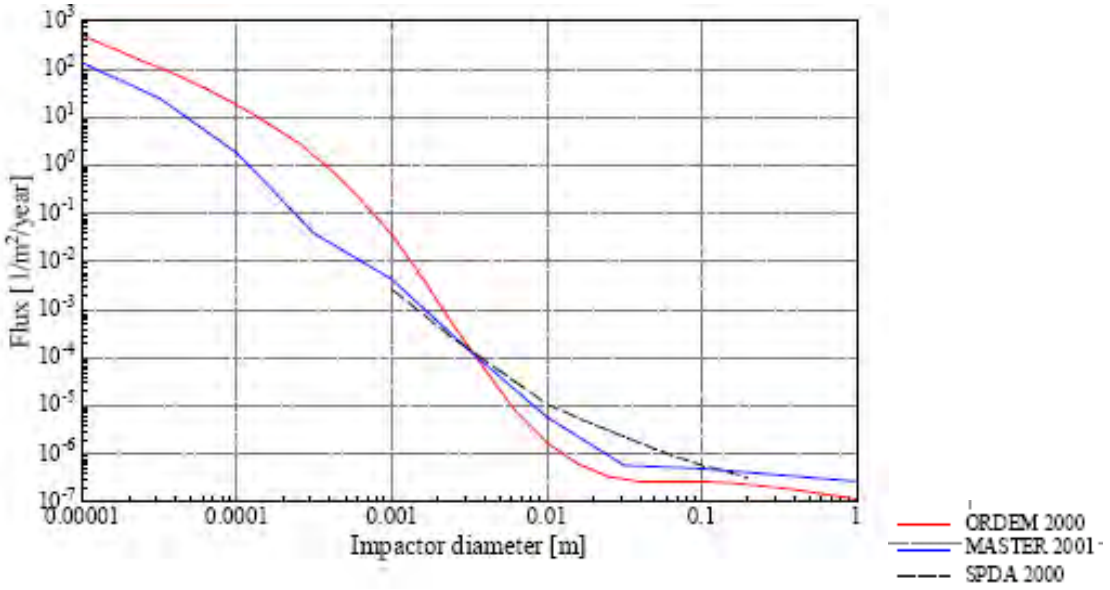

Figure 4.5-20. Model debris fluxes at ISS orbit (400 km altitude, 51.5 deg inclination).

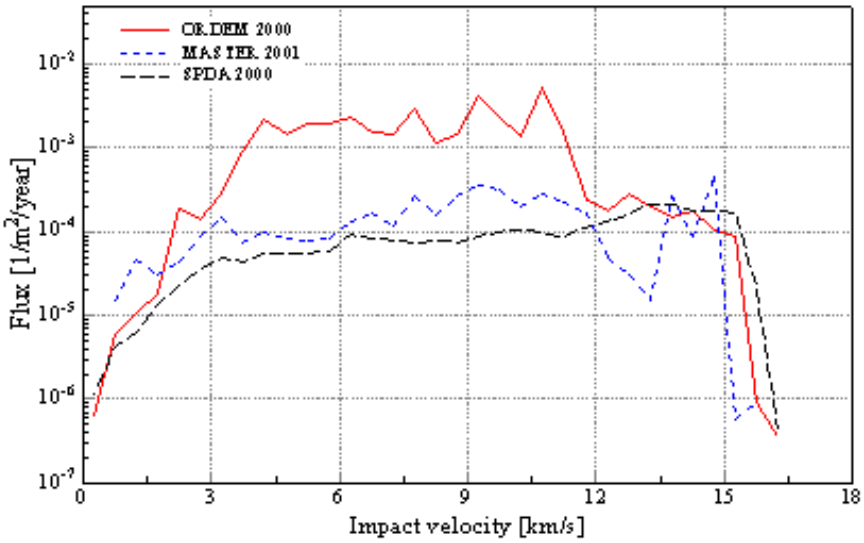

Figure 4.5-21. Flux versus impact velocity of particles larger than 1 mm.

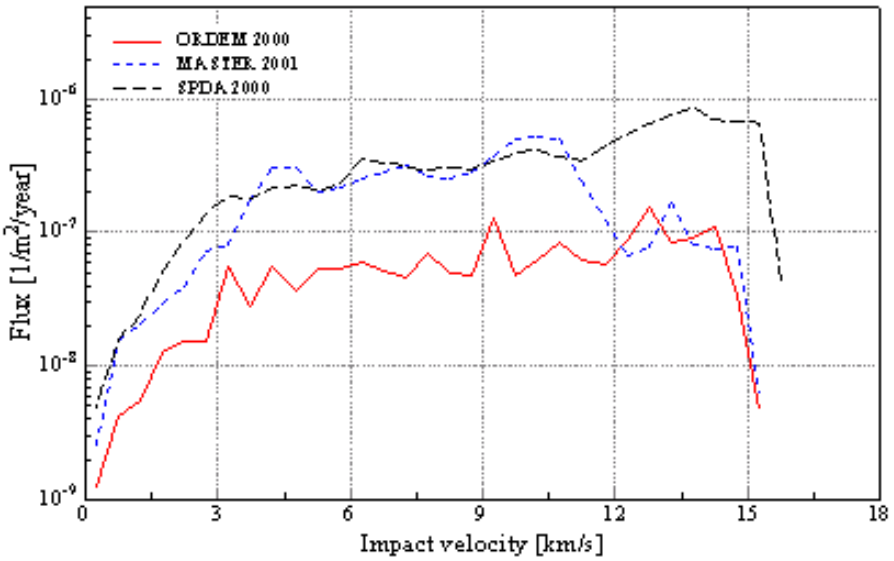

Figure 4.5-22. Flux versus impact velocity of particles larger than 1 cm.

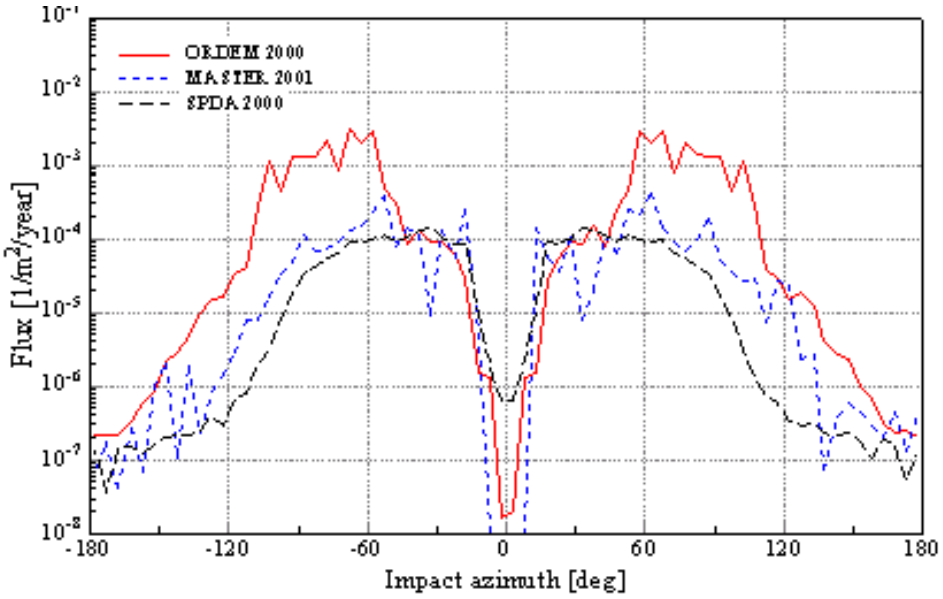

Figure 4.5-23. Flux versus impact azimuth angle of particles larger than 1 mm.

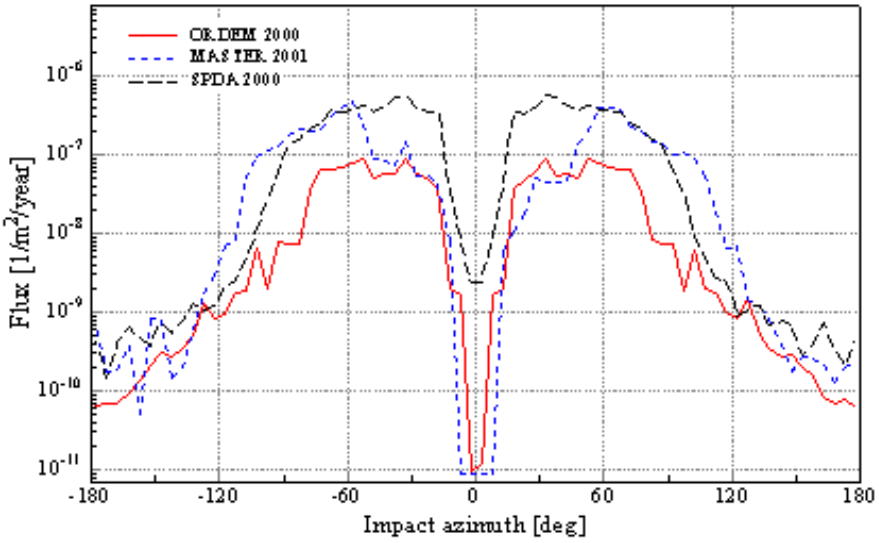

Figure 4.5-24. Flux versus impact azimuth angle of particles larger than 1 cm.

In all cases in Figure 4.5-20, Figure 4.5-21, and Figure 4.5-22 it is clear that the ORDEM2000 environment has a much higher flux below 1 cm then that of either MASTER 2001 or SDPA 2000. ORDEM2000 has a generally smaller flux above 1 cm.

It is important to remember that each model uses different approaches to model the debris population and represents a different snapshot of the environment.

4.5.3 LEGEND

4.5.3.1 History of LEGEND

To continue to improve the knowledge of the orbital debris environment, in 2001, the NASA Orbital Debris Program Office initiated an effort to develop a new debris evolutionary model to replace EVOLVE. The first generation of the EVOLVE model was written in 1986 [Reynolds 1991]. Over the years, several major upgrades were developed and implemented into the main model and supporting models [Reynolds and Eichler 1995, Reynolds *et al.* 1998, Krisko *et al.* 2000]. EVOLVE was a 1-dimensional model describing the LEO debris environment between 200 and 2000 km altitude. For more than a decade it was a leading model providing critical insights into the orbital debris environment. It was also the tool supporting the development and publication of NSS 1740.14 in 1995 [Reynolds 2001].

The motivations to build a new model to replace EVOLVE were twofold. First, a 1-dimensional description and treatment of LEO debris populations might not be adequate to address all issues. For example, the spatial density of debris at the same altitude can vary significantly as a function of latitude. In addition, populations such as objects in GEO and recent breakup fragments from parent objects in sun-synchronous orbits all have strong longitudinal dependence. To describe the orbital debris environment and to analyze its future behavior (such as collisions) with high fidelity, a 3-dimensional model is needed. Second, as the debris populations continue to grow, there is a need to build a full-scale debris model describing the near-Earth environment from LEO to MEO and to GEO. The dated program structure of EVOLVE and the patches added to the model over the years made it difficult to upgrade. It was a more efficient approach to simply start over and totally replace EVOLVE with a new model.

The new model, LEGEND, was completed in 2003. It is capable of simulating the historical and future debris populations in the near-Earth environment [Liou *et al.* 2004, Liou 2006]. The historical simulation in LEGEND covers the period from 1957 to the present epoch. The model adopts a deterministic approach to mimic the known historical populations. Launched rocket bodies, spacecraft, and mission-related debris (rings, bolts, etc.) are added to the simulated environment based on a comprehensive NASA Orbital Debris Program Office internal database. Known historical breakup events [Johnson *et al.* 2004] are reproduced, and fragments down to 1 mm in size are created with the NASA SBM, which describes the size, A/M, and velocity distributions of the breakup fragments [Johnson *et al.* 2001]. All objects are propagated forward in time while decayed objects are removed from the environment immediately. The simulation program outputs the orbital elements and other physical properties of the objects at the end of each year for post-processing analysis. The future projection component of LEGEND covers 200 years from the end of the historical simulation. Orbit propagation is handled in a way identical to the historical simulation.

Explosion probabilities of future rocket bodies and spacecraft are based on an analysis of launch history and recent explosions. The explosion probability of each vehicle is reduced to zero after 10 years of on-orbit lifetime. Vehicles with a history of explosion, but which have had the breakup causes fixed, are not included in future explosion consideration. Collision probabilities among objects are estimated with a fast, pair-wise comparison algorithm in the projection component [Liou 2006]. Only objects 10 cm and larger are considered for potential collisions. This size threshold is historically the detection limit of the SSN sensors, and more than 95% of

the debris population mass is in objects of 10 cm and larger. Fragments down to 1 mm in size are generated based on the NASA SBM and are added to the simulated environment afterward. Each breakup fragment is assigned a unique identification character to track its origin: explosion, intact-intact collision, intact-fragment collision, or fragment-fragment collision.

The LEGEND future projection adopts an MC approach to simulate potential future on-orbit explosions and collisions. The procedure of this MC approach is simple and straightforward. Within a given projection time step, typically set to 5 days, once the explosion probability is estimated for an intact object, a random number is drawn and compared with the probability to determine if an explosion would occur. A similar procedure is applied to collisions for each pair of target and projectile involved within the same time step. Parent objects are removed from the environment once fragments are generated. Due to the nature of the MC processes, multiple projection runs must be performed and analyzed before reliable and meaningful conclusions can be drawn from the outcome. A statistical study of LEGEND, based on the standard bootstrap method, indicates that the mean from 100 MC runs leads to a standard error of the mean, at the end of a 100-year projection, on the order of 1% or less [Liou 2006]. Therefore, averages from 100 MC runs in general should be statistically sound and reliable.

4.5.3.2 Where LEGEND Is Now

4.5.3.2.1 Breakup Model

One of the key components of a debris evolutionary model is the satellite breakup model. This is needed to simulate the outcome of historical and future explosion and collision breakups. The 2001 NASA SBM is based on well-observed, on-orbit explosions and collisions, and ground-based experiments [Johnson *et al.* 2001]. The former includes Landsat and Nimbus explosions and P-78 collisions, while the latter included the Satellite Orbital Debris Characterization Impact Test and HVI experiments. Fragment size distribution, A/M distribution, and their velocity distribution with respect to the parent satellite were derived from a careful analysis of all available data. Figure 4.5-25 and Figure 4.5-26 show the cumulative size distributions of explosion and collisions fragments, respectively, between the data and the final NASA model.

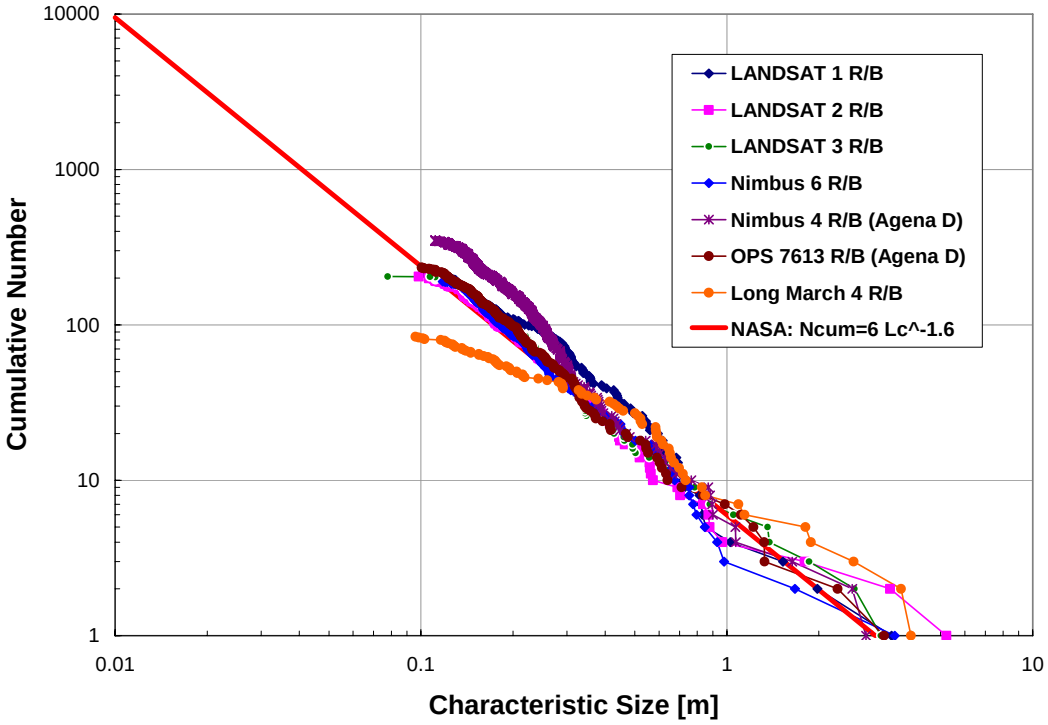

Figure 4.5-25. Sample debris size distributions from seven upper stage explosions, as derived from SSN data.

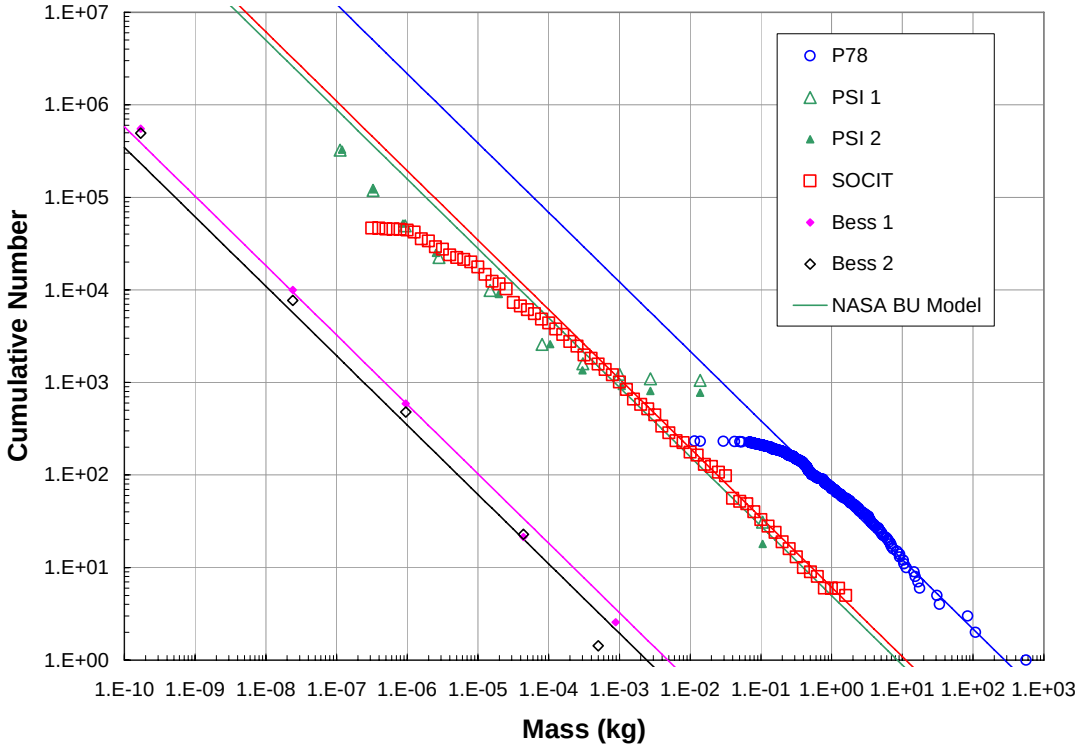

Figure 4.5-26. Sample debris size distributions from on-orbit and laboratory hypervelocity collisions.

4.5.3.2.2 Orbit Propagators

Two orbit propagators GEOPROP and PROP3D were developed for LEGEND. The former is used for GEO and near GEO objects while the latter is used for LEO, MEO, and Geosynchronous transfer orbit (GTO) objects. Perturbations included in PROP3D are solar and lunar gravitational perturbations, solar radiation pressure, atmospheric drag, Earth's shadow effects, and Earth's J_2, J_3, J_4 perturbations. Historical daily solar flux F10.7 values are combined with the J77 atmospheric model for the drag calculation [Jacchia 1977]. The solar flux F10.7 values used in the projection period have two components: a short-term daily projection by the NOAA Space Environment Center, and a long-term projection. The long-term F10.7 projection is a repeat of a sixth-order sine and cosine functional fit to Solar Cycles 18 to 23 [Whitlock 2006]. A simple smoothing function is used to interpolate the two solar flux components during the short- to long-term transition. Perturbations included in GEOPROP are solar and lunar gravitational perturbations, solar radiation pressure, and Earth's zonal (J_2, J_3, J_4) and tesserral ($J_{2,2}$, $J_{3,1}$, $J_{3,3}$, $J_{4,2}$, and $J_{4,4}$) harmonic perturbations. Both PROP3D and GEOPROP have been validated against orbital history records of the SSN objects and are shown to provide adequate description of the long-term orbital evolution of debris objects suitable for LEGEND.

4.5.3.2.3 Collision Probability Evaluation Model

The general consensus in the orbital debris community is collisions will likely produce more fragments than explosions in the future. Therefore, it is critical to have a high fidelity model to analyze future collision activities to ensure reliable environment predictions. The evaluation model developed for LEGEND to determine collision probability is called Cube. It has the ability to identify objects involved in collisions individually. This allows the user to better quantify the characteristics of future collision activities, for example, by orbit type (*e.g.*, LEO/GTO/GEO, inclination, RA of the ascending node), by object type (satellite, rocket body, breakup fragment), by breakup time, by location, and by mass.

Cube is designed specifically to work with an orbital debris evolutionary model to allow for source and sink terms of the objects involved and to utilize their updated orbital elements as they evolve in time. Its underlying principle is to evaluate the long-term collision probabilities of involved objects by means of uniform sampling of the system in time. It is more advanced than a simple particle-in-a-box approach or a 1-dimensional spatial density approach because it does not require any assumptions to simplify the system. A special sorting technique is also implemented within Cube to make it a fast pair-wise comparison algorithm. Cube has been compared and validated with other classical collision probability evaluation approaches. Its unique capability is a key to understand the nature of future collision activities and to develop reliable mitigation measures to control the growth of future debris populations.

4.5.3.2.4 Major Simulation Results

Major utilities of LEGEND are to quantify different mitigation options and to analyze various factors affecting the effectiveness of the options. For example, even with the same 25-year rule for postmission disposal (PMD) compliance, a prolonged spacecraft mission lifetime would decrease the effectiveness of the 25-year decay rule in LEO. This is demonstrated in Figure 4.5-27, where different spacecraft mission lifetimes are tested with the 25-year rule [Liou and Johnson 2005]. All PMD scenarios are shown to reduce the growth of future debris populations

significantly. However, the effectiveness has eroded gradually with increasing spacecraft mission duration.

Potential collision activities among orbiting objects for the next 100 years from LEO, MEO, and GEO regions have been analyzed with LEGEND. Figure 4.5-28 shows the simulated collision events in LEO from a non-mitigation, 100-year future projection [Liou 2005]. It is clear that most collisions occur at altitudes around 800 and 1,000 km; *i.e.*, regions of high spatial density. Although the average impact speed is around 12 km/sec, approximately half of them have impact speeds higher than 14 km/sec. On average, a total of 13 catastrophic collisions are expected in the next 100 years for the non-mitigation scenario. About 70% of the intact-intact type collisions have at least one intact that is launched in the future projection period. About 56% of the intacts in intact-fragment type collisions are also launched in the future projection period. This illustrates the importance of postmission disposal for rocket bodies and satellites to limit the growth of future on-orbit collisions and debris populations. Of all the "fragment projectiles" in intact-fragment type collisions, about 65% originated from future collisions. This demonstrates the nature of the feedback process in future collision activities. On the other hand, future explosion fragments only contribute about 8% to the "fragment projectiles" in intact-fragment type collisions.

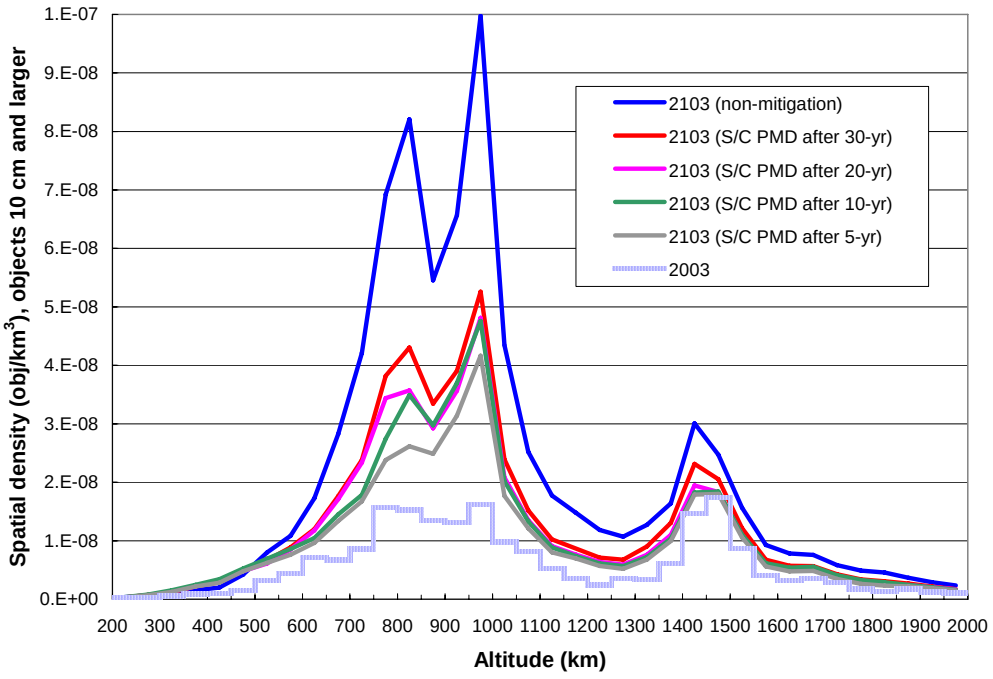

Figure 4.5-27. Spatial density distribution of objects 10 cm and larger as a function of altitude.

The four curves, from top to bottom, are labeled in the same order as those in the key. The four PMD scenarios all follow the same postmission 25-year rule, but with different mission lifetimes for the spacecraft. The histogram near the bottom represents the environment in 2003.

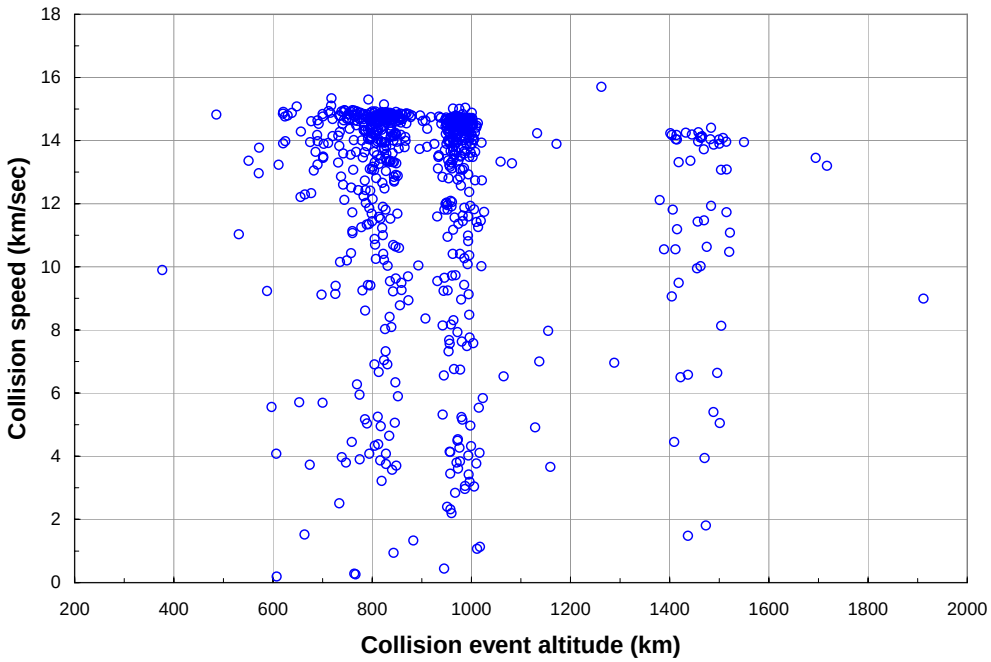

Figure 4.5-28. Impact speed versus collision altitude for LEO collisions - predicted by a special LEGEND 100-year, non-mitigation future simulation.

To provide a bottom-line assessment of the current LEO debris environment, a special LEGEND simulation was carried out in late 2005 [Liou and Johnson 2006, 2007]. The study assumed no satellites were launched after December 2005. A total of 150 MC runs were carried out and analyzed. Each MC run simulated the current debris environment and projected it 200 years into the future. The results indicate that the LEO debris environment has reached a point such that, even if no further space launches were conducted, the Earth satellite population would remain relatively constant for only the next 50 years or so. Beyond that, the debris population would begin to increase noticeably, due to the production of collisional debris (Figure 4.5-29). Detailed analysis shows that this growth is primarily driven by high collision activities around 900- to 1000 km altitude - the region that has a very high concentration of debris at present.

Has the current debris population in the LEO region reached the point where the environment is unstable and collisions will force an uncontrollable population growth in the foreseeable future? Based on this "no new launches" scenario, collisions will continue to occur in LEO over the next 200 years, primarily driven by the high collision activities in the region between 900- and 1000-km altitude. This trend, of course, will not last forever, as long as no new launches are added to the environment. Over time (millennia or longer), the collision cascade process will deplete most massive objects in the environment and lead to a permanent population decrease at the end.

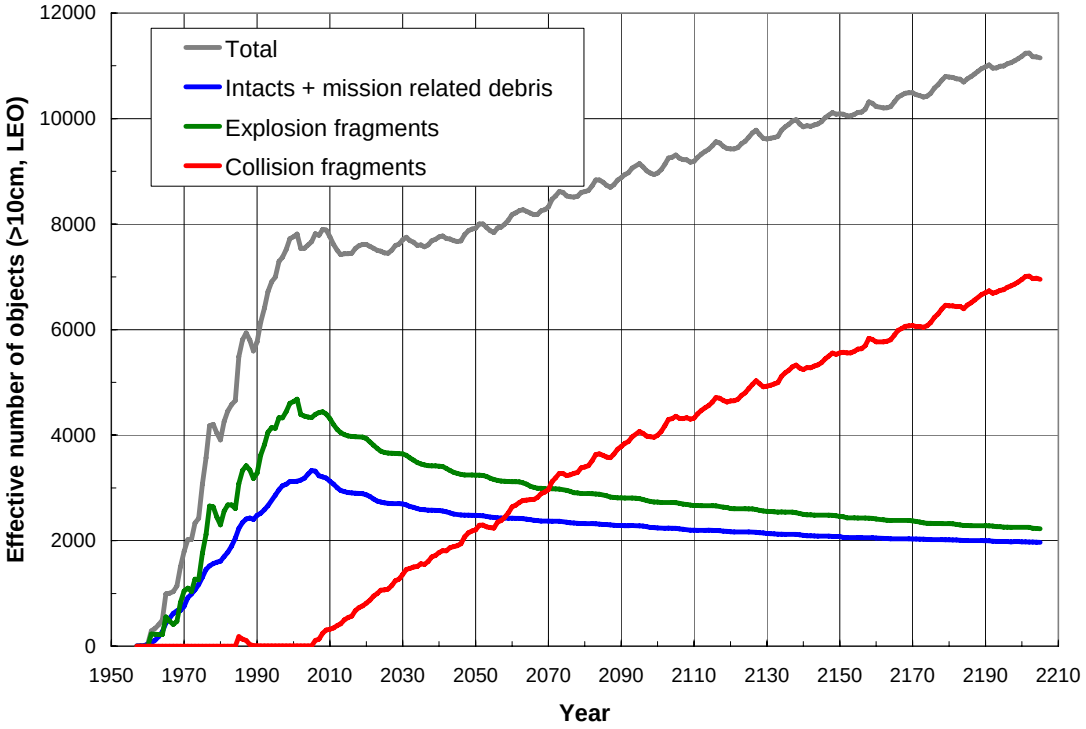

Figure 4.5-29. Effective number of LEO objects, 10 cm and larger, from the LEGEND simulations based on the "no new launches" assumption.

The future projection parts of the curves (years 2006 to 2205) are averages from 150 MC runs. Intacts are rocket bodies and spacecraft that have not experienced breakups.

The "no new launches" assumption adopted for the study is, of course, not practical. However, it does serve as a good benchmark to assess the current debris environment. In reality, the LEO population growth will be greater than that shown in the analysis, as spacecraft and their orbital stages continue to be launched into space. How much greater it will be in 200 years is difficult to predict, due to major uncertainties in future launches, although one can make reasonable assumptions to bound the problem [Krisko 2004].

Commonly adopted mitigation measures, such as limiting postmission orbital lifetimes of satellites to less than 25 years, will slow down the population growth [Krisko *et al.* 2001, Liou and Johnson 2005]. However, these measures will be insufficient to constrain the Earth satellite population. Only remediation of the near-Earth environment; *i.e.*, removing existing large and massive objects from orbit, will likely prevent the undesirable effects predicted in this study (see section 4.7.5.2).

4.5.3.3 Where LEGEND Is Going

Due to the limitation of the ground-based sensors, the environment near GEO is not well-understood. The SSN catalogs only cover objects in GEO about 1 m and larger. Recent optical surveys, however, have unveiled a significant amount of UCTs that might exceed the catalog population in GEO. These UCTs most likely originated from breakups in the region that have

yet to be recognized. In a LEGEND collision study, based on the currently known GEO catalog objects and a non-mitigation scenario, less than one catastrophic collision is expected in GEO in the next 100 years. This prediction is certainly an underestimate. With a more complete population definition by optical telescopes, a new study on the GEO population and its future will be needed to better characterize the environment, and if necessary, to develop aggressive mitigation measures to protect it.

In addition to regular UCTs, a new class of objects in GEO has been recently discovered by the ESA 1 m telescope [Schildknecht *et al.* 2004]. These faint (18^{th} to 19^{th} magnitude) objects have mean motions near 1 rev/day and orbital eccentricities as high as 0.55. A recent NASA GEO survey using the 0.6/0.9 m MODEST in Chile also reveals many faint objects with high hour-angle drift rates that are consistent with highly eccentric orbits [Seitzer *et al.* 2004]. The combination of the 24-hour orbital period and high eccentricity is certainly a surprise to the orbital debris community. However, a simple explanation may solve this puzzle. These may be debris with very high A/M ratios [Liou and Weaver 2004].

A study on the orbital evolution of GEO debris with very high A/M ratio was conducted by the NASA Orbital Debris Program Office in 2004 [Liou and Weaver 2005]. The objective was to find a plausible explanation for the class of objects in GEO. The results indicated that solar radiation pressure could cause a high A/M debris to go through a significant yearly variation in eccentricity and a long-term variation in inclination. The amplitude of the variation increased with increasing A/M. A group of debris with A/Ms on the order of 10 to 20 m^2/kg could produce observable characteristics consistent with the discovered population.

Another objective was to ascertain if a population of debris with A/Ms as high as 20 m^2/kg would match the maximum eccentricity of 0.55. The surfaces of satellites are covered with thermal blankets, or multi-layer insulation (MLI), which often consists of layers of thin aluminized Mylar®, Kapton®, or Nomex®. Typical areal density will give the corresponding A/Ms of the layers, varying from below 10 m^2/kg to more than 20 m^2/kg. Therefore, it is conceivable that surface degradation, impacts by small meteoroids, or explosions of GEO satellites have led to a population of MLI pieces in GEO. This might be the population that was discovered by the ESA 1 m telescope.

The existence of a highly eccentric GEO population may have important implications for the environment. Although this population spends less time in the GEO traffic zone (35,286 to 36,086 km altitude), the encounter speed between it and a GEO operational satellite should be higher than that between two typical GEO objects. Whether or not this population poses significant collision risks to operational satellites in GEO needs to be modeled carefully. How this population affects the overall GEO environment can be evaluated with LEGEND once the population is better defined.

A follow-up study to the "no new launches" LEO environment assessment might identify options to prevent the growth of future LEO debris population. If debris active removal is to be considered, a sensitivity study would be needed to quantify the effectiveness of this remediation measure. A LEGEND analysis is currently underway to address this issue. The results of this analysis will provide the first indication on whether or not debris active removal is a feasible means to control the future LEO environment.

4.5.3.4 Other Agencies' Equivalent Models

Other space agencies have developed similar orbital debris evolutionary models. They include, for example, the Debris Environment Long-Term Analysis (DELTA) model developed for ESA by QinetiQ in the UK [Walker *et al.* 2000] and the Semi Deterministic Model (SDM) developed for ESA, at ISTI/CNR in Italy [Rossi *et al.* 1998]. In general, the main differences in debris evolutionary models are the orbit regime (LEO/GEO), orbit propagator, traffic model, breakup model, collision probability-evaluation model, size/mass threshold for collision consideration, and type of collisions considered.

One of the major factors contributing to the differences among environment predictions by different debris evolutionary models is the breakup model. A consensus recently has been reached to adopt the NASA Breakup Model as the standard. A study comparing the long-term evolution of the LEO debris environment with DELTA, LEGEND, and SDM was carried out by IADC Working Group 2 members in 2004. The results were presented at the 2006 COSPAR Scientific Assembly [Martin *et al.* 2006]. Overall, there was a good agreement between model predictions.

4.5.4 References

Adachi, I. et al., "Study of a Threshold Cherenkov Counter Based on Silica Aerogels with Low Refractive Indices," Nucl. Instrum. Methods Phys. Res. A, 355, pp. 390-398, 1995.

Anon., "Meteoroid Environment Model - 1969 (Near Earth to Lunar Surface)," NASA SP-8013, Washington, DC, 1969.

Christiansen, E.L., Orbiter Meteoroid/Orbital Debris Impacts: STS-50 (6/92) through STS-86 (10/97), JSC-28033, 1998.

Corsaro R. et al., "PINDROP - An Acoustic Particle Impact Detector," The Orbital Debris Quarterly News, NASA JSC, July 2004. Available online at http://www.orbitaldebris.jsc.nasa.gov/newsletter/pdfs/ODQNV8i3.pdf.

Corsaro R. et al., "Continuous Large-Area Micrometeoroid Flux Measuring Instrument," *Proceedings of Dust in Planetary System*, 2006.

Drolshagen, G., et al., "Optical Survey of Micrometeoroid and Space Debris Impact Features on EuReCa," Planet, Space Sci. 44, 1996.

Drolshagen, G., et al., "HST Solar Array Impact Survey: Revised Damage Laws and Residue Analysis," Adv. Space Research, 9, 1997.

Drolshagen, G., H. Svedhem, and E. Grün, "Measurements of Cosmic Dust and Micro-debris with the GORID Impact Detector in GEO," *Proceedings of the 3rd European Conference on Space Debris*, ESA SP-473, pp. 177-184, Darmstadt, Germany, October 2001.

Hörz, F., et al., "Preliminary Analysis of LDEF Instrument A0187-1 'Chemistry of Micrometeoroid Experiment'," *LDEF-69 Months in Space: First Post-retrieval Symposium* (A.S. Levine, Ed.), NASA CP-3134, 1991.

Hörz, F., et al., "Preliminary Analysis of LDEF Instrument A0187-1, the Chemistry of Micrometeoroid Experiment (CME)," Hypervelocity Impacts in Space (J.A.M. McDonnell, Ed.), University of Kent at Canterbury Press, 1992.

Hörz, F. et al., "Optical Analysis of Impact Features in Aerogel From the Orbital Debris Collection Experiment on the Mir Station," NASA TM-1999-209372, 1999.

Humes, D.H., "Large Craters on the Meteoroid and Space Debris Impact Experiment, *LDEF-69 Months in Space: First Post-retrieval Symposium* (A.S. Levine, Ed.), NASA CP-3134, 1991.

Humes, D.H., "Small Craters on the Meteoroid and Space Debris Impact Experiment," *LDEF-69 Months in Space: Third Post-retrieval Symposium* (A.S. Levine, Ed.), NASA CP-3275, 1993.

Humes, D.H., "MEEP Polished Plate Meteoroid and Debris Experiment—Craters in the Aluminum Alloy (6006-T-) Plate," *MEEP Archive System*, NASA Langley Research Center, 1998.

Hyde, J.L., et al., As-Flown Shuttle Orbiter Meteoroid/Orbital Debris Assessment, Phase I, JSC-28768, 2000a.

Hyde, J.L., et al., As-Flown Shuttle Orbiter Meteoroid/Orbital Debris Assessment, Phase II, JSC-29070, 2000b.

Hyde, J.L. and R.P. Bernhard, STS-114 OV-103 Flight 31 Meteoroid/Orbital Debris Post Flight Assessment, JSC-63373, 2006.

Jacchia, L.G., "Thermospheric Temperature, Density and Composition: New Models," *Special Report 375*, Smithsonian Astrophysical Observatory, 1977.

Johnson, N.L., P.H. Krisko, J.-C. Liou, P. Anz-Meador, "NASA's New Breakup Model of EVOLVE 4.0," Adv. Space Research, 28 (9), pp. 1377-1384, 2001.

Kessler, D.J., "Orbital Debris Environment for Space Station," *JSC Internal Note 2001*, 1984.

Kessler, D.J., et al., "Orbital Debris Environment for Spacecraft Designed to Operate in Low Earth Orbit," NASA TM-100471, 1989.

Kessler, D.J., et al., "Meteoroids and orbital debris. In Space Station Program Natural Environment Definition for Design," NASA SSP-30425/Rev. A, 1991.

Kessler, D.J., et al., "A Computer-Based Orbital Debris Environment Model for Spacecraft Design and Observation in Low Earth Orbit," NASA TM-104825, 1996.

Kitazawa, Y., et al., "First Year Mission Results of Passive Measurement Experiment of Dust Particles on ISS (MPAC)," *Presented at the 35th COSPAR Scientific Assembly*, 2004.

Kitazawa, Y., et al., "Passive Measurement of Dust Particles on the ISS (MPAC): Fourth Report on Aerogel Dust Collectors," *Presented at the 36th COSPAR*, Beijing, China, 2006.

Krisko, P.H., et al., EVOLVE 4.0 User's Guide and Handbook, LMSMSS-33020, 2000.

Krisko, P.H., N.L. Johnson, J.N. Opiela, "EVOLVE 4.0 Orbital Debris Mitigation Studies," Adv. Space Research, 28 (9), pp. 1385-1390, 2001.

Krisko, P.H., "EVOLVE Historical and Projected Orbital Debris Test Environments," Adv. Space Research 34 (5), pp. 975-980, 2004.

Kuriki, K., et al., "Meteoroid and Space Debris Impact Investigations in SFU Post Flight Analysis Activities: Preliminary Results and Further Directions, the Institute of Space and Astronautical Science (ISAS)," Report No. 666, 1997.

Levine, A.S. (Ed.), LDEF—69 months in space: The First Post-retrieval Symposium, NASA CP-3134, 1991.

Levine, A.S. (Ed.), LDEF—69 months in space: The Second Post-retrieval Symposium, NASA CP-3194, 1992.

Levine, A.S. (Ed.), LDEF—69 months in space: The Third Post-retrieval Symposium, NASA CP-3275, 1993.

Liou, J.-C., et al., The New NASA Orbital Debris Engineering Model ORDEM2000, NASA TP – 2002-210780, May 2002.

Liou, J.-C., D.T. Hall, P.H. Krisko, and J.N. Opiela, "LEGEND – A Three Dimensional LEO-to-GEO Debris Evolutionary Model," Adv. Space Research, 34 (5), pp. 981-986, 2004.

Liou, J.-C. and J.K. Weaver, "Orbital Evolution of GEO Debris with Very High Area-to-mass Ratios," The Orbital Debris Quarterly News, NASA JSC, July 2004. Available online at http://www.orbitaldebris.jsc.nasa.gov/newsletter/pdfs/ODQNV8i3.pdf.

Liou, J.-C. and N.L. Johnson, "A LEO Satellite Postmission Disposal Study Using LEGEND," Acta Astronautica, 57, pp. 324-329, 2005.

Liou, J.-C. and J. Weaver, "Orbital Dynamics of High A/M Debris and Their Distribution in GEO," *Proceedings of the 4th European Conference on Space Debris*, ESA SP-587, pp. 285-290, Darmstadt, Germany, August 2005.

Liou, J.-C. and N.L. Johnson, "Risks in Space from Orbiting Debris," Science, 311, 340-341, 2006.

Liou, J.-C. and N.L. Johnson, "Instability of the Present LEO Satellite Population," Adv. Space Research, in press, doi:10.1016/j.asr.2007.04.081, 2007.

Liou, J.-C., et al., "Improving the Near-Earth Meteoroid and Orbital Debris Environment Definition with LAD-C," *57th International Astronautical Congress*, Valencia, Spain, 2006.

Liou, J.-C., "Collision Activities in the Future Orbital Debris Environment," Adv. Space Research, 38, pp. 2102-2106, 2006.

Martin, C., J.-C. Liou, and A. Rossi, "Comparing the Long-term Evolution of the Space Debris Environment with DELTA, LEGEND and SDM," *Presented at the 36th COSPAR*, Beijing, China, 2006.

Matney, M., et al., "Recent Results from Goldstone Orbital Debris Radar," Adv. Space Research, 23, 1999.

McDonnell, J.A.M., et al., "Meteoroid and Debris Flux and Ejecta Models: Summary Report," ESA Contract No. 11887/96/NL/JG, 1998a.

McDonnell, J.A.M., et al., "Meteoroid and Debris Flux and Ejecta Models: Final Report," ESA Contract No. 11887/96/NL/JG, 1998b.

Moussi, A., et al., "Results of Impact Analysis on HST Service Mission 3B Solar Arrays," *Proceedings of the 4th European Conference on Space Debris*, ESA SP-587, pp. 207-214, Darmstadt, Germany, August 2005.

Nazarenko, A., "The Development of the Statistical Theory of a Satellite Ensemble Motion and its Application to Space Debris Modeling," *Proceedings of the 2nd European Conference on Space Debris*, ESA SP-393, pp. 99-104, Darmstadt, Germany, May 1997.

Nazarenko, A.I., "Application of Average Contamination Sources for the Prediction of Space Debris Environment," *AAS/AIAA Space Flight Mechanics Meeting*, AAS 98-161, Monterey, California, February 1998.

Nazarenko, A.I., I.L. Menchikov, "Engineering Model of Space Debris Environment," *Proceedings of the 3rd European Conference on Space Debris*, ESA SP-473, Darmstadt, Germany, October 2001.

Neish, M.J., et al. "Passive Measurement of Dust Particles on the ISS Using MPAC: Experiment Summary, Particle Fluxes and Chemical Analysis," *Proceedings of the 4th European Conference on Space Debris*, ESA SP-587, pp. 221-226, Darmstadt, Germany, August 2005.

Reynolds, R.C., "Documentation of Program EVOLVE," Report OD91-002-U-CSP, System Planning Corp, 1991.

Reynolds, R.C. and P. Eichler, "A Comparison of Debris Environment Projections Using the EVOLVE and CHAIN Models," Adv. Space Research, 16 (11), pp. 127-135, 1995.

Reynolds, R.C., A. Bade, P. Eichler, et al., NASA Standard Breakup Model 1998 Revision, LMSMSS-32532, 1998.

Reynolds, R.C., "The NASA Orbital Debris Guidelines: an Historical Perspective on Orbital Debris Modeling Supporting the Development of a Policy on the Use of Space," Space Debris 2000, AAS Science and Technology Series, 103, pp. 315-322, 2001.

Rossi, A., L. Anselmo, A. Cordelli, et al., "Modeling the Evolution of the Space Debris Population," Planet. Space Sci., 46, pp. 1583-1596, 1998.

Schildknecht, T. et al., "Optical Observations of Space Debris in Highly Eccentric Orbits," Adv. Space Research, 35 (5), pp. 901-911, 2004.

Schwanethal, J.P., et al., "Analysis of Impact Data From the DEBIE (DEBris In orbit Evaluator) Sensor in Polar Low Earth Orbit," *Proceedings of the 4th European Conference on Space Debris*, ESA SP-587, pp. 177-182, Darmstadt, Germany, August 2005.

Sdunnus, H., J. Bendisch, H. Klinkrad, "The ESA MASTER 2001 Space Debris and Meteoroid Reference Model," *Proceedings of the 3rd European Conference on Space Debris*, ESA SP-473, Darmstadt, Germany, October 2001.

Seitzer, P. et al., "Results from the GEO Debris Survey with MODEST," The Orbital Debris Quarterly News, NASA JSC, January 2004. Available online at http://www.orbitaldebris.jsc.nasa.gov/newsletter/pdfs/ODQNV8i1.pdf.

Settecerri, T.J., et al., Radar Observations of the Orbital Debris Environment: Haystack and HAX Radars Oct 1990-Oct 1998, JSC-28744, 1999.

Tabata, M. et al., "Development of Silica Aerogel with Any Density," *IEEE Nuclear Science Symposium Conference Record*, p. 818, 2005.

Tuzzolino, A.J., et al., "Final Results from the Space Dust (SPADUS) Instrument Flown Aboard the Earth-orbiting ARGOS Spacecraft," Planet. Space Sci., 53, pp. 903-923, 2005.

Vardi, Y. and D. Lee, "From Image Deblurring to Optimal Investments: Maximum Likelihood Solutions for Positive Inverse Problems," J. R. Statist. Soc., B 55, No. 3, 1993.

Walker, R. et al., "Long Term Space Debris Environment Prediction," Technical Report ESA Contract 12808/98/D/IM(SC), DERA, Farnborough, UK, 2000.

Wegener, P., J. Bendisch, K.D. Bunte, H. Sdunnus, "Upgrade of the ESA MASTER Model," Final Report of ESOC/TOS-GMA contract 12318/97/D/IM, May 2000

Whitlock, D., "Modeling the Effect of High Solar Activity on the Orbital Debris Environment," The Orbital Debris Quarterly News, NASA JSC, p. 1, April 2006. Available online at http://www.orbitaldebris.jsc.nasa.gov/newsletter/pdfs/ODQNV10i2.pdf.

Yano, H., "Japanese Contribution to In-situ Meteoroid and Debris Measurement in the Near Earth Space," Earth, Planets and Space, 51, pp. 1233-1246, 1999.

Zhang, J.-C., and D.J. Kessler, "Orbital Debris and Meteoroid Population as Estimated from LDEF Impact Data," *LDEF—69 months in space: Third post-retrieval symposium* (A.S. Levine, Ed.), NASA CP-3275, 1993.

Zook, H.A., et al., "Meteoroid Impacts on the Gemini Windows," Planet. Space Sci., 18, pp. 953-964, 1970.

4.6 Micro-Meteoroid Orbital Debris (MMOD) Shielding

4.6.1 Introduction

Spacecraft shielding is designed to prevent a majority of the micrometeoroid and orbital debris particles that can impact a spacecraft, during its lifetime, from causing serious damage that would endanger the continuing operation of critical components of the spacecraft needed to comply with the applicable postmission disposal requirements. It can also be used to enhance the probability of mission success and/or enhance crew survivability. Due to spacecraft size and mass constraints, it is not possible with current shielding technology to eliminate completely the

risk from micrometeoroid orbital debris impact. Current practice calls for designing shields to meet or exceed protection limits, which are generally expressed in terms of a minimum acceptable reliability level or success criteria (*i.e.*, a probability of not being struck by an MMOD particle that will completely penetrate through the spacecraft shielding). Shielding can be an important component of the overall strategy used to reduce the risk from meteoroid or orbital debris impact, which can also include other operational means, such as collision warning and avoidance to reduce the risk from orbital debris impact.

4.6.2 Spacecraft MMOD Environment

NASA standard meteoroid and debris environment models are used in risk assessments to determine the cumulative flux of particles with a diameter that exceeds the ballistic limits. The environment models indicate that there are many more smaller than larger particles. Thus, raising the shielding performance in terms of the MMOD particle sizes the shielding can "stop" decreases the flux of penetrating particles and improves spacecraft reliability.

4.6.2.1 Meteoroid Environment Model

Meteoroids are the natural particles in orbit about the sun, which have quite high impact velocities relative to spacecraft in orbit about Earth. Meteoroid velocities range from 11 km/s to 72 km/s, with an average for Earth orbiting spacecraft of about 20 km/s. The majority of meteoroids impacting a spacecraft are thought to originate from comets, with relatively low particle densities of roughly 1 g/cm^3. This is contrasted with the meteorites that survive atmospheric entry and are found on Earth's surface, which are higher density and thought to originate mainly from asteroids. The meteoroid environment model currently used for shielding design is defined in NASA documentation [Anderson and Smith 1994]. A new meteoroid environment model has been recently developed by MSFC and is being implemented into the BUMPER MMOD risk assessment code [Jones 2004, McNamara et al. 2004].

4.6.2.2 Orbital Debris Environment Model

Orbital debris impact velocities are lower than meteoroids, generally impacting spacecraft in LEO at relative speeds of from less than 1 km/s to just over 15 km/s, with an average velocity of about 9 km/s for a 400 km altitude. The debris environment threat is composed of metallic fragments, paint, aluminum-oxide and other components of spacecraft, and SRM exhaust. Typically, for debris risk assessments, orbital debris particle density is assumed to be 2.8 g/cm^3 corresponding to aluminum metal. Because the orbital debris environment is tied to human activities in space, it is much more dynamic than the meteoroid environment, and the orbital debris environment definitions are subject to periodic updates and revisions as more data is collected on the amount and evolution of orbital debris in Earth orbit. The current debris environment model for purposes of shielding design is defined by NASA TP-2002-210780 [Liou *et al.* 2002] and referred to as ORDEM2000.

4.6.3 Shielding Probability of No Penetration Limits

Each program or project sets its own limits for shielding either to improve the probability of mission success or to protect the crew in the case of human space flight. Human space flight

usually has the highest no penetration limits and therefore the highest level of shielding. The process is presented here for illustrative purposes.

4.6.3.1 Process for Human Spaceflight

General vehicle design standards for MMOD protection for human spaceflight projects managed by JSC are given in the NASA JSC Design and Procedural Standards Manual [anon. 2004]. The statement of the standard calls for the following from the MMOD protection system:

- Protection levels against impacts from micrometeoroids and orbital debris (MMOD) for spacecraft structures shall be determined by HVI tests and analysis.
- MMOD risks for loss of crew (LOC), loss of vehicle (LOV), and loss of mission (LOM) shall be no greater than MMOD risks for previous spacecraft (ISS and Space Shuttle) (see Table 4.6-1).
- The MMOD risk assessments shall be updated as the MMOD environment definitions change.
- Actual damage from MMOD impacts shall be identified and compared to predictions to track and trend MMOD effects on the spacecraft.

Crewed vehicles from the early years of space exploration have used the probabilistic approach to design meteoroid shielding. Table 4.6-1 provides a listing of historical MMOD protection design levels for human spaceflight programs along with examples of robotic spacecraft. Generally, “critical” penetrations are defined (for human exploration vehicles) as those that would endanger the survivability of the vehicle and crew. Mission success and functionality criteria have been applied to human exploration as well as non-crewed spacecraft. Criteria are met when the MMOD protection system and operational techniques for the spacecraft meet or exceed the minimum acceptable probability of no penetration causing LOV/LOC or LOM.

Other options have been accepted by various programs to monitor the effects of MMOD impacts by on-board sensors, to inspect particularly sensitive or high-risk areas of the vehicles for MMOD damage, and to carry repair kits that provide a means to patch critical MMOD damage to thermal protection system materials (for Space Shuttle) and pressure shell (for ISS). In addition, operational flight rules have been implemented to operate in attitudes that reduce MMOD risk to the maximum extent possible.

4.6.3.2 ISS Shielding Design Limits

The ISS has meteoroid and debris protection limits consistent with past programs. As such, it carries by far the most capable meteoroid/debris shields ever flown. This is because ISS is larger and exposed longer than other space vehicles. The ISS is the largest spacecraft ever built. When complete in 2010, more than 11,000 m^2 of surface area will be exposed to the space environment. These factors increase the expected number of meteoroid and debris impacts. To meet comparable protection limits, ISS shielding must be more effective. For instance, most ISS critical hardware exposed to the MMOD flux in the velocity vector (front) or port/starboard (sides) directions is protected by shields effective at stopping 1-cm to 1.3-cm-diameter aluminum debris particle at typical impact velocity and angle (9 km/s, 45^o). In comparison, the Mir space station was able to stop 0.3 cm particles, the Space Shuttle Orbiter is capable of stopping 0.2 cm to 0.5 cm particles, and Apollo and Skylab were able to stop 0.15 cm to 0.2 cm particles under similar impact conditions. ISS also has the ability to maneuver to avoid ground-trackable debris

Table 4.6-1. MMOD Shielding Probability of No Penetration Limits for Various Spacecraft

Vehicle	Environ-ments	Failure Mode	Minimum Probability of No MMOD damage causing LOV/LOC or LOM	MMOD Risk per area and time (risk in % per m^2 – year)	Critical Al OD diameter (cm) at 7km/s & 0deg
Apollo Command & Service Module	MM	LOV / LOC (critical TPS damage, etc.)	0.996 per 8.3 day lunar mission	0.25	0.16
Skylab Module	MM	LOV / LOC (pressure shell damage)	0.995 for 8 month mission	0.003	0.2
Shuttle Orbiter	MMOD	LOV / LOC (critical TPS damage, etc.)	0.995 per mission	0.013	0.08 – 0.5
	MMOD	LOM (for radiator leak causing LOM or mission abort)	0.984 per mission	0.5	0.08
Gamma-ray Large Area Space Telescope (GLAST) Anti-Coincidence Detector	MMOD	LOM (no more than 1 light-leak)	0.99 for 5 years	0.02	0.2
Hubble Space Telescope	MMOD	LOM (light leak in aft shroud)	0.95 for 2 years	0.03	0.16
ISS	MMOD	Potential LOM, LOC/LOV (penetration of crew module pressure shell causing air leak, internal fragments, etc.)	0.98 to 0.998 per critical element over 10 years	0.001	0.6 – 1.3
		Potential LOM, LOC/LOV (penetration of crew module pressure shell, external pressure vessel shielding, control moment gyro shielding)	0.76 PNP cumulative over 10 years for all critical elements	0.001	0.6 – 1.3
		LOC	0.95 Probability of no crew loss due to MMOD over 10 years	0.0003	0.6 – 1.3
Crew Exploration Vehicle (CEV)	MMOD	LOV (critical TPS damage, etc.)	0.993 Probability of no vehicle loss due to MMOD over 5 years at ISS	0.0015	0.4 - 0.6
		LOV (critical TPS damage, etc.)	0.9998 Probability of no vehicle loss due to MMOD per Lunar mission	0.0004	0.4 – 0.6

particles (typically >10 cm diameter). By virtue of its large internal volume, the crews of ISS have time to locate and isolate leaks, if they occur, by closing hatches. Hole repair kits are manifested and crews are trained to repair a leak in a module if it occurs. Crew escape vehicles are docked to ISS in the event of a major event requiring evacuation.

4.6.4 Risk Assessment Process

The approach to evaluating and designing protection systems to meet criteria is illustrated in Figure 4.6-1. By using this methodology, an analyst can accurately evaluate spacecraft risks from MMOD impact, identify zones or areas of the spacecraft that are the "risk drivers (areas which contribute the greatest to the overall vehicle/mission risk)" which control the MMOD risk, and evaluate options to reduce risk. Each major step in the risk assessment process is described in the following sections.

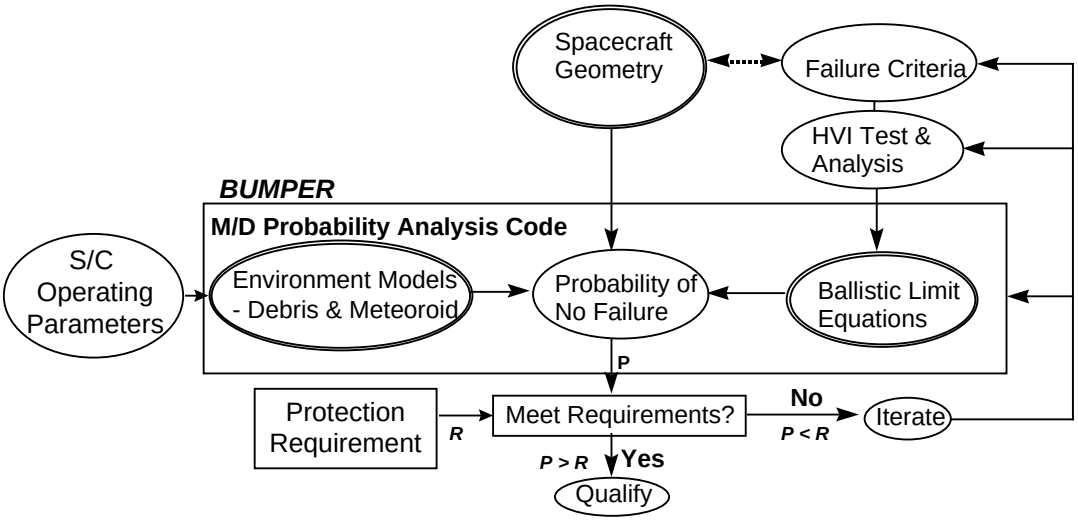

Figure 4.6-1. Meteoroid and orbital debris risk assessment methodology.

4.6.4.1 Spacecraft Geometry

The expected number of impacts, as given in Equation 4-6-1, is directly proportional to spacecraft size. Risk of MMOD impact failure increases as the area and time exposed to the MMOD flux increases.

$$N = \sum_{i=1}^{n} N_i = \sum_{i=1}^{n} \left(F \cdot A \cdot t\right)_i \qquad (4\text{-}6\text{-}1)$$

where N is the number of impacts causing failure and is equal to the sum of the impact failures in each region (N_i) over all regions (i = 1 to n) of the spacecraft. N_i is found from the product of flux (F, number/m^2-year) of meteoroid and debris impacts that exceed the failure ballistic limits of a region, exposed area (A, m^2) and time (t, year). It is important to break down the spacecraft geometry into different regions, each with a different exposed area, different materials of construction, shielding configurations and thickness. For instance, there are over 400 different

shields protecting ISS-habitable modules and external critical items (pressure vessels, control moment gyros) which have been optimized depending on their location and exposure to the MMOD threat to provide the necessary MMOD protection.

4.6.4.2 Impact Directionality

The front and sides of a spacecraft are more exposed to debris impact while the front, sides, and top (zenith) are more exposed to meteoroid impact. The LDEF (see Section 4.4.4.1) had 20 times more craters observed on the forward face compared to the aft, and 200 times more craters on the forward than the Earth facing side. Heavier shielding is typically placed on front and sides of spacecraft with fixed orientation relative to the velocity direction to protect from higher impact rates on these surfaces.

Figure 4.6-2. LDEF.

4.6.4.3 Spacecraft Failure Criteria

A key step in the risk assessment process is to precisely define what is meant by “failure,” that is to define potential damage modes from MMOD impact and to quantify for each the minimum amount of damage that can lead to failure of spacecraft hardware. This definition establishes the failure criterion or criteria that are assigned to each region of the spacecraft geometry model. For instance, MMOD damage modes and failure criteria for elements of the ISS are given in Table 4.6-2.

4.6.4.4 HVI Tests

HVI tests are an integral part of the analyses conducted to ensure adequate design of spacecraft MMOD shielding. Two-stage, light-gas guns (LGG) are used to accelerate projectiles up to 7 km/s (Figure 4.6-3). LGGs are capable of launching a variety of different and well-controlled projectile shapes. A disadvantage is that LGGs are capable of velocities that cover only a fraction of the orbital debris threat. Since average orbital debris velocity in low-Earth orbit is on the order of 9 km/s, LGG can directly simulate only 40% of the orbital debris threat.

Table 4.6-2. Damage Modes and Failure Criteria for ISS Elements.

*(note: critical failure criteria marked with *)*

Critical Elements	Thermal Protection System (TPS) Damage	Spall/Perforation of Shield exterior of Pressure Shell	Perforation of Pressure Shell	Uncontrolled Decompression	Catastrophic Rupture	Detonation
Crew Modules			X*	X	X	
Pressure Vessels (Liquids & Gases)		X*[1]	X*[1]		X	X
Control Moment Gyros (Rotating Equipment)		X*			X	
Crew Return Vehicles	X		X*	X	X	

[1] *Failure criterion for Russian PVs is perforation of pressure shell. Failure criterion of other designs is perforation or detached spall of shielding surrounding PV.*

Functional Elements	Surface Degradation	Leak	Short or Open Circuit
Radiator Panels	X	X	
Radiator Flex/Hard Lines		X	
Thermal loop lines & exchangers		X	
Power cables			X
Batteries		X	X
Solar Arrays	X		X
Data lines/cables			X
Window outer panes	X		

[1]*Failure criterion for US PV is perforation or detached spall of shielding surrounding PV. Failure criterion for Russian PV is critical damage to the pressure shell.*

Figure 4.6-3. NASA JSC-White Sands Test Facility two-stage LGG.

Other techniques exist to launch projectiles over 10 km/s. For instance, an inhibited shaped-charge launcher (ISCL) at Southwest Research Institute (SwRI) is capable of launching aluminum projectiles, 0.25-g to 2-g mass, in the shape of a cylinder to 11.5 km/s (Figure 4.6-4). Another high-speed launcher that has provided useful information on shield capabilities in excess of 10 km/s is the 3-stage hypervelocity launcher developed at Sandia National Laboratories. This launches thin disks (L/d=0.1-0.2, mass=0.2g-1g) of aluminum and titanium from 10-15

km/s with some bowing and tilting of the projectile. Hydrocode simulations are used to assess projectile shape effects on shield response. (Hydrocodes are finite-difference and finite-element computer programs that model the response of materials to very short duration loading. The term alludes to the fluid-like behavior of solid materials at striking velocities much greater than the materials' local sound speed.)

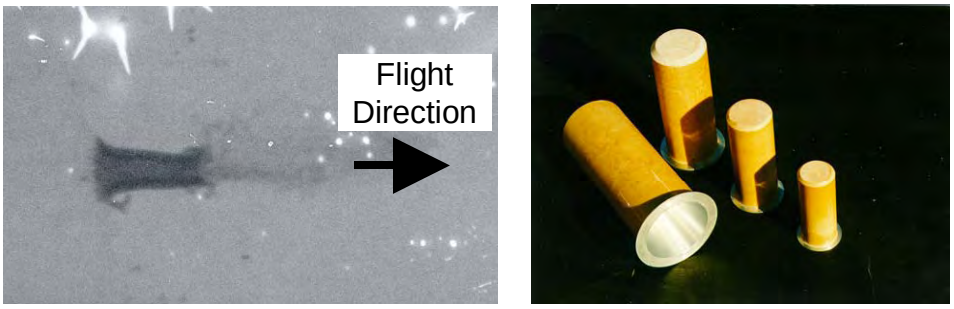

Figure 4.6-4. At SwRI's ISCL, various size charges are available that are capable of launching 0.25-g to 2-g aluminum projectiles up to 11.5 km/s (left).

Projectiles are typically in the shape of a hollow cylinder (right).

4.6.5 Ballistic Limit Equations

Ballistic limit equations (BLEs) or "penetration" equations are developed based on the HVI test results, numerical simulations, and analytical assessments [Christiansen 2003]. BLEs describe the particle sizes that are on the failure threshold of a particular spacecraft component. The ability of a particular shield to withstand HVI is predicted by a BLE. BLEs are a function of the target "failure criteria"; target configuration, materials and thickness, and projectile parameters such as velocity, angle, shape and density. MMOD risk assessments require a BLE defined for each surface of a spacecraft, for each failure criterion assessed. Shield design equations have also been developed that provide a means to estimate shielding parameters needed to defend against specific projectile threats.

Because of the complexity of spacecraft and their HVI failure modes, many different BLEs exist for a wide variety of shielding types, spacecraft components and hardware, and differing damage/failure modes. A description of BLEs for one particular type of shield, the basic Whipple shield, is provided in the following section. This example illustrates the considerations involved in developing BLEs.

4.6.5.1 Whipple Shield BLEs

In the 1940s, Fred Whipple proposed a meteoroid shield for spacecraft consisting of a thin "sacrificial" wall mounted at a distance from a rear wall. The Whipple shield functionality is shown in Figure 4.6-5 and Figure 4.6-6. The function of the first sheet or "BUMPER" is to break up the projectile into a cloud of material containing both projectile and BUMPER debris. This cloud expands while moving across the standoff, resulting in the impactor momentum being distributed over a wide area of the rear wall. The back sheet must be thick enough to withstand the blast loading from the debris cloud and any solid fragments that remain. For most conditions, a Whipple shield results in a significant weight reduction over a single plate, which must contend with deposition of the projectile kinetic energy in a localized area.

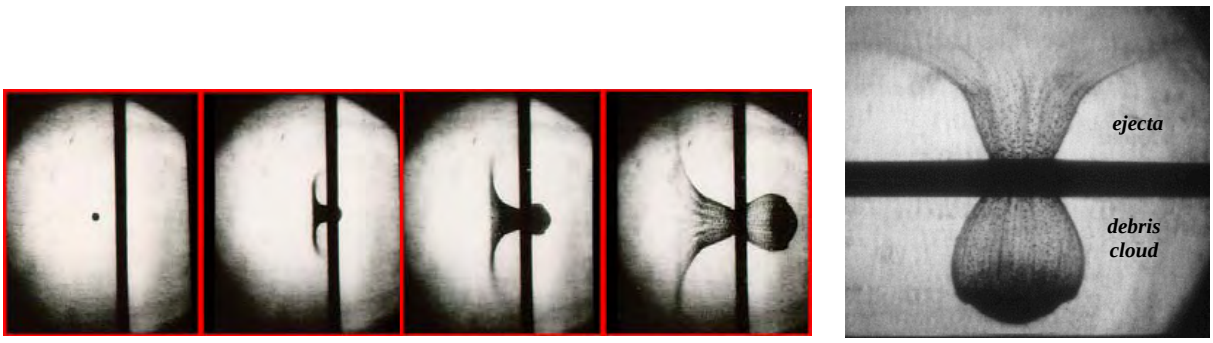

Figure 4.6-5. High-speed camera film (Cordin), 0.32 cm projectile impacts BUMPER at 6.8km/s, left to right, 1µs between frames.

Whipple shields were used to provide protection to the Apollo Command Module and Lunar Lander. Apollo shields were capable of stopping 0.16 cm diameter aluminum particles at 7km/s, normal impact angle (0^o).

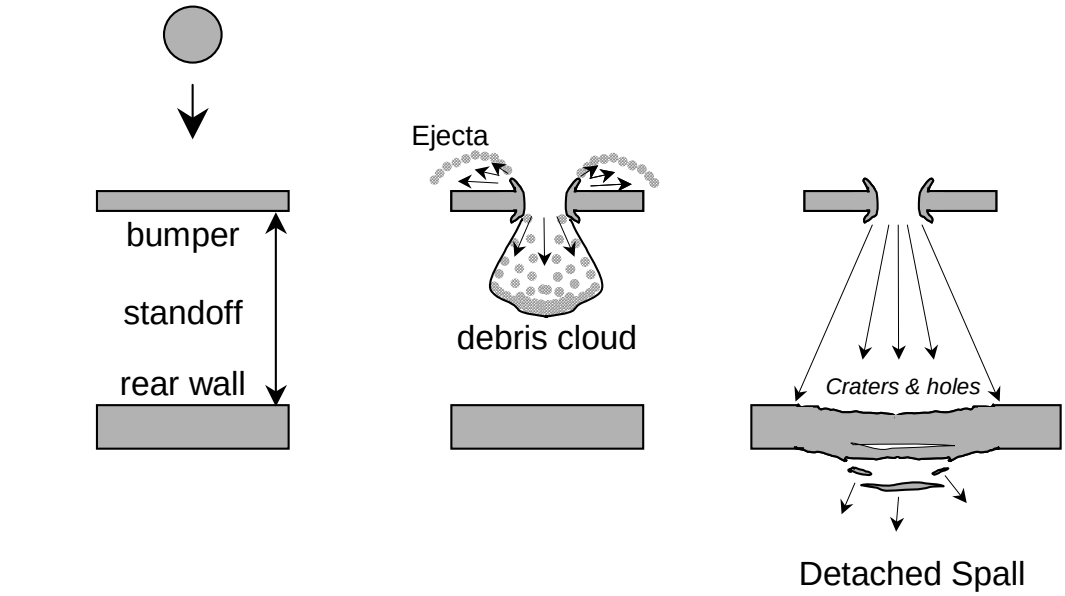

a) Whipple shields consist of a BUMPER, standoff (gap or spacing), and rear wall.

b) HVIs will generate a cloud of BUMPER and projectile debris that can contain solid fragments, liquid, and vapor particles.

c) The rear wall must survive the fragments and debris cloud impulsive loading. It could fail by perforation from solid fragments, spall, or tear and petal from the impulsive loading.

Figure 4.6-6. Whipple shield.

4.6.5.2 Whipple Shield Design Equations

For design purposes, Equations (4-6-2 through 4-6-4) provide BUMPER- and rear wall-thickness to defeat a given threat particle are determined by the following equations (assuming $V_n \geq 7$ km/s).

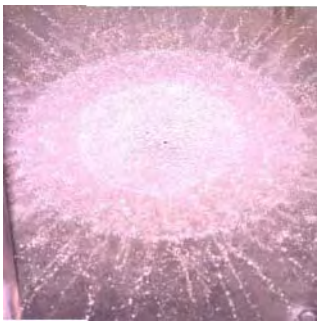

Figure 4.6-7. Rear wall after impact.

$$t_b = c_b\, m_p / \rho_b = c_b\, d\, \rho_p / \rho_b \qquad (4\text{-}6\text{-}2)$$

$$t_w = c_w\, d^{0.5}\, M^{1/3}\, (\rho_p\, \rho_b)^{1/6}\, \rho_w^{-1}\, (V \cos\theta)\, S^{-3/4}\, \sigma'_h{}^{-1/2} \qquad (4\text{-}6\text{-}3)$$

Where:

c_b	coefficient in BUMPER sizing equation (unitless)
c_w	coefficient in rearwall sizing equation ($cm^{-3/4}$ sec $g^{1/3}$ km^{-1})
d	projectile diameter (cm)
ρ_b	BUMPER density (g/cm^3)
ρ_p	projectile density (g/cm^3)
ρ_w	rearwall density (g/cm^3)
m_p	mass per unit area of projectile (g/cm^2)
M	projectile mass (g)
S	shield spacing, distance between BUMPER and rearwall (cm)
$(S/d)_o$	shield standoff to projectile diameter ratio, initial value: $(S/d)_o = 15$
σ	rearwall yield stress (ksi) (Note: 1ksi = 1,000 lb_f/in^2 = 6.895 MPa)
σ'	normalized rear wall yield stress (unitless)
t_b	BUMPER thickness (cm)
t_w	rearwall thickness (cm)
θ	impact angle (deg)
V	impact velocity (km/s).

Where $c_b = 0.25$ when $S/d < 30$, $c_b = 0.20$ when $S/d \geq 30$, and $c_w = 0.79$ {$cm^{-3/4}$ sec $g^{1/3}$ km^{-1}}. Normalized yield stress (unitless) $\sigma'_h = (\sigma/70$ ksi).

The ballistic limit criterion is no perforation or spall of the rear wall. BUMPER fragments become the primary source of rear wall damage at impact angles greater than 65°. Therefore, for oblique angles over 65°, the calculated rear wall thickness should be constrained to 65°. Coefficient, c_w, should be adjusted by the factor, $[(S/d)/(S/d)_o]$ where $(S/d)_o = 15$, when $S/d<15$, as follows.

$$c_w = 0.79\, [(S/d)/(S/d)_o]^{-0.185} \qquad (4\text{-}6\text{-}4)$$

4.6.5.3 Whipple Shield Ballistic Limits for All Impact Velocities

Typical ballistic limits for a Whipple shield at all impact velocities are illustrated in Figure 4.6-8 for normal impact by an aluminum sphere. The Whipple shield ballistic limit is compared to a monolithic, single aluminum plate of same mass as the combined Whipple shield's BUMPER and rear wall. Protection capabilities are defined for three penetration regimes based on normal component velocity (Vn) for an aluminum impact on a Whipple shield: ballistic regime (Vn < 3 km/s), fragmentation regime (3 km/s ≤ Vn ≤ 7 km/s), and melt/vaporization regime (Vn > 7 km/s). Important shield physical and material properties that influence ballistic limits of the shield vary as a function of impact velocity. Equations used to quantify ballistic limits for various types of shields are provided in the literature [Christiansen 2003].

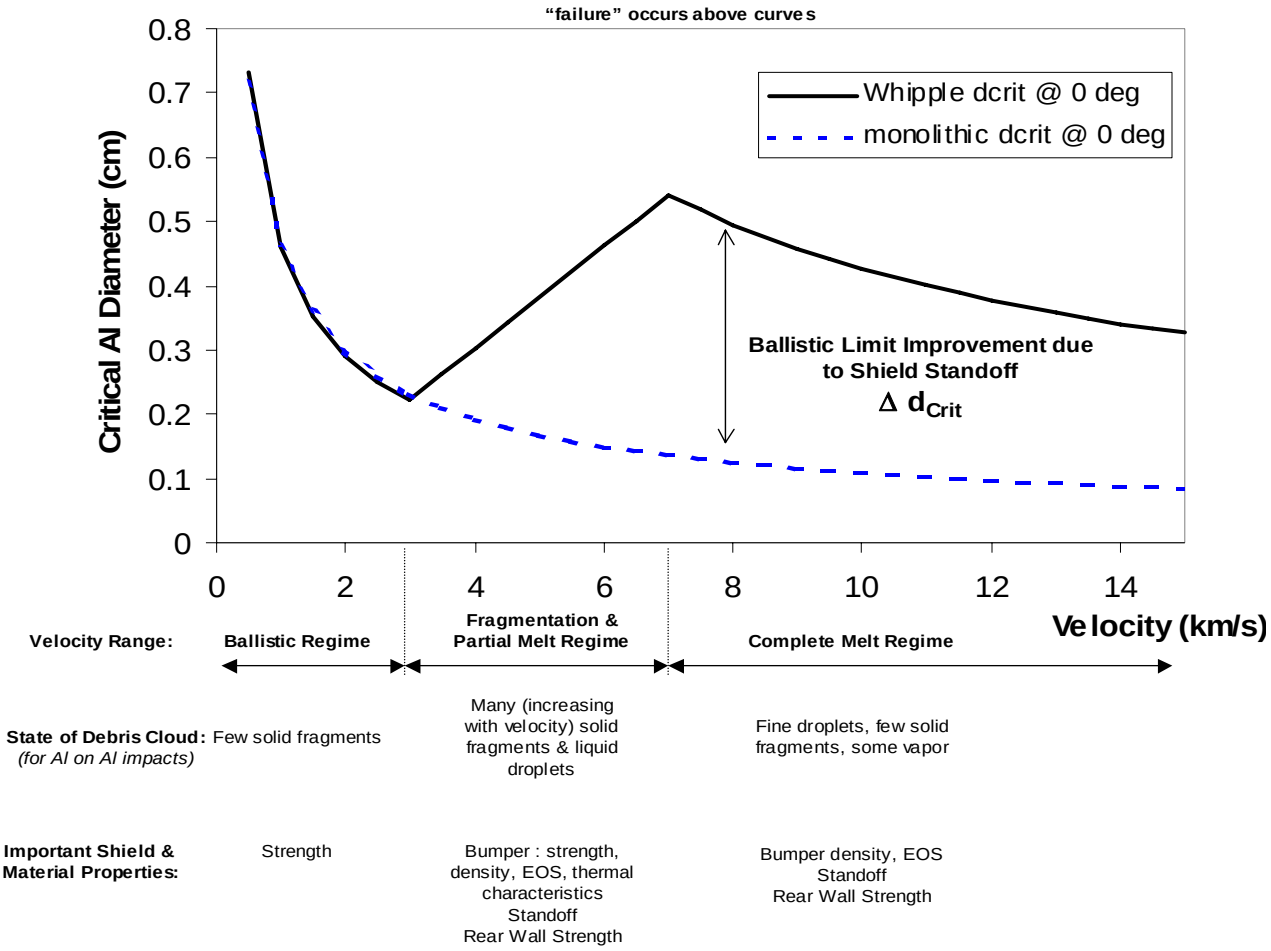

Figure 4.6-8. Ballistic limits for equal mass monolithic target and Whipple shield.

Failure criterion is threshold perforation or detached spall from rear wall. Monolithic target is 0.44 cm thick Al 6061T6. Whipple shield consists of 0.12 cm thick Al 6061T6 BUMPER followed at 10 cm by 0.32 cm thick Al 6061T6 rear wall.

A key factor governing the performance of spaced shields is the "state" of the debris cloud projected from the BUMPER toward the rear wall. The debris cloud may contain solid, liquid, or vaporized projectile and BUMPER materials, or a combination of the three states, depending

on the initial impact pressure. Solid fragments in the debris cloud are generally more penetrating when they contact the rear wall than liquid or vapor particles. Blast loading in the rear wall is a function of shield standoff, which becomes of increasing importance as impact velocity increases above about 5 km/s.

4.6.6 BUMPER Code

The BUMPER code has been the standard in use by NASA and contractors to perform meteoroid and debris risk assessments since the early 1990s. Over that period of time it has undergone extensive revisions and updates. NASA has applied BUMPER to risk assessments for ISS, Space Shuttle, Mir, Extravehicular Mobility Units (*i.e.*, space suits), and other satellites and spacecraft. Significant effort has been expended to validate BUMPER and "benchmark" it to other MMOD risk assessment codes used by some ISS International Partners. Figure 4.6-1 illustrates where BUMPER fits in the risk assessment process. The BLEs and MMOD environment models are embedded into BUMPER. A finite element model (FEM) that describes the spacecraft geometry is created in and input into BUMPER. BUMPER calculates the number of predicted failures by determining the number of MMOD particles that exceed the ballistic limits for each element of the FEM, and calculates the total number of failures by summing the individual elements. BUMPER results are used to determine the "risk drivers," which areas on the spacecraft contribute most to the overall risk. Emphasis on risk reduction is placed on lowering the risk for the "drivers."

4.6.7 Probability of No Penetration and Design Qualification

Probability of no penetration (PNP) failure is assessed based on Poisson statistics (Equation 4-6-5) where N is defined by Equation (4-6-1). This is NASA's standard approach used to assess meteoroid shielding since Apollo. The same probabilistic approach has been extended to designing spacecraft protection systems for the combined meteoroid and debris environments, assessing risks of functional failure, or calculating risks of impact damage exceeding a user defined size (diameter or depth). The same statistical approach is used to assess risks of any kind of damage extent that can be expressed in terms of different BLEs.

$$PNP = \exp(-N) \tag{4-6-5}$$

The risk of penetration is:

$$Risk = 1 - PNP \tag{4-6-6}$$

Assessed PNP is compared to requirements for MMOD protection. The shielding design effort is successful when the assessed PNP is greater than the required PNP. As illustrated in Figure 4.6-1, iteration of the risk assessment and risk reduction process is often necessary to meet protection requirements and optimize the design; *i.e.*, meet the requirements with less weight, lower volume (less standoff), less cost, etc. The last step in the process is to conduct final shield verification by analysis (supported by HVI test as appropriate), prior to final design certification and acceptance.

4.6.8 Risk Reduction Practices

4.6.8.1 Find MMOD Risk Drivers

- Perform detailed assessment of penetration risks for the overall vehicle to determine the zones that present the greatest risks.
- Selectively improve the protection capability in the areas identified as risk drivers.

4.6.8.2 Shielding Enhancement

- Optimize the shielding weight distribution to account for the directional MMOD distribution. Shielding on each critical item is tailored for the environment and its location. Because the MMOD impact rate is highest on forward and side surfaces, more capable shielding (heavier or with greater standoff) is applied to these surfaces and less on the Earth-facing surface. Shielding is also reduced in areas where shadowing from neighboring structure will reduce impacts. The goal of this effort is to equalize the ratio of risk to area for the various vehicle zones. The risk-to-area ratio for each zone is assessed and optimized by repeated BUMPER code runs.
- Incorporate enhancements such as increasing the spacing between BUMPER and rear wall, or using higher performance alloys and materials for the rear wall.
- Implement more fundamental changes such as incorporating more efficient, multi-BUMPER shielding concepts.
- Incorporate toughening materials, such as ceramic fabric and high-strength fabric into the multi-layer insulation thermal blanket that is often integral to the MMOD shielding.

4.6.8.3 Impact Reduction

- Maximize shadowing – Take advantage of shielding and shadowing from neighboring items and locate external critical equipment to trailing or Earth-facing surfaces to reduce MMOD impact rates, or put them in areas highly shadowed by other hardware.
- Select Low-Frontal Area Orientations – The best orientation for a relatively short cylinder (length/diameter of 1.8) in terms of lowest meteoroid and debris impact risk is with the cylindrical length axis oriented perpendicularly to the orbital plane. A vertical (gravity-gradient) orientation (with length axis parallel to Earth radial) has a 30% higher MMOD impact risk. An orientation with the length axis parallel to the velocity vector is in the middle.
- Flight Attitude – Select the best flight attitude by pointing the most vulnerable surfaces aft or toward Earth, a standard procedure for the Space Shuttle. Other spacecraft can take a similar approach.

4.6.8.4 Inert Stored Energy Equipment

After use, stored energy equipment should be made inert if possible. For instance, a storage tank should be completely depressurized after it is emptied. The risk of catastrophic rupture is eliminated when stress levels in the pressure wall are made negligible by depressurizing to a small value. This would require design modifications to implement for propellant tanks and other fluid storage tanks. Another example is to keep spare flywheels, gyros, or other momentum storage devices in an inactive state until required.

4.6.8.5 Reduce Hazards if Shield Penetration Occurs

Design and operational options may exist to reduce hazards if a penetration occurs. For instance, some hatches to unoccupied modules can be kept closed to prevent a depressurization of an entire station if a penetration occurred to the module. A perforation into an unoccupied module with a closed hatch would not result in loss of crew from shrapnel fragments, light flash, acoustic overpressure, or depressurization. Vent lines between modules could be left open to allow for some air circulation and to keep pressures equalized to facilitate hatch opening during normal operations.

4.6.8.6 Critical Damage Detection, Repair, and Replacement

Inspection and repair of impact damage to critical areas of reentry vehicles (such as the crew return vehicle attached to ISS) can be used as a supplement to MMOD shielding for maintaining flight worthiness. Some impact damage to thermal protection systems (TPS) on Earth return vehicles is not a hazard while on-orbit (and may therefore be undetected), but could become hazardous later during reentry aerodynamic heating phases. Properly placed instrumentation with correct sensitivity to detect critical TPS damage can help support the inspection and detection process.

4.6.9 Enhanced Shielding

The primary purpose of developing improved shielding is to provide higher levels of spacecraft meteoroid and debris protection with less weight.

To illustrate the issue, consider the shielding required to stop a 1-cm-diameter aluminum projectile at 7 km/s, 0^{o} impact angle. To meet the requirement, four shield concepts are shown in Figure 4.6-9: a conventional aluminum Whipple shield with a 10.2 cm standoff, a Nextel/Kevlar stuffed Whipple shield with the same standoff, a Whipple shield with a 30 cm standoff, and a Nextel multi-shock shield concept. The stuffed Whipple shield incorporates a blanket between the outer aluminum BUMPER and inner pressure wall that combines two materials: Nextel™ ceramic fabric and Kevlar™ high strength fabric[1.] The shielding mass estimates are made assuming the shielding encloses a cylinder, with a 4.2 m inside diameter and an 8.5 m length. It is clear for this example that there are significant mass savings by using advanced shielding concepts (i.e., up to 50% reduction).

Also, it is possible to trade weight for protection capability (*i.e.*, capability and shield PNP are related), so it can be shown that lower weight and more effective protection in terms of higher PNP are possible using Nextel/Kevlar stuffed Whipple and Multi-Shock shields compared to conventional Whipple shields.

---

1 Nextel is a flexible, ceramic fabric product manufactured by 3M Corporation. Nextel contains alumina, boron oxide, and silica. Kevlar is a product of the E.I. DuPont Co.

Projectile in all cases: 1cm diameter aluminum, 1.5g, 7km/s, normal impact

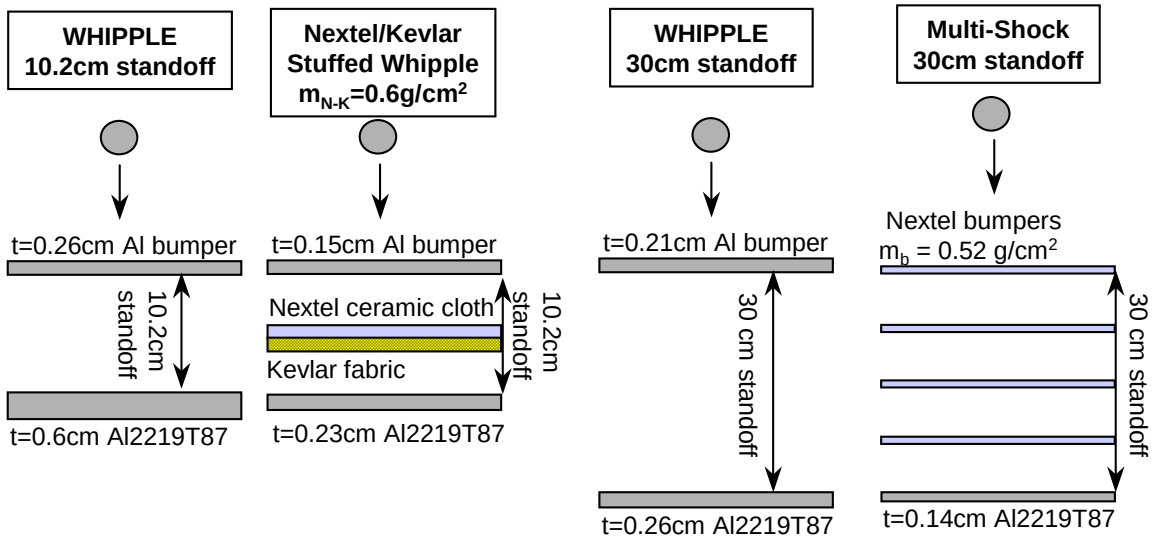

Areal Density (kg/m²)				
	Whipple S=10cm	**Stuffed Whipple S=10cm**	**Whipple S=30cm**	**Multishock S=30cm**
BUMPER:	7.0	10.6	5.6	5.2
Rear wall:	17.2	6.6	7.5	3.8
Total:	**24.2**	**17.3**	**13.1**	**9.0**
Surface Area (m²)				
BUMPER:	152	152	175	175
Rear wall:	141	141	141	141
Mass (kg) including 30% of BUMPER for support mass				
BUMPER:	1060	1620	980	910
Support:	320	490	300	270
Rear wall:	2420	940	1060	540
Total: (include support)	**3800**	**3050**	**2340**	**1720**

Figure 4.6-9. Shielding concepts comparison.

4.6.10 References

Anderson B.J. (Ed.) and R.E. Smith (Compiler), “Natural Orbital Environment Guidelines for Use in Aerospace Vehicle Development,” NASA TM 4527, 1994.

Anon., JSC Design & Procedural Standards Manual, Section M/S-11, Meteoroid and Orbital Debris Protection Levels for Structures, JSC Program Requirements, JPR-8080.5, Revised Dec. 2004.

Christiansen, E.L., Meteoroid/Debris Shielding, NASA TP-2003-210788, 2003.

Jones, J.; "Meteoroid Engineering Model-Final Report;" NASA MSFC SEE/CR-2004-400, June 2004.

Liou, J.-C., et al., The New NASA Orbital Debris Engineering Model ORDEM2000, NASA TP – 2002-210780, May 2002.

McNamara, H., et al.; "Meteoroid Engineering Model (MEM): A Meteoroid Model for the Inner Solar System," Earth, Moon, and Planets 95, pp. 123-139, 2004.

4.7 Mitigation

4.7.1 Introduction

Options are available to control, limit, or reduce the growth of the orbital debris. However, there are currently few options to significantly modify the current debris environment; the focus has primarily been on influencing the future environment. Three generic options of debris control currently exist: design, disposal, and active removal

Improved design options would include booster and payload design, preventing the spontaneous explosion of rocket bodies and spacecraft, as well as improving reliability. Launch vehicles and spacecraft can be designed so that they are litter-free; *i.e.*, they dispose of separation devices, payload shrouds, and other expendable hardware (other than upper stage rocket bodies) at a low enough altitude and velocity as to not become orbital. This becomes more difficult when two spacecraft share a common launch vehicle. In addition, stage-to-stage separation devices and spacecraft protective devices, such as lens covers and other potential debris, can be kept captive to the stage or spacecraft with lanyards or other provisions to minimize debris. Also, when stages and spacecraft do not have the capability to actively deorbit, they need to be made as inert as possible. Expelling all propellants and pressurants and assuring that batteries are protected from spontaneous explosion requires modification in either design or operational practices for both stages and spacecraft.

Disposal or deorbiting of spent upper stages or spacecraft is a more aggressive and effective strategy than merely rendering spent stages and spacecraft inert, since it removes significant mass from the environment that could become debris in the future should an explosion or collision take place. The primary method to achieve this is a perigee lowering maneuver so that the orbital lifetime is constrained to a minimum threshold period such as 25 years. Such a maneuver quickly moves the object from the region of higher collision risk and removes the mass and cross section from orbit in a small fraction of the orbital lifetime that would exist without such a maneuver. A second way to achieve a successful disposal is to relocate the rocket

body into an orbit in which there are few other spacecraft. For instance, very few spacecraft use the region between 2000 km altitude and GEO (the exception being the Global Positioning System constellation). Therefore, moving derelict rocket bodies to a perigee higher than 2000 km, with an apogee lower than GEO, becomes an effective way to preserve the LEO environment for future missions.

Removal is the elimination of space objects by another system than those mentioned above, which for now is not an economically feasible option. Some studies have been done to target certain objects that may present the largest mass or largest risk of explosion. But the cost of actively retrieving the object, or a rendezvous such that a large object might be pushed to a lower orbit or reenter the atmosphere completely, is not a viable option. However, it is understood that in the future, this mechanism of debris mitigation may be employed.

4.7.2 History

Since 1989, the U.S. and a number of foreign governments and international space-faring organizations have addressed issues of orbital debris mitigation independently, including procedures for the disposal of satellites in GEO at the end of their lifetime. These governments and organizations have also taken steps to monitor the space environment and manage data and information on debris, minimize debris generation, and implement measures to survive contact with debris in space. The U.S. has always been a lead in the international consideration of orbital debris issues and plans to continue leading the effort in orbital debris mitigation.

Discussions on the mitigation issue have been taking place at one level or another among international space agency scientists, engineers, and managers since the 1980s. These discussions have occurred at technical society conventions and in regularly scheduled bilateral and multilateral meetings. NASA began to exchange information on mitigation and other aspects of debris with ESA in 1987 and has met with ESA on a biannual basis since 1989. In August 1992, the two agencies finalized a letter agreement documenting their common interest in continuing joint efforts. Also, every four years since 1993, ESA has hosted a conference on space debris open to all space-faring nations. The 2005 conference featured over 300 participants from 18 countries [anon. 2005b]. Coincident with the first European Conference on Space Debris, the IADC was formed, with NASA, ESA, as well as relevant space agencies in Japan and Russia. The IADC members participate in specialized working groups on measurements, the debris environment, databases, and debris protection and mitigation, and as a body, exchange information on debris research, commend cooperative research projects, and identify and evaluate debris mitigation options.

At the June 1993 plenary session of the UN-COPUOS, the U.S. joined a consensus decision to take up consideration of the orbital debris issue beginning at the February 1994 session of the COPUOS STSC. In its 1994 session, the STSC agreed on the importance of having a firm scientific and technical basis for any future action on the issue of debris. STSC members decided that they should first focus on understanding aspects of international research related to debris, including characterizing the debris environment, debris measurement techniques, mathematical modeling, and protective spacecraft design. This session marked the first time that the scientific and technical aspects of the orbital debris issue were considered by a cross section of space and non space-faring governments.

4.7.3 Current Status

4.7.3.1 Techniques

4.7.3.1.1 Twenty-Five Year Rule

One of the more effective ways to reduce clutter in the LEO environment is to limit the lifetime of objects in regions below 2000 km. This can actually have a two-fold benefit: objects spend less time in LEO and are exposed to explosion or collision risk for much less time. Most international standards have set a guideline of 25 years for LEO post-mission object lifetimes for newly launched objects. Setting a limit such as this is a critical step in controlling the growth of intact objects in LEO. Unfortunately, this limit was not uniformly applied until the last decade or so, so the environment is just beginning to see the positive effect of this technique.

As a demonstration, there are 7775 cataloged objects currently in orbit with a perigee less than 2000 km (as of 4 October 2006). Almost half of these (3893) have been in orbit for more than 25 years. It appears that about 80% of LEO objects (6215) will have lifetimes greater than 25 years from today. Of these 6215, less than 15% (796) were launched after 1995, when the 25-year rule began to take form. So it is easy to see that if the 25-year rule was adhered to strictly in the past, there would be only the 3882 objects launched in the past 25 years in LEO today, with all removed from LEO by 2032. Instead, by 2032, over 6200 objects currently in orbit will still be in LEO.

4.7.3.1.2 Design and Shielding of Spacecraft and Rocket Bodies

The need for protection from orbital debris is influencing the design of new spacecraft. In the past, spacecraft design took into account only the natural meteoroid environment. Today, NASA, DoD, and commercial spacecraft designs consider the additional hazards from human-made orbital debris. Examples of this include shielding energized systems from the environment, passivating energized systems, or improving known design flaws such that future explosion events might be avoided.

Spacecraft can be protected from serious damage by using shielding and by designing the spacecraft to be damage tolerant. Damage tolerance can be achieved by providing redundant systems for critical functions with proper separation to prevent single event catastrophes.

Similar to the need to shield energized subsystems, it may be more important to have the capability to de-energize the systems once a spacecraft or rocket body is no longer functional. This technique was not universally employed until a number of rocket body explosions occurred long after the payload associated with the rocket body had been delivered. Once design implementations were put into place, a significant reduction (or elimination) of this explosion risk was seen.

Finally, learning from design mistakes can also prevent future on-orbit explosion catastrophes. As an example, from 1972 to 1981 there were a total of 70 Delta missions, with 8 major fragmentation events occurring long after the payload was delivered (11% of all Delta missions). A design problem was identified and corrected. Since 1982, there have been over 150 Delta second stages to reach orbit, and none have subsequently exploded from the same design flaw. If the same explosion rate from 1972 to 1981 had taken place over the last 25 years, there could

have been more than 16 events, contributing nearly 2000 more debris pieces to the environment [Johnson *et al.* 2004].

Another lesson learned involves the failure to passivate pressurant tanks. The most intense breakup of a U.S. satellite occurred on 3 June 1996, when a 2-year-old, abandoned Pegasus HAPS upper stage exploded. After a thorough investigation the cause was determined to have originated when a pressure regulator failed, allowing highly pressurized helium rapidly into the propellant tank. The leak-before-burst design of the propellant tank was insufficient to prevent a catastrophic fragmentation. In another scenario, a low pressure residual fluid could lead to greater consequences; i.e., more debris generation, if its tank were struck by a small or large hypervelocity particle.

4.7.3.1.3 Storage Orbits

Because of the height of the GEO regime, it becomes impractical to attempt to reenter spacecraft once their operational lifetime has expired. It is practical, however, to move these objects away from the useful GEO belt, such that other missions in the future may utilize these important orbits. Many studies have been performed to determine the precise change in altitude that ensures that a spacecraft will not reenter the GEO belt because of perturbing forces such as solar radiation pressure and lunar perturbations. The spacecraft's area-to-mass ratio can affect exactly how high it needs to be moved above GEO in order to not reenter the belt, but it typically is at least 200 km above, and in many cases can be 300 km above. It is equally important to minimize the eccentricity of the orbit. Long-term orbit prediction is necessary to find an orbit that ensures the object does not reenter the GEO regime over decades or centuries.

Storage orbits may also be between LEO and GEO as long as the perigee does not get below 2000 km height and the apogee does not threaten the GEO regime. Typically, to achieve this, the apogee must be at least 200 km below GEO, with the perigee at or above 2000 km.

4.7.3.1.4 Controlled Reentry

A very effective, yet expensive and technically difficult, technique to reduce the debris in LEO is to use a direct and controlled reentry once the mission is complete. However, this can be complex and require additional weight in fuel and additional risk that a system may not function properly. A controlled reentry is mostly necessary when it is known that a large satellite may not demise upon atmospheric reentry. An example of this is the Mir space station. Therefore, enough fuel reserve must be left to guide the object into unpopulated areas, usually the ocean. Although expensive, a controlled reentry eliminates the long term risk of on-orbit fragmentation by reducing the orbital lifetime to the mission lifetime.

4.7.3.2 U.S. Guidelines and Requirements

The U.S. National Space Policy of 2006, in Section 11 of the Intersector Guidelines, states:

> "Orbital debris poses a risk to continued reliable use of space-based services and operations and to the safety of persons and property in space and on Earth. The United States shall seek to minimize the creation of orbital debris by government and non-government operations in space in order to preserve the space environment for future generations. Toward that end:

- Departments and agencies shall continue to follow the United States Government Orbital Debris Mitigation Standard Practices, consistent with mission requirements and cost effectiveness, in the procurement and operation of spacecraft, launch services, and the operation of tests and experiments in space;
- The Secretaries of Commerce and Transportation, in coordination with the Chairman of the Federal Communications Commission, shall continue to address orbital debris issues through their respective licensing procedures; and
- The United States shall take a leadership role in international fora to encourage foreign nations and international organizations to adopt policies and practices aimed at debris minimization and shall cooperate in the exchange of information on debris research and the identification of improved debris mitigation practices."

From this Policy, NASA, the DoD, the FCC, and the U.S. Department of State each crafts their own guidelines to comply with the U.S. policy.

The National Space Policy requires that orbital debris mitigation measures be "consistent with mission requirements and cost effectiveness." Debris mitigation solutions, as a result of policy, will result in some added cost or payload penalty. By implementing these solutions early in the design process these penalties can be minimized, and that is one of the growing areas of focus for U.S. orbital debris requirements.

NASA Procedural Requirement (NPR) 8715.6 defines the procedures NASA uses to limit the generation of space debris in Earth orbit. This document was approved in early 2007, and was an update to the previous NASA Policy Directive 8710.3, which had most recently been revised in January 2003. In addition to limiting generation of debris in all Earth orbits, NASA also desires to limit the generation of debris in other space locations where future spacecraft may travel. These locations include lunar orbit, the Earth-Sun Lagrange points, Martian orbits, and others.

More specifically, NASA crafted a NASA-STD 8719.14 to which each NASA program that places a satellite in Earth orbit must adhere. NASA-STD 8719.14 uses specific and attainable metrics to define what is and is not compliant with the U.S. Space Policy. These metrics include:

- The limitation of the release of mission-related debris.
- The limitation of risk of collision with both large and small debris.
- A 25-year rule to limit the post-mission lifetime of all NASA payloads, rocket bodies, and mission-related debris to 25 years or less.
- The protection of the GEO belt for active spacecraft, ensuring that any object moved to a super-GEO orbit does not reenter the GEO regime for over 100 years (which usually means it will never reenter the GEO regime).
- Reliability metrics in excess of 90% for systems needed to attain PMD.
- Depleting onboard energy sources after completion of mission.
- The limitation of the risk of human casualty to be less than 1:10,000 for any reentering object.
- The limitation of the lifetime and sever risk of tethers.

Each NASA program must submit an ODAR and an End of Mission Plan at various stages of development, beginning with the PDR, all the way through decommissioning and reentry. These

reports are reviewed for technical content, and any object that is not in compliance with the requirements put forth by NASA-STD 8719.14 must justify the noncompliance in terms of cost and mission after each is reviewed individually to ensure that no other option is available.

The U.S. DoD space policy, dated July 1999, expressly addresses orbital debris as a factor in the planning of military space operations. The DoD space policy states, "The creation of space debris shall be minimized, in accordance with 1996 National Space Policy (the version predating the 2006 National Space Policy). Design and operation of space tests, experiments, and systems shall strive to minimize or reduce the accumulation of such debris consistent with mission requirements and cost effectiveness." The policy adds, "spacecraft disposal shall be accomplished by atmospheric reentry, direct retrieval, or maneuver to a storage orbit to minimize or reduce the impact of future space operations." [anon. 1999]. In 1998, a NASA-DoD working group was organized to meet annually to share information on debris activities within the two organizations. Coordinated programs of observation and modeling of explosions and collisions, with the resulting environment, are conducted by both organizations. The research aids satellite and booster program offices by assessing vehicle-specific debris hazards and debris abatement options.

The FCC first officially noted the issue of debris mitigation in 1994, mostly in connection with large LEO constellations. The FCC participated in the 1995 Interagency Report on Orbital Debris, and in subsequent years participated in the U.S. Government's development of debris mitigation. By 2000, the FCC adopted their first policy, and in June 2004, the FCC adopted a comprehensive set of regulations concerning mitigation of orbital debris. These regulations apply to licensing of commercial U.S. satellites and the use of non-U.S. satellites to provide service in the United States. The rules require disclosure, prior to authorization, of debris mitigation measures, including end-of-life measures. The regulations are consistent with the guidelines adopted by the IADC [Kensinger 2005].

All U.S. commercial activities subject to the DoT authority are subject to the Office of Commercial Space Transportation's regulations established in Chapter III, 14 Code of Federal Regulations Part III. These regulations require each applicant to address safety issues with respect to its launch, including the risks of associated orbital debris, on-orbit safety, and reentry hazards.

4.7.3.3 Improvements Shown Since First Guidelines Were Implemented

As governmental and regulatory agencies have adopted more universal policies in limiting the generation of orbital debris, there has been a cessation in the increase of fragmentation events, but not yet a noticeable decrease. Of course, as many objects stay in orbit for decades, if not centuries, it may take several years to attain measurable success in tangible reduction of breakup events. However, as certain classes of objects show repeated incidents, it can be said that specific debris mitigation measures have reduced certain types of events throughout the last decade and a half.

The rate of satellite breakups increased noticeably in the 1970s, and has continued through the 1990s and into the new millennium at an average pace of approximately five fragmentations per year. Increased awareness of potential hazards has resulted in positive actions to mitigate or eliminate many known breakup causes; *e.g.*, Delta second stages, weapons testing, and Cosmos

699- and 862-type events. Together, these four programs were responsible for half of the breakups in the 1980's. The quick response of Arianespace (and ESA) to the breakup of an Ariane third stage in 1986 is indicative of a desire by almost all space-faring organizations to operate responsibly in near-Earth space. However, as new boosters are designed, there is the potential for new problems to develop, and therefore the need for organizations and companies to respond in a swift manner will remain critical [Johnson *et al.* 2004].

It is inevitable, it should be noted, that some causes of breakup remain unknown. Especially when derelict spacecraft produce relatively few breakup debris, certain causes (like catastrophic explosion or collision) can be ruled out, but the cause may never be known for certain. To date, there have been 34 breakup events of unknown cause, including 6 events since 2004 (almost half of the total breakups in that timeframe).

4.7.4 Other Agencies/UN Guidelines

While NASA was the first space agency in the world to issue a comprehensive set of orbital debris mitigation guidelines, other countries and organizations, including Japan, France, Russia, and ESA have followed suit with guidelines of their own. In 2002, after a multi-year effort, the IADC, comprised of the space agencies of 10 countries as well as ESA, adopted a consensus set of guidelines designed to mitigate the growth of the orbital debris population. These guidelines were formally presented to the STSC of COPUOS in February 2003. In June 2005, representatives from over a dozen member States and ESA (which holds an official Observer status) participated in a session to begin drafting a set of space debris mitigation guidelines. As a result of this 4-day meeting, a consolidated set of draft space debris mitigation guidelines were produced. On 1 March 2006, the Space Debris Working Group formally presented the Subcommittee with a draft document entitled "U.N. COPUOS STSC Space Debris Mitigation Guidelines." The concise document contains seven numbered guidelines addressing debris released intentionally or unintentionally during deployment, operations, and post-mission disposal in all altitude regimes. After a full year of review in 2006, the guidelines were adopted at the 44th meeting of the Subcommittee in February 2007 [anon. 2005a, anon. 2006b, and anon. 2007].

ESA has been a leader in pushing for the adaptation of international debris mitigation guidelines. In June 2004, the European Code of Conduct on space debris mitigation was approved for the first time by ESA and its partner agencies. The elements of the European Code of Conduct are consistent with the IADC Debris Mitigation Guidelines, while providing greater detail and rationale. Like the NASA Standard, the Code of Conduct is intended to be used by projects in the early phases to reduce space debris, while also giving an insight into necessary future practices. It should be noted that the Code of Conduct is technically voluntary, but does require that projects that cannot comply should justify and record the noncompliance. France adopted the European Code later in 2004 [anon. 2004].

In 2000, Russia put into force a "General Requirements for Mitigation of Space Debris Population." The requirements in this standard are consistent with those of other agencies within the IADC [anon. 2006a]. Russia has in place a Space Debris Mitigation Standard, which again follows the IADC guidelines, including special consideration for SOZ motors, which have had a history of explosion post-mission [Johnson 1995, Johnson 2004].

The National Space Development Agency (NASDA [one of the three agencies that later became JAXA]) of Japan first adopted a Space Debris Mitigation Standard in March of 1996, becoming one of the first agencies to do so. The Standard addressed all of the pertinent debris issues, such as collisions, released debris, and maintenance of the GEO belt. The Standard was updated in 2003 to align more closely with the IADC standard [anon. 2003].

All of the above agencies were leaders in establishing the IADC Guidelines, and remain active on the UNCOPUOS-STSC committee.

4.7.5 Software Tools

4.7.5.1 DAS 2.0

NASA developed DAS 2.0 to assess compliance with NASA-STD 8719.14. DAS 2.0 is an upgrade to DAS 1.5.3, which assessed compliance with the previous NSS 1740.14. As in previous versions, the DAS 2.0 software follows the structure of the Standard and provides the user with tools to assess compliance with the requirements. If a project is noncompliant, DAS may also be used to explore debris mitigation options to bring the project within the requirements. DAS can be obtained for free by download from the NASA Orbital Debris Program Office website (www.orbitaldebris.jsc.nasa.gov). Not every requirement from the Standard can be assessed with DAS. Some assessments, like the reliability of a subsystem for PMD, or the probability of controlled reentry, must be done independently from DAS.

DAS uses the latest NASA models, such as ORDEM, PROP3D, GEOPROP, and others, in order to best evaluate compliance with the Standard. A GUI allows the user to set up an entire mission, including launch date, orbital parameters, post-mission disposal plans, and so forth. Several “Science and Engineering” tools are included as well, so that the project or user can do simple calculations (such as orbital lifetime or collision risk with small particles) without having to enter each piece of information. DAS includes a reentry assessment, in which the user can enter up to 200 objects, in up to four nested levels for additional fidelity.

As NASA’s standard method of assessing compliance with NASA-STD 8719.14, the new DAS 2.0 is an important tool for use in space mission design. The many improvements in the interface and the underlying models have yielded a product that is both higher fidelity and easier to use than previous versions of DAS. More information on DAS 2.0 can be found in the Users Guide located in the Appendix of this document.

4.7.5.2 DRAMA

In 2004, the Debris Risk Assessment and Mitigation Analysis (DRAMA) tool was developed by ESA to assess compliance with the European Code of Conduct for Space Debris Mitigation. Like DAS 2.0, DRAMA uses a GUI to utilize five individual software applications. The five applications address collision avoidance maneuvers, collision with small particles (and associated damage), disposal maneuvers and lifetimes, reentry survivability, and reentry risk. The development of this tool was an important step in the proactive implementation of debris mitigation measures in Europe [Martin *et al.* 2005].

4.7.6 Future of Mitigation

4.7.6.1 Improved Design of Space Platforms

As there was an increase in the awareness of the orbital debris problem, both at the national and international level, it became apparent that one of the ways to mitigate the debris problem was to improve the design of space platforms. This improvement continues today, as governments, projects, and programs reevaluate their designs with, in addition to mission requirements, the reduction or elimination of debris as a goal.

Launch vehicles and spacecraft can be designed so that they are litter-free; *i.e.*, they dispose of separation devices, payload shrouds, and other expendable hardware (other than upper stage rocket bodies) at a low enough altitude and velocity that they do not become orbital. This is more difficult to do when two spacecraft share a common launch vehicle. In addition, stage-to-stage separation devices and spacecraft protective devices such as lens covers and other potential debris can be kept captive to the stage or spacecraft with lanyards or other provisions to minimize debris. This is being done in some cases as new projects or new designs allow. These practices should be continued and expanded when possible.

The task of litter-free operations could combine design and operational practices to achieve the goal of limiting further orbital debris created by any space operations. As a result of these efforts, the growth rate of orbital debris will decline, although the overall debris population will still increase.

As mentioned in an earlier section, when stages and spacecraft do not have the capability to deorbit, they need to be made as inert as feasible. Expelling all propellants and pressurants and assuring that batteries are protected from spontaneous explosion requires modifications in either design or operational practices for both stages and spacecraft. These modifications are occurring today, as more governments, programs, and companies have redesigned the “next” generation of launch vehicles and space busses to allow for energized systems to be passivated at the end of mission.

For systems that have multiburn (restart) capability, there are few, if any, design modifications required. For systems that do not have multiburn capability, design modifications to expel propellants are more extensive. Research could be conducted to develop particle-free solid propellants. If successful, this technology research effort could eliminate the Al_3O_2 particulates produced by current SRM propellants. Such a program already exists for tactical missile propellant, but there is no work currently being done for space applications.

Similarly, using materials that tend to demise upon reentry remains one of the more important strategies in reducing the debris risk to persons on the Earth. Advances continue in both of these areas, and as the debris problem becomes more apparent, it can be concluded that more resources will be earmarked for these important issues.

4.7.6.2 Debris Remediation

While the improvement of mission and hardware design will certainly aid in the overall orbital debris problem, recent studies have concluded that it will not be enough to keep the orbital debris population from growing in the 21st century. Even if there were no further launches, in 20-30

years debris producing collisions would slowly add to the population count without control [Liou and Johnson 2006]. This sort of study can lead to the conclusion that some sort of program to actively remove debris from orbit may be necessary to completely control the orbital debris issue. The discussion of debris remediation pertains only to LEO because at present, there is no capability or need for a removal system at GEO.

The removal of large inert objects requires an active maneuver vehicle with the capability to rendezvous with and grapple an inert, tumbling, and non-cooperative target and the ability to properly and accurately apply the required velocity increment to move the object to a desired orbit. While these capabilities have been demonstrated by the Space Shuttle, no uninhabited system has these capabilities for higher altitudes and inclinations. The design, development, and operation of a maneuverable stage to remove other stages and spacecraft requires a high degree of automation in rendezvous, grapple, and entry burn management if operations costs are to be kept practical. The component technologies require study and analysis, followed by breadboard and prototype development.

Small objects would be even less practical to acquire and remove individually. A technique such as an energy-absorbing balloon or laser-type technology would be the most applicable for this sort of removal. But in the larger challenge of limiting the debris in orbit in the future, the smaller objects will not pose as much of a long-term problem because of the smaller masses. Fewer fragments are generated from each potential collision.

The potential for debris remediation hinges on the development of cost-effective and innovative ways to remove existing derelict orbital platforms. Because of the inevitable high cost and lack of immediate financial gain (in terms of dollars and cents), it is apparent that government involvement with the private sector is the only way forward. Without this debris remediation, current policies will only manage to slow down the debris count increase with no realized reduction.

4.7.6.3 Outlook of GEO Regime

As mentioned, there is no apparent, immediate need to actively remove objects from the GEO regime; raised (or graveyard) orbits are more than efficient at preserving the GEO belt for operational satellites while not contaminating any other useful orbital area. It should be noted that disposal orbits are not the only available strategy. The cost effectiveness of a disposal orbit strategy, compared with other strategies, has not been thoroughly examined. If raising the orbit is to be the technique of choice, then it requires planning and reserving the necessary propellant resources to effect the maneuver. To ensure the spacecraft does not reenter the operational GEO belt, an orbit-raising maneuver of at least 200 to 300 km should be performed, which is the rough equivalent of 3 to 6 months of station-keeping fuel.

4.7.6.4 Martian and Lunar Debris Issues

The U.S., India, and China have publicly stated their desire to expand their exploration programs for both the Moon and Mars, while other space-faring nations will likely develop future programs to explore the same. There is increased attention on developing policies and procedures for how to approach the unique debris problems around these heavenly bodies.

Particularly if, and when, humans are sent on missions back to the moon or to Mars, the importance of creating a safe environment to explore will only increase.

Under the NASA-STD 8719.14, programs will be required to consider many of the same debris mitigation requirements that apply to the Earth environment. Specifically, it is recommended that projects limit the release of mission-related debris, ensure that all systems are passivated, adhere to the 25-year rule for leaving objects in orbit, and ensure that tether operations neither collide with resident objects in orbit, nor create unnecessary debris if severed.

4.7.7 References

Anon., "Space Policy," Department of Defense Directive Number 3100.10, United States Department of Defense, 9 July 1999.

Anon., "Space Debris Mitigation Standard," NASDA-STD-18A, National Space Development Agency of Japan; 11 June 2003.

Anon., "European Code of Conduct for Space Debris Mitigation, Issue 1.0," European Space Agency; 28 June 2004.

Anon., "Space Debris Mitigation Guidelines at the UN," The Orbital Debris Quarterly News, NASA JSC, p. 1, July 2005a. Available online at http://www.orbitaldebris.jsc.nasa.gov/newsletter/pdfs/ODQNv9i3.pdf

Anon., Proceedings of the 4th European Conference on Space Debris, ESA SP-587, August 2005b.

Anon, "Presentation to the 43rd session of the Scientific and Technical Subcommittee of the UN Committee on the Peaceful Uses of Outer Spaces (COPUOS)", Federal Space Agency of Russia, Vienna, Austria, 20 February – 3 March 2006a.

Anon., "Draft United Nations Space Debris Mitigation Guidelines," The Orbital Debris Quarterly News, NASA JSC, p. 2, April 2006b. Available online at http://www.orbitaldebris.jsc.nasa.gov/newsletter/pdfs/ODQNv10i2.pdf

Anon., "United Nations Adopts Space Debris Mitigation Guidelines," The Orbital Debris Quarterly News, NASA JSC, p. 1, April 2007. Available online at http://www.orbitaldebris.jsc.nasa.gov/newsletter/pdfs/ODQNv11i2.pdf

Johnson, N.L. et al., History of On-Orbit Satellite Fragmentations, ed. 13, JSC-62530, NASA JSC, Houston, Texas, 2004.

Johnson, N.L. et al., "History of Soviet/Russian Satellite Fragmentations-A Joint U.S.-Russian Investigation," Kaman Sciences Corporation, October 1995.

Kensinger, K. et al., "The United States Federal Communications Commission's Regulations Concerning Mitigation of Orbital Debris," *Proceedings of the 4th European Conference on Space Debris*, ESA SP-587, pp. 571-576, Darmstadt, Germany, August 2005.

Kulik, S., "The Russian Federation Space Plan 2006-2015 and Activities in Space Debris Problems," *Proceedings of the 4th European Conference on Space Debris*, ESA SP-587, pp. 11-15, Darmstadt, Germany, August 2005.

Liou, J.-C. and N.L. Johnson, "Risks in Space from Orbiting Debris," Science, Volume 311, pp. 340-341, 20 January 2006.

Martin, C. et al., "A Debris Risk Assessment Tool Supporting Mitigation Guidelines," *Proceedings of the 4th European Conference on Space Debris*, ESA SP-587, pp. 345-352, Darmstadt, Germany, August 2005.

4.8 Reentry

4.8.1 Introduction

Since the orbital decay of Sputnik almost 50 years ago, approximately 16,000 space objects ranging from 10 cm to more than 25 meters in length that have reentered the atmosphere have been cataloged by the SSN. About one-quarter of all objects are of U.S. origin. On the average, one non-functional spacecraft, launch vehicle orbital stage, or other piece of cataloged debris has reentered the atmosphere every day for more than 40 years. Although more than 200,000 lbs of man-made objects fall back to Earth each year, the majority of these objects do not survive the intense reentry environment.

A photograph of the Compton Gamma Ray Observatory (CGRO) satellite breaking up over the Pacific Ocean in June 2000 is shown in Figure 4.8-1. Most of the objects from targeted or controlled entries, such as the CGRO, that do survive in whole or in part fall harmlessly into the oceans or onto sparsely populated regions such as Siberia, the Australian Outback, or the Canadian Tundra. Occasionally, components of spacecraft and launch vehicles are found. In the recent past, large objects have been recovered in Texas, Guatemala, Saudi Arabia, South Africa, and Uganda. Figure 4.8-2 shows a large (250 kg), stainless steel, cylindrical propellant tank from the Delta II second stage that landed in Georgetown, Texas in January 1997. Usually these large objects that have impacted the ground are from uncontrolled entries or orbital decay, so the impact point cannot be calculated exactly.

Although currently, there is one confirmed hit of a light piece of orbital debris (charred woven material 10 cm by 13 cm) striking a woman at a very low speed in Oklahoma in 1997, no casualties or injuries have been reported from components of reentering spacecraft [anon. 2007]. Nonetheless, debris from space hardware poses a risk to human life and property on the ground.

Generally, orbital reentry is assumed to begin at the entry interface altitude of 122 km (400,000 ft). Spacecraft that reenter from either orbital decay or controlled entry usually break up at altitudes between 84 to 72 km due to aerodynamic forces that cause the allowable structural loads to be exceeded. The nominal break-up altitude for spacecraft is considered to be 78 km. It is believed that larger, sturdier, and denser satellites generally break up at lower altitudes. Solar arrays frequently break off the spacecraft parent body earlier than the main spacecraft, and at higher altitudes (90-95 km), because of the aerodynamic forces that cause the allowable bending moment to be exceeded at the array-spacecraft attachment point.

The two most important parameters in reentry analysis are the ballistic coefficient of the object and its heat of ablation. The ballistic coefficient is dependent on the mass and the geometric shape of the object. It directly affects the trajectory path and velocity of a component and indirectly influences the heating rate of the object. The heat of ablation is based on the thermal properties of the material. Once the heat of ablation of an object has been reached, the object can be considered to have demised or burned up.

After spacecraft (or parent body) breakup, individual components or fragments will continue to lose altitude and experience aeroheating until they either demise or survive to impact the Earth. Many spacecraft components are made of aluminum, which has a relatively low heat of ablation. As a result, these components tend to demise at a higher altitude. Figure 4.8-3 shows the demise altitude for aluminum spheres as a function of both object diameter and object thickness. It is seen that aluminum objects of small diameters and/or thicknesses may demise, whereas aluminum objects with larger diameters and/or thicknesses may survive.

On the other hand, objects made of materials with relatively high heats of ablation (*e.g.*, titanium, stainless steel, beryllium, carbon-carbon), tend to survive reentry for even small diameters and thicknesses. Also, if an object is contained inside a metal housing, the housing must demise before the internal object can receive significant aeroheating and possibly demise.

Some objects may have a very high melt temperature such that they can never demise, but are so light (*e.g.*, tungsten shims), that they impact with a very low velocity. As a result, the kinetic energy at impact is sometimes under 15 J, a threshold below which the probability of human casualty is very low [Cole *et al.* 1996]. Thus, the debris casualty areas computed for these objects do not figure into the total debris casualty area in a reentry survivability analysis.

The precise location of an actual reentry cannot be known beforehand due to disturbances in the atmosphere and modeling inaccuracies (atmosphere density, atmospheric winds, solar cycle, drag coefficient, and others). However, the debris casualty risk due to an object can be quantified. It is driven by year of reentry, the debris casualty area, and orbit inclination. Other qualitative factors in the risk are the mass of the debris and the debris footprint. Reentries compliant with NASA-STD 8719.14 [anon. 2007] must have a risk lower than 1:10,000.

NASA JSC has been developing and modifying Object Reentry Survival Analysis Tool (ORSAT) [Rochelle *et al.* 1999, Smith *et al.* 2006] for over 10 years. This code has evolved into the NASA standard code for ground risk assessment of decaying satellites. The tool simulates the physics of reentry with five general modules: trajectory, atmosphere, aerodynamics, aerothermodynamics, and thermal/ablation. Thus, the tool is able to determine if, when, and how much an object or fragment demises during reentry. The final debris casualty area caused by the surviving objects or fragments is calculated, which is used to determine the reentry risk posed to the Earth's population. More details of the ORSAT code are described in the next section.

4.8.2 Current Status of Reentry Analysis

4.8.2.1 General Discussion of Code

The ORSAT code is the primary NASA computer code for prediction of reentry survivability of satellite and launch vehicle upper stage components entering the Earth's atmosphere from orbital decay or from controlled (targeted) entry. It is frequently used for a higher-fidelity survivability

analysis after the NASA DAS [Opiela and Johnson 2007] has determined that a spacecraft is possibly noncompliant with the NASA-STD 8719.14.

A 3-degree of freedom trajectory is used for either orbital decay or for a controlled entry for the analysis. This trajectory is propagated by integrating relative equations of motion for the time rate of change of altitude, relative velocity, relative flight path angle, latitude, longitude, and heading angle. A fourth-order Runge-Kutta numerical scheme is used to solve these trajectory equations in ORSAT. In the case of a controlled entry, the apogee and perigee are normally entered into the program, while the relative velocity and flight path angle are not included. The parent body trajectory is normally run until an assumed break-up altitude; then trajectories of the individual fragments (components) are run to the point of demise or survival. Controlled entry normally occurs by using a larger amount of propellant with a larger propulsion system to drive the spacecraft to enter the atmosphere at a steeper flight path angle. It will then enter at a more precise latitude, longitude, and footprint in a nearly uninhabited impact region, generally located in the ocean.

The trajectory may be generated using several atmosphere models in ORSAT such as the 1976 U. S. Standard Atmosphere [anon. 1976], the Mass Spectrometer Incoherent Scattering – extended 1990 (MSISe-90) atmosphere [Hedin 1991], or the Global Reference Atmosphere Model-1999 [Justus *et al.* 1999]. An option also exists for the user to enter a customized atmosphere as input to the code.

Objects may be modeled as spheres, cylinders, boxes, cones, disks, and flat plates. ORSAT uses drag coefficients for these objects along with the above atmosphere model and trajectory to examine the path of the object during reentry. Up to 17 modes for these objects may be considered with relative motions such as spinning, tumbling, normal to flow, random tumbling and spinning, end-on spinning, etc. The drag coefficients are defined for continuum flow and free-molecular flow, with curve fits (bridging functions) as functions of Knudsen number in the transition flow regime. These drag coefficients are derived in most cases as a function of diameter and length of the object. Most of the original drag coefficients for spheres and cylinders in ORSAT were based on the relations of Sandia Corporation's Cropp [Cropp 1965] and Klett [Klett 1964], respectively.

Although hypersonic relations were originally used to generate tables of drag coefficients, lower-speed drag coefficients (supersonic, transonic, and subsonic) were added to the code so that the velocity and kinetic energy at ground impact could be computed. Most of these lower-speed drag coefficients are determined as a function of the free stream Mach number. For hypersonic speeds, the ballistic coefficient may vary with time due to the high-temperature ablation of the material, which reduces both mass and area, and in some cases, changes the drag coefficient.

Convective heating rates are computed in ORSAT for the same type of object and mode of entry as the drag coefficients discussed previously. Cold wall stagnation-heating rates to spheres are generated for ideal gas relations using the Detra, Kemp, and Riddell method [Detra *et al.* 1957]. However, for real-gas cases, stagnation heating rates to spheres are computed by the Fay and Riddell method [Fay *et al.* 1958]. Methods exist in the code for analyzing the heating to objects other than spheres by adjusting the object's heating rate to the sphere stagnation point value so that an average value over the body can be obtained if it is spinning or tumbling. Cold wall heating rates are adjusted for hot wall values with a coefficient based on the enthalpy difference.

The net heating rate to a reentering object is computed as the sum of the hot wall heating rate, the oxidation heating rate, and the gas cap radiative heating rate (negligible for orbital or suborbital entry), minus the surface reradiative heating rate. The reradiative heating rate depends on the surface temperature of the body, raised to the fourth power, and the surface emissivity of the material. This emissivity is included in ORSAT as a function of surface temperature for many cases. The oxidation heating rate is based on the heat of oxidation of the material and an oxidation efficiency.

The stagnation value of gas cap radiation is computed in ORSAT 6.0 with the Jones-Park method [Hamilton *et al.* 1991]. It is a function of the atmospheric density, the velocity of the body, and the nose radius. This gas-cap radiation is negligible for objects reentering from Earth orbit; however, for higher speeds, where the reentry velocity may be of the order of 9-11 km/sec (*e.g.*, lunar return missions), this radiation mode of heating can be of the same order as convective heating – especially if the object has a large nose radius.

During the reentry simulation, the net heating rate is summed to obtain the integrated heat load at each time step of the trajectory. The integrated heat load is multiplied by the surface area of the particular object to project the absorbed heat to the body at each time step. When this absorbed heat becomes greater than the material heat of ablation, the object is considered to demise.

Three general models may be used to predict the temperature of the object in ORSAT:

- lumped mass model
- 1-dimensional heat conduction model
- 2-dimensional heat conduction model.

The 2-dimensional model was added to the latest version of ORSAT and is limited to spheres and cylinders. The lumped mass model is normally used for cones and end-on cylinders. When the lumped mass model is used, the temperature of the material is equal to the temperature of the previous time step, plus the integrated heat load, divided by the mass of the object multiplied by its specific heat. When the integrated heat load multiplied by reference area exceeds the heat of ablation of the model, the object is considered to ablate and consequently demise. The heat of ablation per mass of the object is defined as the material heat of fusion plus the specific heat integrated from the initial to melt temperature, multiplied by temperature difference from initial to melt temperature.

The lumped mass method is valid for thin objects of high thermal conductivity (*e.g.*, aluminum). However, for thicker metallic objects and objects of lower thermal conductivity (especially insulation materials), a heat conduction model must be used to compute the transfer of heat through the body and the corresponding temperature gradient. In ORSAT, the temperature response is determined by using a Forward Time Central Space finite difference solution for either hollow or solid spheres and cylinders. Two-dimensional thermal math models were developed for ORSAT 6.0. The advantage of using a 2-dimensional model is that it provides the time when the wall of the object is breached.

Up to six materials may be considered across the body in a single dimension. The material property data base in ORSAT now has approximately 85 materials. Seven properties are included for each material for most cases. These properties are density, specific heat, thermal conductivity, melt temperature, surface emissivity, heat of oxidation, and heat of fusion. In

nearly all cases, the thermal conductivity is included as a function of temperature. In many cases, the emissivity and specific heat also vary with temperature.

After ORSAT has computed the analysis of all components for a particular spacecraft, a number of objects are usually found to survive reentry. These objects that survive will impact the Earth and contribute to the risk for the Earth's population. The debris casualty area is equal to the sum of the individual debris casualty areas of the objects that survive. The individual debris casualty area is calculated by first taking the square root of the debris reference area of the particular object at impact, plus a factor of 0.6 m. This quantity is then squared to obtain units of area. The value 0.6 m represents the square root of the average cross sectional area (0.36 m^2) of a standing individual, as viewed from above.

For an object entering from orbital decay, the expected number of casualties or risk to the population may be computed as the probability of impact in the region, times the population density in the region, times the total debris casualty area as computed above [Opiela and Matney, 2003]. The probability and population density are determined as a function of orbit inclination and apply for the entire range of longitude around the Earth. This is because, for a decaying orbit, it is never known precisely at which longitude region the spacecraft fragment will impact. For targeted entries in which there is a narrow longitude region, the risk may also be computed from the total debris casualty area.

The latest version of ORSAT also contains additional features not contained in earlier versions. These features include a GUI for simplifying the input file; recession rate of ablators; structural failure of solar arrays; tank bursting; Unix and Linux plotting scripts for plotting trajectory, aerodynamics, and aerothermal parameters immediately after each run; and trajectory mapping onto a world map.

4.8.2.2 Application to Specific Spacecraft

The ORSAT code has been used to analyze the reentry survivability of many spacecraft over the years. These spacecraft include both satellites and upper stages of launch vehicles. A number of these spacecraft contain proprietary components (including most of the launch vehicle upper stages), so that references for these analyses will not be given in this handbook.

Specific satellites that were analyzed by ORSAT which do not include proprietary data include the CGRO [Smith and Rochelle 2000], Genesis Bus [Rustick *et al.* 2000 and Smith *et al.* 2004], Extreme Ultraviolet Explorer [O'Hara *et al.* 2001], Earth Observation System(EOS)-Aqua [Rustick *et al.* 2001], EOS-Aura [Smith *et al.* 2001], UARS [Marichalar *et al.* 2002], Tropical Rainfall Measuring Mission [Smith *et al.* 2002], Gamma-ray Large Area Space Telescope [Smith *et al.* 2003], HST [Smith *et al.* 2005], and EOS-Terra [Smith *et al.* 2005].

Other satellites analyzed by ORSAT, but which contain proprietary data, include the German ROentgen SATellit (ROSAT) X-Ray telescope, National Polar-orbiting Operational Environment Satellite System (NPOESS), and the NPOESS Preparatory Project.

Examples of launch vehicle upper stages analyzed by ORSAT, which contain proprietary data, include the Delta IV (4- and 5-m diameters), the Pegasus, and the Atlas V/Centaur. Two major studies of the Space Shuttle vehicle, which do not contain proprietary data analyzed with

ORSAT, were the Space Shuttle Orbiter [Dobarco-Otero *et al.* 2004] and the Space Shuttle External Tank [Smith *et al.* 2004].

A detailed reentry survival analysis of the HST was performed with the ORSAT code [Smith *et al.* 2005]. A cut-out view of the HST is shown in Figure 4.8-4. Figure 4.8-5 presents a typical analysis of the surface temperature of several components that survived from this spacecraft. The Reaction Wheel Assembly (RWA) aluminum housing reaches its melt temperature of 867 K and soon demises, exposing the RWA flywheel, which is made of steel. Although the flywheel reaches its melt temperature of 1700 K as it loses a few layers of material, this was not enough to cause the object to fully demise (*i.e.*, integrated heat load times reference area did not reach the material heat of ablation). The flywheel then begins to cool, and the surface temperature drops as the object falls to the Earth. The other component shown, the Ultra Low Expansion glass primary mirror, never reaches its high melt temperature of 1760 K before it begins to cool and impacts the ground.

In a typical reentry survivability analysis with ORSAT, the demise altitude is frequently plotted as a function of downrange. In this manner, it is possible to see the altitude at which individual objects of the spacecraft demise, and the associated downrange. The shortest distance (heel) usually represents the object with the smallest ballistic coefficient, and the longest distance (toe) usually represents the object with the largest ballistic coefficient. The distance between the heel and toe of these objects is designated as the footprint of the spacecraft.

An example of such a plot is shown in Figure 4.8-6 for the HST spacecraft [Smith *et al.* 2005]. The figure shows the demise altitude of nearly all the 600 objects analyzed falling on top of each other from 78 km (assumed break-up altitude) until around 60 km, where there is a scatter in the demise altitude at various values of downrange. In this case, the footprint was 1219 km. This represents the difference between 1546 km (downrange of base disk) and 327 km (downrange of New Outer Blanket Layer bay).

Based on the computed total debris casualty area of 146 m^2 of the HST, the impact risk was obtained as a function of year of reentry (based on a 28.5° inclination angle). This risk is shown in Figure 4.8-7 for the HST. This risk increases with year of entry because of the increase in world population during this time period. Because of the relative high risk (of the order of 1:340), this spacecraft was noncompliant with the NASA-STD.

4.8.3 Analyses of Reentry Survival by Other Agencies

Two other major groups in the world have also been evaluating reentry survival of spacecraft. These include the group led by Hyperschall-Technologie Gottingen (HTG) in Katlenburg-Lindau, Germany, under contract to the German Center for Aeronautics and Spaceflight Research, and the group at the Center for Orbital and Reentry Debris Studies at Aerospace Corporation in El Segundo, California, under contract to the USAF Space and Missile Systems Center. In addition, a group at JAXA has been performing analyses of spacecraft survival. A group at the Boeing Company in Aurora, Colorado, has also recently been assessing the survival of deorbiting spacecraft. A short discussion and sample references will be given for each of these four groups and their respective computer codes for reentry survival.

4.8.3.1 HTG

The group at HTG has developed a detailed reentry survival code, the Space Craft Atmospheric Reentry and Aerothermal Break-up (SCARAB) code [Lips and Fritsche 2004]. As stated in a paper presented at the 55th IAC, the trajectory in SCARAB is predicted by a numerical integration of the 6-DOF equations of motion for an oblate Earth [Lips and Fritsche 2004]. In continuum flow, the aerodynamic and aerothermodynamic models are based on modified Newtonian theory and modified Lee's theory, respectively. In free-molecular flow, Nocilla or Schaaf-Chambre accommodations are used. The code uses the drag coefficients determined experimentally by Koppenwallner [Koppenwallner 1985].

As stated by Lips and Fritsche, the SCARAB code has a graphical modeling system that has distinct hierarchy levels. These allow composing a complex system by subsystems, compounds, elements, and finally primitives (elementary geometry shapes such as spheres, cylinders, boxes, and so forth) as the lowest level. For each construction element, the mass, center of mass location, and the moment of inertia matrix are generated. The final output of the modeling process is a completely panelized, consistent geometric model of the spacecraft.

Destruction by melting in SCARAB is analyzed on the panel level. Breaking forces can be monitored for predefined cuts. Fragments are either generated if parts of the spacecraft have lost connection because of melting panels, or if the analyzed stress of a cut exceeds the maximum stress. Each fragment is analyzed until it demises completely, fragmentizes again, or reaches the ground.

A number of analyses, including those for specific spacecraft, have been reported by HTG for the SCARAB code, including those in Fritsche *et al*. 1999, Fritsche *et al.* 2000, Lips *et al*. 2002, Lips *et al.* 2003. The first comparison of SCARAB with ORSAT was reported in 1999 [Rochelle *et al.* 1999] for three baseline cases of a 1 m diameter sphere using three different materials (aluminum, titanium, steel) at two angles of inclination, with both codes using the same material properties. Reasonably good correlation was obtained between the two codes for these spherical shapes. A more recent comparison of ORSAT and SCARAB reentry survival results was reported by Lips and Dobarco-Otero in 2005, which described results from additional spherical cases, cylindrical cases, and using another material. Very good correlation was obtained between the two methods in a number of cases. Also, reasonable comparisons were made between the two codes for the entry of the components of the German ROSAT satellite (proprietary data). For a complete spacecraft analysis (such as ROSAT), the main difference between using ORSAT and SCARAB is that, with SCARAB, objects are continuously separated from the parent body, whereas with ORSAT, typically a breakup altitude of 78 km is used.

4.8.3.2 Aerospace Corporation

The analyses previously reported by the group at Aerospace Corporation have centered on implicit expressions for the breakup altitude for spacecraft with thin and thick skin surfaces [Baker *et al.* 1999] and probabilistic estimations of the debris casualty area [Weaver *et al.* 2001]. This group has also been examining debris by laboratory analysis, including both metallurgical and microstructural analyses [Baker *et al.* 1999]. Also, the group has proposed a Reentry Breakup Recorder (REBR) to monitor spacecraft during reentry and transmit the useful data to

ground monitors [Kapoor and Ailor 2003]. The data from the REBR is planned to be used for verification for the various reentry codes.

Recently, the Aerospace group has performed a reentry survival analysis with their new Atmospheric Heating and Breakup (AHaB) code to determine the reentry risk assessment for the NASA Cure-in-Place Ablator Applicator (CIPAA) [Martin and Weaver 2003]. In this analysis, the CIPAA was divided into 87 component types, resulting in 103 total components.

This AHaB code is believed somewhat similar to ORSAT in flight trajectory, heating environment, and body thermal response predictions. However, there has not been a published description of the AHaB code, to date.

4.8.3.3 JAXA

A code used in the JAXA study is called ORSAT-J [Kato *et al.* 2002]. The aeroheating analysis and thermal response analyses in ORSAT-J were imported from the NASA ORSAT code (Version 4.0), but the trajectory module was changed to use the Program to Optimize Simulated Trajectories (POST) code [Brauer *et al.* 1990] for the orbit and trajectory analysis.

4.8.3.4 Boeing

Two recent analyses have been presented which give details of new Boeing studies for disintegrating deorbiting spacecraft without heat shields [Reynerson 2005] and of structural failure due to atmospheric heating [Reynerson 2006]. These papers give the details of the modeling during reentry including trajectory, drag and lift coefficients, object characteristics, reentry envelope, ground track, failure of arrays and appendages due to aerodynamic force, and structural failure due to reentry heating.

4.8.4 Future Improvements

Future improvements to the ORSAT code are being developed. One of these is the ability to override various modules. This includes importing a trajectory from a higher-fidelity model to use in the ORSAT simulation. Also, the aerodynamics calculation can be overridden so that constant ballistic coefficients or drag coefficients may be input as a function of Mach number.

Also, additional relations for the gas cap radiation are being incorporated into ORSAT. These include the method of Tauber-Sutton [Tauber and Sutton 1991], which is another trajectory-based method, and the QRAD code [Rochelle and Rohan 1992]. The QRAD program is a more detailed 4-band model, which computes radiation for infrared lines, visible continuum, ultraviolet lines, and ultraviolet continuum, based on tabulated absorption coefficients as a function of stagnation pressure and enthalpy.

4.8.5 References

Anon., “U.S. Standard Atmosphere, 1976,” NASA-TM-X-74335 NOAA-S/T-76-1562, U.S. Government Printing Office, 1976.

Anon., NASA Standard (NASA-STD) 8719.14, Process for Limiting Orbital Debris, NASA-STD 8719.14, August 2007.

Anon., http://www.aero.org/capabilities/cords/reentry-overview.html, October 2007.

Baker, R.L., M.A. Weaver, D.M. Moody, and C.-C. Wan, "Orbital Spacecraft Reentry Breakup," 50th International Astronautical Congress, IAA-99-IAA.6.7.04, Amsterdam, the Netherlands, 4-8 October 1999.

Brauer, G.L, D.E. Cornick, and R. Stevenson, "Program to Optimize Simulated Trajectories (POST)," Final Report for NASA contract NAS1-18147, Martin-Marietta Corp., September 1990.

Cole, J.K. and W.P. Wolfe, "Hazards to People and Aircraft from Flight Test Data Generated at High Altitudes," AIAA-96-0070, January 1996.

Cropp, L.O., "Analytical Methods used in Predicting the Re-Entry Ablation of Spherical and Cylindrical Bodies," SC-RR-65-187, Sandia Corporation, September 1965.

Detra, R.W., N.H. Kemp, and E.R. Riddell, "Addendum to Heat Transfer to Satellite Vehicles Reentering the Atmosphere," Jet Propulsion, Vol. 27, No. 12, pp. 1256-1257, December 1957.

Dobarco-Otero, J., R.M. DeLaune, and R.N. Smith, "Reentry Survivability Analysis of Shuttle Orbiter Debris," JSC-62672 Rev. A, September 2004.

Fay, J.A. and F.R. Riddell, "Theory of Stagnation Point Heat Transfer in Dissociated Air," Journal of the Aeronautical Sciences, Vol. 25, No. 2, pp. 73-85, February 1958.

Fritsche, B., T. Roberts, M,. Romay, M. Ivanov, E. Grinberg, and H. Klinkrad, "Spacecraft Disintegration during Uncontrolled Atmospheric Re-Entry," *50th International Astronautical Congress*, AIAA 99-IAA.6.7.02 Amsterdam, the Netherlands, 1999.

Fritsche, B., H. Klinkrad, A. Kashkovsky, and E. Grinberg, "Application of SCARAB to Destructive Satellite Re-entries," *51st International Astronautical Congress*, IAA-00-IAA.6.5.08 Rio De Janeiro, Brazil, 2-6 October 2000.

Hamilton, H.H., R.N. Gupta, and J.J. Jones, "Flight Stagnation-Point Heating Calculations on Aeroassist Flight Experiment Vehicle," Journal of Spacecraft and Rockets, Vol. 28, No. 1, pp. 125-127, January – February 1991.

Hedin, A.E., "Extension of the MSIS Thermosphere into the Middle and Lower Atmosphere," Journal of Geophysical Research, Vol. 96, No. A2, pp. 1159-1172, 1 February 1991.

Justus, C.G. and D.L. Johnson, "The NASA/MSFC Global Reference Atmospheric Model – 1999 Version," May 1999.

Kapoor, V.B. and W.H. Ailor, "The Reentry Breakup Recorder: A 'Black Box' for Space Hardware," *17th Annual AIAA/USC Conference on Small Satellites*, SSC02-VIII-3, 2003.

Kato, A., Y. Hyodo, and K. Kishida, "Toward the World Common Re-Entry Safety Assessment Procedure," *Japan Society for Aeronautical and Space Sciences*, ISTS 2002-n-14, 2002.

Klett, R.D., "Drag Coefficients and Heating Ratios for Right Circular Cylinders in Free-Molecular and Continuum Flow from Mach 10-30," SC-RR-64-2141, Sandia Corporation, December 1964.

Koppenwallner, G., "The Drag of Simple Shaped Bodies in the Rarefied Hypersonic Flow Regime," AIAA-85, 0998, Williamsburg, Virginia, 19-21 June 1985.

Lips, T., B. Fritsche, G. Koppenwallner, and H. Klinkrad, "Spacecraft Destruction during Re-Entry – Latest Results and Development of the SCARAB Software System," *2002 World Space Congress*, PEDAS1-B1.4-0030-02, 2002.

Lips, T., B. Fritsche, G. Koppenwallner, A. Zaglauer, and R. Wolters, "Re-Entry Analysis of TERRASAR-X with SCARAB," *54th International Astronautical Congress*, Bremen, Germany, October 2003.

Lips, T. and B. Fritsche, "A Comparison of Commonly Used Re-entry Analysis Tools," *55th International Astronautical Congress*, IAC-04-IAA.5.12.2.09, Vancouver, Canada, 2004.

Lips, T., G. Fritsche, G. Koppenwallner, and H. Klinkrad, "Spacecraft Destruction During Re-entry – Latest Results and Development of the SCARAB Software System," Adv. Space Research, 34, pp. 1055-1060, 2004.

Lips, T., *et al.*, and Dobarco-Otero, J., *et al.*, "Comparison of ORSAT and SCARAB Reentry Survival Results," *Proceedings of the 4th European Conference on Space Debris*, ESA SP-587, pp. 533-538, Darmstadt, Germany, August 2005.

Marichalar, J.J. and W.C. Rochelle, Reentry Survivability Analysis of Upper Atmosphere Research Satellite (UARS), JSC-29647, January 2002.

Martin, G.D. and M.A. Weaver, "Reentry Risk Assessment for Cure-in-Place Ablator Applicator (CIPAA)," *Presented to NASA*, 23 August 2005.

O'Hara, R.E. and N.L. Johnson, "Reentry Survivability Analysis of the Extreme Ultraviolet Explorer (EUVE)," *Proceedings of the 3rd European Conference on Space Debris*, ESA SP-473, Darmstadt, Germany, October 2001.

Opiela, J. N. and M. J. Matney, "Improvements to NASA's Estimation of Ground Casualties from Reentering Space Objects," IAC-03-IAA.5.4.03, 54th International Astronautical Congress, September-October 2003.

Opiela, J., and N. Johnson, "Improvements to NASA's Debris Assessment Software," *58th International Astronautical Congress*, IAA-01-IAA.6.6076, Hyderabad, India, September 2007.

Reynerson, C. M., "Reentry Debris Envelope Model for a Disintegrating, Deorbiting Spacecraft without Heat Shields," *AIAA Atmospheric Flight Mechanics Conference*, AIAA 2005-5916, San Francisco, California, 15-18 August 2005.

Reynerson, C. M., "Reentry Envelope Determination Part II. Structural Failure Due to Atmospheric Heating," *AIAA Atmospheric Flight Mechanics Conference*, AIAA 2006-6275, Keystone, Colorado, 21-24 August 2006.

Rochelle, W. C. and R.A. Rohan, Users Manual for QRAD Entry Radiation Program, JSC-26059, November 1992.

Rochelle, W.C., B.S. Kirk, and B.C. Ting, User's Guide for Object Reentry Survival Analysis Tool (ORSAT) – Version 5.0, Vols. I and II, JSC-28636, July 1999.

Rochelle, W., *et al.*, "Results of IADC Reentry Survivability Benchmark Cases: Comparison of NASA ORSAT 5.0 Code with ESA SCARAB Code," *Presentation at the 17th IADC meeting*, Darmstadt, Germany, October 1999.

Rustick, J. P. and W.C. Rochelle, Reentry Survivability Analysis of GENESIS Spacecraft Bus, LMSEAT 33557, December 2000.

Rustick, J.P. and W.C. Rochelle, Reentry Survivability Analysis of Earth Observing System (EOS) – Aqua Spacecraft, LMSEAT-33622, March 2001.

Smith, R. N. and W.C. Rochelle, "Reentry Survivability Analysis of Compton Gamma Ray Observatory (CGRO)", JSC-28929, March 2000.

Smith, R. N., R.M. DeLaune, and J. Dobarco-Otero, Reentry Survivability Analysis of the Genesis Spacecraft Bus for Off-Nominal Trajectories, JSC-62665 Rev. A, August 2004.

Smith, R.N., J. Dobarco-Otero, K.J. Bledsoe, and R.M. DeLaune, User's Guide for Object Reentry Survival Analysis Tool (ORSAT) – Version 6.0, JSC-62861, January 2006.

Smith, R.N. and W.C. Rochelle, "Reentry Survivability Analysis of Earth Observing System (EOS) – Aura Spacecraft," LMSEAT-33712, July 2001.

Smith, R.N., J. Dobarco-Otero, J.J. Marichalar, and W.C. Rochelle, Tropical Rainfall Measuring Mission (TRMM) – Spacecraft Reentry Survivability Analysis, JSC-29837, September 2002.

Smith, R.N., J. Dobarco-Otero, and W.C. Rochelle, Reentry Analysis of Gamma-ray Large Area Space Telescope (GLAST) Satellite, JSC-49775, July 2003.

Smith, R.N., K.J. Bledsoe, and J. Dobarco-Otero, Reentry Survivability Analysis of the Hubble Space Telescope (HST), JSC-62599, May 2004.

Smith, R.N., J. Dobarco-Otero, and R.M. DeLaune, "Reentry Survivability Analysis of Shuttle External Tank Debris," JSC-62683, December 2004.

Smith, R.N., J. Dobarco-Otero, and R.M. DeLaune, "Reentry Survivability Analysis of the Terra Satellite," JSC-63042, June 2005.

Tauber, M. E. and K. Sutton, "Stagnation Point Radiative Heating Relations for Earth and Mars Entries," Journal of Spacecraft and Rockets, Vol. 28, No. 1, pp. 40-42, January – February 1991.

Weaver, M.A., R.L. Baker, and M.V. Frank, "Probabilistic Estimation of Reentry Debris Area," *Proceedings of the 3rd European Conference on Space Debris*, ESA SP-473, Darmstadt, Germany, October 2001.

Figure 4.8-1. CGRO breaking up over Pacific Ocean during reentry in June 2000

Figure 4.8-2. Fuel tank orbital debris from Delta II second stage that landed near Georgetown, TX in January 1999

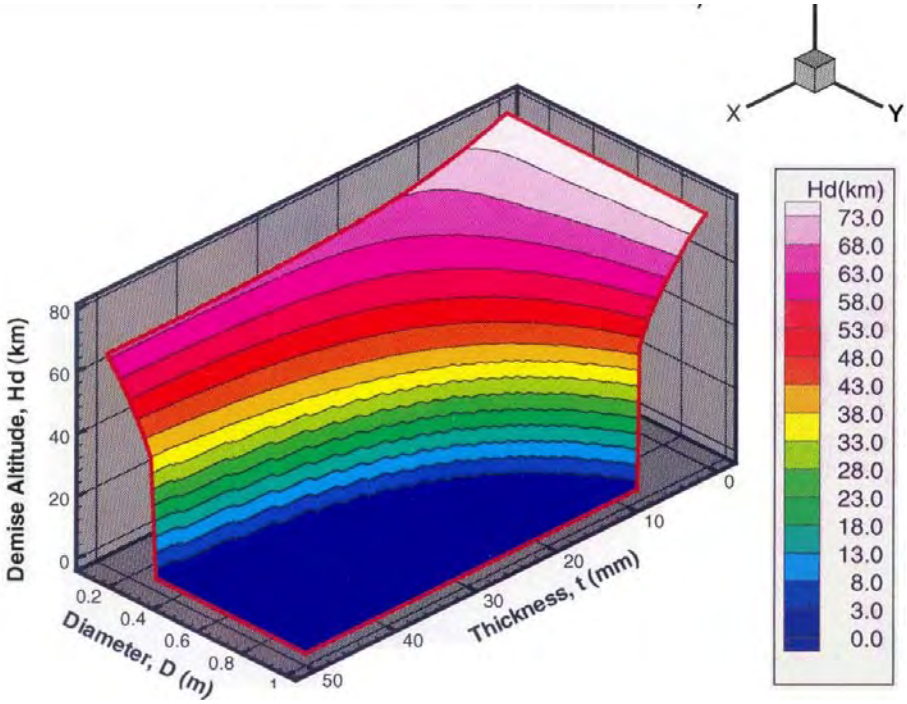

Figure 4.8-3. Demise altitude vs. diameter and wall thickness for aluminum spheres

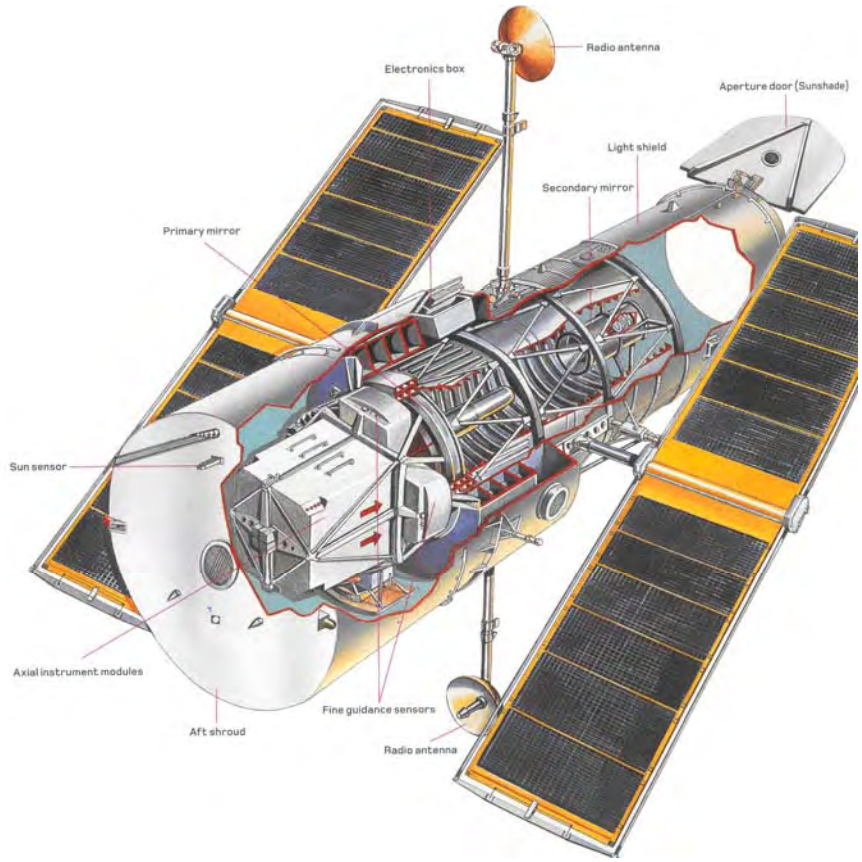

Figure 4.8-4. Cut-out view drawing of the HST.

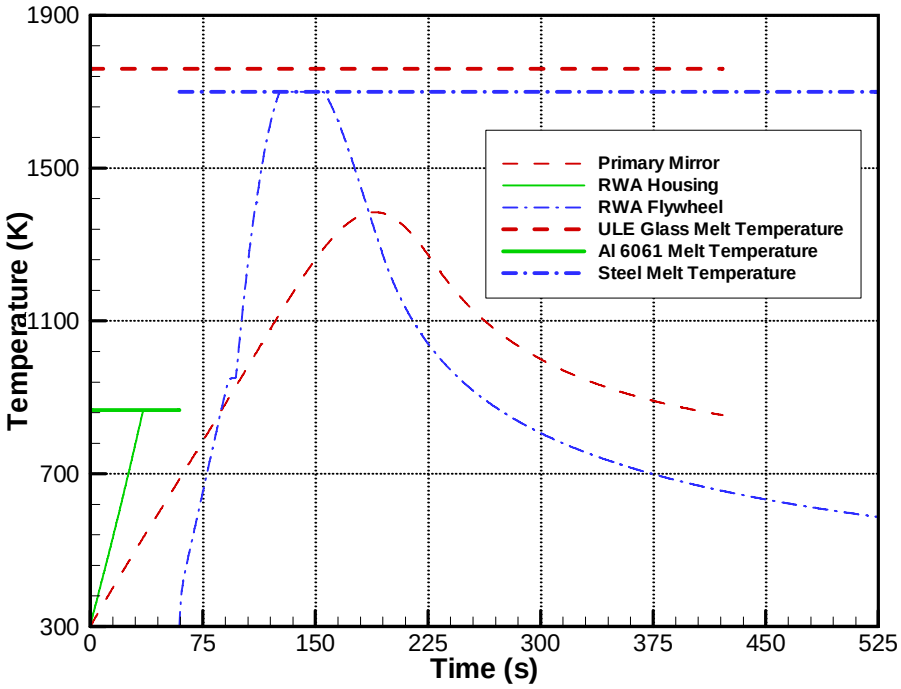

Figure 4.8-5. Surface and melt temperature for sample HST surviving components

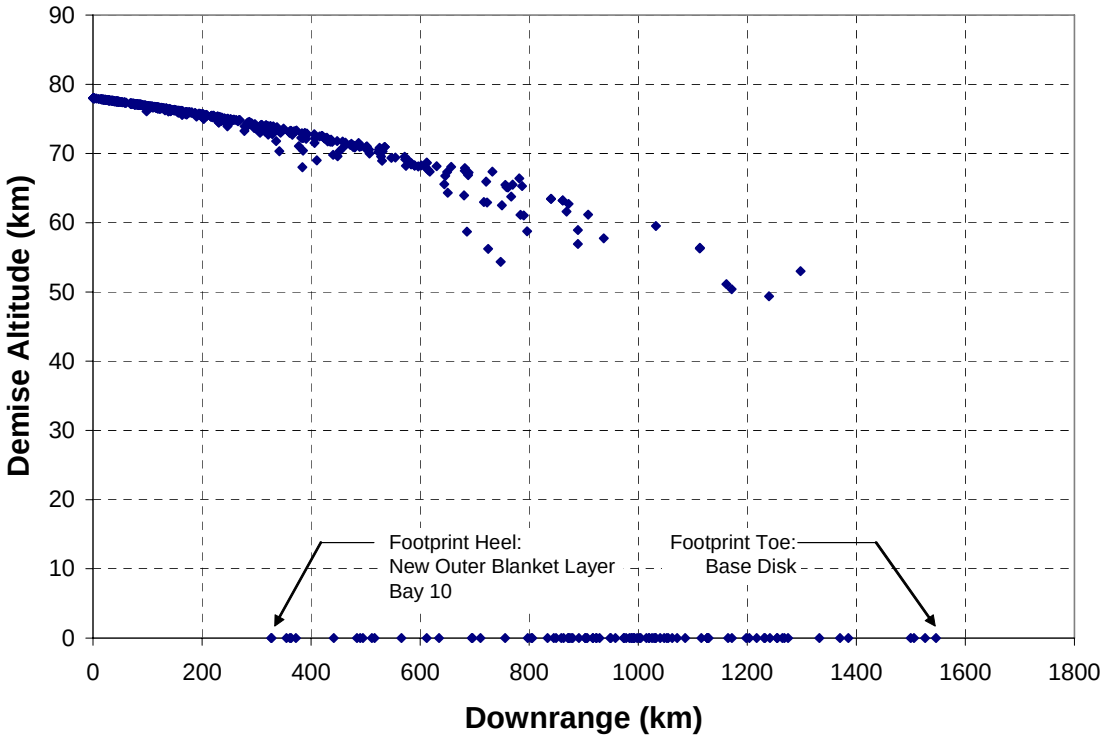

Figure 4.8-6. Demise altitude vs. downrange for HST components

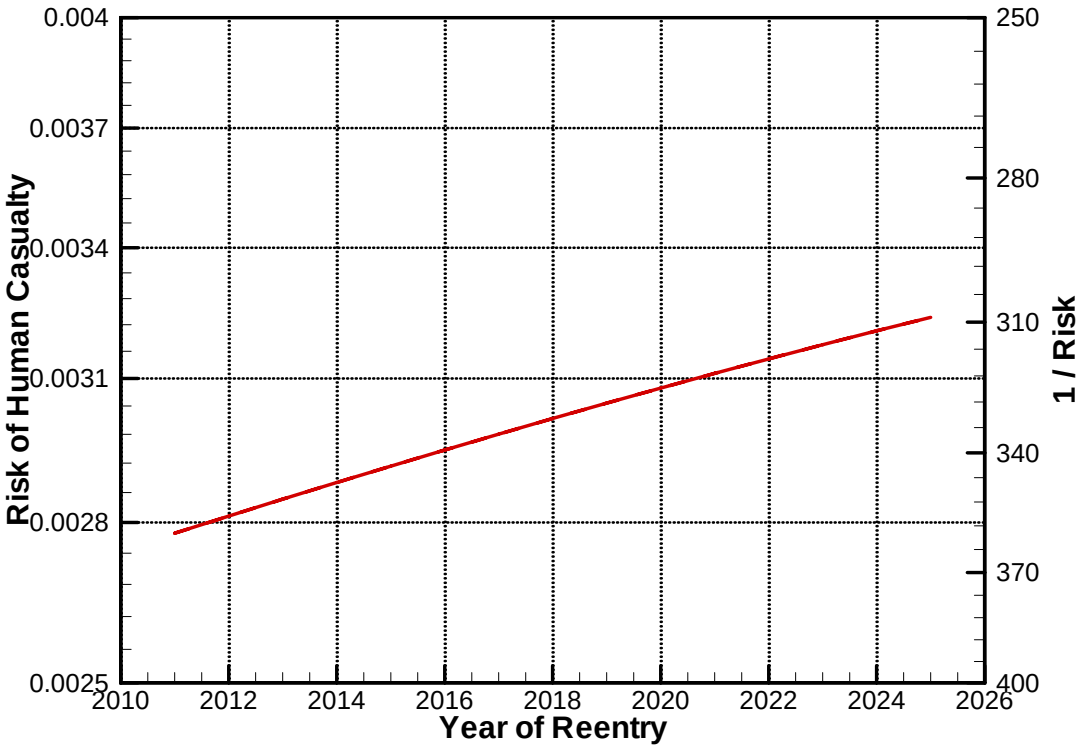

Figure 4.8-7. Calculation of risk for HST as a function of reentry year